

CAPITAL UNIVERSITY OF SCIENCE AND
TECHNOLOGY, ISLAMABAD



Unified Framework for Detection and Mitigation of Cyclic Torque Imbalance in Gasoline Engines

by

Raheel Anjum

A thesis submitted in partial fulfillment for the
degree of Doctor of Philosophy

in the

Faculty of Engineering

Department of Electrical Engineering

2020

Unified Framework for Detection and Mitigation of Cyclic Torque Imbalance in Gasoline Engines

By

Raheel Anjum

(DEE 143006)

Dr. Tielong Shen, Professor

Shen Laboratory, Sophia University, Japan

(Foreign Evaluator 1)

Dr. Marco Baglietto, Associate Professor

University of Genoa, Italy

(Foreign Evaluator 2)

Dr. Aamer Iqbal Bhatti

(Thesis Supervisor)

Dr. Noor Muhammad Khan

(Head, Department of Electrical Engineering)

Dr. Imtiaz Ahmed Taj

(Dean, Faculty of Engineering)

**DEPARTMENT OF ELECTRICAL ENGINEERING
CAPITAL UNIVERSITY OF SCIENCE AND TECHNOLOGY
ISLAMABAD**

2020

Copyright © 2020 by Raheel Anjum

All rights reserved. No part of this thesis may be reproduced, distributed, or transmitted in any form or by any means, including photocopying, recording, or other electronic or mechanical methods, by any information storage and retrieval system without the prior written permission of the author.

Dedicated to my Parents, Siblings, Wife and Daughters



CAPITAL UNIVERSITY OF SCIENCE & TECHNOLOGY ISLAMABAD

Expressway, Kahuta Road, Zone-V, Islamabad
Phone: +92-51-111-555-666 Fax: +92-51-4486705
Email: info@cust.edu.pk Website: <https://www.cust.edu.pk>

CERTIFICATE OF APPROVAL

This is to certify that the research work presented in the thesis, entitled “**Unified Framework for Detection and Mitigation of Cyclic Torque Imbalance in Gasoline Engines**” was conducted under the supervision of **Dr. Aamer Iqbal Bhatti**. No part of this thesis has been submitted anywhere else for any other degree. This thesis is submitted to the **Department of Electrical Engineering, Capital University of Science and Technology** in partial fulfillment of the requirements for the degree of Doctor in Philosophy in the field of **Electrical Engineering**. The open defence of the thesis was conducted on **December 19, 2019**.

Student Name: Mr. Raheel Anjum (DEE143006)

The Examining Committee unanimously agrees to award PhD degree in the mentioned field.

Examination Committee :

(a) External Examiner 1: Dr. Abdul Qayyum Khan,
Professor
PIEAS, Islamabad

(b) External Examiner 2: Dr. Ammar Hassan,
Associate Professor,
SEECs, NUST, Islamabad

(c) Internal Examiner : Dr. Raza Samar
Professor
CUST, Islamabad

Supervisor Name : Dr. Aamer Iqbal Bhatti
Professor
CUST, Islamabad

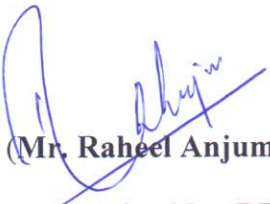
Name of HoD : Dr. Noor Muhammad Khan
Professor
CUST, Islamabad

Name of Dean : Dr. Imtiaz Ahmad Taj
Professor
CUST, Islamabad

AUTHOR'S DECLARATION

I, **Mr. Raheel Anjum (Registration No. DEE-143006)**, hereby state that my PhD thesis titled, '**Unified Framework for Detection and Mitigation of Cyclic Torque Imbalance in Gasoline Engines**' is my own work and has not been submitted previously by me for taking any degree from Capital University of Science and Technology, Islamabad or anywhere else in the country/ world.

At any time, if my statement is found to be incorrect even after my graduation, the University has the right to withdraw my PhD Degree.


(**Mr. Raheel Anjum**)
Registration No : DEE-143006

Dated: 19 December, 2019

PLAGIARISM UNDERTAKING

I solemnly declare that research work presented in the thesis titled “**Unified Framework for Detection and Mitigation of Cyclic Torque Imbalance in Gasoline Engines**” is solely my research work with no significant contribution from any other person. Small contribution/ help wherever taken has been duly acknowledged and that complete thesis has been written by me.

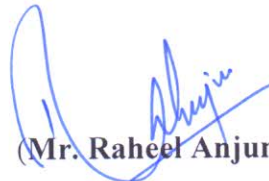
I understand the zero tolerance policy of the HEC and Capital University of Science and Technology towards plagiarism. Therefore, I as an author of the above titled thesis declare that no portion of my thesis has been plagiarized and any material used as reference is properly referred/ cited.

I undertake that if I am found guilty of any formal plagiarism in the above titled thesis even after award of PhD Degree, the University reserves the right to withdraw/ revoke my PhD degree and that HEC and the University have the right to publish my name on the HEC/ University Website on which names of students are placed who submitted plagiarized thesis.

Dated:

19

December, 2019


(Mr. Raheel Anjum)

Registration No : DEE-143006

List of Publications

It is certified that following publications have been made out of the research work, that has been carried out for this thesis:-

Journal Publications

1. **R. Anjum**, A. I. Bhatti, A. Yar and Q. Ahmed, “*Cyclic Torque Imbalance Detection in Gasoline Engines using a Uniform Second Order Sliding Mode Observer*”, Proceedings of the Institution of Mechanical Engineers, Part D: Journal of Automobile Engg. vol. 233, no. 13, pp. 3515-3527, 2019.

Conference Publications

1. **R. Anjum**, A. Yar, S. R. Shah, Q. Ahmed and A. I. Bhatti, “*Observer based Robust Control Design for Mitigation of Cyclic Torque Imbalance in Gasoline Engines*”, 3rd IEEE Conference on Control Technology and Applications (CCTA), Hong Kong, China, 19-21 Aug 2019, IEEE CSS.
2. **R. Anjum**, A. Yar, I. Khan, Q. Ahmed and A. I. Bhatti, “*Dual Loop Speed Tracking Control for Torque Management of Gasoline Engines*”, European Control Conference, Naples, Italy, 24-28 June 2019, pp. 3084-3089. IEEE.
3. **R. Anjum**, A. Yar, I. Khan, Q. Ahmed and A. I. Bhatti, “*Second Order Sliding Mode based Speed Tracking Control for Torque Management of Gasoline Engines*”, 12th Asian Control Conference, Fukuoka, Japan, 9-12 June 2019, pp. 555-560. IEEE.
4. **R. Anjum**, A. Yar, Q. Ahmed and A. I. Bhatti, “*Cyclic Torque Imbalance Detection in Gasoline Engines using Second Order Sliding Mode*”, 2nd IEEE Conference on Control Technology and Applications (CCTA), Copenhagen, Denmark, 21-24 Aug 2018, pp. 1046-1051. IEEE CSS. DOI: 10.1109/CCTA.2018.8511522.
5. **R. Anjum**, A. Yar, I. Khan, Q. Ahmed and A. I. Bhatti, “*Speed Tracking of Spark Ignition Engines using Higher Order Sliding Mode Control*”, 16th International Bhurban Conference on Applied Sciences and Technology (IBCAST),

Islamabad, Pakistan, 8-12 Jan 2019, pp. 576-581. IEEE. DOI: 10.1109/IB-CAST.2019.8667231.

6. **R. Anjum**, I. Khan, A. Yar and A. I. Bhatti, “*Air-to-Fuel Ratio Control of Gasoline Engines using Smooth Sliding Mode Algorithm*”, 13th International Conference on Emerging Technologies (ICET), Islamabad, Pakistan, 27-28 Dec 2017, pp. 1-6. IEEE. DOI: 10.1109/ICET.2017.8281731.

Other Publications

1. A. Yar, **R. Anjum**, Q. Ahmed and A. I. Bhatti, “*A Framework for Model Based Detection of Misfire in a Gasoline Engine with Dynamic Skip Fire*”, SAE Technical Paper 2019-01-1288, 2019, <https://doi.org/10.4271/2019-01-1288>.
2. G. Murtaza, A. I. Bhatti, Y. A. Butt and **R. Anjum**, “*FTC for Air Path Actuators of a Diesel Engine using VGSTA* ”, 13th International Conference on Emerging Technologies (ICET), Islamabad, Pakistan, 27-28 Dec 2017, pp. 1-6. IEEE. DOI: 10.1109/ICET.2017.8281652.
3. I. Khan, A. I. Bhatti, **R. Anjum** and Q. Khan, “*Constructive Mechanism of Lead/Lag Design for a Class of Linear Systems*”, 12th International Conference on Emerging Technologies (ICET), Islamabad, Pakistan, 18-19 Oct 2016, pp. 1-6. IEEE. DOI: 10.1109/ICET.2016.7813226.

Raheel Anjum

(DEE 143006)

Acknowledgements

All Praises to ALLAH Almighty, the Most Gracious and the Most Merciful.

I am highly grateful to my supervisor Dr. Aamer Iqbal Bhatti, whose persistent guidance and inspiration has always been a source of motivation since start of my post-graduation studies. I am especially thankful to my co-supervisor Dr. Qadeer Ahmed for his invaluable support and technical guidance, not only in PhD research work but also during MS. I also wish to thank Dr. Ahmed Yar, who has been a mentor throughout my PhD research work for his assistance, encouragement and constructive feedback.

I would like to thank Dr. Fazal ur Rehman, Dr. Raza Samar, Dr. Imtiaz Taj and Dr. Noor Muhammad Khan for their guidance and inspirational teaching during PhD course work. I am also grateful to Dr. Sami ur Rehman Shah from SMME, NUST, as technical discussions with him have aided to understand working of IC engines; as well as Mr. Saad Saleem for his support and assistance to learn GT-Suite.

I am thankful to all members of Control and Signal Processing Research Group (CASPR), Dr. Yasir Awais, Dr. Imran Khan, Dr. Qudrat Khan, Dr. Ali Arshad, Dr. Ghulam Murtaza, Dr. Ghulam Murtza Kiani, Dr. Ussama Ali, Dr. Zeeshan Babar, Dr. Abdul Rehman Yasin and Dr. Mudassir Rizvi for their assistance on various technical topics and support during my research work. I am also thankful to my colleagues, Mr. Farhan, Mr. Usman, Mr. Zohaib, Mr. Atif, Mr. Rizwan Azam, Mr. Asghar, Mr. Waiz, Mr. Azmat, Mr. Ahmed Mahmood, Mr. Yasir Naeem and Mr. Abrar for their guidance and encouragement.

Above all, I am highly grateful to my parents, my siblings who have always provided me motivation and relentless support to pursue higher studies and my spouse for her cooperation, support and assistance during my doctorate's tenure.

In the last, I acknowledge Higher Education Commission (HEC), Islamabad for financial support to carry out this research work.

Abstract

Torque imbalance is a wide-ranging problem, common in all internal combustion engines irrespective of their type. It is desirable to achieve consistent torque contribution from engine cylinders to prevent excessive torsional vibrations in the crankshaft. Torque generation is not smooth in internal combustion engines as successive work phases of the combustion cycle produce periodically time-varying torque. Thus, the role of torque imbalance control is significant in reducing such variations. In the last three decades, considerable research efforts have been made to improve engine control systems for compliance with policies and regulations to minimize exhaust emissions and enhance fuel economy. Progression in the field of electronics and embedded systems has made it possible to implement complex control techniques in a small-scale engine control unit.

Cyclic torque imbalance is one of the types of engine torque imbalance, which exists due to variations in the torque, generated by combustion cycles in an engine cylinder. It causes non-smooth engine power and excessive stresses in engine components. Minimizing imbalance in the cyclic torque is important to achieve better fuel economy, reduced exhaust emissions and limit degradation as well as aging effects of engine components. Although, cyclic torque imbalance was sporadically studied; however, it was not considered a concern until measurement of consecutive engine cycles was made possible. Cyclic torque balancing approach is comprised of detecting imbalance in the torque and mitigating its causes to decrease the difference between work output of successive combustion cycles in an engine cylinder.

In this dissertation, a model based novel unified framework is proposed for detection and mitigation of cyclic torque imbalance in gasoline engines. First Principle Based Engine Model is employed to formulate the proposed framework, which is comprised of sliding mode based observer and fault tolerant controller. Uniform second order sliding mode observer is used for estimation of the unknown input i.e. net piston force (f_n) from engine speed dynamics to detect imbalance in the cyclic torque. No extra sensors and hardware are required for evaluation of the proposed

estimation technique. Fault in fuel injection subsystem is induced to generate imbalance in the cyclic torque. Model of single cylinder gasoline engine is developed in GT-Power to validate the proposed estimation technique. First Principle Based Engine Model is transformed to get direct relation between engine speed and injector pulse width. Estimated net piston force (\hat{f}_n) is used to design the control law for observer based fault tolerant control techniques to mitigate imbalance in the cyclic torque by reconfiguration of the control input and attenuation of the fault in fuel injection subsystem. Results of numerical simulation have demonstrated that desired objective is achieved by the proposed model based unified framework.

Another contribution of the research work presented in this dissertation is to propose a fault tolerant speed tracking control technique for gasoline engines. Variations appear in engine speed due to torque imbalance. Output speed of the engine is kept at prescribed set-points, despite occurrence of the fault in fuel injection subsystem. The proposed technique is also robust to disturbances in the form of fluctuating load torque. Transformation in First Principle Based Engine Model is employed for torque management by tracking varying speed profile of the engine. Reference data is acquired from engine test rig to validate the proposed fault tolerant speed tracking control technique.

Contents

Author’s Declaration	v
Plagiarism Undertaking	vi
List of Publications	vii
Acknowledgments	ix
Abstract	x
List of Figures	xvi
List of Tables	xix
Abbreviations	xx
Symbols	xxii
1 Introduction	1
1.1 Gasoline Engines	2
1.2 An Overview of Engine Torque Imbalance	5
1.3 Motivation and Objectives	7
1.4 Research Contributions	9
1.5 Overview of the Dissertation	11
2 Cyclic Torque Imbalance in IC Engines	13
2.1 Engine Balancing	14
2.1.1 Fluid Dynamics Engine Balancing	15
2.1.2 Thermal Engine Balancing	15
2.1.3 Mechanical Engine Balancing	16
2.1.3.1 Static Balancing	16
2.1.3.2 Dynamic Balancing	16
2.1.3.3 Torque Balancing	16
2.2 Classes of Engine Torque Imbalance	17
2.2.1 Cylinder to Cylinder Torque Imbalance	17

2.2.2	Cyclic Torque Imbalance	18
2.2.2.1	Causes of Cyclic Torque Imbalance	20
2.2.2.2	Impact of Cyclic Torque Imbalance	21
2.2.2.3	Cyclic Torque Imbalance and Variable Cylinder Displacement Engines	21
2.3	Methodologies for Detection and Mitigation of Engine Torque Im- balance	23
2.3.1	In-Cylinder Pressure	24
2.3.2	Exhaust Oxygen Concentration	24
2.3.3	Engine Rotational Speed	25
2.4	Existing Approaches for Detection and Mitigation of Engine Torque Imbalance	26
2.4.1	Detection of Imbalance in Cyclic Torque	26
2.4.2	Engine Rotational Speed based Approaches	29
2.4.2.1	Frequency Domain Approaches	29
2.4.2.2	Time Domain Approaches	32
2.5	Research Analysis	35
2.6	Problem Statement	37
2.7	Chapter Summary	37
3	Mathematical Models of Gasoline Engine	38
3.1	Working Principle of Otto Cycle	39
3.2	Modeling Approaches of Gasoline Engine	41
3.2.1	Mean Value Models of Gasoline Engine	42
3.2.2	Cylinder by Cylinder Models of Gasoline Engine	44
3.3	Models of Engine Crankshaft	45
3.3.1	Lumped Inertia Parameter Model	46
3.3.2	Continuous Mass Model	48
3.3.3	Multi-Segment Concentrated Mass Model	48
3.3.4	Soft Body Dynamics Model	49
3.4	Engine Models Incorporating Torque Production Subsystem	49
3.5	First Principle based Engine Model with Lumped Cylinder Dynamics	52
3.5.1	Torque Producing Mechanism Model	54
3.5.2	Analytical Cylinder Pressure Model	60
3.5.3	Model Integration	63
3.5.3.1	Air Intake Subsystem	63
3.5.3.2	Intake Manifold Subsystem	64
3.5.3.3	Fuel Dynamics Subsystem	65
3.5.4	Attributes of First Principle based Engine Model	67
3.6	Engine Modeling in GT-Suite	68
3.6.1	Validation of FPEM in GT-Power	69
3.6.1.1	Sub-Models of GT-Power based Engine Model	70
3.6.1.2	Model Validation	71

3.7	Chapter Summary	77
4	Detection of Cyclic Torque Imbalance	78
4.1	Fuel Injection Subsystem	79
4.1.1	Working of Fuel Injector	79
4.1.2	Faults in Fuel Injection Subsystem	81
4.2	Unknown Input Observer	82
4.2.1	Review of Unknown Input Observers	83
4.2.2	Unknown Input Observers based on Second Order Sliding Mode	84
4.3	Sliding Mode Control	86
4.3.1	Design of Sliding Mode Control	87
4.3.2	Chattering Phenomenon	89
4.3.3	Higher Order Sliding Mode	90
4.3.4	Second Order Sliding Mode Algorithms	92
4.3.4.1	Real Twisting Algorithm	92
4.3.4.2	Super Twisting Algorithm	94
4.4	FPEM based USOSM Observer	95
4.4.1	Unknown Input Estimation using USOSM Observer	96
4.4.2	Relation between Generation of Cyclic Torque and Net Piston Force	97
4.4.3	Observer Design	98
4.4.4	Observability	101
4.4.5	Boundedness Analysis	102
4.4.6	Error Dynamics Analysis and Convergence	103
4.5	Results and Discussions	106
4.5.1	MATLAB and GT-Power Co-Simulation Environment	106
4.5.2	Imbalance Generation in Cyclic Torque	107
4.5.3	Detection of Cyclic Torque Imbalance	109
4.6	Chapter Summary	116
5	Mitigation of Cyclic Torque Imbalance	117
5.1	Fault Tolerant Control	118
5.1.1	Fault Tolerant Control for Vehicle Powertrain	119
5.2	Observer Based Fault Tolerant Control Design	120
5.2.1	Existing Approaches for Mitigation of Cyclic Torque Imbalance	121
5.2.2	Unified Framework for Detection and Mitigation of Cyclic Torque Imbalance	122
5.2.3	Assumptions for Control Design	124
5.2.4	Transformation in First Principle based Engine Model	124
5.3	STA based FTC Technique	127

5.3.1	Controller Structure	128
5.3.2	Existence of Sliding Mode	128
5.3.3	Control Law	130
5.3.4	Results and Discussion-STA based FTC Technique	132
5.4	CESTA based FTC Technique	137
5.4.1	Controller structure	138
5.4.1.1	Lyapunov Stability Analysis-I	139
5.4.1.2	Lyapunov Stability Analysis-II	141
5.4.2	Control Law	145
5.4.3	Results and Discussion-CESTA based FTC Technique	147
5.5	Chapter Summary	153
6	Robust Speed Tracking Control	154
6.1	Engine Speed Tracking and Torque Management	155
6.2	Existing Approaches for Engine Speed Tracking Control	158
6.3	Robust Speed Tracking Control	160
6.3.1	Smooth Super-Twisting Algorithm	162
6.3.2	Control Law	163
6.4	Engine Test Rig	166
6.4.1	On-board Diagnostic Interface	166
6.4.2	Data Acquisition	167
6.5	Results and Discussion	168
6.6	Chapter Summary	172
7	Conclusion and Future Work	173
7.1	Contributions of Research Work	175
7.2	Future Directions	176
	Bibliography	178
	Appendix A	
	Mathematical Expressions of FPEM	198

List of Figures

1.1	Cross-Section View of the Gasoline Engine	2
1.2	Phases in the Gasoline Engine	4
1.3	Crankshaft Failure due to Torque Imbalance	6
1.4	Proposed Methodology	10
2.1	Groups of Engine Balancing	14
2.2	Schematic Diagram of the Engine Cylinder	19
2.3	Basic Concept of DSF [37]	22
2.4	Methodologies for Torque Imbalance Detection and Mitigation	23
3.1	Ideal Otto Cycle [1]	40
3.2	Modeling Approaches of Gasoline Engine [79]	42
3.3	Lumped Inertia Parameter Model of Engine Crankshaft [97]	46
3.4	Torque Producing Mechanism-Lumped Cylinder Engine [117]	54
3.5	Constraints for Motion of Torque Producing Mechanism	57
3.6	Inputs and Outputs of Cylinder Pressure Model	61
3.7	Structure of Torque Production Subsystem [14]	63
3.8	Structure of the FPEM [117]	64
3.9	GT-Power based Model of Single Cylinder Gasoline Engine	70
3.10	Engine Angular Position (θ_1); FPEM and GT-Power based Engine Model	73
3.11	Engine Rotational Speed (ω_1); FPEM and GT-Power based Engine Model	74
3.12	Engine Rotational Speed Comparison for Single Combustion Cycle a) Angular Position versus Rotational Speed b) Time versus Rotational Speed	75
3.13	Net Piston Force (f_n); FPEM and GT-Power based Engine Model	76
4.1	Cross Section View of the Fuel Injector	80
4.2	Type of System Faults [132]	81
4.3	Phases of Sliding Mode Control	88
4.4	Chattering during Sliding Motion of the System	89
4.5	(a) Signum Function (b) Saturation Function [157]	90
4.6	System Trajectories on Sliding Surface (a) First Order SMC (b) HOSM	91
4.7	Real Twisting Algorithm	92

4.8	Super Twisting Algorithm	94
4.9	Proposed Framework for Detection of Cyclic Torque Imbalance	99
4.10	Estimated Net Piston Force (f_n) for Balanced Cyclic Torque Generation	108
4.11	Magnified View of Estimated Net Piston Force (f_n) for Balanced Cyclic Torque Generation	108
4.12	Fault Induced in Injected Fuel Mass	109
4.13	Estimation of Engine Angular Position (θ_1)	110
4.14	Error in Estimation of Engine Angular Position	111
4.15	Estimation of Engine Rotational Speed (ω_1)	111
4.16	Error in Estimation of Engine Rotational Speed	112
4.17	Estimated Net Piston Force (f_n) for Imbalanced Cyclic Torque Generation	113
4.18	Magnified View of Estimated Net Piston Force (f_n) for Imbalanced Cyclic Torque Generation	113
4.19	Detection of Cyclic Torque Imbalance	114
4.20	Estimated Net Piston Force (f_n)	115
4.21	Magnified View of Estimated Net Piston Force (f_n)	115
5.1	Proposed Unified Framework for Detection and Mitigation of Cyclic Torque Imbalance	123
5.2	Intake Manifold Pressure	133
5.3	Estimation of (a) Engine Angular Position (b) Engine Rotational Speed	133
5.4	Estimation Error (a) Engine Angular Position (b) Engine Rotational Speed	134
5.5	Estimation of Net Piston force (f_n) by FPEM based USOSM Observer	135
5.6	Mitigation of Cyclic Torque Imbalance by STA based FTC Technique - Desired and Actual Net Piston force (f_n)	135
5.7	(a) Fuel Mass Injected per Combustion Cycle (b) Control Input (c) Sliding Surface	136
5.8	Intake Manifold Pressure	147
5.9	Estimation of (a) Engine Angular Position (b) Engine Rotational Speed	148
5.10	Estimation Error (a) Engine Angular Position (b) Engine Rotational Speed	149
5.11	Estimation of Net Piston force (f_n) by FPEM based USOSM Observer	150
5.12	Mitigation of Cyclic Torque Imbalance by CESTA based FTC Technique - Desired and Actual Net Piston force (f_n)	150
5.13	(a) Fuel Mass Injected per Combustion Cycle (b) Control Input	151
5.14	Fault Induced in Fuel Injection Subsystem at $t \geq 15$ sec	152
5.15	Sliding Surface of STA based FTC Technique	152
5.16	Sliding Surface of CESTA based FTC Technique	153
6.1	Speed Generation Subsystems in Gasoline Engine	156

6.2	Map between Torque Demand, Position of Accelerator Pedal and Engine Speed [182]	157
6.3	Proposed Framework for Engine Speed Tracking Control	161
6.4	Engine Experimental Setup	165
6.5	Data Acquisition System based on OBD-II	167
6.6	Plot of (a) Throttle Valve Angle (b) Load Torque	168
6.7	Plot of Engine States (a) Manifold Pressure (b) Engine Output Speed	169
6.8	Net Piston Force (f_n)	170
6.9	Fuel Mass Injected per Combustion Cycle (m_{fo}) with Faults in Fuel Injection Subsystem	171
6.10	Fuel Mass Injected per Combustion Cycle (m_{fo}) with no Fault in Fuel Injection Subsystem	171
6.11	Plot of (a) Sliding Surface (b) Control Input	172

List of Tables

3.1	Detail of Generalized Coordinates	55
3.2	Comparison of FPEM and MVEM [16]	67
3.3	Specifications of Single Cylinder Gasoline Engine	72
6.1	Specifications of Test Rig Engine	166

Abbreviations

AFR	Air to Fuel Ratio
BSFC	Brake Specific Fuel Consumption
BDC	Bottom Dead Center
BIBO	Bounded Input and Bounded Output
CESTA	Certainty Equivalence Super Twisting Algorithm
CI	Compression Ignition
CCEM	Cylinder to Cylinder Engine Model
COV	Coefficient of Variations
COVIMEP	Coefficient of Variation in Indicated Mean Effective Pressure
DSF	Dynamic Skip Fire
DFT	Discrete Fourier Transform
DEM	Discrete Event Model
DAE	Differential Algebraic Equation
EFI	Electronic Fuel Injection
ECU	Engine Control Unit
EoC	End of Combustion
EoM	Equation of Motion
EGR	Exhaust Gas Recirculation
FTC	Fault Tolerant Control
FFT	Fast Fourier Transform
FPEM	First Principle based Engine Model
FRF	Frequency Response Functions
HOSM	Higher Order Sliding Mode
HCCI	Homogenous Compression Charge Ignition

IMEP	Indicated Mean Effective Pressure
IPW	Injector Pulse Width
IAT	Intake Air Temperature
IC	Internal Combustion
LMI	Linear Matrix Inequalities
LPF	Low Pass Filter
MAP	Manifold Air Pressure
MFB	Mass Fraction Burnt
MVEM	Mean Value Engine Model
MPC	Model Predictive Control
MIMO	Multi Input-Multi Output
NVH	Noise, Vibration, Harshness
OBD-II	On Board Diagnostics-II
PID	Proportional Integral Derivative
PI	Proportional Integral
RTA	Real Twisting Algorithm
RGF	Residual Gas Fraction
SOSM	Second Order Sliding Mode
SMC	Sliding Mode Control
SI	Spark Ignition
SA	Spark Angle
SoC	Start of Combustion
STA	Super Twisting Algorithm
SSTA	Smooth Super Twisting Algorithm
TDC	Top Dead Center
USOSM	Uniform Second Order Sliding Mode
UIO	Unknown Input Observer
UKF	Unscented Kalman Filter
VCD	Variable Cylinder Displacement
VVT	Variable Valve Timing
VSC	Variable Structure Control

Symbols

Symbol	Description	Units
α	Throttle Valve Angle	<i>rad</i>
\dot{m}_{ai}	Mass Flow Rate of Air Past the Throttle	<i>kg/sec</i>
\dot{m}_{aio}	Intake Manifold Model Fitting Variable	<i>kg/sec</i>
m_{ao}	Air Mass Inducted into Engine Cylinder	<i>kg</i>
P_{amb}	Ambient Pressure	P_a
T_{amb}	Ambient Temperature	<i>K</i>
D	Diameter of the Throttle	<i>m</i>
P_{man}	Intake Manifold Pressure	P_a
T_{man}	Intake Manifold Temperature	<i>K</i>
P_{exh}	Exhaust Manifold Pressure	P_a
V_{man}	Intake Manifold Volume	m^3
P_{comb}	Combustion Pressure	P_a
T_{comb}	Combustion Temperature	<i>K</i>
ΔT	Change in Temperature due to Combustion	<i>K</i>
V_d	Engine Displacement Volume	m^3
V_c	Cylinder Clearance Volume	m^3
η_v	Volumetric Efficiency	%
m_{total}	Total Charge Trapped in Engine Cylinder	<i>kg</i>
\dot{m}_{ao}	Mass Flow Rate of the Air into Engine Cylinder	<i>kg/sec</i>
\dot{m}_{fi}	Mass Flow Rate of the Injected Fuel	<i>kg/sec</i>
\dot{m}_{fo}	Mass Flow Rate of Fuel Injected into Cylinder	<i>kg/sec</i>
\dot{m}_{fv}	Mass Flow Rate of the Fuel Vapors	<i>kg/sec</i>

Symbol	Description	Units
$\dot{m}_{f inj}$	Mass Flow Rate of the Fuel Injector	kg/sec
m_{fo}	Fuel Mass Injected per Combustion Cycle	kg
τ_f	Fuel Film Evaporation Time Constant	sec^{-1}
τ_N	Net Torque	Nm
τ_L	Load Torque	Nm
τ_{int}	Instantaneous Cylinder Torque	Nm
τ_{gas}	Combustion Torque	Nm
τ_{mass}	Inertia Torque	Nm
τ_i	i^{th} Inertia Torque	Nm
θ_0	Position at SoC	rad
$\delta\theta_1$	Combustion Duration	rad
KE	Kinetic Energy	J
PE	Potential Energy	J
K	Structural Stiffness	N/m
B	Structural Damping	kg/s
F_c	Force Acting on Piston Head	N
F_{crk}	Force Acting on Crank Case Side of the Piston	N
A_P	Area of the Piston	m^2
P_{cyl}	Pressure in the Cylinder	Pa
P_{ck}	Crank Case Pressure	Pa
f_n	Net Piston Force	N
f_n^d	Desired Net Piston Force	N
f_n^a	Actual Net Piston Force	N
\hat{f}_n^a	Estimated Value of Actual Net Piston Force	N
ω_1^d	Desired Engine Speed	rad/sec
ω_1^a	Actual Engine Speed	rad/sec
P_{man}^a	Actual Manifold Pressure	Pa
Q_{HV}	Fuel Heating Value	J/kg
c_v	Specific Heat at Constant Volume	$kJ/kg - K$
η_c	Combustion Efficiency	$\%$

Symbol	Description	Units
$V(\theta_1)$	Instantaneous Volume of the Engine Cylinder	m^3
V_{ivc}	Cylinder Volume at Intake Valve Close	m^3
R	Universal Gas Constant	$J.kg^{-1}.K^{-1}$
P_i	Pressure in i^{th} Phase of Otto Cycle	P_a
T_i	Temperature in i^{th} Phase of Otto Cycle	K
V_i	Volume in i^{th} Phase of Otto Cycle	m^3
C_D	Coefficient of Discharge of the Throttle	
X_f	Fuel Separation Parameter	
γ	Ratio of Specific Heats	
γ_c	Exponent of Polytropic Compression	
γ_e	Exponent of Polytropic Expansion	
m_{fb}	Mass Fraction Burnt	
Δm_{fb}	Change in Mass Fraction Burnt per Combustion Cycle	
Δ	Unknown Parameter	
L	Lagrangian of the System	
$S_i(x)$	i^{th} Sliding Surface	
q_i	i^{th} Generalized Coordinate	
ϕ_i	i^{th} Constraint of Motion	
λ_i	i^{th} Lagrange Multiplier	
e_i^s	i^{th} Generalized Effort	
Γ	Set of parameters of Torque Producing Mechanism	
ω	Angular Velocity ¹	rad/sec
θ	Angular Position ¹	rad
x	X Component of Center of Mass of a Rigid Body ¹	m
y	Y Component of Center of Mass of a Rigid Body ¹	m
m	Mass ¹	kg
J	Moment of Inertia ¹	$kg.m^2$
l	Length ¹	m

¹Subscript (whereas applicable) will correspond to respective body

Chapter 1

Introduction

Control technology has played an important role to improve the overall performance of automotive vehicles. Control of many vehicle subsystems have been converted from mechanical to electrical/electronic based solutions, such as fuel injection, throttle control, cruise control, anti-lock braking system, active suspension and many more. Role of control systems in reducing the air pollution, that is caused by undesired engine emissions was acknowledged by the automotive industry in last decades of the 20th century. As a result, On Board Diagnostics-II (OBD-II) regulations were introduced to detect as well as isolate the faults and failures automatically in engine systems; which enabled immediate rectification of the system malfunction.

Progression in the field of electronics and embedded systems has made it possible to implement complex control algorithms within an Engine Control Unit (ECU), which aided to meet the regulations i.e., OBD-II and euro emission standards. For example, Electronic Fuel Injection (EFI) is a standard feature in present day engines, that has allowed online adjustment of injection timing and duration. It has made it possible to develop the techniques for cylinder-wise features estimation and control.

Map-based solutions were mostly developed for engine control systems in the past due to computation limitations. These maps were manually tuned along with

different engine parameters. Complex control algorithms were proposed due to increasing demand of compliance with regulation and policies for reduction in exhaust emissions and improving the fuel efficiency. Model-based control techniques can assist in reducing the use of empirical relationship maps and enhance engine performance. Research work presented in this dissertation is focused to propose model-based solutions for detection and mitigation of cyclic torque imbalance.

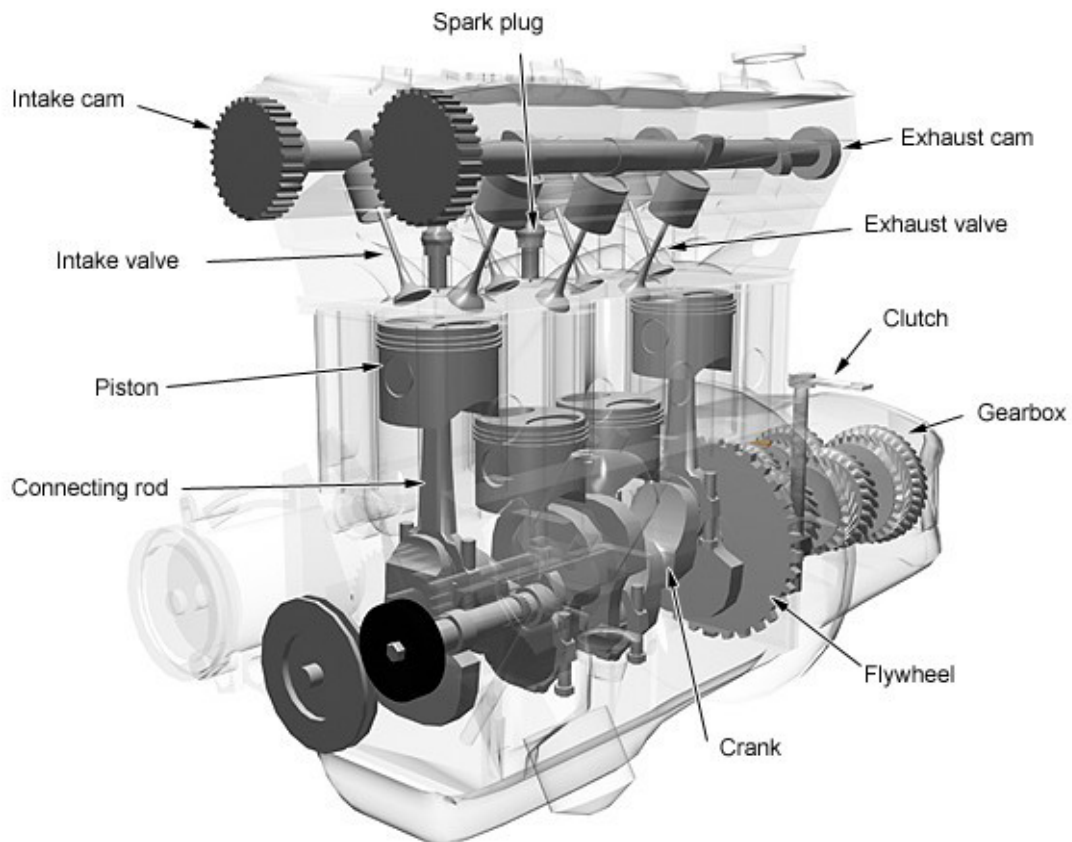


FIGURE 1.1: Cross-Section View of the Gasoline Engine

1.1 Gasoline Engines

In the history of mankind, invention of Internal Combustion (IC) engine during second industrial revolution has proved to be an important scientific event. Since its invention in 1870s, IC engines have not only transformed the means of transportation but also found wide range applications from lawnmowers to power

generators and marine vessels. IC engine produces mechanical energy through combustion from chemical energy of fossil fuels. Combustion of the fuel results in the form of undesirable emissions, that includes particulate matter, nitrogen oxides, unburned hydrocarbons and carbon monoxide. Reduction in these undesired emissions and improving fuel efficiency have remained the main driving force behind evolution of IC engines.

As highlighted in [1], various designs of the IC engine were developed in second half of the 19th century, which operated with variable success. First practical engine was invented by J.J.E. Lenior around 1860s. Relatively successful Otto-Langen engine was introduced in 1867, which was claimed to have 11% efficiency. It was atmospheric engine in which power stroke was driven by atmospheric pressure that acted against a vacuum. In this era, basic four stroke engines started to evolve.

Many scientists worked on the design of four stroke engine but Nicolaus A. Otto has been credited with the invention of modern automobile Spark Ignition (SI) engine in 1876. IC engines have first appeared in road vehicles during 1880s. Two stroke engines also evolved during this era. Rudolf Diesel developed Compression Ignition (CI) engine in 1892, which was more efficient than the gasoline engine. In 1954, Wankel engine was proposed, which used eccentric rotary design instead of reciprocating piston design to transform combustion pressure into rotational motion.

Classification of IC engines can be carried out on the basis of various parameters; such as, type of ignition, engine cycle, basic design, air intake process, position and number of cylinders, fuel type and fuel input method. Though much research effort was carried out to develop various designs of the IC engine; however, based on type of ignition, SI and CI engines have remained at forefront in application of the IC engine. Gasoline engines have been established as one of the main types of the IC engine, that are mostly used in passenger cars. Cross-section view of the gasoline engine is shown in Figure 1.1. Success of gasoline engine can be attributed to combination of different characteristics and ability to adapt

technological advancements, such as exhaust emissions requirement was met with the addition of a three-way catalytic converter.

Basic working principle of gasoline engine is same as that of the IC engine; which acts as a heat engine to produce mechanical energy in the form of rotational motion of the crankshaft from chemical energy of fossil fuels. Phases in four strokes of the gasoline engine are illustrated in Figure 1.2. Initially, thermal energy is produced from chemical energy of the fuel by combustion. Due to thermal energy, pressure as well as temperature of gases inside the cylinder raises, which causes expansion of these gases against torque producing mechanism of the gasoline engine. This mechanism is comprised of crankshaft, connecting rod and piston that converts expansion of gases on the piston head to rotational movement of the crankshaft, which is engine output speed. Crankshaft is coupled to transmission unit of vehicle power-train to transmit the rotational motion for desired use.

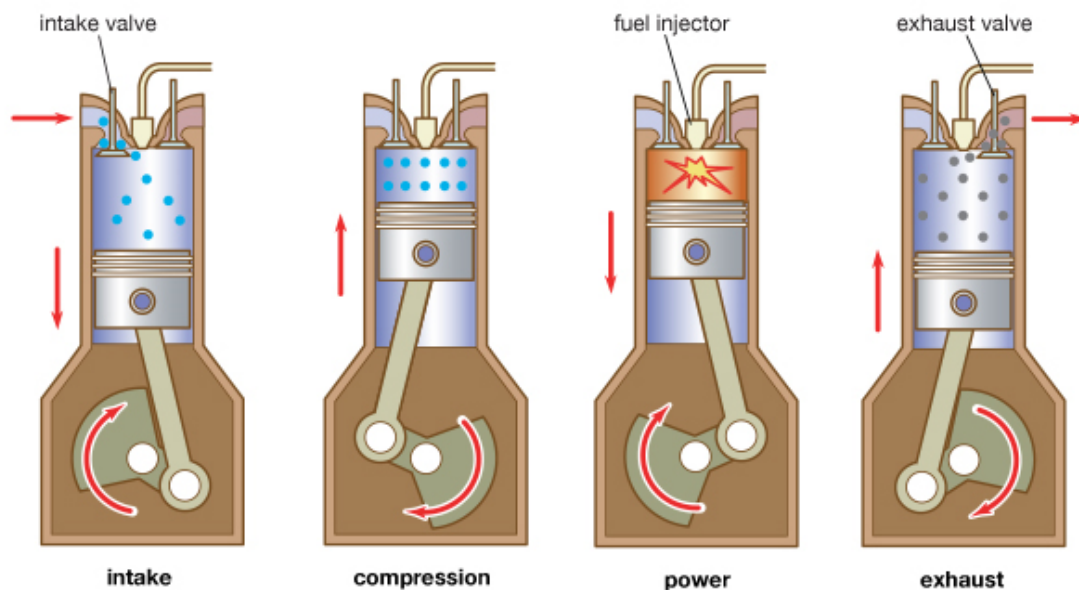


FIGURE 1.2: Phases in the Gasoline Engine

In gasoline engines, spark timing as well as fuel injection are set to acquire useful mechanical work near Top Dead Center (TDC) from chemical energy of the combustion mixture. Pressure inside the engine cylinder increases tremendously due to release of chemical energy and produce net combustion force, which pushes the piston toward Bottom Dead Center (BDC).

1.2 An Overview of Engine Torque Imbalance

Engine torque imbalance is mainly caused due to non-uniform contents of the engine cylinder. Torque generation is not smooth in gasoline engines as consecutive work phases of the combustion cycle produces periodically time-varying torque. Also, discontinuous combustion and geometry of the torque producing mechanism cause torsional vibrations.

Torque imbalance has remained a critical problem since invention of the gasoline engine. It affects the engine performance by reducing drivability, increase in Noise, Vibration, Harshness (NVH) and rise in undesired exhaust emissions. Torque imbalance becomes significant when Air to Fuel Ratio (AFR) changes from stoichiometric value in either a rich or lean direction. Such degradation of combustion process limits maximum AFR that can be used to achieve low fuel consumption and reduced emissions with satisfactory drivability of the vehicle.

Causes of engine torque imbalance includes disparities in fuel injection or air intake path, production error between cylinders and stochastic features of the combustion process. Moreover, fuel injectors could have manufacturing variances and aging due to which variations may occur in the fuel mass that is injected in the engine cylinder. Torque imbalance in gasoline engines could also be caused due to:

- Variations in mechanical design; i.e., stroke length, piston design, gasket, rings size, fuel manifold and camshaft profile condition.
- Degradation of engine components, such as worn rings, leakage in valves, weak action of valve lifters, clogged or leaked fuel injector, spark plug gap wear and faulty ignition coil.
- Malfunction in combustion control such as AFR control, ignition timing, engine cooling, fuel mass injection and its timing.

It is desired to generate balanced torque from engine cylinders as it increases engine reliability and reduce consumption of fuel as well as exhaust emissions. Peak combustion pressure in engine cylinders can be controlled by torque balancing;

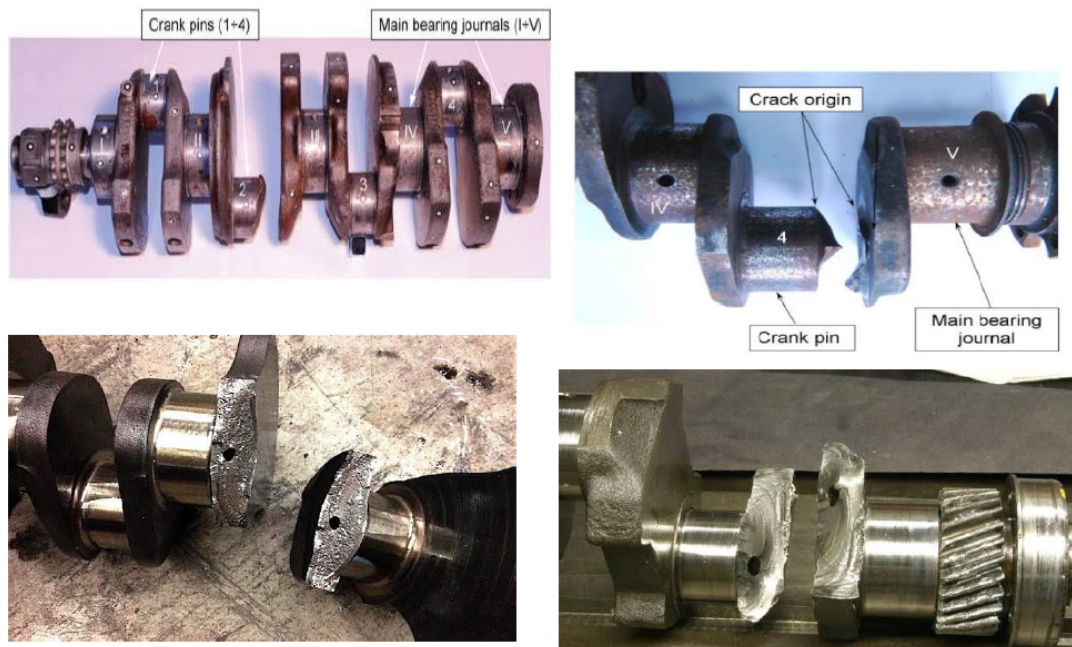


FIGURE 1.3: Crankshaft Failure due to Torque Imbalance

also, it reduces unbalanced crankshaft torsional forces which can lead to crankshaft failure. Few examples of crankshaft failure, as shown in Figure 1.3.

Combustion variations in SI engine are caused by different factors that could be stochastic or deterministic in nature. Initially stochastic characteristics of the combustion phase were investigated to study torque imbalance in gasoline engines [2, 3]. However, it was analyzed that engine performance can also be improved by considering the deterministic nature of combustion variations. Oscillations in engine rotational speed have been usually employed to study various features of the gasoline engine; such as cylinder pressure [4], misfire detection [5] and torque estimation [6]. Engine rotational speed based approaches were grouped as frequency domain and time domain techniques [7]. Frequency domain approaches had used order domain method [8]; whereas different techniques were proposed as time domain approaches [9, 10]. Engine rotational speed based approaches is discussed in detail in Subsection 2.4.2 in Chapter 2.

Engine torque imbalance can be classified as cylinder to cylinder and cyclic torque imbalance. Cyclic combustion variations in gasoline engines were observed and researched since start of the 20th century. Various factors were attributed as

cause of cyclic variations, which ranged from deterministic effects of residual gases to stochastic effects such as turbulent, in-cylinder mixing fluctuations. Cyclic variations have remained critical as combustion instabilities produce undesired emissions, limit lean-fueling levels and Exhaust Gas Recirculation (EGR) [11].

Cyclic variations are produced due to non-repeatability of the combustion process on a cycle resolved basis, resulting in inconsistent output work. In each cycle, combustion force acts on the piston head during power stroke and produce torque at the crankshaft end. It can be said that “*cyclic torque imbalance in an engine cylinder occurs due to difference between work output of combustion cycles, producing inconsistent varying profile of the output torque*”. It is also termed as cyclic torque variations.

Variations in combustion process between consecutive cycles have been considered as direct cause of variance in net piston force (f_n), which manifests itself as imbalance in engine output torque. Minor variations in conditions are incessant part of the combustion process in gasoline engines and do not contribute significantly to cyclic torque imbalance. Major contributors to imbalance in the cyclic torque include variable air intake, disparities in fuel injection and variations in spark duration or energy that alter the combustion conditions significantly, which leads to large variations in engine torque.

1.3 Motivation and Objectives

Due to swift progress in the field of engine technology, research community in automotive industry has always looked forward to develop novel control techniques to improve the engine performance. Increasing environmental awareness and introduction of more strict legislation have led to global demand of reduction in exhaust emissions from road car engines [12]. Introduction of Euro Standards in 1990s have led to intensive research for development of control methodologies for various processes in gasoline engines, such as fuel injection, spark timing, EGR flow, AFR and output speed. Engine control systems were mostly developed by

using map-based solutions along with various manually tuned parameters. Accordingly, functionality dependencies became further complex and made it difficult to analyze the system.

As already mentioned, control functions are growing continuously to abide by the performance objectives. It has remained important to achieve performance objectives and robust control over complete engine life. These performance objectives are often interrelated or conflict with each other. This necessitated development of optimal and high-performance engine control algorithms. Development of model-based control strategies can assist to reduce the number of maps and simplify performance dependencies.

In existing literature, Mean Value Engine Model (MVEM) of gasoline engine was predominately used for diagnosis and control due to its simplicity and control oriented nature. However, lumped parameter approach was followed in MVEM to model different processes and generation of output torque. Due to lumped approach, individual contribution of cylinders could not be observed in MVEM. Also, this model does not depict system dynamics with high fidelity. Few assumptions were made to develop MVEM, including the analogy to use continuously operating volumetric pump to model the torque production subsystem [13].

First Principle Engine Model (FPEM) was proposed to address such modeling limitations of MVEM [14]. In FPEM, assumption of volumetric pump was replaced by torque production subsystem model, that enabled to describe oscillations in engine rotational speed. Also, assumption of considering one bigger cylinder instead of multi-cylinders arrangement is addressed in FPEM [15]. Enhanced computational power of embedded systems has given the opportunity to focus on comprehensive study of torque generation processes in gasoline engines.

It is desired to produce consistent output torque by an engine cylinder, when it is operating under same conditions. Cyclic torque imbalance is generated due to any impediment in it, which causes excessive stresses in engine components and non-smooth output power. As mentioned in [16], FPEM can be employed for various engine diagnosis and control problems. Engine power balancing is one

of the problems that requires uniform torque contribution from engine cylinders. Mitigation of cyclic torque imbalance ensure smooth power contribution by engine cylinders. However, detection of cyclic torque imbalance is essential to develop such control techniques. Also, engine power balancing assist to design more fuel-efficient engine technologies, such as Variable Cylinder Displacement (VCD) and Dynamic Skip Fire (DSF).

Mitigation of cyclic torque imbalance has diverse objectives. It limits torsional vibration in engine crankshaft that is caused due to non-uniform torque contributions from engine cylinders. Secondly, it ensures even distribution of mechanical stresses on components of the engine, especially crankshaft. Reduction in torque imbalance contribute to limit degradation and aging effects in engine components, apart from improving its fuel efficiency. It reduces exhaust emissions and harshness due to roughness of the engine. Even if torque variations are limited and has less influence on engine performance, it is still important to detect irregularity in torque production for prognosis and to avoid eventual failure of the engine. The proposed methodology to attain desired objectives is shown in Figure 1.4. Chapter wise brief overview of the proposed methodology is presented in Section 1.5, whereas it is discussed point by point in next chapters.

1.4 Research Contributions

Main contribution of the research work presented in this dissertation is the development of model based novel unified framework for detection and mitigation of cyclic torque imbalance. As this framework is proposed for nonlinear model of the gasoline engine, thus no limit exist for its operating range. The novel FPEM is employed to estimate net piston force (f_n), which gives a direct measure of the torque generated by the engine cylinder. Proposed estimation technique is validated by using speed dynamics of GT-Power based model of the gasoline engine.

FPEM is transformed to get direct relation between engine states and fuel input, which was not established in the conventionally employed MVEM. Observer based

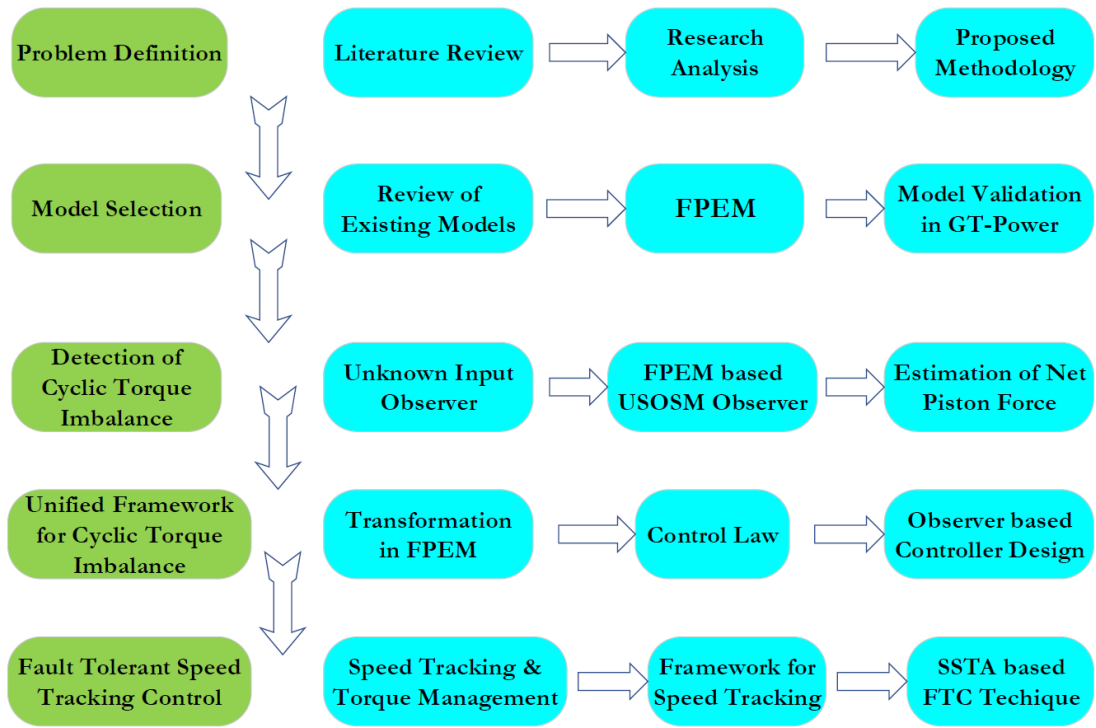


FIGURE 1.4: Proposed Methodology

Fault Tolerant Control (FTC) techniques are proposed to mitigate imbalance in the cyclic torque. Also, robust speed tracking control for engine torque management is proposed, which keeps the output speed at desired set points despite occurrence of the fault in fuel injection subsystem. It also demonstrated significance of the transformation in FPEM for engine diagnosis and control.

Research work presented in this dissertation has following major contributions:

- Development of model based unified framework for detection and mitigation of cyclic torque imbalance.
- Detection of cyclic torque imbalance by estimation of net piston force (f_n), as unknown input to engine speed dynamics.
- Mitigation of cyclic torque imbalance in gasoline engines by observer based FTC techniques.
- Transformation in FPEM to develop the direct relation between engine states and fuel input.
- Validation of torque production subsystem model in FPEM by using speed dynamics of GT-Power based engine model.

- Robust speed tracking control for torque management of gasoline engines, despite occurrence of the fault in fuel injection subsystem.

1.5 Overview of the Dissertation

In this chapter, general essence of the proposed research work is discussed. Chapter 2 and 3 cover background of the research problem. In these chapters, cyclic torque imbalance and gasoline engine models are discussed, respectively. Main contributions of the research work, i.e. detection and mitigation of cyclic torque imbalance are presented in Chapter 4 and 5. Apart from it, robust speed tracking control for engine torque management is described in Chapter 6, followed by conclusion and future research directions in Chapter 7.

Engine torque imbalance is discussed in Chapter 2. Different classes of torque imbalance are briefly discussed along with causes, impact and application of cyclic torque imbalance; followed by three main methodologies to detect and mitigate torque imbalance. A detailed literature review of cyclic torque imbalance as well as its detection and mitigation by using engine rotational speed is presented in this chapter. Both frequency and time domain approaches for engine speed based torque imbalance detection and mitigation are described. Based on the literature review, research analysis is presented to identify the gap and formulate research problem.

In Chapter 3, modeling approaches for gasoline engines are discussed with a focus on MVEM and Cylinder to Cylinder Engine Models (CCEM). Engine crankshaft models are also presented, which were developed to model oscillations in engine rotational speed. Different modeling techniques to incorporate torque production subsystem in IC engine models are reviewed before going through FPEM. Derivation of torque production subsystem model is discussed in detail, along with its integration with model of other engine subsystems to present FPEM. Main attributes of FPEM are also described to highlight its significant features. Model of

torque production subsystem in FPEM is validated by comparing its results with GT-Power based gasoline engine model.

In Chapter 4, FPEM is employed to develop the framework for detection of cyclic torque imbalance. The proposed technique is applied under lab conditions as gasoline engine is operated under steady state conditions. The FPEM based observer is proposed for estimation of net piston force (f_n) from speed dynamics of the gasoline engine. Estimated net piston force (f_n) gives a direct measure of variations in the cyclic torque. Fault in fuel injection subsystem is induced to vary injected fuel mass and generate imbalance in the cyclic torque. Validation of the proposed framework is carried out by using speed dynamics of GT-Power based model of the gasoline engine.

In Chapter 5, two observer based FTC techniques are proposed for mitigation of imbalance in the cyclic torque. In both FTC techniques, the sliding surface is designed to detect torque imbalance and mitigate it by re-configuring the controller. Model of engine speed dynamics in FPEM is transformed to develop direct relationship between engine speed dynamics and Injector Pulse Width (*IPW*). Model based novel unified framework for detection and mitigation of cyclic torque imbalance is accomplished by FPEM based observer and observer based FTC techniques.

In Chapter 6, a framework is proposed to carry out robust speed tracking control for engine torque management. Variations appear in engine speed due to torque imbalance. Desired speed set points are required to be followed by mitigating the fault that cause torque imbalance. As already discussed, one of the research contributions is transformation in FPEM, which is employed to propose robust technique to achieve the desired control objective in the presence of faults in fuel injection subsystem by proposed sliding mode control based technique. Reference data is acquired from a 1300 cc, four-cylinder SI engine test rig for validation of the proposed technique.

In Chapter 7, proposed research work is concluded along with possible future directions.

Chapter 2

Cyclic Torque Imbalance in IC Engines

Cyclic torque imbalance is one of the major problems for gasoline engines that is caused due to variations between combustion cycles. Consecutive combustion cycles are usually not uniform even under consistent conditions. If combustion process does not progress in similar way between two consecutive cycles, then it results in different cylinder pressure curves [17]. Variations in cyclic torque become noteworthy when AFR changes significantly due to different causes, as discussed in subsequent sections. Study of cyclic torque imbalance is essential to meet engine performance requirements. Advantages of mitigating imbalance in the cyclic torque include reduction in engine surge, improvement in fuel efficiency and decrease in exhaust emissions.

With brief introduction of gasoline engines and cyclic torque imbalance in Chapter 1, this chapter begins with detailed discussion on engine balancing in Section 2.1. Groups of engine balancing are discussed in this section; however, main focus is to present engine torque balancing. Classes of torque imbalance are presented in Section 2.2. Cyclic torque imbalance is discussed in detail in Subsection 2.2.2, along with its causes, impact and application. In Section 2.3, three main methodologies, which are used for detection and mitigation of engine torque imbalance

are described. Review of cyclic torque imbalance is presented in Section 2.4, along with detailed discussion on engine rotational speed based approaches to detect and mitigate imbalance in the engine torque. Various frequency and time domain approaches are discussed in this section, followed by research analysis in Section 2.5 and problem statement in Section 2.6.

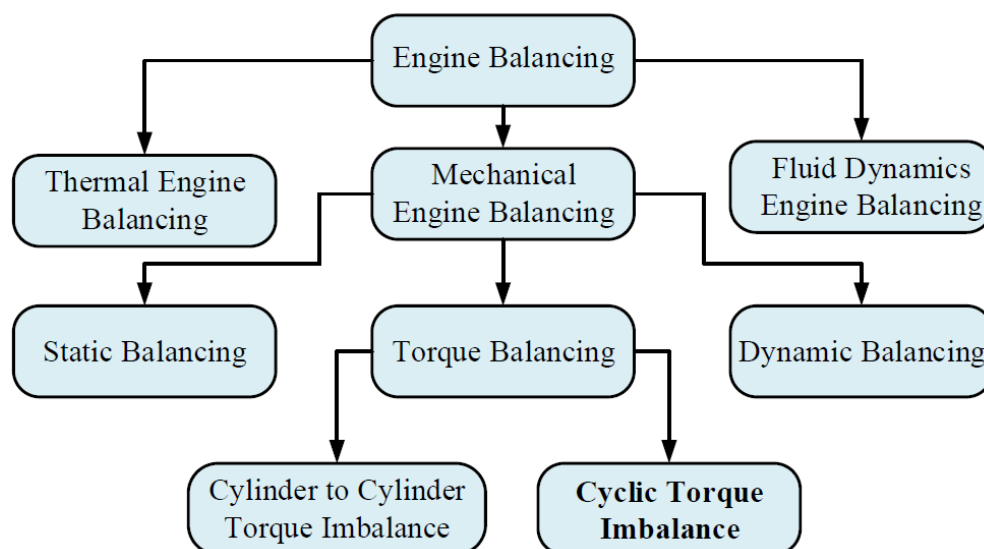


FIGURE 2.1: Groups of Engine Balancing

2.1 Engine Balancing

Engine balancing is critical for IC engines, irrespective of their type. It is discussed in general in this section as engine imbalance could occur in SI as well as CI engines. Numerous factors in design, production, operation, tuning and maintenance can affect balance of the engine. No engine can be perfectly balanced due to different factors but overall balance of the engine can be improved. During engine balancing, key considerations are, balancing of structural and operational elements; performance and durability; output power and efficiency; physical parameters; environmental effects and NVH reduction factors.

Engine balancing is kept in consideration during engine manufacturing. It reduces internal loads and vibrations, which could produce stresses in metal and eventually lead to failure of a component. Generally, balancing a reciprocating engine

is a complex issue as a well-balanced engine for a specific use may exhibit unacceptable level of vibrations in another application due to variation in load and mounting technique. Intermittent energy source in the presence of high number of reciprocating parts, such as piston and connecting rod makes the engine naturally prone to vibrations. As shown in Figure 2.1, engine balancing can be grouped as mechanical [18], fluid dynamics and thermal [19], depending on the factors that affect the engine balance.

2.1.1 Fluid Dynamics Engine Balancing

During working of an IC engine, certain pressures are generated in it along with various forces and torques. Apart from compression pressure inside the cylinder, positive oil pressure as well as negative intake manifold pressure act as source of resistance, which is required to be uniform. If one of the engine cylinders has a restrictive exhaust port, then it periodically increases resistance for every 720 degrees of crankshaft rotation in a four-stroke IC engine. There is kinetic resistance due to air, water, gas and oil that are required to be accelerated during engine operations. Crank throws hit lubrication oil in the oil pan, which acts as a source of vibration. Also, engine components usually do not touch each other and separated by thin oil films. Such oil films oppose shearing forces and could act as vibration source in overheated engine.

2.1.2 Thermal Engine Balancing

Thermal engine balance depicts the equilibrium between energy generated due to combustion in IC engines and flow of energy from engine to the environment [20]. Thermal balancing is critical for durability and strength of the IC engine. It also affects mechanical and fluid dynamics balancing of the engine. In an IC engine, temperature gradient exists between cylinders on radiator side and on flywheel side, especially in air-cooled engines. Such thermal imbalance generates variation in manufacturing tolerances and cause sliding friction in engine cylinders.

2.1.3 Mechanical Engine Balancing

Mechanical engine balancing can be sub-grouped into following classes, depending on the factors that cause the imbalance [18].

2.1.3.1 Static Balancing

Balancing of the weight and center of gravity of moving parts in IC engines is termed as “*Static Balancing*”. It requires that all reciprocating masses such as piston, connecting rod as well as rotating masses such as crank web weight, flywheel have uniformity in weight and center of gravity.

2.1.3.2 Dynamic Balancing

It refers to balancing of the forces that act on different components of the engine. In an IC engine, piston mass accelerates and decelerates, which resists smooth rotation of the crankshaft. Also, big end of the connecting rod rotates as well as reciprocate during engine operation. “*Phase balance*” as well as “*Plane balance*” is required for reciprocating and rotating masses of the engine. The ‘*Phase*’ refers to crankshaft rotation timings, whereas ‘*Plane*’ refers to location of crankshaft rotation axis. Crank-throws, that are farthest from flywheel side of the crankshaft also display torsional deflection that necessitates “*Torsional balancing*”. Static mass of the engine also plays an important role in dynamic balancing. Vibrations are also caused due to small engine movements and determined by engine weight distribution, center of gravity and rigidity.

2.1.3.3 Torque Balancing

Torque balancing has remained an important research area of the engine control. In an IC engine, it is essential to attain uniform torque generation from engine cylinders. However, small measurable fluctuations could exist in the engine torque. In a four-stroke IC engine, generation of the torque is not smooth as combustion

in a cylinder occurs after every 720 degrees of the crankshaft rotation. Also, combustion force generated in the cylinder applies torque on the crankshaft at connecting rod location, which is at different distance from power take off point in inline IC engines. Torque balancing problem is comparable to estimation of the torque and detection of misfire in IC engines.

Effects of engine torque imbalance are severe in low load and speed conditions than high load and speed conditions [21]. Torque balancing ensures that peak combustion pressure is within the specified limits and distribute the load across engine cylinders. It can reduce fuel consumption, minimize unbalanced crankshaft torsional forces and reduce excessive stress on engine components due to unbalanced pressures as well as detonation. Thus, it increases engine reliability, control combustion temperature and reduces exhaust emissions.

2.2 Classes of Engine Torque Imbalance

Torque imbalance in IC engines can be further classified as follows [22]:

1. Cylinder to cylinder torque imbalance
2. Cyclic torque imbalance

2.2.1 Cylinder to Cylinder Torque Imbalance

Cylinder to cylinder torque imbalance refers to the condition when “*one or more than one engine cylinder contribute unequal torque compared to other cylinders of the engine during each combustion cycle*”.

There are different causes of cylinder to cylinder torque imbalance in IC engines. Non-identical torque could be produced by engine cylinders as fuel injectors may have part to part variability or difference in air charge may be caused due to asymmetries in the air intake subsystem. For each cylinder, intake and exhaust runners may have different physical characteristics, which can cause variations in

air dynamics. It also affects distribution of burned recirculated gases, despite presence of EGR subsystem. Distinct combustion profiles may be caused in cylinders due to variations in the combustion mixture. Also, variance in combustion and air induction could be caused by soot deposits on valves as well as in the cylinder [23]. Difference between engine cylinders in terms of fuel mass, injection timing, valve timing, deviations in ignition as well as fuel injection subsystems can be caused during manufacturing of the components as well as due to prolong usage.

Cylinder to cylinder torque imbalance cause various undesired effects, out of which few are perceptible by the driver. Human ear can detect cylinder to cylinder torque imbalance at low engine speed. Cylinder to cylinder torque imbalance could raise speed fluctuations, increase torsional vibrations as well as engine noise. Different approaches were proposed to study cylinder to cylinder torque imbalance, which can be broadly grouped as estimation of cylinder wise output power or relative torque contribution of engine cylinders.

2.2.2 Cyclic Torque Imbalance

Although cyclic torque imbalance has been briefly discussed in Section 1.2, a detailed description of cyclic torque imbalance is presented in this section. In an engine cylinder, cyclic torque imbalance can be identified by monitoring variations in net piston force (f_n) from one combustion cycle to another. Due to cyclic torque imbalance, variations appear in net piston force (f_n) around averaged mean value, instead of similar time evolution of the net force generated on piston head. Thus, torque produced by each combustion cycle differs from the mean torque that is design target of the engine; as it is desired to achieve consistent torque from a cylinder for emission compliant operations. Schematic diagram of the engine cylinder is shown in Figure 2.2 to illustrate generation of net piston force.

The term cyclic torque imbalance covers different types of variations in engine cylinder, depending upon the following [24, 25]:

1. Variations of gaseous mixture motion in engine cylinder during combustion.

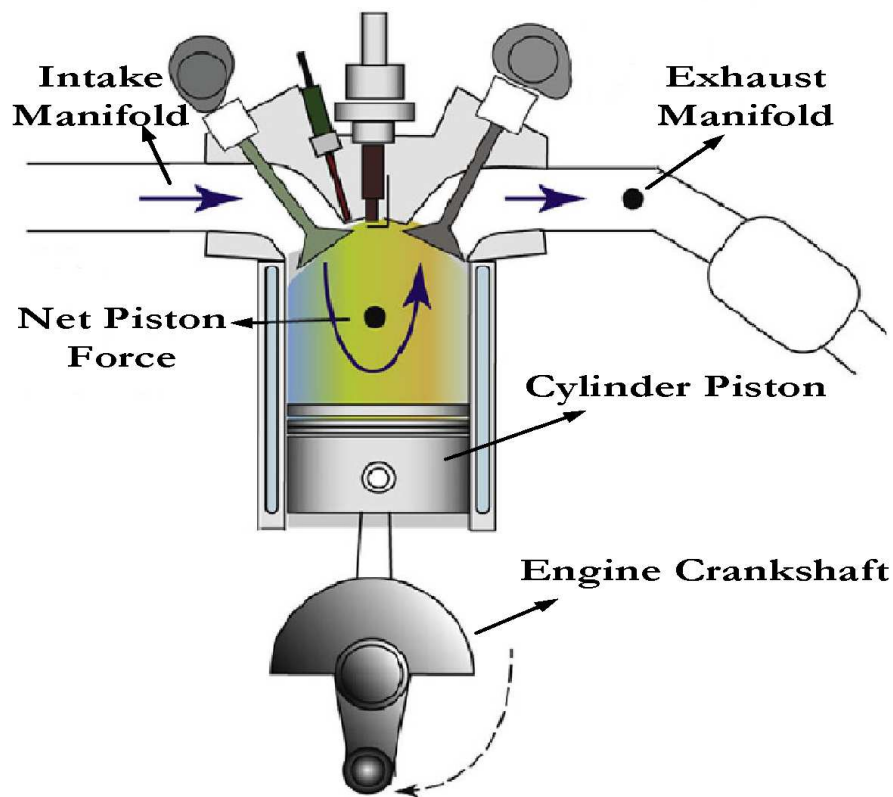


FIGURE 2.2: Schematic Diagram of the Engine Cylinder

2. Variations in mass of air, fuel mass and recirculated or residual exhaust gases in the cylinder.
3. Variations in uniformity of mixture composition, mainly in spark plug neighborhood. It is also related with imperfect mixing of air as well as fuel and recirculated exhaust gases.
4. Variations in spark duration and energy, spark discharge features such as initial flame kernel position and breakdown energy.

Causes of cyclic torque imbalance have been grouped as deterministic or stochastic one. Variations in the mass of air, fuel or in spark duration and energy are deterministic causes of cyclic torque imbalance. Such variations in air, fuel or spark can be exactly expressed using mathematical models. Whereas, mixture turbulence during combustion and uniformity of mixture composition especially near spark plug are stochastic phenomenon that cause cyclic torque imbalance. Such variations in combustion process cannot be exactly expressed by mathematical model. Thus, compared to stochastic factors, deterministic causes of cyclic torque

imbalance can be employed to develop model-based framework for detection and mitigation of cyclic torque imbalance.

2.2.2.1 Causes of Cyclic Torque Imbalance

As already mentioned, cyclic torque imbalance is an undesirable phenomenon in SI engines. It is caused due to variations of in-cylinder conditions for consecutive combustion cycles at nominally identical operating conditions. Few of the causes of cyclic torque imbalance include faults in fuel injection or ignition subsystems and loss of compression due to cylinder air or fuel leakage. Manufacturing tolerances, aging of engine components and external disturbances also cause cyclic torque imbalance. Substantial dispersion can be observed in AFR due to such variations, inducing partial or total loss of indicated torque.

Turbulence in combustion mixture is another major cause of cyclic torque imbalance. Turbulence can be divided into small-scale and large-scale motions. Small-scale turbulence affects the initial flame kernel whereas large scale turbulence affects the flame propagation. Turbulence is influenced by different engine parameters; however, mainly it depends on output speed. Mixture turbulence is increased due to increase in engine speed, which causes high variations in flame speed and result in high combustion variations [26]. Turbulence represent stochastic aspect of cyclic torque variations, whereas deterministic aspects such as residual gas cause oscillations in dilute combustion. In [27], it was proposed that high residual gas quantity and decreased combustion pressure in a cycle is caused due to high combustion pressure of the preceding cycle. Composition of the mixture can also effects burn rate, as fast burn cycles are produced due to locally rich mixtures around spark plug, whereas ignition may not occur if mixture is too lean [28].

As mentioned above, one of the main causes of cyclic torque imbalance is fault in the fuel injection subsystem. Higher peak pressure, increase in burn rate and minimum variations in heat release may occur due to slightly rich fuel mixture [29]. There can be difference between demanded and actual amount of the injected fuel due to different physical attributes of the fuel injector. It includes clogged nozzle of

the injector, fuel leakage from injector nozzle, variable function of solenoid valve, fluctuations in fuel injection pressure and aging effects. Such faults may deteriorate precision requirements of fuel injection control, which can cause variance between average torque contribution of combustion cycles.

2.2.2.2 Impact of Cyclic Torque Imbalance

Cyclic torque imbalance has numerous effects on working of the gasoline engine and acts as a limiting factor to enhance the engine performance. Variations in cyclic torque can affect fuel economy [30] and increase undesired exhaust emissions, especially during idling condition. In addition to environmental effects, cyclic torque imbalance also causes degradation of ride quality, deteriorate vehicle drivability by causing fluctuations in output speed, fast aging of three way catalytic converter and vibrations in the driveline [31].

Cyclic torque imbalance also causes wear and degradation of engine parts due to excessive periodic loading of the engine components. In an unbalanced engine, torque output is lower than the balanced engine, which causes loss of maximum available torque. Cyclic torque imbalance also leads to loss of thermal efficiency, reduced power contribution of the engine cylinder, increase in engine harshness and rise in indicated torque fluctuations at a given operating point [32].

2.2.2.3 Cyclic Torque Imbalance and Variable Cylinder Displacement Engines

Reduction in cyclic torque imbalance can increase the engine output power up to 10% for same fuel consumption [33]. In 2012, VCD technology was assessed as one of the future technologies in automotive rule-making [34]. Fuel economy can be enhanced up to 18% by DSF, which is one of the recent VCD techniques [35]. Analysis of cyclic torque variations is significant to understand cylinder-wise contributions in engine output torque. Thus, it has a crucial role to mitigate NVH effects for implementation of VCD strategies, such as DSF [36].

DSF is the extension of VCD, which was developed by Tula Technology in collaboration with Delphi Automotive in recent years. In VCD, fixed number of engine cylinders are deactivated, depending on requirement of torque generation. DSF is considered as software enabled variable displacement of the engine [37]. Basic concept of DSF is based on torque production management, shown in Figure 2.3. Instead of throttle, desired brake torque is obtained by selective torque production as response to the driver command.

In DSF, selective firing or skipping of the fuel is carried out in all engine cylinders; according to the requirement of torque generation. Each firing cylinder performance can be optimized for better thermal efficiency, which is affected by constraints such as AFR, peak cylinder pressure and combustion temperature [37]. Cylinder firing or skipping event determine the actuation of intake and exhaust valves, fuel injection and spark ignition.

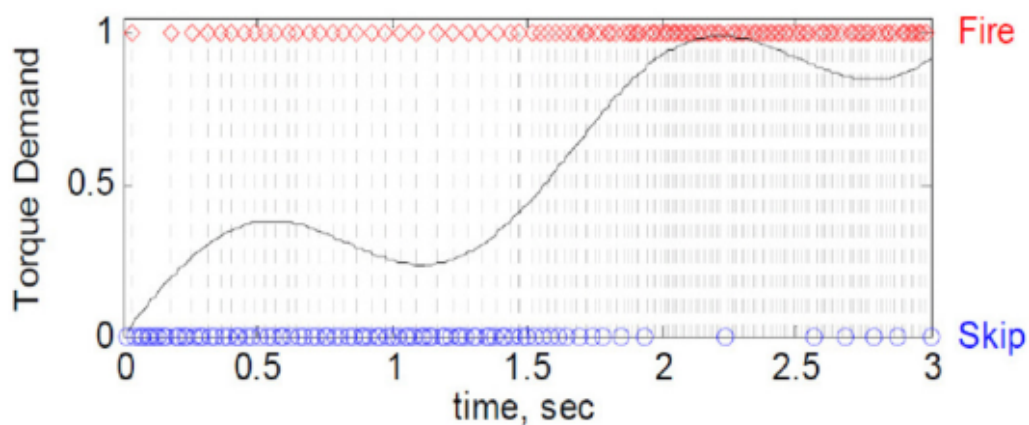


FIGURE 2.3: Basic Concept of DSF [37]

In DSF, firing density decisions are based on fuel economy, which can induce undesirable NVH characteristics. Each firing event in engine cylinder produces torque, that exerts an acceleration on the crankshaft. Vibrations are caused by such acceleration; whose frequency is function of the firing pattern as well as density [36]. Mitigation of such undesirable vibrations has remained the main objective in DSF. Detection of cyclic torque imbalance can assist to realize torque contribution of the engine cylinder and reduction of NVH in DSF.

2.3 Methodologies for Detection and Mitigation of Engine Torque Imbalance

First essential step to mitigate engine torque imbalance is detection of variations in the torque. This information is used to impart corrections to overcome the imbalance in torque contributions. As shown in Figure 2.4, three methodologies are predominantly used for torque imbalance detection and mitigation, that are based on following variables [38]:

1. In-cylinder pressure.
2. Exhaust oxygen concentration.
3. Engine rotational speed.

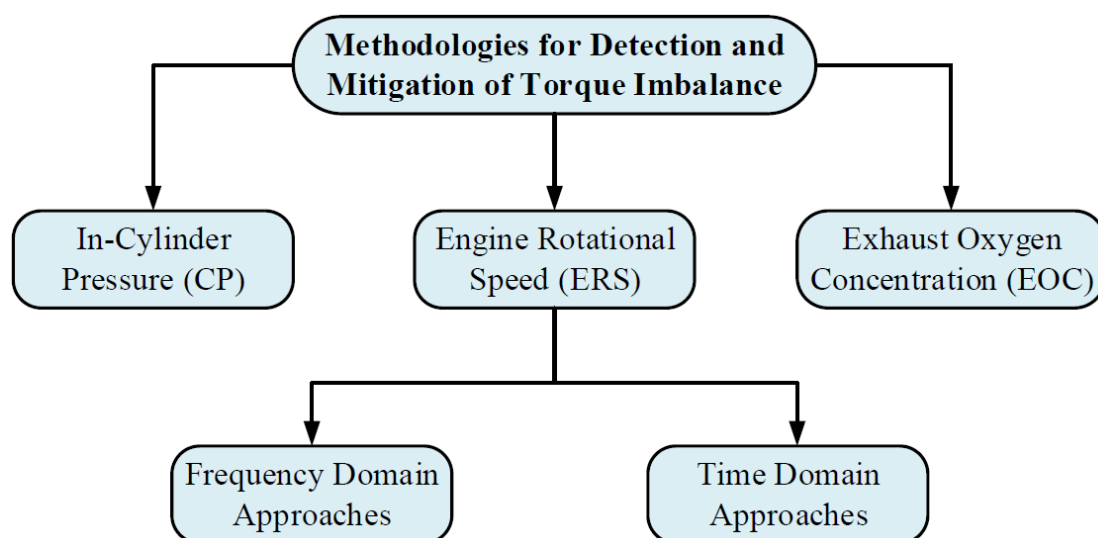


FIGURE 2.4: Methodologies for Torque Imbalance Detection and Mitigation

Exhaust oxygen concentration based techniques were focused on estimation of imbalance in AFR, whereas engine rotational speed and in-cylinder pressure based techniques had addressed engine torque imbalance by using fuel as control variable. Although, torque imbalance can be caused due to variations in air intake or fuel injection path; however, injected fuel mass is regulated both cases to mitigate imbalance in the engine torque.

The above mentioned three methodologies are discussed briefly in following sub-sections:

2.3.1 In-Cylinder Pressure

Direct control of combustion process in engine cylinder can be attained by in-cylinder pressure sensor. Error in both fuel mass injection and timing can be found by using cylinder pressure sensor data, as most of the combustion controllers were based on cylinder pressure and designed for injection timing regulation. Due to combustion requirements, this method is mostly used in alternative combustion mode engines [39], like Homogeneous Compression Charge Ignition (HCCI) for tightly regulated combustion process, which evades unstable combustion; although it can also be applied in conventional combustion engines [40]. Also, heat release rate and cylinder pressure can be computed from cylinder pressure measurements.

Keeping cost of cylinder pressure sensor in consideration along with their vulnerability to the noise, cylinder pressure-based techniques for combustion control and cylinder balancing is yet to be adopted by automotive industry for use in commercial cars.

2.3.2 Exhaust Oxygen Concentration

Engine torque imbalance can be detected from instantaneous fluctuations in the measured exhaust oxygen concentration by its comparison with cycle average value; as long as contribution of each cylinder in exhaust oxygen can be estimated. Model-based techniques were not extensively used for exhaust oxygen concentration-based torque imbalance detection and control; though several models-based techniques were used for pre-catalyst and post-catalyst AFR control.

In the existing literature, some of the torque imbalance control techniques were based on input-output relationship of exhaust oxygen concentration. In these techniques, measurements of the oxygen sensor were denoted as weighted summation of oxygen concentration of the combustion mixture in each cylinder [41]. Whereas, weighted factor in summation was used as ratio between total mass of the combustion gases and mass of combustion gases from the engine cylinder that passes the oxygen sensor in a specified time window. In [41], control of individual cylinder

AFR was proposed by using multi-rate sampling technique. Individual cylinder AFR was estimated by using input observability concept, that was based on the proposed model. Decoupled Proportional Integral (PI) compensator was designed from estimated individual cylinder AFR to reduce torque variations.

Another technique for individual cylinder AFR estimation was discussed in [42], in which a single sensor was placed downstream the turbine. In this technique, injected fuel quantity of engine cylinders was controlled by PI compensator to vary AFR balance of the cylinder. In [43], cyclic variations of Residual Gas Fraction (RGF) for AFR control of gasoline engines were studied. These cyclic variations were modeled as Markov process, which was motivated by the observation that current cycle combustion state is influenced by previous cycle combustion state and RGF. Based on this model, a stochastic optimal control technique was proposed.

Requirement of additional sensors to estimate oxygen concentration from exhaust gases of cylinders and high computational requirements have made the online implementation of this methodology a challenging task.

2.3.3 Engine Rotational Speed

Engine rotational speed measurements have been extensively used for estimation of operational conditions in the engine cylinder, torque estimation and detection of engine misfire. Engine speed can be measured from crankshaft position sensor that is installed in every present day commercial vehicle engine. Thus, no extra sensor is required for implementation of this methodology.

Compared to other two methodologies, engine rotational speed based methodology was found more appropriate for detection and mitigation of engine torque imbalance as it does not require additional sensors and have relatively less computational requirements. However, a unified framework for torque imbalance detection and mitigation was rare in all three methodologies.

A detailed review of engine rotational speed based techniques is presented in next section.

2.4 Existing Approaches for Detection and Mitigation of Engine Torque Imbalance

2.4.1 Detection of Imbalance in Cyclic Torque

Cyclic torque imbalance has remained an active area of study since initial times of the gasoline engine. However, it was not considered a concern until measurement of consecutive engine cycles was made possible. Extensive work can be found in existing literature to study cyclic torque variations as it is considered an undesired phenomenon that affects performance of the gasoline engine. Combustion in SI engine has variations due to both deterministic and stochastic factors. Most of the earlier research work on cyclic torque variations was focused on stochastic aspects [2, 3]. Nevertheless, these variations also displayed a high degree of low-dimensional deterministic structure [44], which implied predictability and real-time control of cyclic torque imbalance [45].

For gasoline engines, both stochastic and deterministic factors that affect cyclic variations were investigated to study their impact on engine performance. In [46], causes of cyclic torque variations were classified as effects of previous or same cycle. *Previous cycle effects* refer to variations in the residual gas, whereas *same cycle effects* represent combustion mixtures variations in the engine cylinder. RGF was assumed as a deterministic parameter of cyclic torque variations, as combustion and emissions of current cycle are affected by residual gases of the previous cycle.

Different techniques were proposed to study the impact of various parameters on cyclic torque imbalance, such as effect of charge dilution and combustion position were discussed in [47]. A database of measurements from a set of test engines was developed by applying different operational approaches. Cyclic variations at full load, knock limit and due to dilution approaches, such as lean operation and internal EGR were investigated. Effects of residual gas feedback were also discussed in this work. Correlations between burn rate, knock and cyclic variations were investigated experimentally in [48]. It was proposed that cyclic variations are

linearly correlated with burn rate and relative AFR. Also, raise in cyclic variations could increase tendency to knock due to nonlinear relationship between Indicated Mean Effective Pressure (IMEP) and peak pressure.

In [49], simulation model was proposed to study cyclic torque variations in combustion phase. For different operating points, cylinder pressure traces of 300 cycles were analyzed to observe high and low cyclic torque variations. A quasi dimensional ignition model was derived and combined with combustion model. Growth of early flame kernel that included modeling of electric spark phenomenon, spark plug geometry, heat transfer, interaction of flame kernel with turbulence and in-cylinder flow near spark plug were studied. At different ignition timings, effects of cyclic variations in combustion were represented by proposed model through statistical analysis of normalized heat release rate, IMEP and compared with the experimental data.

A hybrid model for gasoline engines was presented in [50], as both event-based cyclic state transitions and continuous-time dynamic behavior of the engine were studied. It included transition model of residual gas mass that is discrete-time event, dynamics of actuator response and air intake path, which are continuous-time events. Cyclic states were estimated in real time by using extended Kalman filter, whereas combustion process parameters such as IMEP and combustion phasing were modeled by using data-driven method. In [51], effects of RGF and AFR on combustion duration and efficiency were studied by simulating the deterministic aspects of cyclic variations on cylinder pressure, heat release and IMEP.

In [52], standard deviation of mass fraction burn rate was proposed as a new parameter for analysis of cyclic torque variations in SI engines. Effects of engine speed and air to fuel equivalence ratio on cyclic torque variations were studied. An estimator was proposed, that was based on mass burn rate and its deviations to describe cyclic torque variations. Mass burn rate for each combustion cycle was acquired from measured data of the combustion pressure for each engine speed and air to fuel equivalence ratio. For combustion diagnosis, optimal value of various parameters was obtained by applying a genetic algorithm-based technique.

In [53], effects of EGR, boost pressure and compression ratio on cyclic variations in gasoline engines were discussed. It was proposed that cyclic variations increased with increase of EGR ratio for lower laminar flame speed. However, relatively low cyclic variations were observed due to combination of appropriate boost pressure or compression ratio with EGR. Cyclic variations in a turbocharged gasoline engine were analyzed at different operating conditions in [54]. Both numerical and experimental analysis were carried out at different output speeds and AFR values. A spark timing sweep was executed for each operating condition, which moved from knock free to knock limited operation. Cyclic variations were statistically characterized in term of IMEP and maximum in-cylinder pressure. A complete 1-D model of the gasoline engine was developed in GT-Power to simulate cyclic variations in term of Gaussian distributed stretching of predicted burning rate to obtain numerical pressure cycle. It had statistical distribution of in-cylinder pressure and matched with experimental results.

In [55], combustion variations were studied in the gasoline engine by placing analyzer in exhaust manifold to study cycle resolved emissions from one of the cylinders. A piezoelectric transducer was integrated with spark plug to measure the in-cylinder pressure. Effect of engine operating parameters, which included ignition timing, engine speed, air to fuel equivalence ratio and load torque on combustion as well as emission variations were analyzed. It was suggested that impact on combustion variations was caused due to variance in mixture stoichiometry. Lower coefficient of variations in IMEP and Nitric Oxide (NO) emissions were observed due to rich composition of cyclic mixture. Mean value of Carbon Dioxide (CO_2) emissions was affected by stoichiometry, whereas lambda fluctuations affected coefficient of variations in CO_2 . Also, ignition timings effected the combustion and NO emissions.

It was concluded by review of different techniques in existing literature that cyclic torque variations effect a wide range of engine parameters, due to which conspicuous changes can be observed in engine performance. Both stochastic as well as deterministic factors were investigated in the past to analyze impact of these factors on cyclic torque imbalance. Deterministic factors can be influenced by

engine control techniques to reduce imbalance in the cyclic torque. Research work presented in this dissertation is focused to study deterministic factors to develop model based unified framework for detection and mitigation of cyclic torque imbalance.

2.4.2 Engine Rotational Speed based Approaches

Oscillations in engine rotational speed are influenced by combustion forces that are generated in engine cylinders. These oscillations describe the contribution of each cylinder in total output torque of the engine, which can be measured by crankshaft position sensor [8].

Oscillations in engine rotational speed were used for various engine diagnostic and control techniques, such as torque estimation [6, 56] and misfire detection [5, 57]. Apart from estimation of indicated torque and misfire detection, these oscillations were also used for fault diagnosis [58, 59], in-cylinder pressure estimation [4, 60], parameter estimation [61, 62] and cylinder balancing [23, 63]. Frequency as well as time domain approaches have been applied to detect and control torque imbalance, using engine rotational speed oscillations. These approaches are discussed in detail in following subsections:

2.4.2.1 Frequency Domain Approaches

Most of the proposed techniques had used ‘order domain method’ in frequency domain approaches [8]. This approach is based on lowest harmonic order information of output speed measurements. Based on this information, magnitude and phase plots of 0.5, 1 and 1.5 harmonics were drawn by taking Fast Fourier Transform (FFT) of engine rotational speed.

Changes in amplitude of order components of instantaneous speed waveform were examined in [8]. Engine rotational speed was measured from the experimental setup of two IC engines and correlated indicated torque with lowest harmonic

order amplitude of the engine rotational speed spectra. Torque imbalance was identified from phase plot of engine rotational speed oscillations spectrum by analyzing lowest order components.

In [64], Frequency Response Function (FRF) was used to estimate cyclic cylinder pressure, load torque and indicated torque by measuring first five harmonics of engine rotational speed oscillations. Multi-layer neural network was applied to map FRF as function of Discrete Fourier transform (DFT) of manifold pressure, engine speed and mean speed. FRF was computed at different output speeds and load torque. These FRF were mapped over entire operating range of the test engine through multi-layer neural network, which provided FRF between cylinder pressure and engine speed oscillations. Cylinder pressure was estimated by DFT and FRF of the engine speed and converted to crank domain by inverse DFT. Also, an indirect method to estimate cyclic values of IMEP and peak pressure from engine speed oscillations was presented in [65]. It was transformed to frequency domain by applying DFT and used as input to multi-layer perceptron. Peak pressure and IMEP were proposed as indicators of cyclic variations in the cylinder and it was suggested that change in burning phase could cause variations in peak pressure. The 10% deviation in IMEP from nominal value was considered as allowable limit of Coefficient of Variations (COV) in cyclic torque, that can cause problem in drivability of the vehicle.

In [23], detection and control of torque imbalance was discussed in direct injection engines. Cylinder pressure and indicated torque were estimated by using mass and energy balance to model properties of in-cylinder gas, apart from turbocharger and manifold dynamics. Proposed control algorithm provided fuel mass correction command for fuel injector to balance the engine torque. However, it did not consider the actual fuel mass that was injected in the cylinder. Three different methods were proposed for cylinder balancing. These techniques were based on estimated crankshaft acceleration, measurements of cylinder pressure and exhaust manifold pressure measurements. In first method, crankshaft acceleration was used to detect torque imbalance in the cylinder by selecting a crank angle window. In second method, in-cylinder pressure was measured to develop the

control methodology for mitigation of torque imbalance. Cycle-average cylinder torque was calculated by using in-cylinder pressure sensor and crank position. A simple integral control technique was used for generation of fuel correction from imbalance indicator. In third method, use of high-resolution sensor was discussed for exhaust manifold pressure to inject fuel in the engine cylinder without creating torque imbalance. Symmetric exhaust manifold configuration was assumed and injected fuel mass was balanced by equalizing pulses of the exhaust manifold pressure.

In [66], control technique to reduce torque variations by processing of engine rotational speed was presented. Proposed technique was based on PI controller, in which variations level index between peak and valley values of the oscillations in engine speed were used as feedback variable. In each cycle, variations index from the cylinder was extracted by comparison of acceleration characteristics of the oscillations. Peak and valley value of engine rotational speed were used to estimate acceleration capability of the cylinder by taking difference of these values. The estimated acceleration capability was used as index of torque variations. Based on detection of variations level, injection of fuel in engine cylinder was regulated by control algorithm. Excitation torque phase diagram in low frequencies of order 0.5, 1 and 1.5 were plotted. It was suggested that low order torsional vibrations were developed due to imbalance of lower order torque of the cylinder, which was caused due to combustion non-uniformity. This work had few limitations, which included improvement of accurate acquisition of engine speed and data processing for efficient control strategy. Secondly, suggested control technique tends to be inefficient in case of small torque variations. Thus, a precision bound existed for the proposed technique.

In [63], cylinder balancing problem was addressed by adjusting fuel injection to suppress variations in the engine torque. This algorithm used engine speed measurements to draw phase angle diagrams. Also, relation between cylinder firing order with phase and amplitude of torque frequencies was developed by defining a complex valued torque order component. In this work, torque balancing problem was framed to minimize the cost function of torque order components by changing

fuel injection duration for the cylinder that generated imbalanced torque. Engine speed measurements were used for reconstruction of torque order components. A model was proposed to relate components of the torque order with fuel injection duration.

Problem of reducing the torsional vibrations in IC engines was also discussed in [67]. Control strategy was presented to regulate fuel injection for balancing the torque contributions from engine cylinders. Torsional vibrations in the engine were determined from output speed to estimate components of the torque. A model was proposed to develop the relation between engine firing order and torque oscillations. This relationship was used for fuel injection control to reduce engine torsional vibrations. Non-uniform behavior of torque contributions by engine cylinder was estimated from analysis of phase angle diagram, which was developed from lowest deflection orders.

Decrease in engine torsional vibrations was treated as an optimization problem in [68]. Online minimization of the cost function was proposed, which was based on frequencies of engine speed vibrations and exhaust gas temperature deviations. Proportional torque contribution of the cylinder was observed from superimposed indicated torque components, which were applied to the crankshaft. Torque contribution of the engine cylinder was obtained by observing variations in kinetic energy of the crankshaft and correlating these variations with engine firing order. Torque balancing method was generalized by phase angle diagram analysis to carryout adjustment of torque contributions by the engine cylinder. An iterative procedure was proposed to minimize amplitude of torsional vibrations by varying quantity of the injected fuel.

2.4.2.2 Time Domain Approaches

Various research efforts were carried out to detect and mitigate engine torque imbalance by applying time domain approaches. In [7], a convergent time domain method was proposed for power balancing and its results were analyzed to study effects of flexible crankshaft on torsional vibration frequencies. In [9], a method

for cylinder balancing control was discussed that was based on torque reconstruction by using state space model of dual mass flywheel. It was suggested to use reconstructed torque, instead of engine speed dynamics to detect as well correct the torque imbalance.

In [10], a hybrid technique to detect torque imbalance in gasoline engines was presented by using dynamic signal measurements, which were coupled with gas dynamics and thermodynamic processes. Instead of fuel injection, this study was focused on air intake path to control imbalance in the engine torque. It was proposed that intake average pressure in low to medium speed range could influence the torque imbalance of excess air coefficient. However, in high load and high speed, RGF and exhaust pressure are main influencing factors. Also, variations in IMEP are caused by combined effects of RGF and non-uniform excess air coefficient. In this work, fuel injection in the cylinder was assumed uniform; whereas, online implementation of the proposed technique required additional sensors in air path.

In [69], an algorithm was proposed that was comprised of IMEP estimation model and model reference adaptive control technique. Based on measurement of pressure in a single cylinder and crankshaft speed, IMEP of all cylinders was estimated. Indicated torque from the cylinder was represented by a relationship between IMEP and engine speed. Estimated IMEP was used for torque control by applying model reference adaptive control technique. However, the proposed control technique required high cost in-cylinder pressure sensor. A similar approach was discussed to estimate combustion features of each cylinder and instantaneous torque from cylinder pressure and speed of the engine in [70].

In [71], neural network based technique was applied to propose the relationship between cylinder pressure parameters and engine speed. Non-intrusive estimation of cylinder pressure and evaluation of combustion quality were carried out in the proposed technique. Another approach for cylinder to cylinder and cyclic in-cylinder pressure reconstruction was presented in [72]. Linear correlation between engine

rotational speed and in-cylinder pressure was used to develop the proposed technique. Such linear correlation was characterized by FRF. Estimation of indicated torque was also carried out by using the reconstructed in-cylinder pressure.

In [73], estimation of pressure traces of individual cylinders was proposed by applying adaptive sliding mode observer, which was derived analytically. In [60], cylinder pressure reconstruction was carried out by employing crank kinematics and a recurrent nonlinear auto-regressive neural network with exogenous input. The proposed adaptive gradient descent technique was tuned by using the measured crank kinematics and validated by test engine data.

Apart from above mentioned techniques, which were based on engine speed oscillations, few other approaches were also proposed to study imbalance in the engine torque. In [74], torque variations in a dual fuel engine were analyzed to get insight of the combustion modes that have influenced port-injection strategy along with late intake valve closing. It was proposed that simultaneous use of late intake valve closing and dual fuel combustion can lead to uneven distribution of fuel in cylinders, which could affect overall engine performance and efficiency. Main parameters that can affect distribution of fuel were discussed as well as trends were identified between operating conditions and fuel flow. However, a control strategy was not proposed to mitigate torque imbalance due to non-uniform fuel distribution.

In [75], a model was proposed to estimate oxygen mass fraction in the engine cylinder. This experimental study highlighted the relationship between mass fraction of in-cylinder oxygen and ignition delay; as non-uniform trapped mass was suggested as another cause of torque imbalance. In-cylinder oxygen concentration was used to predict combustion characteristics and develop a control technique to reduce engine torque imbalance. It was proposed that IC engines with advanced combustion modes have variations in cylinder contents, that are generated by recirculation of exhaust gases in intake manifold. Accurate information of cylinder composition was considered important to reduce torque imbalance and improve thermal efficiency of the engine. Relationship between mass fraction of oxygen,

ignition delay, pressure and temperature during ignition delay was developed from measurement of cylinder emissions to estimate pre-combustion concentration of the oxygen in engine cylinder.

In [76], two methods were proposed to detect imbalance in the engine torque, which were based on instantaneous turbocharger speed signal. Contribution of engine cylinders was considered by analyzing the turbocharger speed signal. In first case, integral of the speed signal was analyzed, whereas in second case derivative of turbocharger speed was studied. In [77], control technique for cylinder balancing of gasoline HCCI engine was discussed. Based on air mass flow rate and AFR, width of the injector fuel pulse was adjusted in this technique. An optimal spark timing and combustion phasing control technique was also proposed in this work.

2.5 Research Analysis

Existing literature has been extensively reviewed to study torque imbalance in IC engines. Three main methodologies are discussed to detect and mitigate engine torque imbalance in Section 2.3. In-cylinder pressure based approaches require high cost sensors to measure the cylinder pressure, which are also vulnerable to signal noise. Thus, this approach has not been generally adopted by automotive industry for commercial road cars. Exhaust oxygen concentration-based approaches lack full model-based techniques. Furthermore, additional sensors are also required to monitor individual cylinder contributions in overall exhaust emissions.

Compared to these two approaches, engine rotational speed based techniques can be implemented in real time. Engine output speed can be measured by using crankshaft position sensor, installed on engine flywheel. Thus, no additional equipment is required to implement such approach. In the existing literature, many estimation and control techniques were proposed that are based on engine speed oscillations to estimate indicated torque, misfire detection, fault diagnosis and estimation of in-cylinder pressure as well as engine parameter. Torque imbalance was analyzed by employing the estimated indicated torque or cylinder pressure.

Torque imbalance detection and mitigation techniques by using engine speed oscillations are grouped as frequency domain and time domain approaches. A comparison between these two approaches was discussed in [7]. In frequency domain approaches, identification of torque imbalance is carried out when engine speed differs most from average value of the output speed. Variations in engine speed oscillations are caused due to torque imbalance. Phase-angle diagrams of engine speed are developed to analyze superimposed cylinder torques, that are applied on crankshaft. Based on phase-angle diagram analysis, fuel mass injected in the cylinder is adjusted to balance the engine torque. Time domain approaches have less computational requirement as compared to frequency domain approaches. Computational requirements are relatively less in time domain approaches as compared to frequency domain approaches. Model based unified framework for detection and mitigation of cyclic torque imbalance can be proposed by employing time domain approaches.

Engine rotational speed oscillations are analyzed by using different models, which are discussed in Section 3.3. Lumped inertia parameter model of engine crankshaft is extensively used to model engine speed oscillations. This model does not depict the oscillations due to inertia mass of torque production subsystem, which comprises of piston, connecting rod and crankshaft. Though a simple linear model, lumped inertia parameter model is only useful for engine diagnosis and estimation techniques. Also, MVEM is generally employed to develop engine control techniques. However, application of MVEM to develop a model based unified framework for simultaneous engine diagnosis and control was not discussed in earlier research work. Individual models were proposed to detect torque imbalance due to faults in fuel injection, ignition or air intake path. However, a model based unified framework to detect and mitigate the engine torque imbalance is rare in the existing literature.

In this research work, a model based novel unified framework is proposed for detection and mitigation of torque imbalance in gasoline engines. This framework can facilitate in reducing exhaust emissions, NVH as well as improving fuel efficiency of the engine. As already stated, engine torque imbalance is a wide-ranging

problem that is common in all types of IC engines and classified as cylinder to cylinder and cyclic torque imbalance. Research work presented in this dissertation is focused to study cyclic torque imbalance in gasoline engines and comprised of two parts. In the first part, detection of cyclic torque imbalance is carried out, whereas in the second part, control techniques are proposed to mitigate imbalance in the cyclic torque. By appropriate selection of the engine model, the proposed unified framework can also be applied to CI engine.

2.6 Problem Statement

To develop a model based unified framework for detection and mitigation of cyclic torque imbalance in gasoline engines.

2.7 Chapter Summary

In this chapter, an overview of engine torque imbalance has been presented. Different groups of engine balancing have been described along-with classes of torque imbalance. Cyclic torque imbalance has been reviewed in detail to present its causes, impact and application. Three main methodologies, that are employed to detect and mitigate torque imbalance have been discussed and engine rotational speed based approaches have been extensively analyzed. Detailed literature review of cyclic torque variations and both frequency as well as time domain approaches in engine rotational speed based techniques to detect and mitigate torque imbalance have been presented. In research analysis, significance of time domain approaches has been elaborated to present the research problem.

In Chapter 3, modeling approaches of gasoline engines as well as crankshaft models are discussed. The novel FPEM is presented in this chapter. Based on FPEM, detection and mitigation of cyclic torque imbalance is proposed in subsequent chapters.

Chapter 3

Mathematical Models of Gasoline Engine

Progression in the field of embedded systems and electronics has made the application of complex control algorithms possible to improve the engine performance. Dynamic engine models for development of control techniques have remained an active research area since 1970s. Dynamic model of any physical system is comprised of a set of differential equations, which are formulated under certain assumptions. Such models represent the system accurately, depending upon precision of assumptions to develop the model and value of parameters in the dynamic model. Dynamic models are usually generic, which could be used for all systems that are working on same principle.

Different approaches have been proposed to model gasoline engines, which are discussed in this chapter. In the start, Otto cycle is briefly discussed in Section 3.1 to explain the combustion cycle of gasoline engines. Modeling approaches for gasoline engines are presented in Section 3.2 and MVEM as well as CCEM are reviewed briefly in this section. Engine crankshaft models are given in Section 3.3; whereas, lumped inertia parameter model is discussed in detail in this section. Different modeling techniques are reviewed in Section 3.4, which were proposed to incorporate torque production subsystem in engine models. FPEM with lumped

cylinder dynamics is discussed in Section 3.5. In this section, torque production subsystem model and its integration with model of other subsystems is presented. Prominent attributes of FPEM are also highlighted in this section. Engine modeling in GT-Suite is briefly discussed in Section 3.6, followed by validation of engine speed dynamics in FPEM by using GT-Power based engine model.

3.1 Working Principle of Otto Cycle

Before going through modeling approaches, working principle of gasoline engines is discussed in this section. Thermodynamic cycle of a naturally aspirated, four-stroke SI engine is called “*Otto cycle*” [1]. Otto cycle is comprised of four processes, which are described by movement of the cylinder piston. In a four-stroke engine, crankshaft completes two revolutions during one combustion cycle. Four phases in ideal Otto cycle are discussed as follows:

1. **Intake Phase:** Otto cycle starts with intake phase, when piston in a cylinder begin to move from TDC to BDC. In Figure 3.1, process 6-1 represents the intake phase, which is an isobaric process. Inlet pressure is equal to one atmosphere during intake phase, whereas in real engine the pressure during intake is slightly less than atmospheric pressure due to pressure losses during air flow in the inlet.
2. **Compression Phase:** Compression is second phase of Otto cycle, during which isentropic compression takes place. It is represented by process 1-2 in Figure 3.1, as piston moves from BDC to TDC. In actual phase, spark plug fires before piston reaches TDC, due to which end of compression is affected. Both pressure as well as temperature increases during compression phase. Both compression as well as expansion phases are assumed as adiabatic as well as frictionless and approximated as isentropic processes.

Constant volume heat input occurs toward end of the compression phase, known as “*combustion process*”. It is represented by process 2-3 in Figure

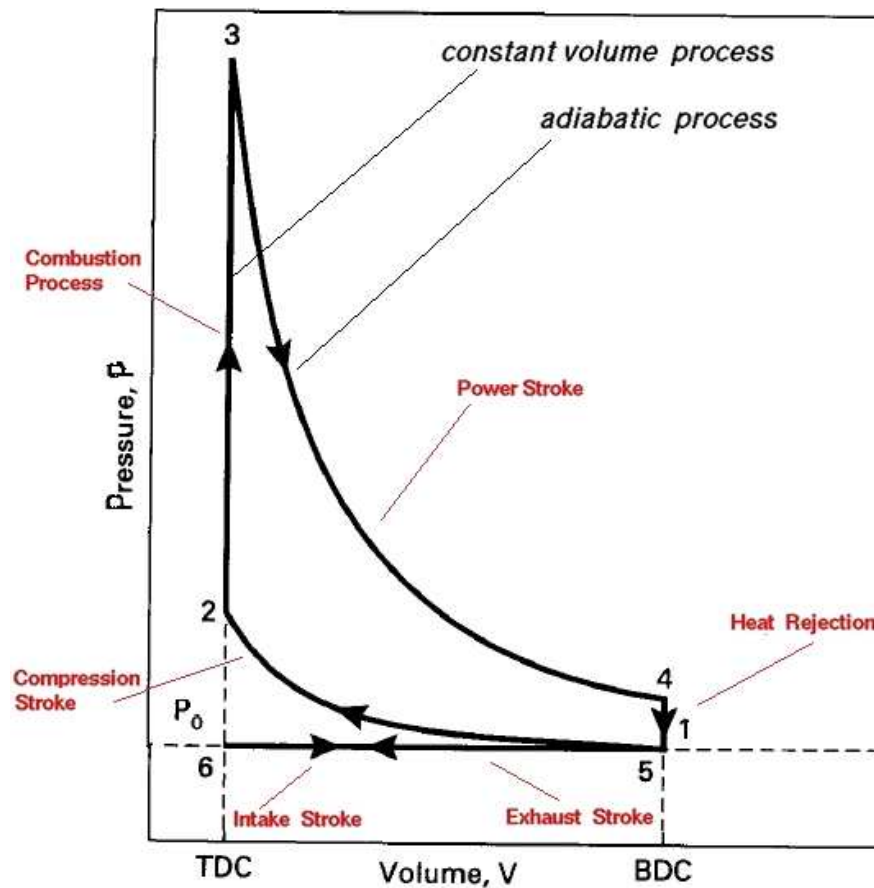


FIGURE 3.1: Ideal Otto Cycle [1]

3.1 and ideally piston is at TDC during this process. Combustion starts before TDC and ends after TDC in real engines. Heat energy is added in the system during combustion process. Due to heat energy, temperature increases at constant volume, which also causes rise in pressure. At point 3, maximum cylinder pressure is achieved.

3. **Expansion Phase:** It is also called “*power stroke*” and shown as process 3-4 in Figure 3.1. Pressure is very high at start of the expansion phase as it follows the combustion process. High pressure forces the piston to move from TDC to BDC, due to which power and output work of the engine is generated. In Otto cycle, expansion phase is approximated with the isentropic process. Both pressure and temperature decrease as piston moves from TDC to BDC. Exhaust valve opens when piston reaches near BDC, due to which exhaust blow down occur. Pressure inside the cylinder reduces to a great extent as exhaust gases are released from the cylinder. In ideal cycle, blow down is desired to

be completed as piston reaches BDC to avoid resistance to piston movement during exhaust phase. Blow down is assumed to take place at constant volume in Otto cycle and represented by process 4-5 in Figure 3.1. Massive heat rejection takes place during this process. It is assumed that pressure is equal to one atmosphere and temperature reduces in this process due to expansion cooling.

4. **Exhaust Phase:** It is last phase of Otto cycle, which is represented by process 5-6 in Figure 3.1. It is a constant pressure process as piston travel from BDC to TDC. Pressure is assumed to be equal to one atmosphere as exhaust valve is opened in this phase. In real engine, pressure drops in exhaust manifold, due to which exhaust pressure is marginally high than the atmospheric pressure. Intake valve opens and exhaust valve closes as piston reaches TDC to start next combustion cycle.

3.2 Modeling Approaches of Gasoline Engine

SI engine is a complex nonlinear system, which comprises of different subsystems such as air, fuel, output speed, cooling and lubrication. All these subsystems are modeled by using different methodologies that are based on model complexity level. Main objective of engine modeling is the formulation of input-output relations to accurately describe the engine dynamics.

Gasoline engine modeling can be categorized into three main approaches [13, 78], which are shown in Figure 3.2. In the first approach, which represents empirical methods, engine models are formulated from experimental data by different methods. These methods include dynamic models, fitting of engine variable polynomials and phenomenological models, fitted with constants that are determined experimentally as well as empirical relations which are specific to the engine under study. This modeling approach is usually described by a set of look up tables.

Different modeling approaches, such as MVEM, CCEM, Discrete Event Model (DEM) and hybrid models have been developed for gasoline engines by using basic

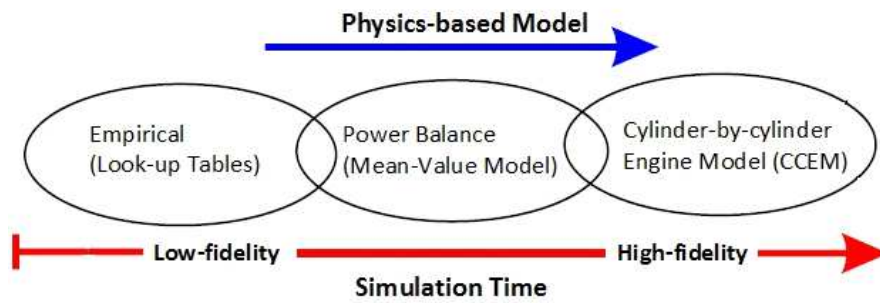


FIGURE 3.2: Modeling Approaches of Gasoline Engine [79]

physical laws. One of the approaches is DEM, which is based on reciprocating nature of the engine. If engine processes are assumed of continuous nature, in which discrete cycles of the gasoline engine are not considered; then such model is known as MVEM. Application of a modeling approach depends on the control objectives; as DEM is preferred for misfire detection, whereas MVEM is used for development of control and diagnosis techniques for slow engine processes [80, 81].

3.2.1 Mean Value Models of Gasoline Engine

Second approach is comprised of the control oriented MVEM, which contains physics-based equations as well as empirical data and use time scale domain. MVEM encompasses physical feature of the engine in more detail than empirical models; however, these model are relatively simple as compared to CCEM [78, 79]. In MVEM, average value of states over few engine cycles is evaluated, whereas engine discrete events are neglected. Operating time scale is assumed to be of prolong duration than combustion cycle [78]. MVEM predicts principal external variables of the engine, which includes output speed and intake manifold pressure; as well as important internal variables of the engine, such as volumetric and thermal efficiencies. MVEM is the amalgamation of look-up tables and physics-based components that permit to evaluate as well as control physical parameter effects. Such features have made MVEM appropriate for real time control applications [13, 82], as it has less computational demand.

In [82, 83], Dobner discussed a model of the gasoline engine along with carburetor model. Carburetor model was comprised of empirical look-up tables, which were

function of manifold pressure, throttle valve angle and AFR. This engine model was comprised of time delay integration of the dynamic equations. Being a discrete model, the computations were carried out for each firing instant of the engine. Aquiono [84] used output speed and volumetric efficiency to develop the model of fuel dynamics. In this work, fuel dynamics model was proposed for the first time; however, continuous flow model was in contrast to Dobner's model.

In [85], Powell et.al., presented a basic nonlinear model of the gasoline engine. This model included dynamics of engine subsystems such as intake manifold, throttle body, fuel injection and EGR. A regression model was used to calculate mass of intake air as function of speed dynamics and manifold pressure. Indicated torque was calculated as function of output speed by using another regression equation. In [86], nonlinear engine model was proposed, which was similar to Powell's model by replacing throttle angle approximate function by a polynomial. Output torque was used as function of AFR, air mass flow at throttle valve, Spark Angle (SA) and output speed. In this model, inlet air flow, throttle body, generated torque and pumping of the engine were expressed by nonlinear algebraic relations. Speed dynamics and air flow in intake as well as exhaust manifolds were modeled by differential equations; though, model of the fuel dynamics was not discussed in this work.

In [87], Yuen et.al., presented an engine model with similar approach that was discussed in [83], by modeling the carburetor instead of throttle body. Unlike Dobner's model, manifold pressure in transient conditions and variations in intake manifold temperature along with its effect on fuel evaporation were considered. Emission gases were described as function of AFR, whereas throttle mass flow was correlated to geometry and characteristics of the throttle area.

Moskwa contributed a detailed account of MVEM in [88]. In this work, area of throttle body was expressed as function of throttle angle, bore and pin diameter. Engine torque was stated in term of AFR, Spark Advance (SA) and look-up tables of friction. Manifold pressure, cylinder geometries and compression ratio were used to express thermal energy of the gasoline engine. In [78], Hendricks presented the

most widely used MVEM of the gasoline engine and gave additional details in [89]. Proposed model was comprised of three main states, which included manifold pressure, injected fuel mass and engine speed. Unlike [84], model of fuel dynamics was based on fuel flow in the intake manifold. In [90], effects of spark timing were discussed by employing the thermal efficiency in MVEM that was proposed in [91]. Engine thermal efficiency was expressed as product of four engine variables, which included manifold pressure, AFR, engine speed and spark timing.

3.2.2 Cylinder by Cylinder Models of Gasoline Engine

CCEM is the third modeling approach of gasoline engines, which are developed in crank angle domain. Compared to MVEM, these models are more precise and depict subsystem processes in more detail. This model is used to evaluate fuel injection, engine diagnosis, exhaust emissions and fuel consumption. Engine parameters, such as temperature, pressure, area and volume of cylinder as well as valve lift, engine power and burning rate of the fuel mass can be calculated at specified crank angle. CCEM can predict cylinder peak pressure and instantaneous torque in crank angle domain, whereas control techniques can affect the engine on per cycle basis. In this approach, cycle average torque can be calculated by integration of net torque over complete combustion cycle [92]. Engine performance can be predicted in more detail by using CCEM, as each phase of Otto cycle, shown in Figure 3.1, can be modeled to develop complete simulation of Otto cycle. Characteristics of each phase of Otto Cycle can be analyzed by CCEM [24].

In [93], CCEM of gasoline engines was presented by using both physical and empirical formulations. Cylinder pressure was integrated over one engine cycle to evaluate torque and power; as well as engine performance. Proposed model was comprised of tuning parameters set, which included AFR, geometry of the engine, heat transfer and ignition. Exact data of cycle states was difficult to obtain, that was required for simulation and analysis of the engine cycle. In [92], CCEM of Variable Valve Timing (VVT) engine was proposed. This model was comprised of 24 states, which included temperature, manifold air mass, burned gas residual,

pressure, combustion and exhaust process dynamics. This model predicted instantaneous torque at a given crank angle, whereas algorithms based on this model can control the engine on per-cycle basis.

In [94], a comparison between MVEM and CCEM was presented. This comparison was based on utility of the model and possible application in model based power-train control design. Comparison of complexity between MVEM and CCEM for control of engine power-train was primary objective of this study. It was concluded in [78, 89], that complexity of the model depended on its application.

MVEM was found more appropriate model to develop the techniques for state estimation and nonlinear control; as both MEVM and CCEM offer similar dynamic response in simulations. MVEM is more suitable for analysis and development of engine control algorithms [13, 94] due to inherent limitations of CCEM. Many constraints, such as complexity, control design and difficulty to analyze are associated with CCEM. Being control oriented model, MVEM is employed for simulations, systematic analysis, control-based applications and estimation techniques.

3.3 Models of Engine Crankshaft

Generally, main components of the IC engine have remained same for past 100 years or so; comprising of engine block, engine head, intake and exhaust manifolds, cylinder, piston, connecting rod, intake and exhaust valves, camshaft and crankshaft. All these components have significant role in the performance of IC engines; nevertheless, crankshaft is the main component which translates reciprocating motion of piston in the cylinder to rotational motion. This rotational motion at flywheel end of the crankshaft is used as output torque of IC engines. Crankshaft does not only provide mechanical energy from chemical energy of fuel; but oscillations in engine rotational speed can be employed for diagnosis and control of combustion process in engine cylinders. Different models of crankshaft were developed to study oscillations in engine rotational speed. Four basic crankshaft

models have been used for analyzing rotational speed oscillations [95], which are discussed as follows:

3.3.1 Lumped Inertia Parameter Model

Based on simple principles of mechanics, lumped inertia parameter model was the initial model, that is used for crankshaft vibrational analysis [96]. It is also termed as “Simple Mass Spring Model”. To illustrate the model, crankshaft of a multi-cylinder engine is represented by lumped inertia parameter model in Figure 3.3. Depending upon number of cylinders, a similar crankshaft model can be developed for any IC engine.

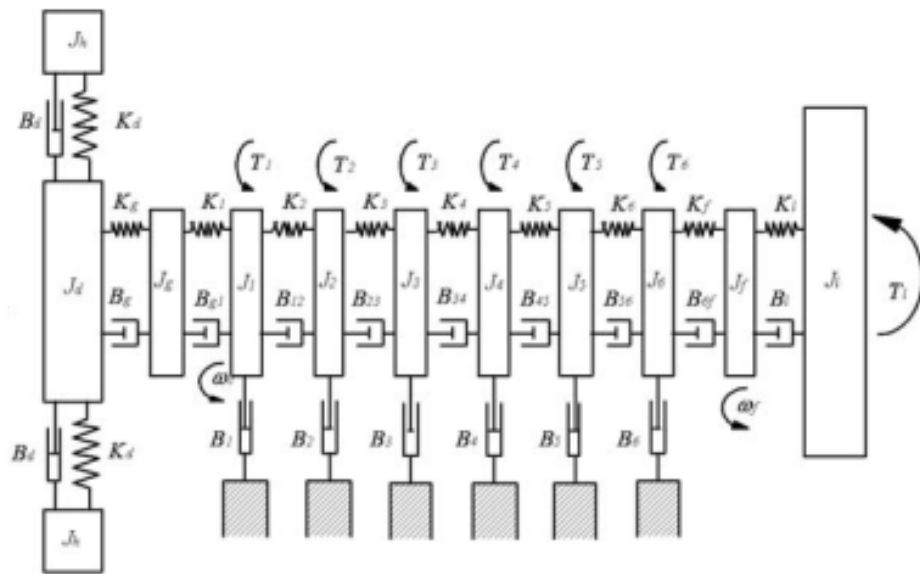


FIGURE 3.3: Lumped Inertia Parameter Model of Engine Crankshaft [97]

In this model, crankshaft was grouped into concentrated inertia moment discs, mass-less elastic axis and external as well as internal damping. Rotational inertia of each disc included piston, equivalent rotational inertia of connecting rod and rotational inertia of crank. To attenuate torsional vibrations in crankshaft, a harmonic damper was attached at crank-nose side, whereas load side of the crankshaft

was connected to flywheel. As mentioned in [97], following assumptions were made to develop lumped inertia parameter model of the crankshaft:

- For each cylinder, crankshaft inertia was lumped at respective crank that resulted in moments of inertia as J_1, \dots, J_6 .
- Crankshaft structural stiffness and structural damping were assumed locally linear and expressed as $K_g, K_1, \dots, K_6, K_f, K_l$ and $B_g, B_{gl}, B_{12}, \dots, B_{56}, B_{6f}, B_l$, respectively.
- Damping due to pumping, piston friction, main bearing friction and ring friction were supposed to be locally linear. These were expressed by B_1, \dots, B_6 .
- Damping and stiffness of harmonic damper were also supposed to be linear as K_d and B_d .
- Input torques were expressed by τ_1, \dots, τ_6 , which represented sum of friction torque, indicated torque and periodic inertia torques; that acted at each crank throw.
- Load torque was assumed slowly varying or constant.

Lumped inertia parameter model was extensively employed to analyze oscillations in engine rotational speed for torque estimation and cylinder health diagnosis [97, 98]. In [97], an unknown input observer based method was proposed for reconstruction of cylinder-wise indicated torque. By using lumped inertia parameter model, combustion torque was estimated by model inversion [99], Kalman filtering [100] and frequency analysis [56, 98]. Imbalance in engine torque can also be detected by analysis of oscillations in engine rotational speed. In [101], torque imbalance was identified from speed difference of engine phase. Torque imbalance was detected by calculating elapsed time in a certain fixed region of crank angle domain in [23]. Lumped inertia parameter model is linear and simple.

However, certain limitations are associated with this model, which includes:

- Lumped inertia parameter model is applicable for engine diagnosis only and does not present control design framework.
- Order of the model increases as number of cylinders increases in the engine.

- Oscillations due to varying inertia of torque producing mechanism are suppressed in this model.

3.3.2 Continuous Mass Model

This model is based on continuum theory, in which crankshaft is assumed as an elastomer that is developed in finite element method. In literature, this model is also termed as “*Distributed Mass Model*” [102]. By applying finite element method, this model divided crankshaft objects into finite element calculation model of division. In this model, crankshaft mass was continuously distributed along entire crankshaft length, unlike lumped inertia parameter model. Also, partial differential equations were used, that can precisely account for vibrations in the crankshaft. Low and high frequency components of crankshaft speed oscillations can be computed by using numerical methods. This model can also compute arbitrary section stress.

Continuous mass model is the complex description of engine speed oscillations, in which computation of low speed could cause large cumulative error. Thus, it is difficult to apply this model for system design and simulation. Continuous mass model is mostly used in calculation of free vibrations, which are hard to realize due to calculation method. Two models are further derived from continuous mass model, which are “*Multi-Diameter Model*” and “*Framework Model*”.

3.3.3 Multi-Segment Concentrated Mass Model

This model is analogous to lumped inertia parameter model. Nevertheless, depending upon structure characteristic requirements for analysis demand, multi-segment concentrated mass model is divided into sections as per analysis requirements. This model can compute torsional oscillation frequencies of higher order, which cannot be found by lumped inertia parameter model. Multi-segment concentrated mass model evades substantial computational load as needed in continuous mass model.

3.3.4 Soft Body Dynamics Model

In this model, crankshaft is characterized as modal flexible body to calculate its rotational speed dynamics. Series of modals are contained in a flexible body. State variables of the system are required for each modal unit during breakdown steps to calculate relative amplitude of each characteristic vector. Total deformation of flexible body was computed by using linear superposition principle and integrating deformation of nod at each time interval.

3.4 Engine Models Incorporating Torque Production Subsystem

Various research efforts were found in existing literature in which kinetics of torque producing mechanism were modeled; instead of considering the analogous subsystem of volumetric pump to overcome modeling inadequacy present in MVEM. Such studies have also considered lumped inertia parameter model to analyze various engine features.

In [103], a model based on rotational velocity of engine flywheel was proposed to simulate disturbances and misfire condition. This model used multi-body dynamics of crankshaft with torsional flexibility to analyze oscillations, which were produced in engine speed and drive-line. Cylinder torque was modeled by using analytical cylinder pressure model [104], along with model of moving piston mass [105]. Also, a drive-line model was employed to evaluate torsional vibration modes of the drive-line. Although, crankshaft model was considered as interconnected flexible body; however, cylinder torque was calculated for single cylinder only. Effect of torque generated by other cylinders was not included in crankshaft model and mass of connecting rod was not considered to model torque producing mechanism. Model extension for multicylinder engines could make its application difficult as model complexity increased with rise in number of engine cylinders. Also, it was a diagnostic model and not proposed as a control oriented model.

A simulation model for IC engines was presented in [106]. This model was based on nonlinear first order differential equations, in which dynamics of crankshaft were stated as interconnected spring-mass-damper systems. In this model, individual cylinder pressure was taken as input and brake torque was measured by torque sensor as system output. Cylinder-wise combustion information was obtained from the measured instantaneous crankshaft torque, which was also used to propose the torque control technique. Proposed model had the limitation of torque sensor to measure crankshaft torque, as torque sensor is expensive and not installed in the engine of commercial road cars. It also had high requirement of computational load, as flexible crankshaft model was considered and information about large number of parameters was required by this model. Thus, online implementation of proposed model became a challenging task.

In some techniques, torque producing mechanism was modeled as slider-crank mechanism, as it was comprised of a slider in the form of cylinder piston; whereas, connecting rod acted as linkage and crankshaft resembled the crank. Torque production subsystem of multi-cylinder engine was modeled in [107]. In this model, equations for torque balancing and kinematic analysis of slider-crank mechanism were derived in Newtonian mechanics. Model of single cylinder was proposed, which can be extended to multi-cylinder engine. However, in Newtonian mechanics, model for constrained motion of the mechanism became further complex. Also, model complexity increased with rise in number of engine cylinders.

A modified model of torque production subsystem was discussed in [108], which proposed a combustion model for estimation of in-cylinder pressure and instantaneous torque by modeling the torque producing mechanism as slider-crank mechanism. Instead of the analogy of volumetric pump, torque producing mechanism was modeled as two lumped masses in this model. One mass modeled rotational motion, whereas other mass modeled reciprocating motion of the mechanism. These lumped masses were used to calculate rotational and translational inertia of the mechanism. Orthogonal force component, which acted on crank-offset was transformed as output torque by using trigonometry relations.

Crankshaft was modeled as a rigid body in this model. Nevertheless, complete model of torque producing mechanism in multi-cylinder engine was not derived. Kinetic analysis of torque producing mechanism was carried out to propose this model for estimation of torque that is generated due to combustion force, i.e.,

$$F_c(\theta) = A_p P_{cyl}(\theta) \quad (3.1)$$

where, A_p , $F_c(\theta)$ and $P_{cyl}(\theta)$ denote piston area, force applied on piston and cylinder pressure, respectively. Although, this model included dynamics of the slider-crank mechanism to represent torque producing mechanism but extension of proposed model to multi-cylinder engines was not derived. Also, addition of multi-cylinder dynamics does not give any further information about the engine, apart from modeling the oscillations in engine rotational speed.

In [109], a model was derived with time-varying mass moment of inertia, instead of constant inertia model. Two approaches were proposed to develop the nonlinear engine model. First approach used Newtonian method, whereas in other approach Lagrangian method was applied to drive kinematics and dynamic forces of the engine. Individual force balance equations for crankshaft, connecting rod and piston were computed to derive dynamic equations of the engine. The proposed approach was not extended to develop control-oriented engine model, as it only focused to derive the model with time varying mass moment of inertia.

In another technique, engine rotational position was used to estimate pressure, fuel mass and output torque of the engine in [110]. Projection method was used to drive piston-crank model, which described motion of the engine; whereas, combustion process was represented by Wiebe function. Both piston-crank model and Wiebe function were integrated to propose model of the torque production subsystem. Unscented Kalman Filter (UKF) based observer was employed to estimate desired variables. This model was proposed for single cylinder engine and extension of the model for multi-cylinder engines was not discussed. Also, proposed model was not control-oriented and can be used for engine diagnosis only.

Different techniques were also proposed to reconstruct indicated torque and cylinder pressure by employing the models that incorporated torque production subsystem or used oscillations in engine rotational speed, such as lumped inertia model [106], stochastic method [111] and neural network based method [64]. Although, various observers were presented to estimate indicated torque [112] and cylinder pressure [73]; however, these techniques did not capture the oscillations that were produced due to reciprocating motion of torque producing mechanism. Also, constrained motion of torque producing mechanism was not considered during engine modeling [113, 114].

3.5 First Principle based Engine Model with Lumped Cylinder Dynamics

As discussed in Section 3.2, CCEM gives more physical attribute of engine subsystems but numerical complexity and order of the model increases if number of cylinders are increased. MVEM is the simpler class of control-oriented engine models, that possess physical information about engine subsystems, along with certain assumptions and analogies. Although, MVEM is mostly employed as control-oriented model but it does not depict system dynamics with high fidelity. Few assumptions were made to develop MVEM, including the analogy to use continuously operating volumetric pump model instead of torque production subsystem [13]. Due to such assumptions, some important output response elements were suppressed, that include engine rotational speed oscillations. Also, MVEM had limited ability to represent system dynamics under faulty conditions, such as misfire in the cylinder; as this model take average value over few combustion cycles and also uses empirical relations. Different techniques to incorporate torque production subsystem in model of gasoline engines were discussed in Section 3.4; however as highlighted, these models had certain limitations.

As highlighted in Subsection 3.2.1, MVEM has been formulated on the basis of physical principles. Throttle valve angle is considered as model input, whereas

engine rotational speed is taken as output of the model. In MVEM, an assumption has been made to model the torque producing mechanism as a volumetric pump [13]. Oscillations in engine rotational speed are generated due to combustion in each cylinder. In MVEM, supposition of volumetric pump in place of torque producing mechanism has suppressed oscillatory behavior of output speed. Oscillations in engine rotational speed are mainly caused by:

- Cylinder pressure does not remain constant during combustion process and generates non-uniform force. As already mentioned in Section 3.1, nature of work performed by all four phases of the combustion cycle is different in an engine cylinder. Power is produced only in combustion phase; whereas, remaining three phases consume some portion of this power.
- Torque producing mechanism has varying inertia as it is an oscillating system. Torque producing mechanism in the engine cylinder is comprised of piston, connecting rod and crankshaft. This mechanism resembles the slider-crank mechanism and generate oscillating torque, which is termed as “*inertia*” torque. Effective inertia of oscillating mass in torque producing mechanism vary twice for one crankshaft revolution [115]. Secondary resonance in engine rotational speed oscillations are produced if inertia torques have large variations. Such phenomenon of secondary resonance and instability region are termed interesting but of less significance. In [116], it was proposed that instantaneous torque contribution τ_{int} from the cylinder act on the crankshaft as $\tau_{int} = \tau_{gas} + \tau_{mass}$, where τ_{gas} is combustion torque that is produced by combustion of air fuel mixture and τ_{mass} is inertia torque that is generated due to oscillating movement of torque producing mechanism.

FPEM is a recently developed, control-oriented gasoline engine model. Oscillations in engine rotational speed were modeled in FPEM, which were suppressed in MVEM. In FPEM, model of torque producing mechanism was derived with lumped cylinder assumption using constrained Equation of Motion (EoM) in Lagrangian mechanics [14]. Apart from modeling oscillations in engine speed, FPEM also stated the relationship between engine speed and net piston force (f_n). This

model was extended by integrating the closed form analytical cylinder pressure model of gasoline engine [117] to model the net piston force (f_n) acting on the piston head. Torque produced by the engine depends on this force, generated in the engine cylinder.

Model of the torque production subsystem was comprised of torque producing mechanism model for lumped cylinder engine and analytical cylinder pressure model of gasoline engines. In FPEM, assumption of volumetric pump in MVEM was replaced by torque producing mechanism model and phases of Otto cycle, that displayed output speed oscillations. Engine output was comprised of average speed profile in MVEM, whereas oscillations in engine output speed were displayed in FPEM.

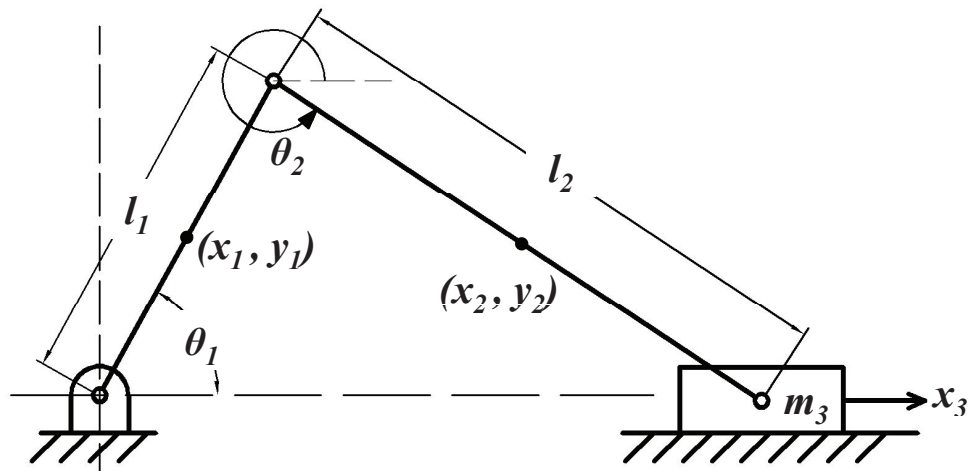


FIGURE 3.4: Torque Producing Mechanism-Lumped Cylinder Engine [117]

3.5.1 Torque Producing Mechanism Model

The FPEM with lumped cylinder dynamics was presented in [14] and generic model of torque producing mechanism was derived. Schematic diagram of torque producing mechanism in an engine with lumped cylinder dynamics is shown in Figure 3.4. This mechanism is comprised of piston, which is connected to crankshaft via

connecting rod. Following assumptions were made to derive the torque producing mechanism model:

1. Elements of the mechanism were assumed to be inflexible and rigid.
2. Potential energy was assumed constant with negligible change in it ($\partial PE/\partial q_i, \partial PE/\partial \dot{q}_i \approx 0 \forall q_i$).
3. Lumped approach was adopted to model the friction. Friction from all components was applied as frictional torque to crankshaft.

Detail of generalized coordinates, which were defined for physical variables in torque producing mechanism are given in Table. 3.1:

TABLE 3.1: Detail of Generalized Coordinates

Generalized Coordinate	Mechanism Variables	Description of Variables
q_1	x_1	Center of mass of crankshaft
q_2	y_1	
q_3	θ_1	Angular position of crankshaft
q_4	x_2	Center of mass of connecting rod
q_5	y_2	
q_6	θ_2	Angular position of connecting rod
q_7	x_3	Position of cylinder piston

Constrained EoM in Lagrangian mechanics, given in Eq. (3.2), was used to drive the model of torque producing mechanism.

$$\frac{d}{dt} \frac{\partial L}{\partial \dot{q}_i} - \frac{\partial L}{\partial q_i} + \sum_{j=1}^k \lambda_j \frac{\partial \phi_j}{\partial q_i} = e_i^s \quad (3.2)$$

which was subjected to following constraints.

$$\phi_j(q, t) = 0, \quad j = 1, 2, 3, \dots, k \quad (3.3)$$

where subscript j denotes j^{th} constraint, k means total number of constraints and i denotes i^{th} generalized coordinate. Term e represent generalized effort and L represents Lagrangian of the mechanism, which is given as following:

$$L = KE - PE \quad (3.4)$$

where, PE represent total potential energy and KE represent total kinetic energy of the mechanism.

Total kinetic energy of the mechanism (KE) can be expressed as follows:

$$KE = KE_1 + KE_2 + KE_3 \quad (3.5a)$$

$$KE_1 = \frac{1}{2}m_1(\dot{x}_1^2 + \dot{y}_1^2) + \frac{1}{2}J_1\dot{\theta}_1^2 \quad (3.5b)$$

$$KE_2 = \frac{1}{2}m_2(\dot{x}_2^2 + \dot{y}_2^2) + \frac{1}{2}J_2\dot{\theta}_2^2 \quad (3.5c)$$

$$KE_3 = \frac{1}{2}m_3\dot{x}_3^2 \quad (3.5d)$$

It was assumed that potential energy of the subsystem did not change significantly. Motion of the bodies in torque producing mechanism had following constraints, which are also explained in Figure 3.5.

$$\phi_1 = x_1 - \frac{l_1}{2}\cos\theta_1 = 0 \quad (3.6a)$$

$$\phi_2 = y_1 - \frac{l_1}{2}\sin\theta_1 = 0 \quad (3.6b)$$

$$\phi_3 = x_2 - (l_1\cos\theta_1 + \frac{l_2}{2}\cos\theta_2) = 0 \quad (3.6c)$$

$$\phi_4 = y_2 - (l_1\sin\theta_1 + \frac{l_2}{2}\sin\theta_2) = 0 \quad (3.6d)$$

$$\phi_5 = l_1\cos\theta_1 + l_2\cos\theta_2 - x_3 = 0 \quad (3.6e)$$

$$\phi_6 = l_1\sin\theta_1 + l_2\sin\theta_2 = 0 \quad (3.6f)$$

For each coordinate q_i , term $\frac{d}{dt} \frac{\partial L}{\partial \dot{q}_i}$ in Eq. (3.2) was solved, which resulted as :

$$\begin{aligned} \text{Crankshaft} &\Rightarrow \frac{d}{dt} \frac{\partial KE}{\partial \dot{x}_1} = m_1\ddot{x}_1 & \frac{d}{dt} \frac{\partial KE}{\partial \dot{y}_1} = m_1\ddot{y}_1 & \frac{d}{dt} \frac{\partial KE}{\partial \dot{\theta}_1} = J_1\ddot{\theta}_1 \\ \text{Connecting Rod} &\Rightarrow \frac{d}{dt} \frac{\partial KE}{\partial \dot{x}_2} = m_2\ddot{x}_2 & \frac{d}{dt} \frac{\partial KE}{\partial \dot{y}_2} = m_2\ddot{y}_2 & \frac{d}{dt} \frac{\partial KE}{\partial \dot{\theta}_2} = J_2\ddot{\theta}_2 \\ \text{Piston} &\Rightarrow \frac{d}{dt} \frac{\partial KE}{\partial \dot{x}_3} = m_3\ddot{x}_3 \end{aligned}$$

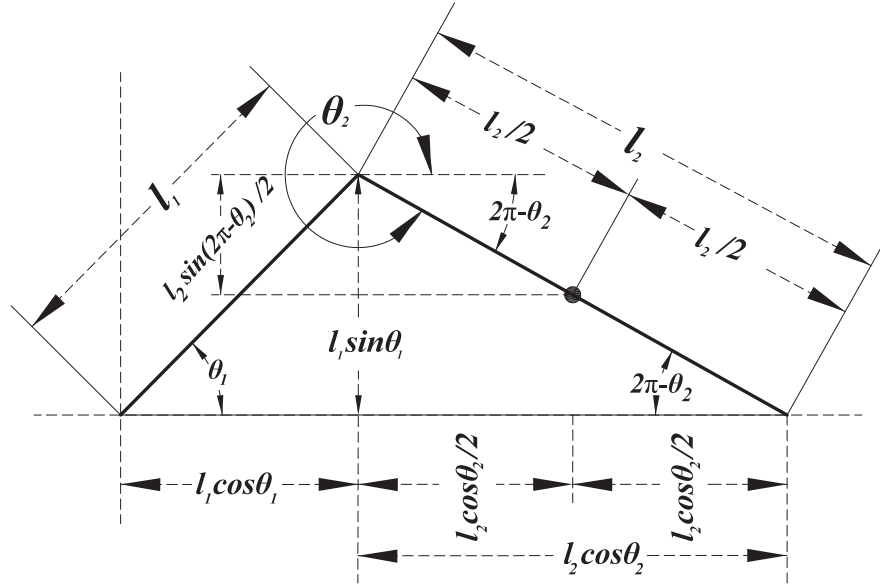


FIGURE 3.5: Constraints for Motion of Torque Producing Mechanism

Following equations were obtained by applying constrained EoM to generalized coordinate, i.e., $q_1 = x_1$, which is mass center of the crankshaft along x-axis. No external input was applied to the mechanism along this generalized coordinate:

$$\frac{d}{dt} \frac{\partial KE}{\partial \dot{x}_1} - \frac{\partial KE}{\partial x_1} + \sum_{j=1}^6 \lambda_j \frac{\partial \phi_j}{\partial x_1} = 0 \quad (3.8a)$$

$$m_1 \ddot{x}_1 + \lambda_1 \frac{\partial}{\partial x_1} \left[x_1 - \frac{l_1 \cos \theta_1}{2} \right] = 0 \quad (3.8b)$$

$$m_1 \ddot{x}_1 + \lambda_1 = 0 \quad (3.8c)$$

For generalized coordinate $q_2 = x_2$, i.e., center of mass of the crankshaft along y-axis, following equations were obtained by applying constrained EoM. Also, no external input was applied along this generalized coordinate:

$$\frac{d}{dt} \frac{\partial KE}{\partial \dot{y}_1} - \frac{\partial KE}{\partial y_1} + \sum_{j=1}^6 \lambda_j \frac{\partial \phi_j}{\partial y_1} = 0 \quad (3.9a)$$

$$m_1 \ddot{y}_1 + \lambda_2 \frac{\partial}{\partial y_1} \left[y_1 - \frac{l_1 \sin \theta_1}{2} \right] = 0 \quad (3.9b)$$

$$m_1 \ddot{y}_1 + \lambda_2 = 0 \quad (3.9c)$$

Following equations resulted by applying constrained EoM to angular position of the crankshaft, i.e., $q_3 = \theta_1$. External input τ_N was applied along this generalized coordinate:

$$\frac{d}{dt} \frac{\partial KE}{\partial \dot{\theta}_1} - \frac{\partial KE}{\partial \theta_1} + \sum_{j=1}^6 \lambda_j \frac{\partial \phi_j}{\partial \theta_1} = \tau_N \quad (3.10a)$$

$$\begin{aligned} J_1 \ddot{\theta}_1 + \lambda_1 \frac{\partial}{\partial \theta_1} \left[x_1 - \frac{l_1 \cos \theta_1}{2} \right] + \lambda_2 \frac{\partial}{\partial \theta_1} \left[y_1 - \frac{l_1 \sin \theta_1}{2} \right] + \\ \lambda_3 \frac{\partial}{\partial \theta_1} \left[x_2 - \left(l_1 \cos \theta_1 + \frac{l_2 \cos \theta_2}{2} \right) \right] + \\ \lambda_4 \frac{\partial}{\partial \theta_1} \left[y_2 - \left(l_1 \sin \theta_1 + \frac{l_2 \sin \theta_2}{2} \right) \right] + \end{aligned} \quad (3.10b)$$

$$\begin{aligned} \lambda_5 \frac{\partial}{\partial \theta_1} [l_1 \cos \theta_1 + l_2 \cos \theta_2 - x_3] + \lambda_6 \frac{\partial}{\partial \theta_1} [l_1 \sin \theta_1 + l_2 \sin \theta_2] = \tau_N \\ J_1 \ddot{\theta}_1 + \lambda_1 \left[\frac{l_1}{2} \sin \theta_1 \right] - \lambda_2 \left[\frac{l_1}{2} \cos \theta_1 \right] + \lambda_3 l_1 \sin \theta_1 \\ - \lambda_4 l_1 \cos \theta_1 - \lambda_5 l_1 \sin \theta_1 + \lambda_6 l_1 \cos \theta_1 = \tau_N \end{aligned} \quad (3.10c)$$

Application of constrained EoM to center of mass of the connecting rod along x-axis, i.e., $q_4 = x_2$, resulted in following equations. No external force was applied along this generalized coordinate:

$$\frac{d}{dt} \frac{\partial KE}{\partial \dot{x}_2} - \frac{\partial KE}{\partial x_2} + \sum_{j=1}^6 \lambda_j \frac{\partial \phi_j}{\partial x_2} = 0 \quad (3.11a)$$

$$m_2 \ddot{x}_2 + \lambda_3 \frac{\partial}{\partial x_2} \left[x_2 - \left[l_1 \cos \theta_1 + \frac{l_2 \cos \theta_2}{2} \right] \right] = 0 \quad (3.11b)$$

$$m_2 \ddot{x}_2 + \lambda_3 = 0 \quad (3.11c)$$

Constrained EoM was applied to mass center of the connecting rod along x-axis, i.e., $q_5 = y_2$. No external force was applied along this generalized coordinate and yielded following equations:

$$\frac{d}{dt} \frac{\partial KE}{\partial \dot{y}_2} - \frac{\partial KE}{\partial y_2} + \sum_{j=1}^6 \lambda_j \frac{\partial \phi_j}{\partial y_2} = 0 \quad (3.12a)$$

$$m_2 \ddot{y}_2 + \lambda_4 \frac{\partial}{\partial y_2} \left[y_2 - \left[l_1 \sin \theta_1 + \frac{l_2 \sin \theta_2}{2} \right] \right] = 0 \quad (3.12b)$$

$$m_2\ddot{y}_2 + \lambda_4 = 0 \quad (3.12c)$$

Next generalized coordinate was angular position of the connecting rod, i.e., $q_6 = \theta_2$ and no external input was applied along it. Application of constrained EoM resulted in following equations:

$$\frac{d}{dt} \frac{\partial KE}{\partial \dot{\theta}_2} - \frac{\partial KE}{\partial \theta_2} + \sum_{j=1}^6 \lambda_j \frac{\partial \phi_j}{\partial \theta_2} = 0 \quad (3.13a)$$

$$J_2 \ddot{\theta}_2 + \lambda_3 \frac{\partial}{\partial \theta_2} \left[x_2 - \left[l_1 \cos(\theta_1) + \frac{l_2 \cos(\theta_2)}{2} \right] \right] +$$

$$\lambda_4 \frac{\partial}{\partial \theta_2} \left[y_2 - \left[l_1 \sin \theta_1 + \frac{l_2 \sin \theta_2}{2} \right] \right] +$$

$$\lambda_5 \frac{\partial}{\partial \theta_2} (l_1 \cos(\theta_1) + l_2 \cos(\theta_2) - x_3) + \quad (3.13b)$$

$$\lambda_6 \frac{\partial}{\partial \theta_2} (l_1 \sin(\theta_1) + l_2 \sin(\theta_2)) = 0$$

$$J_2 \ddot{\theta}_2 + \lambda_3 \frac{l_2}{2} \sin \theta_2 - \lambda_4 \frac{l_2}{2} \cos \theta_2 - \lambda_5 l_2 \sin \theta_2 + \lambda_6 l_2 \cos \theta_2 = 0 \quad (3.13c)$$

Last generalized coordinate was position of the cylinder piston, i.e., $q_7 = x_3$. Along this generalized coordinate, external input *net piston force* (f_n) was applied. Following equations resulted by applying constrained EoM:

$$\frac{d}{dt} \frac{\partial KE}{\partial \dot{x}_3} - \frac{\partial KE}{\partial x_3} + \sum_{j=1}^6 \lambda_j \frac{\partial \phi_j}{\partial x_3} = f_n \quad (3.14a)$$

$$m_3 \ddot{x}_3 + \lambda_5 \frac{\partial}{\partial x_3} (l_1 \cos \theta_1 + l_2 \cos \theta_2 - x_3) = f_n \quad (3.14b)$$

$$m_3 \ddot{x}_3 - \lambda_5 = f_n \quad (3.14c)$$

As constrained EoM for each generalized coordinate, q_1 through q_7 were solved; following differential equations were obtained for all generalized coordinates:

$$m_1 \ddot{x}_1 + \lambda_1 = 0 \quad (3.15a)$$

$$m_1 \ddot{y}_1 + \lambda_2 = 0 \quad (3.15b)$$

$$J_1 \ddot{\theta}_1 + \lambda_1 \left[\frac{l_1}{2} \sin \theta_1 \right] - \lambda_2 \left[\frac{l_1}{2} \cos \theta_1 \right] + \lambda_3 l_1 \sin \theta_1$$

$$- \lambda_4 l_1 \cos \theta_1 - \lambda_5 l_1 \sin \theta_1 + \lambda_6 l_1 \cos \theta_1 = \tau_N \quad (3.15c)$$

$$m_2\ddot{x}_2 + \lambda_3 = 0 \quad (3.15d)$$

$$m_2\ddot{y}_2 + \lambda_4 = 0 \quad (3.15e)$$

$$J_2\ddot{\theta}_2 + \lambda_3 \left[\frac{l_2}{2} \sin \theta_2 \right] - \lambda_4 \left[\frac{l_2}{2} \cos \theta_2 \right] + \lambda_5 l_2 \sin \theta_2 + \lambda_6 l_2 \cos \theta_2 = 0 \quad (3.15f)$$

$$m_3\ddot{x}_3 + \lambda_5 = f_n \quad (3.15g)$$

Torque producing mechanism model was expressed by Differential Algebraic Equations (DAE) as it had seven differential equations from generalized variables along with six algebraic equations for constraints of motion. It resulted in one degree of freedom of torque producing mechanism. This model was simplified in *Mathematica*[®]; whereas model parameters were tuned using optimization techniques and discussed in detail in [16].

Following form was obtained after simplification of the model:

$$\dot{\omega}_1 = \mathbf{g}_1(\theta_1(t), \Gamma) \omega_1^2(t) + \mathbf{g}_2(\theta_1(t), \Gamma) \tau_N + \mathbf{g}_3(\theta_1(t), \Gamma) f_n \quad (3.16)$$

Complete expressions of $\mathbf{g}_1(\theta_1(t), \Gamma)$, $\mathbf{g}_2(\theta_1(t), \Gamma)$ and $\mathbf{g}_3(\theta_1(t), \Gamma)$ [118] are presented in **Appendix A**.

3.5.2 Analytical Cylinder Pressure Model

Model of torque producing mechanism was integrated with analytical parametric cylinder pressure model of the SI engine, which was presented in [104]. Cylinder pressure model provided net piston force (f_n) by incorporating the forces produced due to combustion, power phase of the cycle and pumping losses. Inputs as well as outputs of the cylinder pressure model are shown in Figure 3.6.

Net piston force (f_n) was calculated by following formulation:

$$\begin{aligned} F_c &= P_{cyl} A_P \\ F_{crk} &= P_{crk} A_P \\ f_n &= F_c - F_{crk} = (P_{cyl} \times A_P) - (P_{crk} \times A_P) \end{aligned} \quad (3.17)$$

where, F_c represents the force acting on piston head, F_{crk} represents the force acting from crank-case side on the piston, A_P is area of the piston, P_{cyl} is pressure in cylinder and P_{crk} is pressure in crank-case.

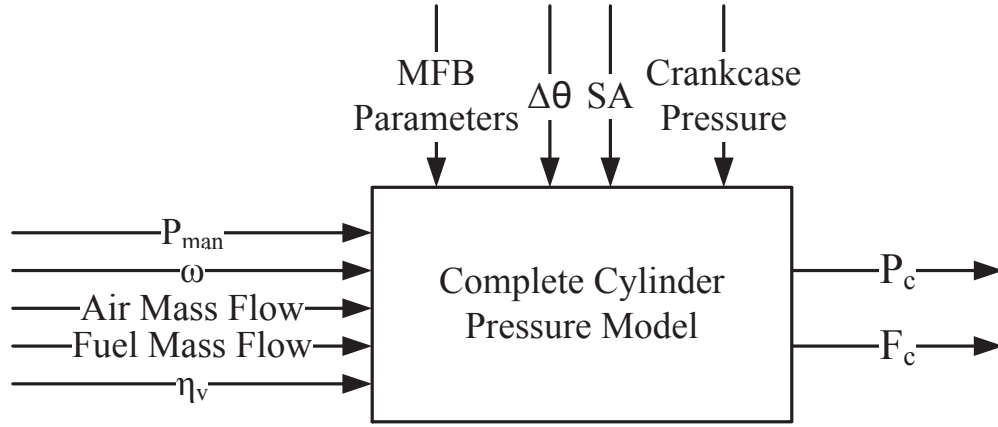


FIGURE 3.6: Inputs and Outputs of Cylinder Pressure Model

Cylinder pressure model was derived by linking the asymptotes of intake, compression, combustion, expansion and exhaust phases. Each phase of the four-stroke engine was realized by its own physical principle. Volumetric efficiency and intake manifold pressure of the engine were used to estimate in-cylinder pressure during intake phase. Also, mass of the air and inducted fuel mass in the cylinder were calculated for a given AFR. Similar procedure was also adopted for exhaust phase.

Compression Phase: For compression phase, asymptote was described by a poly-tropic process with compression exponent (γ_c). Initial conditions for poly-tropic compression process were assumed at the end of intake phase. Thus, asymptotes of intake and compression phases were automatically joined.

During compression, pressure and temperature were modeled as:

$$\begin{aligned}
 P_c(\theta_1) &= P_{ivc} \left(\frac{V_{ivc}}{V(\theta_1)} \right)^{\gamma_c} \\
 T_c(\theta_1) &= T_{ivc} \left(\frac{V_{ivc}}{V(\theta_1)} \right)^{\gamma_c-1}
 \end{aligned} \tag{3.18}$$

where, $V(\theta_1)$ and V_{ivc} are instantaneous volume of the cylinder taken as function of engine angular position and cylinder volume at intake valve close, respectively.

Combustion Phase: This phase initiated from Start of Combustion (SoC) and lasts till End of Combustion (EoC). Duration between these two events was termed as *Combustion Phasing*, which was expressed by Mass Fraction Burnt (MFB). Combustion phasing and mass fraction burnt is mostly modeled by Wiebe function [119, 120], which was expressed as:

$$m_{fb}(\theta_1) = 1 - \exp \left[-a \left(\frac{\theta_1 - \theta_0}{\delta\theta_1} \right)^{m+1} \right] \quad (3.19)$$

where, m_{fb} is mass fraction burnt, θ_0 is start of combustion, $\delta\theta_1$ is burn duration and m, a are Wiebe shape factor. In [104], approximation of these shape factors was described. Average value of $\delta\theta_1$ for gasoline engines is used as calculated in [119] and spark timing is assumed as SoC. Also, nominal values of $\delta\theta_1$ and combustion parameter values for SI engines were described in [119].

Expansion Phase: Asymptote of expansion phase was also represented by a poly-tropic process with exponent (γ_e). Pressure and temperature during expansion phase were expressed as:

$$\begin{aligned} P_e(\theta_1) &= P_3 \left(\frac{V_3}{V(\theta_1)} \right)^{\gamma_e} \\ T_e(\theta_1) &= T_3 \left(\frac{V_3}{V(\theta_1)} \right)^{\gamma_e - 1} \end{aligned} \quad (3.20)$$

where P_3, T_3, V_3 are cylinder pressure, temperature and volume at the end of combustion phase.

Overall closed form expression of in-cylinder pressure was presented in [104]. Structure of torque production subsystem, which was developed by integrating models of torque producing mechanism and cylinder pressure is shown in Figure 3.7.

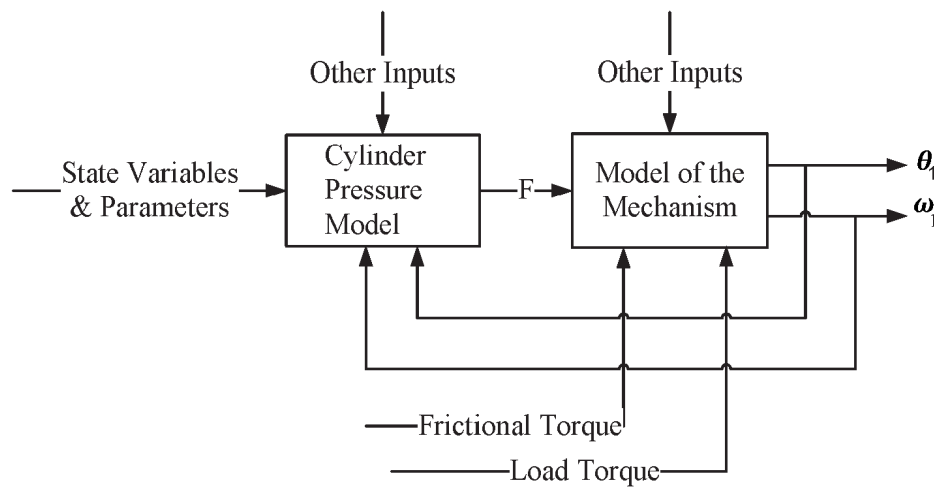


FIGURE 3.7: Structure of Torque Production Subsystem [14]

3.5.3 Model Integration

As shown in Figure 3.8, structure of FPEM was formed by integrating following engine subsystems:

1. Air intake subsystem.
2. Intake manifold subsystem.
3. Fuel dynamics subsystem.
4. Torque production subsystem.
 - (a) Model of torque producing mechanism.
 - (b) Model of cylinder pressure.

As mentioned before, model of torque production subsystem was comprised of torque producing mechanism model for lumped cylinder engine and analytical cylinder pressure model of gasoline engines. Air intake and fuel dynamics subsystems were incorporated from [78], whereas intake manifold model was taken from [13] to develop the complete model.

3.5.3.1 Air Intake Subsystem

Although different models of air intake subsystem exist in the literature; however, model presented by Hendricks and Sorenson in [78] was integrated due to its

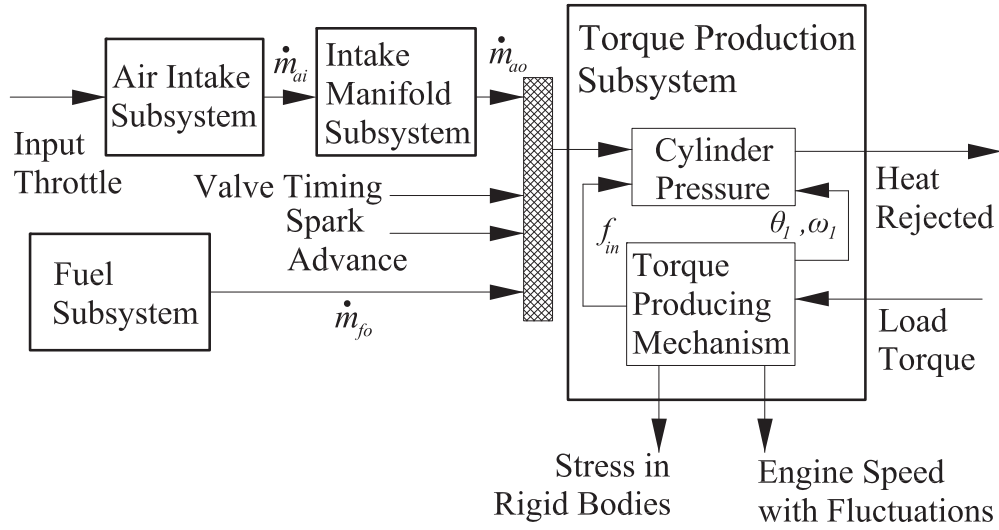


FIGURE 3.8: Structure of the FPEM [117]

simplicity. Model of mass flow rate of air (\dot{m}_{ai}), which enters the intake manifold was given as following:

$$\dot{m}_{ai} = C_D \frac{P_{amb} \sqrt{\gamma'}}{\sqrt{RT_{amb}}} \times A_E(\alpha) f(P_{man}) + \dot{m}_{aio} \quad (3.21)$$

where

$$A_E(\alpha) = \frac{\pi}{4} D^2 \times (1 - \cos(\alpha)) \quad (3.22)$$

$$f(P_{man}) = \begin{cases} \sqrt{P_r^{\frac{2}{\gamma}} - P_r^{\frac{\gamma+1}{\gamma}}} & \text{if } P_r \geq \left[\frac{2}{\gamma+1} \right]^{\frac{\gamma}{\gamma+1}} \\ \sqrt{\left[\frac{1}{\gamma} \right] \left[\frac{2}{\gamma+1} \right]^{\frac{\gamma+1}{\gamma-1}}} & \text{, otherwise} \end{cases} \quad (3.23)$$

whereas, α is throttle valve angle, \dot{m}_{aio} is model fitting variable, P_r is P_{man}/P_{amb} , and $\gamma' = 2\gamma/\gamma - 1$. Discontinuity in Eq. (3.23) was due to *choked flow* phenomena.

3.5.3.2 Intake Manifold Subsystem

Model of intake manifold subsystem, presented in [13] was used to represent manifold pressure dynamics. This model was based on filling and emptying concept.

Intake manifold was filled by the air that enters into intake manifold (\dot{m}_{ai}) and emptied due to air that enter into engine cylinder (\dot{m}_{ao}). Model of intake manifold subsystem under isothermal condition was given as following:

$$\dot{P}_{man} = \frac{T_{amb}\gamma R}{V_{man}} \{\dot{m}_{ai} - \dot{m}_{ao}\} \quad (3.24)$$

where

$$T_{man} = T_{amb}$$

Mass flow rate of the air entering into cylinder (\dot{m}_{ao}) was given as:

$$\dot{m}_{ao} = \eta_v \times \frac{V_d \omega_1 P_{man}}{4\pi R T_{man}} \quad (3.25)$$

where η_v is volumetric efficiency of the engine, V_d is engine displaced volume and R is universal gas constant.

By using the expressions given in Eq. (3.21) and Eq. (3.25) in Eq. (3.24), manifold pressure was expressed as:

$$\dot{P}_{man} = \{f(P_{man}) A_1(C_D, \alpha) - A_2 \omega_1 P_{man}\} \quad (3.26)$$

where

$$\begin{aligned} A_1(C_D, \alpha) &= \frac{RT_{man}}{V_{man}} \gamma C_D A_E(\alpha) P_{amb} \gamma_c \\ A_2 &= \frac{V_d \eta_v}{4\pi V_{man}} \\ \gamma_c &= \sqrt{\frac{2\gamma}{(\gamma - 1)RT_{man}}} \end{aligned}$$

3.5.3.3 Fuel Dynamics Subsystem

For model integration, model of port injected fuel subsystem was adopted from [78]. Injected fuel flow rate (\dot{m}_{fi}) is controlled by pulse width of the injection

signal (*IPW*). After injection into intake manifold, fuel flow is divided into two portions, which are:

1. Flow of slow fuel.
2. Flow of fast fuel.

Fast part of the fuel reached the cylinder in immediate induction cycle, whereas slow component of the fuel reached the cylinder with a time delay.

Fuel dynamics of gasoline engine can be expressed by following relation [78]:

$$\dot{m}_{fo} = \dot{m}_{fv} + \dot{m}_{ff} \quad (3.27)$$

where,

$$\begin{aligned} \dot{m}_{fv} &= (1 - X_f)\dot{m}_{fi} \\ \ddot{m}_{ff} &= \frac{1}{\tau_f}(-\dot{m}_{ff} + X_f\dot{m}_{fi}) \end{aligned} \quad (3.28)$$

whereas, \dot{m}_{ff} is mass flow rate of fuel film, \dot{m}_{fv} is mass flow rate of fuel vapors, τ_f is time constant of fuel evaporation and X_f is injected fuel fraction that is deposited in intake manifold. Also, \dot{m}_{fi} is mass flow rate of injected fuel and output m_{fo} is fuel mass injected per combustion cycle.

Injector Pulse Width (IPW) signal controls the mass flow rate of injected fuel (\dot{m}_{fi}). As mentioned in Eq. (3.27) and Eq. (3.28), mass flow rate of injected fuel (\dot{m}_{fi}) regulates the mass of fuel injected into engine cylinder (m_{fo}) for varying amount of air flow rate to maintain the required AFR. Although, *IPW* is usually calculated in milliseconds (*ms*); however, it is converted into crank angle rotation to calculate mass flow rate of injected fuel (\dot{m}_{fi}) from mass flow rate of fuel injector (\dot{m}_{fInj}) [1]:

$$\dot{m}_{fi} = \frac{\dot{m}_{fInj} \times IPW}{4\pi} \quad (3.29)$$

The FPDM with lumped cylinder dynamics was validated by using the engine data sets that were acquired from experimental setup of 1300cc gasoline engine through OBD-II interface. Brief description of engine test rig is discussed in Section 6.4.

Validation of FPEM was reported in detail in [14, 16, 117]. These engine data sets were also employed for tuning of model parameters by application of optimization technique, that was described in detail in [16]. Numeric value of tuned parameters was also given in [16].

Complete FPEM was stated as follows:

$$\dot{P}_{man} = \{f(P_{man}) A_1(C_D, \alpha) - A_2 \omega_1 P_{man}\} \quad (3.30a)$$

$$\dot{m}_{fo} = \dot{m}_{fv} + \dot{m}_{ff} \quad (3.30b)$$

$$\dot{\omega}_1 = \mathbf{g}_1(\theta_1(t), \Gamma) \omega_1^2(t) + \mathbf{g}_2(\theta_1(t), \Gamma) \tau_N + \mathbf{g}_3(\theta_1(t), \Gamma) f_n \quad (3.30c)$$

3.5.4 Attributes of First Principle based Engine Model

FPEM possesses few additional attributes as compared to MVEM. FPEM has diagnostic as well as control attributes. Model-based interpretation of engine rotational speed oscillations is one of the significant features of FPEM. A comparison of FPEM and MVEM is given in Table 3.2. In-cylinder conditions directly

TABLE 3.2: Comparison of FPEM and MVEM [16]

Attribute	MVEM	FPEM
Engine speed	$\dot{\omega} = \frac{1}{J} \tau_b$	$\dot{\omega}_1 = \mathbf{g}_1(\theta_1(t), \Gamma) \omega_1^2(t) + \mathbf{g}_2(\theta_1(t), \Gamma) \tau_N + \mathbf{g}_3(\theta_1(t), \Gamma) f_n$
Speed dynamics	Based on approximation	Based on the first principle
Engine speed oscillations	Oscillation are not modeled	Oscillations are modeled
VVT and SA	Indirectly modeled	Modeled directly with f_n
System dynamics under fault conditions	Limited description capability	Describe system dynamics under fault conditions
Extension to multi-cylinder engines	Dynamics of multi-cylinder engine cannot be shown	Model extended to show multi-cylinder engine dynamics

corresponded with oscillations in engine speed. Thus, model-based diagnosis techniques can be proposed by employing FPEM. Unlike the engine models that incorporated torque production subsystem, complexity of FPEM did not increase

to a great deal as number of engine cylinder increased. Although, FPEM is a control-oriented model; however, it can also depict system response under fault conditions. Unified diagnostic and control framework can be formulated by employing FPEM to describe system dynamics under various fault conditions. Thus, conventional model-based FTC techniques can be proposed for engine faults [16]. Further extension of such unified framework included cylinder power balancing, fault diagnosis, condition monitoring and engine thermo-management. FTC techniques for gasoline engines can assist to meet the requirements of limp home mode [121] and model based VCD.

Empirical relations were used for spark advance in conventional control-oriented models, whereas spark advance was not defined through empirical formulation in FPEM. Thus, conventional diagnostic observer can be used to estimate spark health of the gasoline engine, which serve as basis for prognosis of misfire condition. Tension in individual bodies of torque producing mechanism could also be analyzed by this model. Heat rejected during combustion cycles can be mathematically expressed in FPEM. Thus, model-based representation of heat rejected during combustion cycles might be used to integrate diagnosis and control framework with engine thermo-management.

3.6 Engine Modeling in GT-Suite

Advancement in software technology has led to variety of 1D engine simulation software packages to achieve optimized engine design. These software packages have helped to improve the engine performance and provide data on various parameters of IC engines. 1-D engine simulation require less computational effort than multidimensional models. Results can be obtained faster and a desktop computer is sufficient in terms of hardware requirements, even for real time simulations. GT-Suite, Ricardo Wave, Dynomation Engine Simulation, Lotus Engine Simulation and AVL Boost are some of the widely used engine simulation software packages. Among these packages, GT-Suite is considered most accomplished and

widely accepted by industry as well as academia to simulate various subsystems of both gasoline as well as diesel engine.

GT-Suite is a software package that contained various modules, such as GT-Cool, GT-Fuel, GT-Crank, GT-Vtrain, GT-Drive and GT-Power for modeling and simulation of different processes and subsystems operation in an automotive system. GT-Suite provided the platform that is based on many physical laws and various toolboxes are accessible for modeling of different subsystems of a vehicle [122]. GT-Suite models can be simulated in conjunction with other software packages to model the complex engine subsystems. Simulink in *MATLAB*[®] is one of the modeling packages that can be integrated with GT-Suite. Complete engine, powertrain and vehicle subsystems are modeled in GT-Power, whereas control techniques are implemented in Simulink-*MATLAB*[®]; to create a GT-Suite and Simulink integrated environment. Control signals in GT-Suite can be passed or received from Simulink-*MATLAB*[®] via ‘SimulinkHarness’ component. For example, vehicle speed can be measured in GT-Suite and passed to Simulink-*MATLAB*[®], which regulate the control signal of throttle valve angle in GT-Suite to change engine speed.

3.6.1 Validation of FPEM in GT-Power

GT-Power is one of the modules of GT Suite, specifically designed for simulation and analysis of IC engines. It is a prime engine simulation software that is acknowledged for its high accuracy to simulate various engine operations. GT-Power solves one dimensional Navier-Stokes equations, i.e., conservation of continuity, energy and momentum. IC engine flows, combustion, in-cylinder turbulence as well as motion, temperatures, pressures, exhaust emissions and fuel flow rate are few of the important parameters that can be simulated in GT-Power. Motion of flows can be evaluated in GT-Power by using models of different engine subsystems, which are based on experimental analysis and data curve fitting. These models provide better accuracy of macro level attributes like airflow, Brake Specific Fuel

Consumption (BSFC), torque as well as micro level features, which include crank angle resolved cylinder pressure and emissions.

3.6.1.1 Sub-Models of GT-Power based Engine Model

Sub models of GT-Power based engine model are discussed briefly in this section. However, detail of these sub models can be found in [122]. GT-Power based engine model of a single cylinder gasoline engine is shown in Figure 3.9.

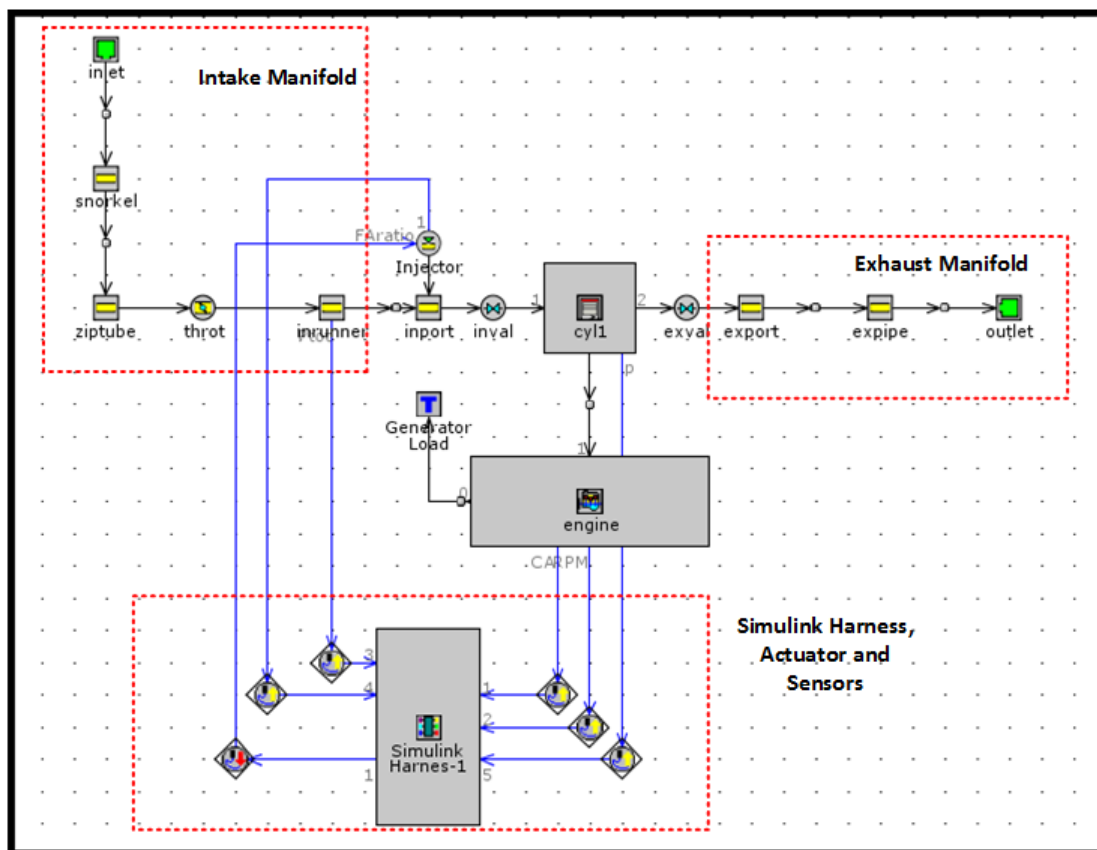


FIGURE 3.9: GT-Power based Model of Single Cylinder Gasoline Engine

The 'cyl1' object was developed from 'EngCylinder' template. Object 'cyl1' has many attributes, out of which one of the attributes is 'combustion object'. The 'EngCylCombSIWiebe' template was used in this object to model the combustion process. This template imposes combustion for gasoline engines using *Wiebe function*. The 'engine' object was developed from 'EngineCrankTrain' template. Attributes of engine crank train were specified by this template. These attributes

were employed to model rigid dynamics and kinematics of the crank-train configurations. Engine geometry in ‘cylinder Geometry’ attribute folder of ‘EngineCrank-Train’ was created by using ‘EngCylGeom’ template.

‘EngCylHeatTr’ attribute in ‘Heat Transfer Object’ of ‘cyl1’ object was used to incorporate heat transfer from engine cylinder and crankcase parts in GT-Power based engine model. In-cylinder heat transfer was calculated by this object by applying ‘WoschniGT’ template, which closely matched classical *Woschni* correlation without swirl [24]. Cylinder wall temperatures were used to model in-cylinder heat transfer. ‘Twall’, ‘TwallDetail’ and ‘TWallSoln’ attributes were used in this object.

Gas properties were defined by using ‘FluidInitialState’ template in intake manifold object, exhaust manifold object and ‘cyl1’ object. Attributes such as pressure, temperature and composition of the air were defined in this template. Inlet and exhaust processes were defined in ‘inval’ and ‘exval’ objects in intake and exhaust manifold sub-systems, which were part of gas exchange dynamics. These objects were defined by using ‘ValveCamConn’ template. Cam angle versus lift array was defined in ‘Lift Arrays’ attribute folder, whereas coefficient of discharge was defined in ‘Flow Arrays’ attribute folder.

3.6.1.2 Model Validation

Model of torque production subsystem in FPEM was simulated in *MATLAB*[®]/Simulink, using specifications of a 550 cc, single cylinder SI engine. Specifications of the engine are mentioned in Table 3.3.

Model of torque production subsystem was validated by using GT-Power based engine model [123], shown in Figure 3.9. Standard values from one of the existing GT-Power benchmark examples, which are available in GT-Suite, were used to develop GT-Power based engine model. These benchmark examples have been extensively employed to analyze various systems and processes of IC engines [124–126]. GT-Power based engine model was developed with Simulink harness module

and engine crank-train module with one-cylinder object. Intake and exhaust manifolds were developed from various flow objects, as shown in Figure 3.9.

TABLE 3.3: Specifications of Single Cylinder Gasoline Engine

Parameter	Unit	Value
Compression ratio	-	8.9
Mass of the piston	<i>g</i>	450
Engine displacement	<i>cm</i> ³	550
Engine stroke length	<i>cm</i>	8.1
Diameter of the cylinder	<i>cm</i>	9.3
Mass of connecting rod	<i>g</i>	600
Inertia of connecting rod	<i>kg.m</i> ²	2.25×10^{-3}
Length of connecting rod	<i>cm</i>	15.7

This model was run in co-simulation environment of MATLAB-Simulink and GT-Power at steady state conditions. Load torque and throttle valve angle were kept constant throughout the simulation. In this research work, load torque was assumed to be known as measurement of load torque is a different research problem. Load torque is the external torque which is applied to the engine. It is equal and opposite to drive torque that is generated by the IC engine, when it is operated at constant speed. In most of the existing literature, calculation or estimation of load torque has been treated as separate engine problem. Thus, load torque has been taken as known input to propose different estimation and control techniques related to IC engines [13, 112]. However, there are further four approaches for on-road conditions measurement of load torque, stated as follows:

1. Techniques based on static maps to calculate load torque by ECU and implemented in accordance with OBD-II specifications. A suitable parameter to indicate load torque is *manifold absolute pressure*. During on-road conditions, load torque can be accessed via OBD-II data logging and scanning device.
2. Unknown input observer-based techniques, which have been applied to estimate load torque as unknown input to IC engines [127, 128].
3. Another way to estimate load torque is based on calculation of vehicle longitudinal dynamics as road load translate to engine load. It depends on many factors that contribute longitudinal load, few of these factors are, aerodynamic drag, inertial load, climbing resistance and road conditions [129]. Longitudinal

dynamics depend on velocity profile of the vehicle, which usually remain close to optimal vehicle speed.

4. Installation of sensors to measure load torque, as fitted in formula one cars.

Thus, In the proposed research work, load torque was assumed as known input for detection of cyclic torque imbalance as it was carried out under lab conditions. Whereas, unified framework for detection and mitigation of cyclic torque imbalance was applied during runtime of the vehicle, as per existing technique in the literature and it was assumed that exact estimate of load torque was available to implement the proposed framework.

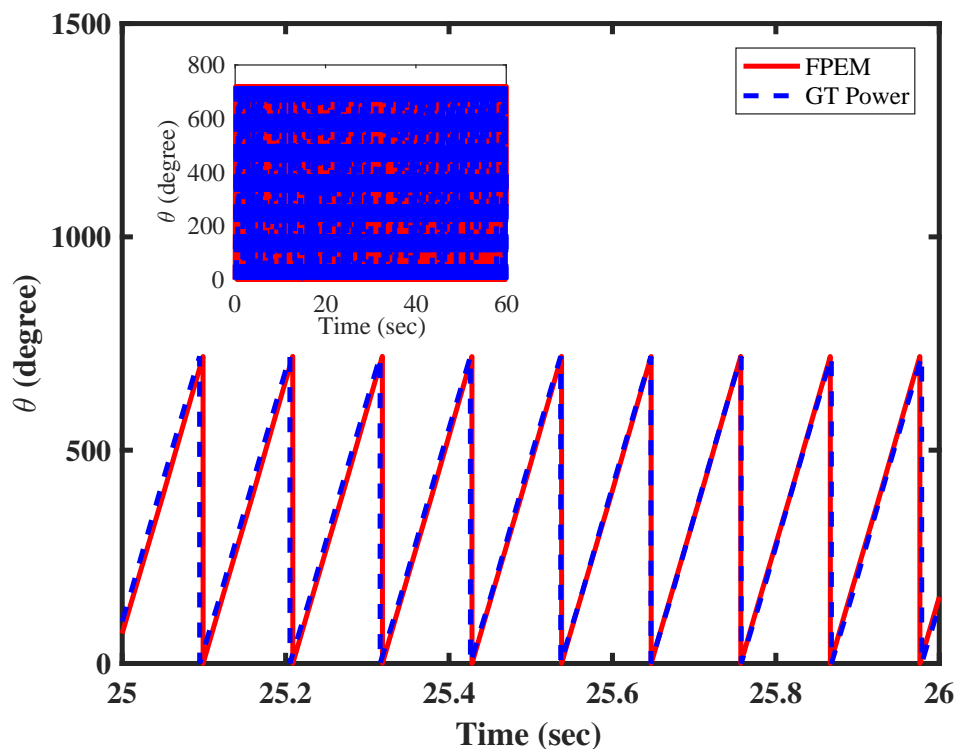


FIGURE 3.10: Engine Angular Position (θ_1); FPEM and GT-Power based Engine Model

Engine angular position, rotational speed and net piston force (f_n) from FPEM were compared with GT-Power based engine model. Enlarged view of engine angular position is shown in Figure 3.10, whereas complete plot of engine angular position of both models is shown in the inset. Each cycle of engine angular position was comprised of 720 degree of crankshaft rotation. Engine angular position of

FPEM was closely matched with angular position of GT-Power based engine model and both models showed similar frequency of combustion cycles.

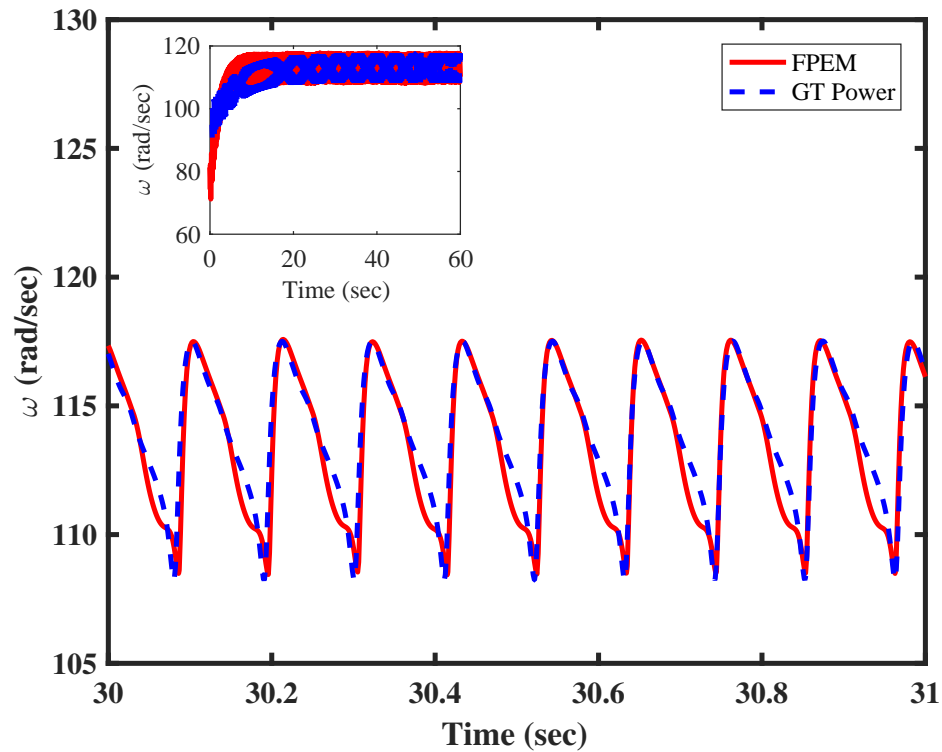


FIGURE 3.11: Engine Rotational Speed (ω_1); FPEM and GT-Power based Engine Model

Enlarged view of engine rotational speed of both FPEM and GT-Power based engine models is presented in Figure 3.11, whereas complete plot of engine speed is shown in the inset. Although initial conditions of engine speed were different; however, it converged to approximately same steady state value in both models. Magnitude and frequency of oscillations in engine speed, that was reconstructed by FPEM matched with speed oscillations of GT-Power based engine model. Plots of engine angular position and rotational speed displayed precise description of engine speed dynamics in FPEM.

In Figure 3.11, it was observed that speed traces from FPEM and GT-Power models followed each other, except during intake and compression phases. Such differences may occur due to inaccuracies in the modeling. Assumptions and simplifications during modeling are considered as main reasons for such imprecision.

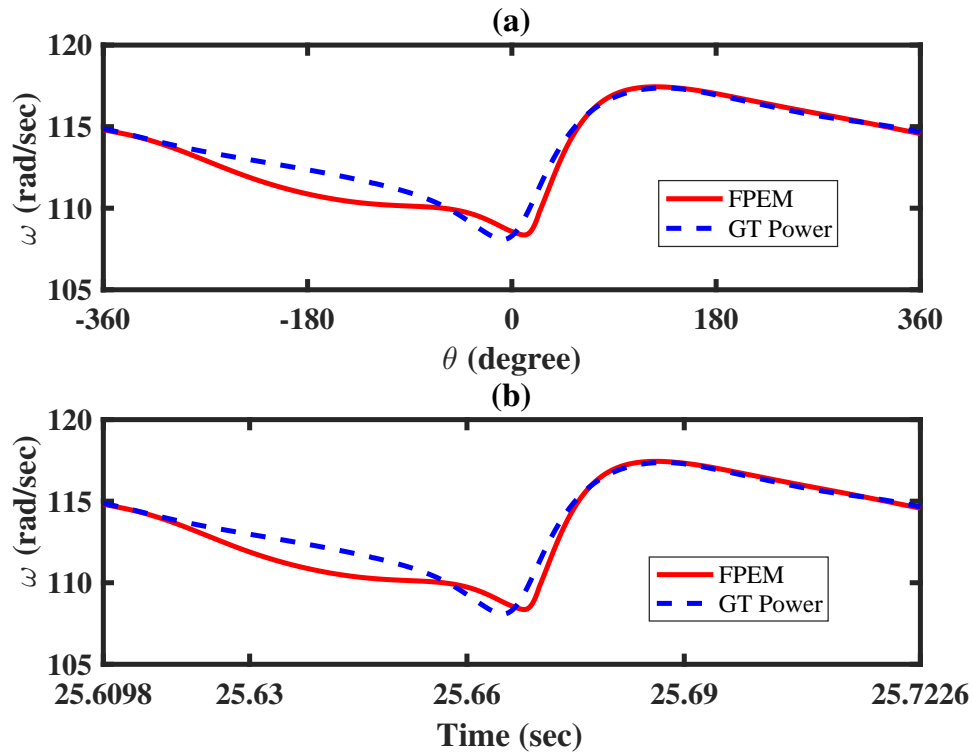


FIGURE 3.12: Engine Rotational Speed Comparison for Single Combustion Cycle a) Angular Position versus Rotational Speed b) Time versus Rotational Speed

It is pertinent to mention that FPEM is the control oriented model, which is based on ordinary differential equations; whereas, GT-Power is based on one dimensional gas dynamics, which represented flows and heat transfer in piping and related components.

Initial pressure of compression stroke can be approximated by manifold pressure expression in the FPEM. However, pressure drops occur over flow turns and valves in intake runner; which influence the pressure of intake air [104]. These phenomena were not modeled in control-oriented models and could affect engine rotational speed during intake and compression phases. Also, heat transfer and heat exchange processes were assumed implicitly during compression phase in cylinder pressure model [104]. Selection of polytropic exponent values can also affect modeling of the compression phase. Whereas, in GT-Power based engine model, “EngCylHeatTr” attribute in “Heat Transfer Object” of “cyl1” object calculated the heat transfer from crankcase parts and cylinders of the engine. This object

used “*WoschniGT*” template that calculated in-cylinder heat transfer by a mathematical relation, which closely emulated the *Woschni* correlation without swirl [24]. Cylinder wall temperatures were used to model in-cylinder heat transfer. The “*Twall*”, “*TwallDetail*” and “*TWallSoln*” attributes were also employed in this object. Mean square error between rotational speed of FPEM and GT-Power model was calculated for single combustion cycle. Value of the mean square error was around 4.5%, which is within allowable error limit.

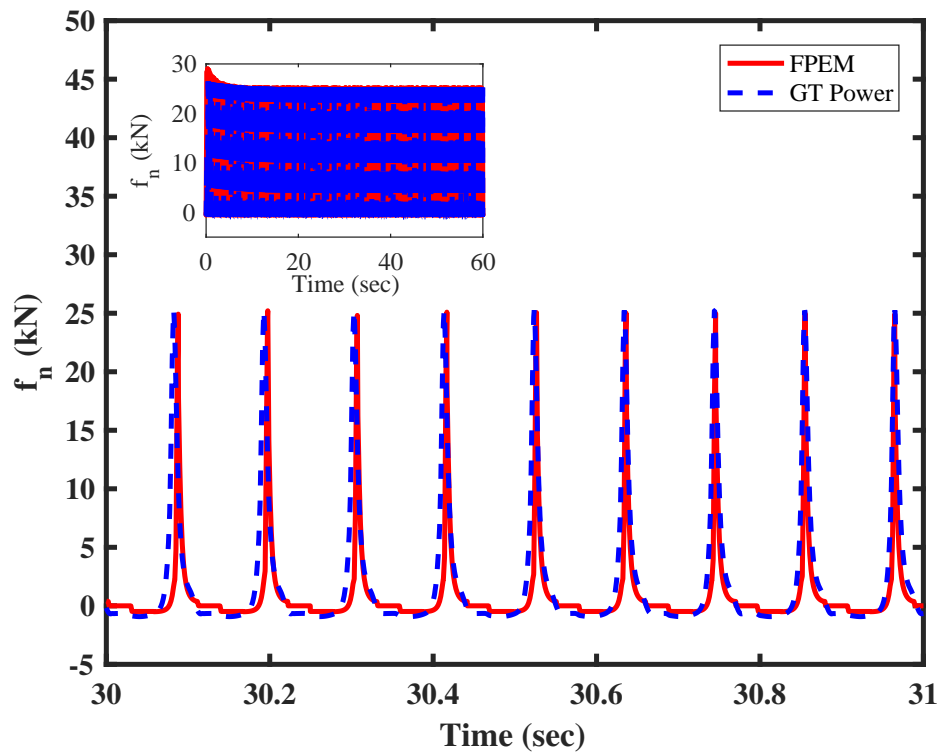


FIGURE 3.13: Net Piston Force (f_n); FPEM and GT-Power based Engine Model

Comparison between rotational speed of FPEM and GT-Power based engine model for single combustion cycle is shown in Figure 3.12 to further evaluate the speed traces from these models. Comparison of engine rotational speed in crank angle domain is shown in Figure 3.12(a), whereas in time domain it is shown in Figure 3.12(b). This comparison for single combustion cycle displayed behavior of engine speed during different phases of four-stroke combustion cycle. It can be noted that such oscillations in engine speed represented the combustion cycles in engine

cylinder. Based on such oscillations, engine diagnosis techniques can be developed to analyze combustion process in the cylinder and detect engine faults.

Enlarged view of net piston force (f_n) from FPEM and GT-Power based engine model is shown in Figure 3.13, whereas complete plot of net piston force (f_n) is shown in the inset. Net piston force (f_n) in FPEM closely matched with net piston force (f_n) that was generated in GT-Power based engine model. Accuracy of FPEM to model gasoline engines is highlighted from Figure 3.10, 3.11, 3.12 and 3.13.

3.7 Chapter Summary

This chapter has been aimed to explore mathematical models of gasoline engines. After going through thermodynamic cycle, modeling approaches of the gasoline engine have been discussed. Crankshaft models have also been presented in this chapter, which were employed to model oscillations in engine rotational speed. Lumped inertia parameter model has been discussed in detail, which is most commonly used to model oscillations in engine speed. Various modeling approaches to incorporate torque production subsystem have also been reviewed before going through FPEM.

Derivation of torque production subsystem model has been discussed in detail along with its integration with models of air intake as well as fuel dynamics subsystems. Main attributes of FPEM have been discussed to highlight significant features of the model. Torque production subsystem in FPEM has been validated by its comparison with speed dynamics of GT-Power based engine model. In the next chapter, detection of cyclic torque imbalance by applying the FPEM based observer is presented.

Chapter 4

Detection of Cyclic Torque Imbalance

Output torque generated by the engine cylinder is required to be same for consecutive combustion cycles; nevertheless, variations occur in cyclic torque due to disturbances in the torque generation. Difference between work output of consecutive combustion cycles is considered as direct cause of cyclic torque imbalance. These variations manifest themselves as inconsistent output torque and effect engine fuel efficiency as well as exhaust emissions. Detection of cyclic torque imbalance is essential to develop control techniques for mitigation of imbalance in the cyclic torque. Torque imbalance detection is first step to formulate the proposed model based unified framework for detection and mitigation of cyclic torque imbalance. Variations in net piston force (f_n) provide a direct indication of imbalance in the cyclic torque and Unknown input observer (UIO) was used to estimate net piston force (f_n) as it cannot be measured directly.

In this chapter, detection of imbalance in cyclic torque is focused, which is caused due to faults in fuel injection subsystem, which are discussed in Section 4.1. UIO is discussed in Section 4.2, along with review of sliding mode based UIO. A brief overview of Sliding Mode Control (SMC) is presented in Section 4.3 to discuss basic concepts of SMC. In Section 4.4, FPEM based Uniform Second Order Sliding Mode

(USOSM) observer is derived for estimation of variations in net piston force (f_n) to detect cyclic torque imbalance. In Section 4.5, numerical simulation results of the proposed observer are presented for detection of cyclic torque imbalance by employing speed dynamics of GT-Power based engine model. Implementation of the observer is carried out under workshop conditions by operating the engine at steady state conditions. Summary of the chapter is presented in Section 4.6.

4.1 Fuel Injection Subsystem

Variations in injected fuel mass is one of the main causes of cyclic torque imbalance. Different causes of imbalance in the cyclic torque have been described in Subsection 2.2.2. However, faults in fuel injection subsystem are common cause of torque imbalance. Thus, in this research work faults in fuel injection are considered, assuming all other systems as fault free.

Fuel is delivered to the injector at predefined pressure by fuel supply subsystem to inject it directly into intake manifold or combustion chamber. Fuel is kept pressurized by fuel pump throughout the engine operation, which supply pressurized fuel to the cylinder from fuel tank. Fuel injection subsystem is kept free from particles and contamination by fuel filter. Generally, fuel is distributed to the injectors by fuel rails/lines, which also acted as storage to level out pressure and minimize pulses in fuel line. Fuel pressure is controlled by pressure regulator to keep it at predetermined value. Fuel injector and faults in fuel injection are discussed briefly in next subsections.

4.1.1 Working of Fuel Injector

During intake phase, fuel injector sprays desired fuel quantity into intake manifold or combustion chamber in the form of individual pulses. Fuel injector is used in almost all present day IC engines, irrespective of their type. Fuel injector regulate injected fuel mass and increase its surface area. Thus, it improves the heat transfer

from surrounding ambient to fuel droplets and consequently speeds up the mixture formation, which lead to more efficient chemical reaction [130].

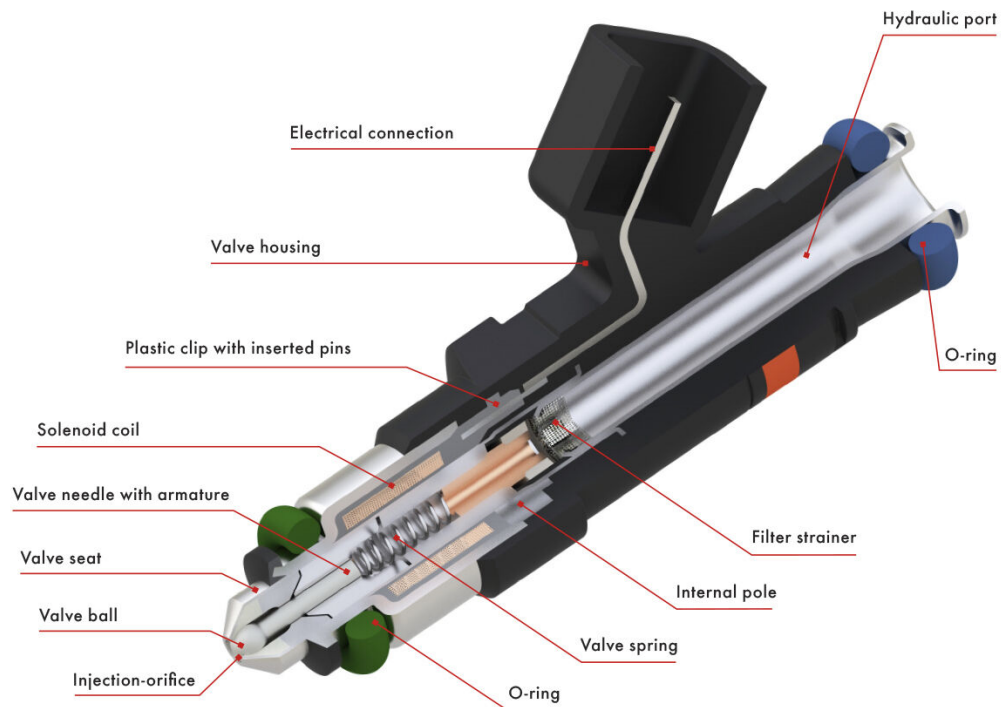


FIGURE 4.1: Cross Section View of the Fuel Injector

Cross section view of fuel injector is shown in Figure 4.1. Injection of fuel by the injector is controlled by ECU. Fuel pump passes pressurized fuel to the injector. Electric current governs movement of the valve arm through an induction coil, which allows pressurized fuel to periodically pass into final orifice disk. There are single or multiple outlet holes present in the orifice disk to discharge fuel at high velocity. Accurate control of injection pulse width, frequency response, reliability and durability are desired characteristics of the fuel injector.

Fuel injector is attached to throttle body or intake runner. Throttle body regulate air mass flow into intake manifold by varying throttle valve angle. Fuel injector is designed to generate fuel droplets as small as possible for better mixing with air that is induced in the engine cylinder. A set of sensors, which includes air flow, temperature and crankshaft position sensor are used to continuously pass the information about engine operating conditions to ECU. Switching mechanism

of the fuel injector is limited by the time that is required by electric current to develop required electromagnetic force in the coil to oppose spring force and move valve arm of the injector. An offset time between pulse trigger and flow lift off point is caused due to such delay. Thus, fuel delivery rate increases gradually during injection. Ratio of maximum to minimum duration of fuel injection is called “*dynamic range of the injector*”. Engine speed determine the maximum duration for which fuel is required to be injected; whereas, minimum duration is decided by injector design [131].

Type of Faults		Components			
		Mechanical Components	Electrical Components	Electronic Hardware	Software
Form	Systematic	√		√	√
	Random		√	√	
Time Behavior	Permanent			√	√
	Transient	√	√	√	
	Intermittent		√	√	√
	Noise		√	√	
	Drift	√	√	√	
Extent	Local	√	√	√	√
	Global			√	√

FIGURE 4.2: Type of System Faults [132]

4.1.2 Faults in Fuel Injection Subsystem

Variations in injected fuel mass are caused due to different faults. Usually faults show a regular behavior for different components of the system. Faults can be differentiated by their extent, form and time behavior. The *form* of the fault can be either systematic or stochastic. The *time behavior* is described by transient, intermittent and permanent nature of the fault. Stochastic faults are applied to the system hardware components and caused by physical degradation, such as thermal stresses, corrosion and wear of the component. Statistical information

can be measured of such faults from historical data due to its random nature. On the other hand, systematic faults are produced during system development or operations due to human error. These faults could be generated during a systems life cycle that includes design, specification, development, operation and maintenance. Until cause of a systematic fault is not removed, it could always occur under certain conditions. Few type of system faults are summarized in Figure 4.2.

In fuel injection subsystem, systematic faults are caused due to error in specifications i.e., manufacturing tolerances, selection of incorrect pressure value for fuel pump designed or bug in ECU software. Whereas, stochastic faults are the one that occurs as result of wear or deterioration of system components. For fuel injection subsystem, stochastic faults include dirty fuel injector due to residue of fuel additives, clogged nozzles of the injectors, variable function of the solenoid valves, fluctuating injection pressure and leakage in fuel injection. Stochastic faults in fuel injection causes various snags that effect overall engine performance. Inconsistent engine power and uneven engine idling is caused due to dirty fuel injector. Misfire occur if fuel injector sprays less fuel due to dirty or clogged fuel injector; or does not inject fuel at all. Diminished fuel mileage is obtained due to fuel injector leakage or fault in solenoid valve function.

Stochastic faults effect run time performance of the engine and required to be mitigated immediately by applying control techniques. Such faults could cause under flow or over flow of the fuel injected in engine cylinder for each combustion cycle. In this research work, FTC techniques are formulated to mitigate cyclic torque imbalance to address such anomalies, that are generated during run time of the fuel injection.

4.2 Unknown Input Observer

UIO is a class of observer algorithms that is employed to estimate unmeasured inputs to a dynamic system from system states and output measurements. Such

observers are important for systems that are subjected to inaccessible inputs or disturbances. UIO has application in fault detection, identification as well as estimation of parameters and unknown input estimation.

Generally, UIO is designed for non-linear systems, given as follows:

$$\begin{aligned}\dot{x}(t) &= f(x(t)) + g u(t) + p d(t) \\ y(t) &= h(x(t))\end{aligned}\tag{4.1}$$

where, state vector is given as $x(t) = [x_1(t), x_2(t), \dots, x_n(t)]^T$, $u(t)$ is known input to the system; p , g are distribution vector of unknown and known inputs, respectively. System output is given as $y(t)$, whereas $f(x(t))$ and $h(x(t))$ represent non-linear functions that depends on state vector $x(t)$ and $d(t)$ represents unknown input to the system.

4.2.1 Review of Unknown Input Observers

Different approaches were used to design UIO for linear as well as nonlinear systems, which are briefly reviewed in this section.

For linear systems, many techniques for UIO design were found in the literature. Observer proposed in [133] was among the earlier work on UIO. This observer reconstructed all states of the linear system, despite existence of unknown inputs. However, proposed observer lacked systematic design guidelines. Inverse of multivariate systems was used in [134].

Observer design based on generalized inverse of the matrices, along with conditions for UIO existence was proposed in [135]. Another approach for observer design to estimate states of a linear system, that had known as well as unknown inputs was given in [136]. System equations were rearranged to remove unknown inputs from part of the system by use of algebraic expressions as well as system analysis. Linear system was divided into two subsystems, which were interconnected; whereas

one of the subsystems was driven by unknown input. This modification made it possible to apply Luenberger observer for state estimation.

For nonlinear systems, various techniques were also proposed for UIO design. In [137], an H_∞ reduced order observer was proposed to estimate both unknown inputs and state variables for uncertain nonlinear systems. In [138], high gain observer was proposed with multiple sliding modes to simultaneously estimate faults as well as states of the nonlinear system with Multi Inputs Multi Outputs (MIMO). In this observer, robust term tracked the fault signals and reconstructed it from respective sliding surface. Compared to other sliding mode observers, the proposed observer had less restrictive conditions for Lipschitz nonlinear systems.

In [139], an observer was proposed to simultaneously estimate unknown inputs and state variables of nonlinear systems. For estimation of unknown inputs, a set of cascaded high gain observers were designed for sequential reconstruction of unknown input without any prior information. In [140], design problem for UIO was discussed for the class of non-linear Lipschitz systems. It was demonstrated that with sufficient and necessary conditions, design problem of UIO is identical to find solution for an H_∞ optimal control problem; which satisfied all of the regularity assumptions. A dynamic framework was presented in [140], in which synthesis of Lipschitz UIO was given by using H_∞ optimization.

4.2.2 Unknown Input Observers based on Second Order Sliding Mode

Second Order Sliding Mode (SOSM) based observers have been applied for state estimation [141], parameter estimation [142] and detection of fault [143]. Identification of uncertainties can be performed with one filtering by using SOSM based observer. This feature has made SOSM based observers more suitable for estimation of system parameters, unknown inputs and fault detection. Also, complete system information and distribution of noise may not be required for SOSM based observer, which is compulsory for Kalman-filter based observers for estimation of

states and parameters [142]. SOSM based estimation techniques are computationally efficient that can be implemented online, as it does not require multiple matrix evaluation; that is required during prediction stage in Kalman-filter.

Fridman et.al., proposed an SOSM based observer in [144] for estimation of observable as well as unobservable states of MIMO systems with stable internal dynamics and unknown inputs. Unknown inputs can be asymptotically identified by using this observer. In [145], Floquet et.al., presented a step by step SOSM based observer for nonlinear systems, subjected to unknown inputs. Super Twisting Algorithm (STA) based observer was proposed, which has specific application to systems with observability singularities and hybrid systems. Structural matching condition was also derived to design the observer and reconstruction of unknown inputs.

In [146], Saif et.al., proposed a SOSM based observer for health monitoring and fault diagnosis of nonlinear systems. Among different uncertainties, unknown input was considered as one form of the uncertainty applied to the system; which can be estimated from the proposed observer. In [147], SMC based observer design was presented for multivariable linear systems with unknown inputs. It was proposed that condition of relative degree can be relaxed by combination of observer and exact differentiator, that are based on SMC. SOSM differentiator-based observer for nonlinear systems was discussed in [144]. System states and unknown inputs were estimated by proposed observer, whereas internal dynamics were assumed stable. SOSM based observer was presented for mechanical systems with uncertainty by Davila et al., in [148]. The proposed observer estimated the velocity by using measurements of the position. In addition to satisfy separation principle, finite time convergence of the observer was also established.

In [149], Cruz-Zavala et.al., proposed USOSM based observer that was extension of SOSM based observer, presented in [148]. Apart from finite-time convergence and exactness of the observer, convergence of the proposed observer was made *uniform* for any initial condition. Errors during observer application would reach at the origin; robustly and exactly. Also, time required for error convergence is bounded

uniformly above the observer initial conditions. Thus, USOSM observer was found more appropriate for detection of imbalance in the cyclic torque. USOSM observer was proposed for second order system; whereas, engine speed dynamics in FPEM was also described by a second order system. This system was represented by the states of engine angular position ($\omega_1(t)$) and rotational speed ($\dot{\omega}_1(t)$). Also, USOSM observer can be applied to estimate unknown input as uncertainty to the system.

4.3 Sliding Mode Control

SMC is a special form of Variable Structure Control (VSC), which apply discontinuous control signal to change dynamics of nonlinear as well as linear systems. Features of SMC, such as better convergence rate as well as robustness to system parametric variations, uncertainties and disturbances have given SMC based techniques a significant advantage as compared to other control techniques. SMC was introduced by V. Utkin in 1977 [150]. Since then, it has evolved into a topic of immense research in control theory and applied in many control applications.

Although, first order SMC has showed robustness to parameter uncertainties; however, it has exhibited significant chattering around sliding surface. SOSM has proved effective to reduce chattering, without compromising benefits of first order SMC. Another reason attributed to apply SOSM control based observers for unknown input estimation is utility of SOSM observers for the systems that have relative degree greater than one.

Observers based on SMC have valuable features, such as insensitivity to unknown inputs and utilization of equivalent output error injection as information source. Such features have made sliding mode observation techniques more suitable for estimation of unknown inputs. First order SMC has showed robustness with respect to external disturbances and parameter uncertainty. Presence of delays, especially delayed inputs within sliding mode can cause parametric uncertainty, which would

induce oscillations around sliding surface [151]. These oscillations are known as “chattering”, which have finite frequency and amplitude.

4.3.1 Design of Sliding Mode Control

Consider following affine nonlinear system:

$$\dot{x}(t) = f(x, t) + g(x, t)u(t) \quad (4.2)$$

where state vector is represented by $x(t) \in \mathfrak{R}^n$, system dynamics by $f(x, t) \in \mathfrak{R}^n$, control vector is given as $u(t) \in \mathfrak{R}^m$ and input dynamics are represent by $g(x, t) \in \mathfrak{R}^{n \times m}$. Also, each entry in $f(x, t)$ and $g(x, t)$ is assumed to be continuous with bounded continuous derivative with respect to $x(t)$.

Switched control $u_i(t) \in \mathfrak{R}^m$ in SMC has following form:

$$u_i(x, t) = \begin{cases} u_i^+(x, t) & \text{with } S_i(x) > 0 \\ u_i^-(x, t) & \text{with } S_i(x) < 0 \end{cases} \quad \forall i = 1, 2, \dots, m \quad (4.3)$$

where $S_i(x) = 0$ is i th sliding surface and given as:

$$S_i(x) = [S_1(x), S_2(x), \dots, S_m(x)]^T \quad (4.4)$$

In SMC design, system state variables are forced to reach a given manifold, known as “sliding surface”; shown in Figure 4.3. Set of relationships between system state variables define the sliding manifold. Original system “slide” along intersection of sliding manifold, whereas desired system dynamics are determined by designed manifold. On sliding surface, system states do not depend on system parameters and determined by sliding manifold. Thus, any perturbation to the system is rejected by SMC.

SMC design is comprised of two phases. In “reaching phase”, trajectories of system states are derived towards sliding manifold by application of appropriate control

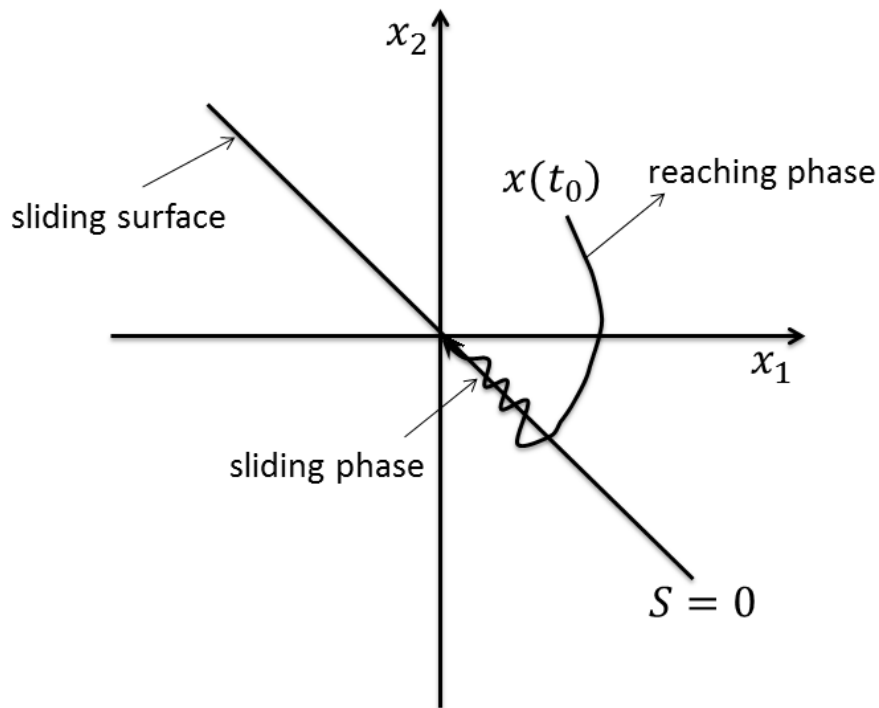


FIGURE 4.3: Phases of Sliding Mode Control

law, as shown in Figure 4.3. In “*sliding phase*”, trajectories of system states reach the sliding manifold by following prescribed constraints as system states slide to the equilibrium point, as displayed in Figure 4.3. The closed loop system become a reduced order system when it is confined to sliding manifold. At sliding surface, closed loop system is robust to external disturbances and matched uncertainties, that are within range space of the input $g(x, t)$. Design of sliding surface is important to obtain desired tracking characteristics and stability.

Usually, following two steps are required to design SMC based controller [152]:

- Sliding surface is defined in accordance with the control objective as well as required features of the closed loop system.
- Discontinuous control law is designed, which force trajectories of system states to reach sliding surface in finite time. Despite modeling uncertainties and external disturbances, states of the system stay on the sliding manifold.

Sliding surface design effect performance of the system. SMC consists of discontinuous and continuous part. The discontinuous part determines robustness of SMC; as it drive system states toward sliding surface under disturbances and modeling

uncertainty. Continuous part becomes more dominant than discontinuous part, when system states reach sliding surface and driven to the equilibrium point.

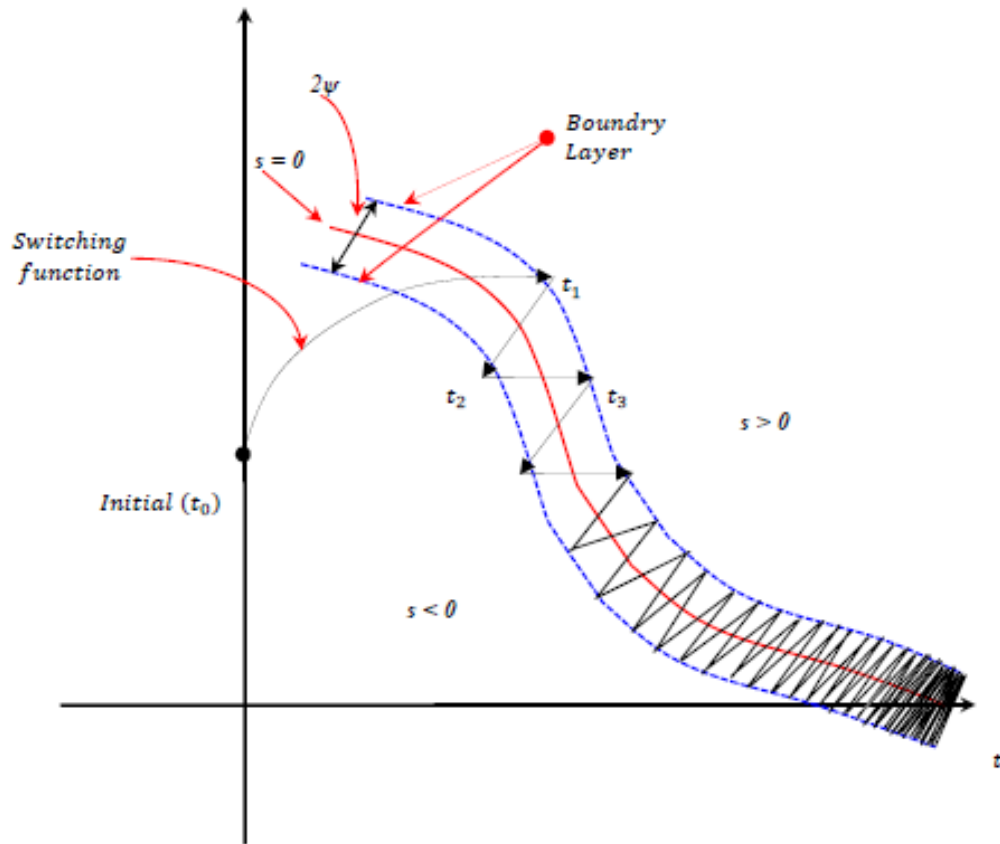


FIGURE 4.4: Chattering during Sliding Motion of the System

4.3.2 Chattering Phenomenon

Instead of infinite high gains in classical continuous control, SMC has discontinuous finite control action that has infinite frequency switching. Invariance of SMC is due to infinity frequency switching, which is impractical in real systems. The actuators have delays in practical electrical or mechanical systems, due to which control switching has finite frequency, which cause “chattering” in SMC, as shown in Figure 4.4.

Control accuracy is decreased due to chattering, which cause wear of moving parts in mechanical actuators and loss of heat in electrical power circuits. Unmodeled

high frequency dynamics of the system may also be excited by chattering, which degrade system performance and may lead to instability.

Different techniques were proposed to reduce chattering in SMC, which include equivalent control [153], Higher Order Sliding Mode (HOSM) [154], dynamic SMC [155], boundary layer [152] and saturation approximation [156]. Saturation approximation function is used in place of *signum function* to change sliding dynamics in near vicinity of discontinuous surface [152], as shown in Figure 4.5.

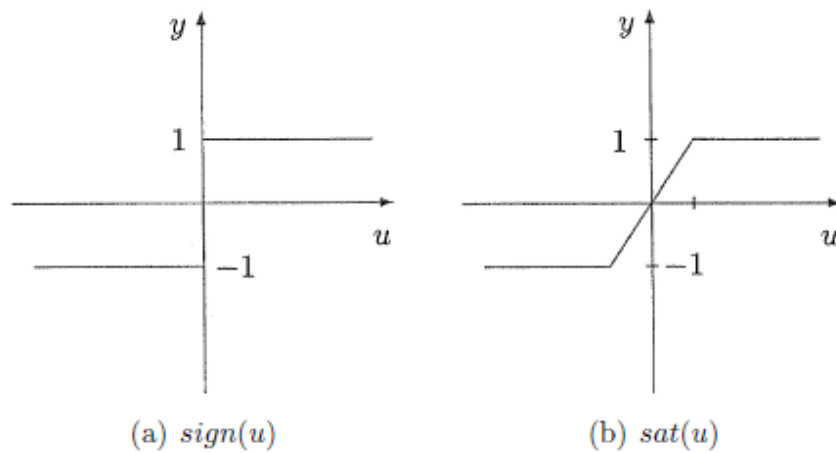


FIGURE 4.5: (a) Signum Function (b) Saturation Function [157]

This technique was extensively used to avoid chattering in many problems; as smooth transition is provided near switching surface. Saturation function can be described as:

$$\text{sat}(s, \psi) = \begin{cases} \text{sign}(s/\psi) & \text{for } |s/\psi| > 1 \\ s/\psi & \text{for } |s/\psi| \leq 1 \end{cases} \quad (4.5)$$

Decrease in chattering depends on $\psi \leq 1$. Chattering could be less at cost of robustness for smaller value of ψ .

4.3.3 Higher Order Sliding Mode

One of the effective methods to attenuate chattering is HOSM [158]. Apart from chattering, another constraint to use first order SMC is relative degree of the

system. Different sliding mode approaches were proposed to overcome such constraints, which include HOSM, dynamic SMC, terminal SMC and integral SMC. These techniques retained main concept of SMC and provided improved accuracy and reduced chattering.

Main concept of HOSM is to act on higher order derivatives of sliding surface to reach and remain on sliding manifold; instead of first order derivatives as in conventional SMC. Sliding variable and its higher time derivatives converges to equilibrium point as discontinuous control is applied on higher order derivatives of the sliding variable. Discontinuous control does not act directly on system input, which reduces the chattering. Apart from chattering reduction, HOSM relax the relative degree constraint; as it can be applied to the systems that have relative degree greater than one. In first order SMC and HOSM, infinitely high frequency switching of control signal provide exact tracking of constraint function. In HOSM, trajectories of system states move on discontinuous surface of closed loop system in Filippov's sense [159]. System trajectories reach the sliding surface vertically in first order SMC, as shown in Figure 4.6(a). In HOSM, chance for trajectories to leave the sliding surface are reduced as system trajectories reach the surface tangentially, as illustrated in Figure 4.6(b).

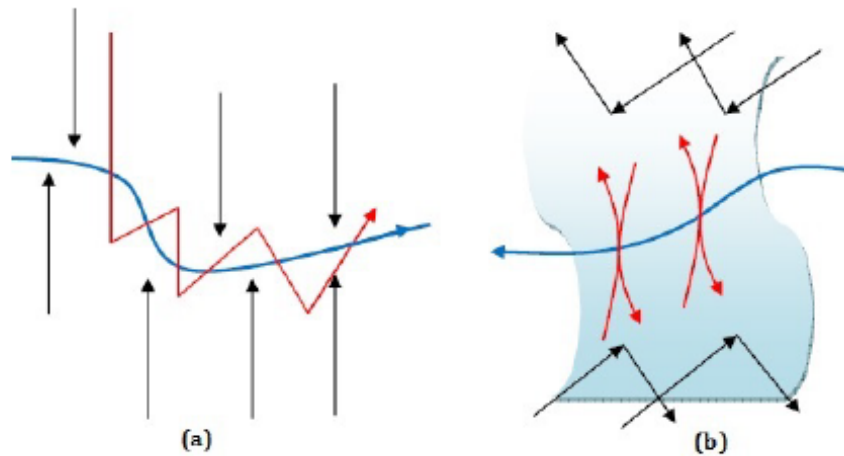


FIGURE 4.6: System Trajectories on Sliding Surface
 (a) First Order SMC (b) HOSM

Among HOSM, most frequently applied technique is SOSM based algorithms, which have lower information demand and simple to use. Real Twisting Algorithm

(RTA), hybrid 2-sliding algorithm, drift algorithm and STA are few variants of SOSM, which ensure finite time convergence of trajectories of the system to sliding surface i.e., $S = \dot{S} = 0$.

4.3.4 Second Order Sliding Mode Algorithms

Objective of SOSM based algorithms is to keep the switching function and its first order derivatives on a certain manifold in state space of the closed-loop system. Usually, SOSM is applied to reduce chattering and design control techniques for the systems that have relative degree two with respect to its output constraint function; while zeroing output of the systems that have relative degree one. RTA and STA are most commonly used SOSM algorithms.

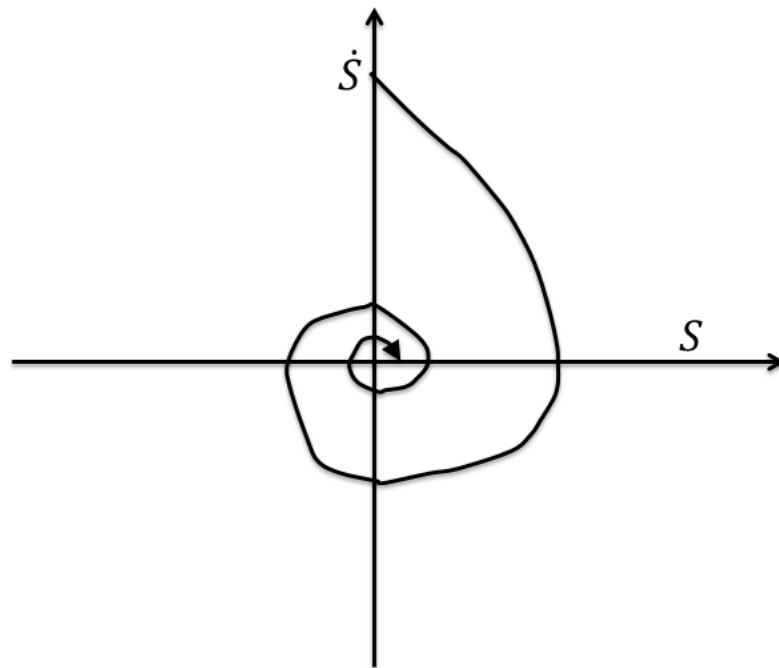


FIGURE 4.7: Real Twisting Algorithm

4.3.4.1 Real Twisting Algorithm

The first known SOSM technique is RTA [158]. In RTA, trajectories of the system twist around the origin of second order sliding surface and converge to it in finite time, as shown in Figure 4.7.

RTA provide better robustness than first order SMC and can be applied to the systems that have relative degree one as well as two. For implementation, RTA require measurement of first order derivatives of the sliding variable. Also, sensitivity to sampling time is another limitation of RTA. For relative degree one systems, control law is mentioned as follows [158]:

$$\dot{u} = \begin{cases} -u & \text{if } |u| > 1 \\ -\mu_m \text{sign}(S) & \text{if } S\dot{S} \leq 0; |u| \leq 1 \\ -\mu_M \text{sign}(S) & \text{if } S\dot{S} > 0; |u| \leq 1 \end{cases} \quad (4.6)$$

where,

$$\begin{aligned} \mu_M &> \mu_m > 0 \\ \mu_M &> \frac{4K_M}{S_0} \\ \mu_m &> \frac{C_0}{K_m} \\ K_m\mu_M - C_0 &> K_M\mu_m + C_0 \end{aligned}$$

The sign of sliding variable \dot{S} is required at each axis crossing to compute \dot{u} . The $\text{sign}(\Delta S)$ replaces $\text{sign}(\dot{S})$ if \dot{S} is not accessible. Thus,

$$\Delta S = S(t) - S(t_i - t_{i-1}) \quad \text{and } t \in [t_i - t_{i-1}]$$

Eq. (4.6) can be expressed as:

$$\dot{u} = \begin{cases} -u & \text{if } |u| > 1 \\ -r_1 \text{sign}(S) - r_2 \text{sign}(\dot{S}) & \text{if } |u| \leq 1 \end{cases} \quad (4.7)$$

where,

$$\begin{aligned} r_1 &> r_2 > 0 \\ \mu_M &= r_1 + r_2 \end{aligned}$$

$$\mu_m = r_1 - r_2$$

For systems with relative degree 2, control law can be expressed as:

$$\dot{u} = \begin{cases} -K_m \text{sign}(S) & \text{if } |u| > 1 \\ -K_M \text{sign}(S) & \text{if } |u| \leq 1 \end{cases} \quad (4.8)$$

where K_m and K_M are controller gains.

4.3.4.2 Super Twisting Algorithm

Trajectories of system states twist around the origin of second order sliding manifold in STA, as shown in Figure 4.8 and converge to the origin within finite time. Compared to other SOSM techniques, derivatives of sliding variable are not required in STA. Also, this algorithm is not sensitive to sampling time interval and can be applied to systems that have relative degree one. STA has displayed robustness and finite time convergence beside reducing the chattering.

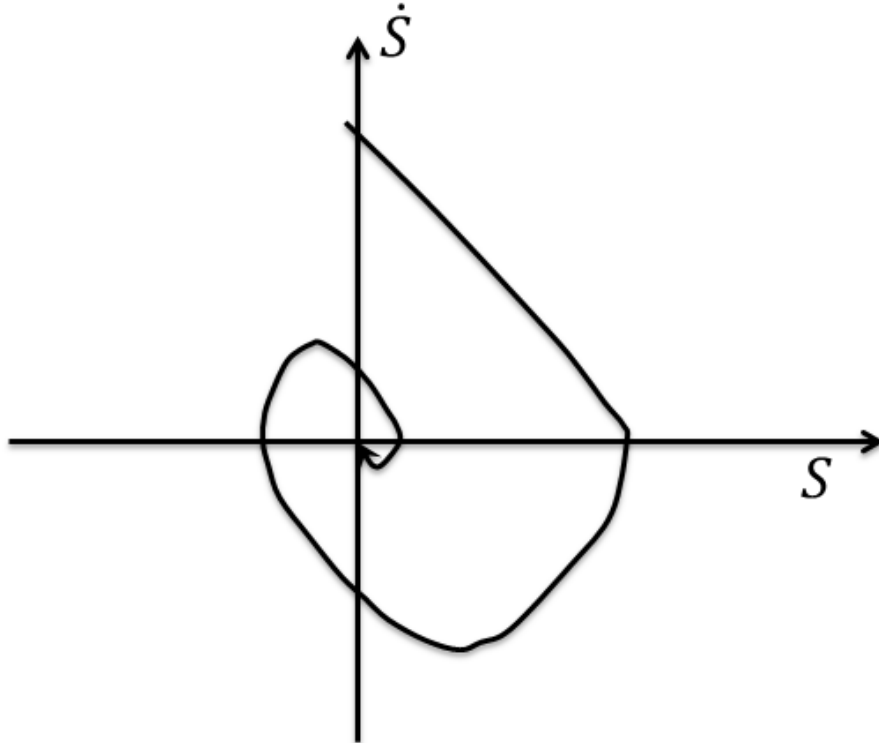


FIGURE 4.8: Super Twisting Algorithm

STA control law is combination of two terms. First term is continuous function of sliding variable, whereas second term contains integral of discontinuous function of sliding variable. STA is expressed as follows [158]:

$$\bar{u} = u_a(t) + u_b(t) \quad (4.9a)$$

$$u_a(t) = \begin{cases} -k_1 |S_0|^\rho \text{sign}(S) & |S| > |S_o| \\ -k_1 |S|^\rho \text{sign}(S) & |S| \leq |S_o| \end{cases} \quad (4.9b)$$

$$\dot{u}_b(t) = \begin{cases} -\bar{u} & |\bar{u}| > 1 \\ -k_2 \text{sign}(S) & |\bar{u}| \leq 1 \end{cases} \quad (4.9c)$$

For finite time convergence, essential conditions are expressed as follows:

$$\begin{aligned} k_2 &> \frac{\Phi}{\Gamma_m} \\ k_1^2 &\geq \frac{4\Phi \Gamma_M (k_2 + \Phi)}{\Gamma_m^2 \Gamma_m (k_2 - \Phi)} \\ 0 &< \rho \leq 0.5 \end{aligned} \quad (4.10)$$

where k_1 , k_2 , Γ_M , Φ , Γ_m are positive constants [158].

Another variant of STA is Smooth Super Twisting Algorithm (SSTA), that produce control action with reduced chattering and effective in many applications. SSTA based robust speed tracking technique is also proposed in this research work, which is discussed in Chapter 6.

4.4 FPEM based USOSM Observer

Derivation of FPEM based USOSM observer for detection of cyclic torque imbalance is described in this section [118, 123]; which is pre-requisite to develop the control techniques for mitigation of imbalance in the cyclic torque. Usually, estimation of engine output torque and cylinder pressure were carried out to detect cyclic torque imbalance, instead of direct estimation of net piston force (f_n); due to inadequacy in models of the gasoline engine, that has already been discussed

in Section 3.4. As already reviewed in Subsection 2.4.2; data driven methods, such as frequency domain approaches were mostly employed to estimate indicated torque and in-cylinder pressure by using oscillations in engine speed, instead of model-based techniques.

4.4.1 Unknown Input Estimation using USOSM Observer

Instead of first order SMC based observers, use of SOSM based observer can aid to compensate the sensor delays by reducing the chattering. SOSM based observers have been reviewed in Subsection 4.2.2 and USOSM observer [149] is applied to achieve the desired objective, as input can be estimated by applying this observer.

For any initial condition, convergence of the USOSM observer is *uniform* as estimation error reaches the origin in finite time, robustly and exactly. Thus, for every initial condition, the convergence time is uniformly bounded.

Definition 4.1: Any system can be termed *uniformly convergent* with respect to initial conditions, if for any initial condition the time required for convergence to a compact set that contain the origin is bounded by same constant for the trajectories of the system.

Definition 4.2: Any system can be termed *uniformly exact convergent* with respect to initial conditions, if from any initial condition the time required for convergence to a compact set that contain the origin is bounded by same constant for every trajectory of the system.

Apart from state estimation, SOSM observers have been employed for estimation of unknown inputs, system parameters and fault diagnosis due to its inherent feature of uncertainty identification.

Sliding mode-based observers have following distinct features [160, 161]:

- Insensitive with respect to unknown inputs.
- Unknown input, parameter and fault can be reconstructed by using the equivalent output injection.

USOSM observer was proposed for second order systems. Apart from state estimation, USOSM observer can be applied for estimation of unknown input [149]. USOSM was extension of the SOSM observer that was mainly used for mechanical systems [148] and also applied for estimation of unknown input [162, 163]. The USOSM observer was employed to propose the estimation framework for detection of imbalance in the cyclic torque.

In the FPEM based USOSM observer, unknown input of net piston force (f_n) was treated as uncertainty and estimated from injection term z_2 . As sliding mode was achieved by the observer, the estimated states of engine speed dynamics converged to actual states and injection term Z_2 became equal to uncertainty, i.e. net piston force (f_n). Thus, proposed FPEM based USOSM observer was termed unknown input observer as it estimated the unknown input i.e. net piston force (f_n), with injection term z_2 as estimation term.

4.4.2 Relation between Generation of Cyclic Torque and Net Piston Force

Torque is tendency of a force to rotate about a point that is not on line of action of that force. It is also known as *moment of a force*. In IC engines, cyclic torque is generated as net piston force (f_n) acts on torque producing mechanism in the engine cylinder. Thus, net piston force (f_n) is a direct measure of cyclic torque that is produced by combustion cycles as engine output. Imbalance in the cyclic torque was generated as variations arise in net piston force (f_n), under identical input conditions. Relation of net piston force (f_n) with engine speed dynamics was given in Eq. (3.30c). Thus, imbalance in the cyclic torque was represented by above mentioned relation in FPEM.

Different causes of imbalance in the cyclic torque were described in Subsection 2.2.2.1. However, fault in fuel injection subsystem is one of the main causes of cyclic torque imbalance. Variations in net piston force (f_n) were induced by varying the injected fuel mass (m_{fi}), which caused imbalance in the cyclic torque.

Mathematical expression of injected fuel mass is shown in Eq. (4.11).

$$m_{fi} = \Delta_{fault} \times \frac{P_{man} \times (V_d + V_c)}{AFR \times R \times T_{man}} \quad (4.11)$$

where, Δ_{fault} represented fault in fuel injection which could increase or decrease fuel mass injected per combustion cycle (m_{fo}). The value of Δ_{fault} remains between 0 and 1; where, $\Delta_{fault} = 1$ represented no fault in fuel injection and $\Delta_{fault} = 0$ represented complete failure of fuel injection subsystem. As a result of Δ_{fault} , fuel mass injected per combustion cycle (m_{fo}) was increased or decreased. In Subsection 5.2.4, FPEM was transformed to drive the relation between net piston force (f_n) and fuel mass injected per combustion cycle (m_{fo}), given in Eq. (5.10).

4.4.3 Observer Design

The proposed framework for torque imbalance detection is shown in Figure 4.9. FPEM based USOSM observer was employed for estimation of net piston force (f_n), which was assumed as unknown input to engine speed dynamics. Imbalance in the cyclic torque was generated by variations in the net piston force (f_n). The fuel mass injected per combustion cycle (m_{fo}) was reduced to cause variations in the net piston force. The proposed framework for detection of cyclic torque imbalance was implemented by using speed dynamics of the GT-Power based engine model [123].

Rotational speed dynamics in FPEM can be described by a second order system, as given below:

$$\begin{aligned} \dot{\theta}_1 &= \omega_1 = h_1(x, t, u) \\ \dot{\omega}_1 &= \mathbf{g}_1(\theta_1(t)) \omega_1^2 + \mathbf{g}_2(\theta_1(t)) \tau_N + \mathbf{g}_3(\theta_1(t)) f_n = h_2(x, t, u) \end{aligned} \quad (4.12)$$

Net torque (τ_N) was assumed as known input and net piston force (f_n) was taken as unknown input to engine speed dynamics. Net torque (τ_N) is the sum of load torque and frictional torque. States of engine speed dynamics were defined as

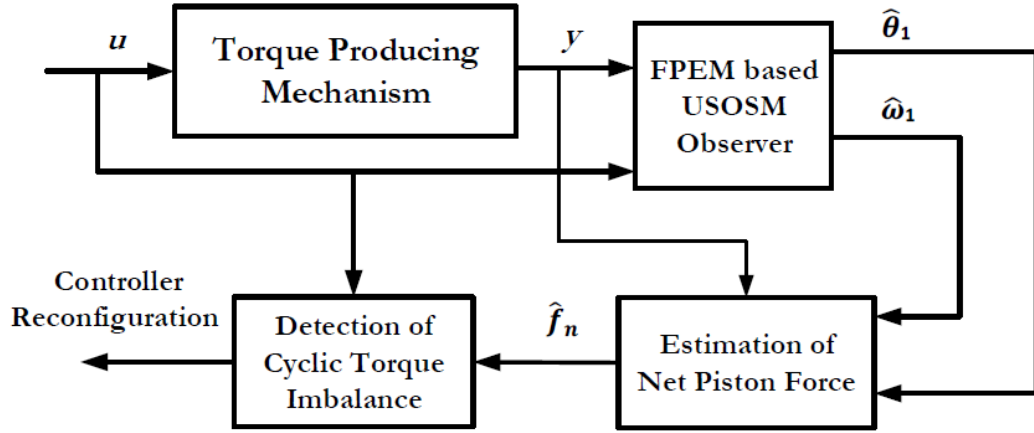


FIGURE 4.9: Proposed Framework for Detection of Cyclic Torque Imbalance

$x = ([x_1, x_2])^T = ([\theta_1, \omega_1])^T$; whereas, engine angular position (θ_1) was taken as output of the system.

Based on state redefinition, engine speed dynamics in Eq. (4.12) can be expressed by following generalized expression:

$$\begin{aligned} \dot{x}_1 &= x_2 \\ \dot{x}_2 &= h(t, x, u) + \xi(t, x, u) d(t) \\ y &= x_1 \end{aligned} \quad (4.13)$$

where, $x \in \mathfrak{R}^n$ is system states vector, $u = (\tau_N, f_n) \in \mathfrak{R}^m$ is control input to engine speed dynamics, $y \in \mathfrak{R}^r$ represent system output and $\xi \in \mathfrak{R}^q$ is unknown input dynamics.

Eq. (4.13) is the standard state space form of the second order systems for application of the USOSM observer as described in [149]. In Eq. (4.13), known nonlinear dynamics of the engine along with known input were represented by:

$$h(x, t, u) = \mathbf{g}_1(\theta_1(t)) \omega_1^2 + \mathbf{g}_2(\theta_1(t)) \tau_N \quad (4.14)$$

whereas, unknown input along with associated dynamics was assumed as uncertainties:

$$\xi_1(t, x, u) = \xi(t, x, u) d(t) = \mathbf{g}_3(\theta_1(t)) f_n \quad (4.15)$$

Dynamics of $h(x, t, u)$ and $\xi_1(t, x, u)$ were Lebesgue-measurable in a compact region of system states x . States of engine speed dynamics were non-zero under steady-state conditions.

Based on the observer in [149], following observer was employed for estimation of states and extraction of unknown input:

$$\begin{aligned}\dot{\hat{\theta}}_1 &= \hat{\omega}_1 + k_1 z_1(e_1) \\ \dot{\hat{\omega}}_1 &= \mathbf{g}_1(\theta_1(t)) \hat{\omega}_2^2 + \mathbf{g}_2(\theta_1(t)) \tau_N + k_2 z_2(e_1)\end{aligned}\quad (4.16)$$

where estimated state variables for engine angular position and rotational speed were represented as $\hat{\theta}_1, \hat{\omega}_1$.

Errors in estimation of engine speed states were expressed as $e_1 = \theta_1 - \hat{\theta}_1$ and $e_2 = \omega_1 - \hat{\omega}_1$. Observer gains k_1, k_2 were required to be designed, whereas output injection terms $z_1(e_1), z_2(e_1)$ were based on STA.

Both injection terms z_1 and z_2 acted to remove the estimation error between actual states θ_1, ω_1 and estimated states $\hat{\theta}_1, \hat{\omega}_1$ of the system. Based on [149], the injection terms with $\beta_1 \geq 0$ and $\beta_2 \geq 0$ were defined as follows:

$$\begin{aligned}z_1(e_1) &= \beta_1 |e_1|^{\frac{1}{2}} \text{sign}(e_1) + \beta_2 |e_1|^{\frac{3}{2}} \text{sign}(e_1) \\ z_2(e_1) &= \frac{\beta_1^2}{2} \text{sign}(e_1) + 2\beta_1 \beta_2 e_1 + \frac{3}{2} \beta_2^2 |e_1|^2 \text{sign}(e_1)\end{aligned}\quad (4.17)$$

When $\beta_1 = 1$ and $\beta_2 = 0$, then SOSM observer proposed in [148] is obtained. Values of $\beta_1 = 1$ and $\beta_2 = 1$ were chosen for the observer design.

Engine angular position (θ_1) can be measured by crankshaft position sensor. Based on measured and estimated values of engine angular position; estimation error (e_1) was calculated.

Theorem 4.1: Observer gains k_1, k_2 are chosen to satisfy either of the inequalities, given in Eq. (4.18) or (4.19), where ρ is known positive constant, such that $|H(t, \theta_1, \omega_1, \hat{\omega}_1)| \leq \rho/2$. Such selection of k_1 and k_2 ensured convergence of $\hat{\theta}_1$ to θ_1 in finite time and made the system in Eq. (4.13) uniformly, exact convergent.

$$k_1^2(k_2 - \frac{1}{4}k_1^2) > \rho^2 \quad ; \quad 2k_2^2 > k_1^2 \quad (4.18)$$

or

$$k_2 > \rho \quad ; \quad k_1^2 > 2k_2 \quad (4.19)$$

Remark 4.1: Selection of k_1 and k_2 depended on uncertainty bound. It also depended on initial value of position estimation error (e_1), whereas $|H(t, \theta_1, \omega_1, \hat{\omega}_1)|$ was bounded for engine speed dynamics. Based on values of $|\{\mathbf{g}_1(\theta_1(t))\omega_1^2 + \mathbf{g}_2(\theta_1(t))\tau_N\}|$ and $|\{\mathbf{g}_1(\theta_1(t))\hat{\omega}_1^2 + \mathbf{g}_2(\theta_1(t))\tau_N\} + \mathbf{g}_3(x_1)f_n|$, a positive value ρ was calculated.

4.4.4 Observability

Definition 4.3: A system is called observable if there exist a finite $t_1 > 0$ for any unknown initial state $x(0)$, such that input u as well as output y information over the interval $[0, t_1]$ are sufficient to obtain initial state $x(0)$ [164].

Assumption 4.1: The nonlinear system in Eq. (4.12) is termed observable if following rank condition of observability matrix (J_o) is satisfied by the given system and observability matrix (J_o) does not lose the rank i.e. $|J_o| \neq 0$. This observability matrix is also called Jacobian matrix.

$$\text{rank}(J_o) = \text{rank} \left[\frac{\partial f_i}{\partial x_j} \right] = n \quad (4.20)$$

where, $i = 1, 2, \dots, n$, $j = 1, 2, \dots, n$ [164].

For engine speed dynamics in Eq. (4.12), the observability matrix in Eq. (4.20) can be written as following:

$$J_o = \begin{bmatrix} \frac{\partial h_1}{\partial x_1} & \frac{\partial h_1}{\partial x_2} \\ \frac{\partial h_2}{\partial x_1} & \frac{\partial h_2}{\partial x_2} \end{bmatrix} \quad (4.21)$$

or

$$J_0 = \begin{bmatrix} 0 & 1 \\ -0.898 & \frac{\partial h_2}{\partial x_2} \end{bmatrix} \quad (4.22)$$

The engine was operated under steady state conditions to evaluate the observability condition. Rotational speed of the engine was taken as 110 rad/sec , load torque (τ_L) was taken as 34.5 Nm and net piston force (f_n) was 25 kN .

The Jacobian matrix (J_o) was solved in *Mathematica* and found full ranked under above mentioned conditions, as $|J_0|$ was not equal to zero:

$$|J_0| = 0.898 \neq 0 \quad (4.23)$$

Thus, engine speed dynamics was found observable in nature and USOSM observer can be designed for it. It was assumed that given system is differentially flat, which satisfied definition 4.4.

Definition 4.4: A system is termed flat, if any of its parameter, state or input can be expressed as a function of flat outputs as well as its derivatives, up to some finite order. Any flat output component can be expressed as function of system variables and its derivatives up to some finite order.

Most of chemical and mechanical systems exhibit the flatness property. In [165], flatness for the class of nonlinear and linear systems was discussed using differential algebra.

4.4.5 Boundedness Analysis

A gasoline engine that is equipped with ECU operates under bounded input ($\alpha < 90^\circ$), such that engine speed dynamics also remain bounded. Such system is characterized as Bounded Input and Bounded Output (BIBO) system. Thus, uncertain function $\xi_1(t, x, u)$ in Eq. (4.15) along with its time derivative remain bounded by positive numbers ξ_1^+ and $\delta\xi_1^+$, respectively. Convergence of the proposed observer is ensured by boundedness of engine speed dynamics.

Definition 4.5: If h^+ and δh^+ are two positive numbers $\forall x, \forall t \in \mathfrak{R}^+$ and $u < u^+$ for the system expressed in Eq. (4.13), such that the given system satisfy following relations, then it is assumed as bounded in nature.

$$\begin{aligned} |h(t, x, u)| &< h^+ \\ \left| \frac{dh(t, x, u)}{dt} \right| &< \delta h^+ \end{aligned} \quad (4.24)$$

Assumption 4.2: The known function $h(x) = [h_i(x_1, x_2, \dots, x_i)]$ was considered bounded with respect to its arguments. It was also assumed as global Lipschitz function with respect to x .

Assumption 4.3: It was considered that unknown input to the system was bounded as $|d(\cdot)| \leq \bar{d}$.

4.4.6 Error Dynamics Analysis and Convergence

Error dynamics of the observer were given by [149]:

$$\begin{aligned} \dot{e}_1 &= -k_1 z_1(e_1) + e_2 \\ \dot{e}_2 &= -k_2 z_2(e_1) + H(t, \theta_1, \omega_1, \hat{\omega}_1) \end{aligned} \quad (4.25)$$

where

$$\begin{aligned} H(t, \theta_1, \omega_1, \hat{\omega}_1) &= \{\mathbf{g}_1(\theta_1(t)) \omega_1^2 + \mathbf{g}_2(\theta_1(t)) \tau_N\} \\ &\quad - \{\mathbf{g}_1(\theta_1(t)) \hat{\omega}_1^2 + \mathbf{g}_2(\theta_1(t)) \tau_N\} + \mathbf{g}_3(\theta_1(t)) f_n \end{aligned} \quad (4.26)$$

or

$$H(t, x, \hat{x}, u) = h_1(x, t, u) - h_1(\hat{x}, t, u) + \xi_1(x, t, u) \quad (4.27)$$

Convergence of proposed observer for engine speed dynamics, given in Eq. (4.16) was analyzed and it was assumed that $\forall \alpha < 90^\circ$, $\forall t \in \mathfrak{R}^+$ and $\forall x, \exists \chi_1$ and χ_2

which satisfy Assumption 4.4. Thus, estimation errors e_1 , e_2 remain bounded and converge to origin as estimated states become equal to actual states.

The error dynamics e_1 and e_2 reached the sliding surface recursively, one after the other. After convergence of the error e_1 to sliding manifold, dynamics of the error e_2 can be expressed as:

$$\dot{e}_2 = H(t, \theta_1, \omega_1, \hat{\omega}_1) - k_2 z_2 \quad (4.28)$$

As SOSM was established, term e_1 approached to zero and \dot{e}_1 vanished. It can be deduced that

$$\dot{e}_1 = e_2 - k_1 \bar{z}_1 \quad (4.29)$$

$$0 = e_2 - k_1 \bar{z}_1 \quad (4.30)$$

Thus, following relation was obtained from Eq. (4.29),

$$k_1 \bar{z}_1 = x_2 - \hat{x}_2 \quad (4.31)$$

As convergence of error e_1 was established; convergence of error e_2 was also ensured, i.e., $e_2 = 0$ and $\dot{e}_2 = 0$.

Following error dynamics were obtained from Eq. (4.28):

$$\dot{e}_2 = H(t, \theta_1, \omega_1, \hat{\omega}_1) - k_2 \bar{z}_2 \quad (4.32)$$

As error e_2 converged to zero, then $\dot{e}_2 = 0$.

Thus, Eq. (4.32) can be expressed as

$$0 = \xi_1(t, x, u) - k_2 \bar{z}_2 \quad (4.33)$$

or

$$\bar{z}_2 = \frac{\xi_1(t, x, u)}{k_2} \quad (4.34)$$

where

$$\xi_1(t, x, u) = \xi(t, x, u) d(t) = \mathbf{g}_3(\theta_1(t)) f_n \quad (4.35)$$

The unknown input was estimated as follows from Eq. (4.34) [118]:

$$\bar{z}_2 = \frac{\mathbf{g}_3(\theta_1(t)) f_n}{k_2} \quad (4.36)$$

or

$$\hat{f}_n = \frac{\bar{z}_2 k_2}{\mathbf{g}_3(\theta_1(t))} \quad (4.37)$$

Estimated value of net piston force \hat{f}_n can be extracted from Eq. (4.37) by applying the Low Pass Filter (LPF). Thus, the unknown input was reconstructed by using the equivalent output injection.

Remark 4.2: Term \bar{z}_1 and \bar{z}_2 were taken as LPF version of the injection terms z_1 and z_2 . First order LPF was applied to handle switching of discontinuous injection terms during estimation of unknown input. Phase lag was reduced by varying the time constant of LPF.

Assumption 4.4: It was assumed that two positive constants χ_1 and χ_2 exist such that

$$\begin{aligned} |h_1(x_1, x_2, t, u)| - |h_1(\hat{x}_1, \hat{x}_2, t, u)| &\leq \chi_1 |e_1| \\ \frac{d}{dt} |h_1(x_1, x_2, t, u)| - \frac{d}{dt} |h_1(\hat{x}_1, \hat{x}_2, t, u)| &\leq \chi_2 |e_2| \end{aligned} \quad (4.38)$$

Based on BIBO behavior of engine speed dynamics and Assumption 4.4; $\forall t \in \mathfrak{R}^+$ and $\forall x, \hat{x}$ as well as u , following relation was obtained:

$$\begin{aligned} |H(t, x, \hat{x}, u)| &< \chi_1 |e_1| + \xi_1^+ \\ \frac{d}{dt} |H(t, x, \hat{x}, u)| &< \chi_2 |e_2| + \delta \xi_1^+ \end{aligned} \quad (4.39)$$

where e_1, e_2 are errors in the estimation of angular position and rotational speed of the engine, $H(t, x, \hat{x}, u)$ represent the system dynamics; whereas, χ_1 and χ_2 are positive constant values.

4.5 Results and Discussions

4.5.1 MATLAB and GT-Power Co-Simulation Environment

Evaluation of the proposed FPEM based USOSM observer was performed by employing GT-Power based engine model [123]. It is pertinent to mention here that detection of cyclic torque imbalance was conducted under lab conditions. The engine was operated at steady state by keeping throttle valve angle and load torque at constant values. This scenario has been implemented in lab conditions using the “Active Diagnosis” [166], which recommend conducting the diagnosis under controlled environment. In active diagnosis, a problem is formulated in a manner to generate a sequence that enforce diagnosable action for iterative refinement of ambiguous diagnosis. Thus, system is manipulated in such a way that hidden faults are exposed for diagnosis. Also, known load torque is applied to the engine.

Following assumptions were made to implement the proposed observer for detection of cyclic torque imbalance.

1. All subsystems of the engine are fault free, except fuel injection subsystem.
2. Faults in fuel injection subsystem are not of extreme nature that may result in complete failure of the system.

Net piston force (f_n) was estimated by applying the proposed observer to detect imbalance in the cyclic torque. Engine speed dynamics were passed to *MATLAB*[®]-Simulink from GT-Power based engine model to estimate net piston force (f_n).

A systematic procedure was followed to estimate the unknown input i.e., net piston force (f_n). Outline of the procedure is as follows:

1. Data was acquired from GT-Power based model of the gasoline engine and passed to FPEM based USOSM Observer.
2. Convergence of FPEM based USOSM observer was ensured by selecting appropriate observer gains.

3. Estimation of the states of engine speed dynamics, i.e. engine angular position θ_1 and engine rotational speed ω_1 after convergence of FPEM based USOSM observer.
4. After convergence, injection term of the observer was used for estimation of the unknown input.

4.5.2 Imbalance Generation in Cyclic Torque

In IC engines, net piston force (f_n) is taken as unknown input that acts on torque producing mechanism to generate engine output torque. Estimation of net piston force was carried out by applying the proposed FPEM based USOSM observer in the co-simulation environment of *MATLAB*[®]-Simulink and GT-Power, as explained in previous section. No Variations existed in estimated net piston force (\hat{f}_n) as fault was not induced in fuel injection subsystem. Plot of estimated net piston force (\hat{f}_n) with no fault in fuel injection is shown in Figure 4.10. Whereas, magnified view of the estimated net piston force (\hat{f}_n) with no fault in fuel injection subsystem is shown in Figure 4.11.

Imbalance in cyclic torque is generated due to various causes, i.e. variations in the mass of inducted air, injected fuel or spark duration and energy. Out of which, fault in fuel injection subsystem is the most common cause of cyclic torque imbalance, which was considered in this research work. Such faults in fuel injection subsystem may increase or decrease the injected fuel mass. Variations in net piston force (f_n) were induced by varying the injected fuel mass injected (m_{fo}), that caused imbalance in the cyclic torque. Mathematical expression of injected fuel mass is shown in Eq. (4.40).

$$m_{fi} = \Delta_{fault} \times \frac{P_{man} \times (V_d + V_c)}{AFR \times R \times T_{man}} \quad (4.40)$$

where, Δ_{fault} represented fault in fuel injection which could increase or decrease fuel mass injected per combustion cycle (m_{fo}). The value of Δ_{fault} remains between 0 and 1; where, $\Delta_{fault} = 1$ represented no fault in fuel injection and $\Delta_{fault} = 0$

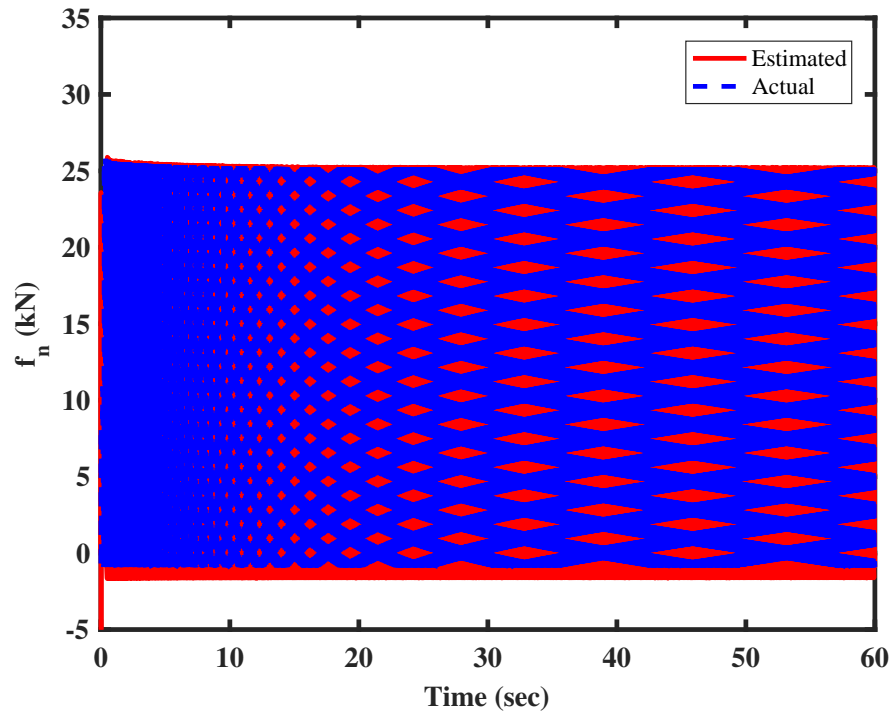


FIGURE 4.10: Estimated Net Piston Force (f_n) for Balanced Cyclic Torque Generation, ($\alpha = 7^\circ$, $\tau_L = 34.5 \text{ Nm}$, $P_{man} = 31 \text{ kPa}$ and $\omega = 110 \text{ rad/sec}$)

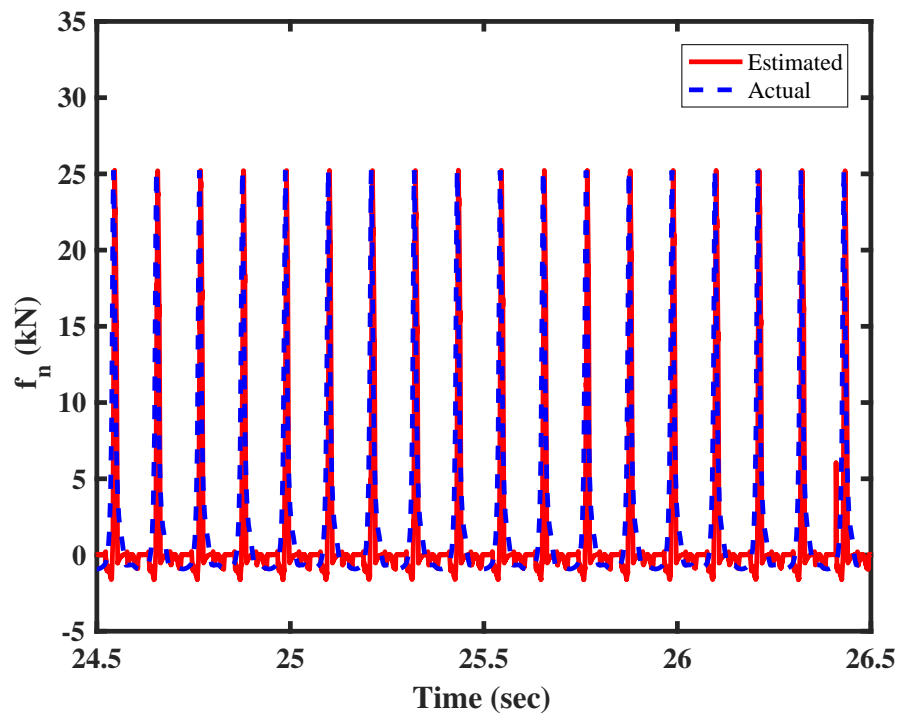


FIGURE 4.11: Magnified View of Estimated Net Piston Force (f_n) for Balanced Cyclic Torque Generation, ($\alpha = 7^\circ$, $\tau_L = 34.5 \text{ Nm}$, $P_{man} = 31 \text{ kPa}$ and $\omega = 110 \text{ rad/sec}$)

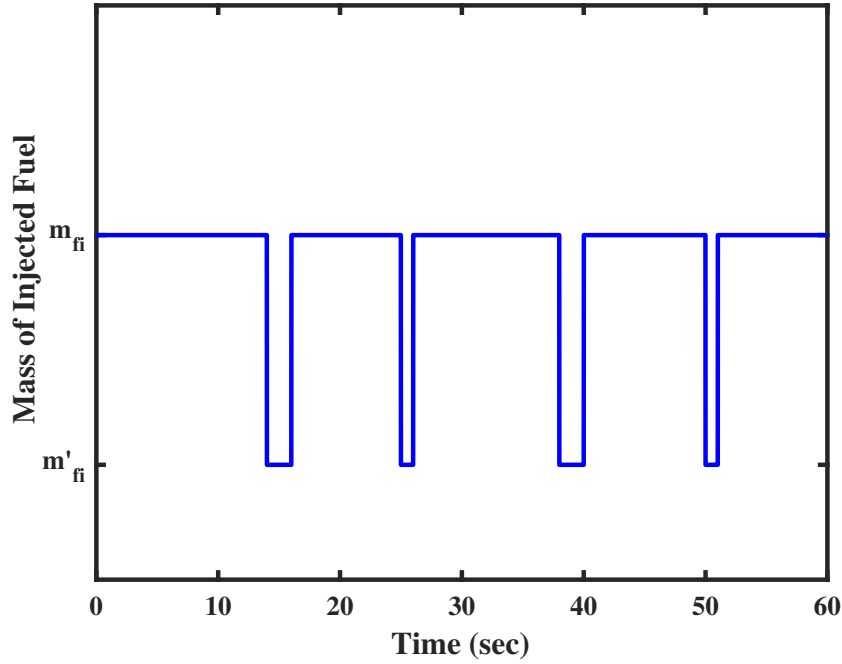


FIGURE 4.12: Fault Induced in Injected Fuel Mass, (m_{fi} is Injected Fuel Mass without Fault and m'_{fi} is Injected Fuel Mass with Fault)

represented complete failure of fuel injection subsystem. As a result of Δ_{fault} , fuel mass injected per combustion cycle (m_{fo}) was increased or decreased. In Subsection 5.2.4, FPEM was transformed to drive the relation between net piston force (f_n) and fuel mass injected per combustion cycle (m_{fo}), given in Eq. (5.10).

To generate cyclic torque imbalance at multiple instances, injected fuel mass was reduced by 20% of the desired fuel quantity that was required to be injected. Injected fuel mass was varied at 12 sec, 25 sec, 38 sec and 50 sec for duration of 2 sec, 1 sec, 2 sec and 1 sec, respectively. Plot of variations in injected fuel mass (m_{fi}) is shown in the Figure 4.12, where m_{fi} represented injected fuel mass when no fault was present in fuel injection subsystem and m'_{fi} represented injected fuel mass when fault was induced in fuel injection subsystem.

4.5.3 Detection of Cyclic Torque Imbalance

Estimated states of engine angular position and rotational speed converged to actual states as proposed observer attained sliding mode dynamics. Enlarged

view of engine angular position (θ_1) estimation is shown in Figure 4.13, whereas full plot of position estimation is shown in the inset. Convergence of $\hat{\theta}_1 \rightarrow \theta_1$ was essential for implementation of the proposed observer. Position estimation error (e_1) converged to the origin as estimated state of angular position $\hat{\theta}_1$ converged to actual position θ_1 , as shown in Figure 4.14.

Enlarged view of estimated engine rotational speed is shown in Figure 4.15 and full plot is shown in the inset. Speed Estimation error (e_2) converged to the origin as estimated state of rotational speed ($\hat{\omega}_1$) converged to actual speed (ω_1), as shown in Figure 4.16. Oscillations in engine rotational speed are modeled in FPEM, which were suppressed in MVEM due to analogy of volumetric pump to model torque producing mechanism. Analysis of oscillations in engine rotational speed can be significant for fault diagnosis and control [16].

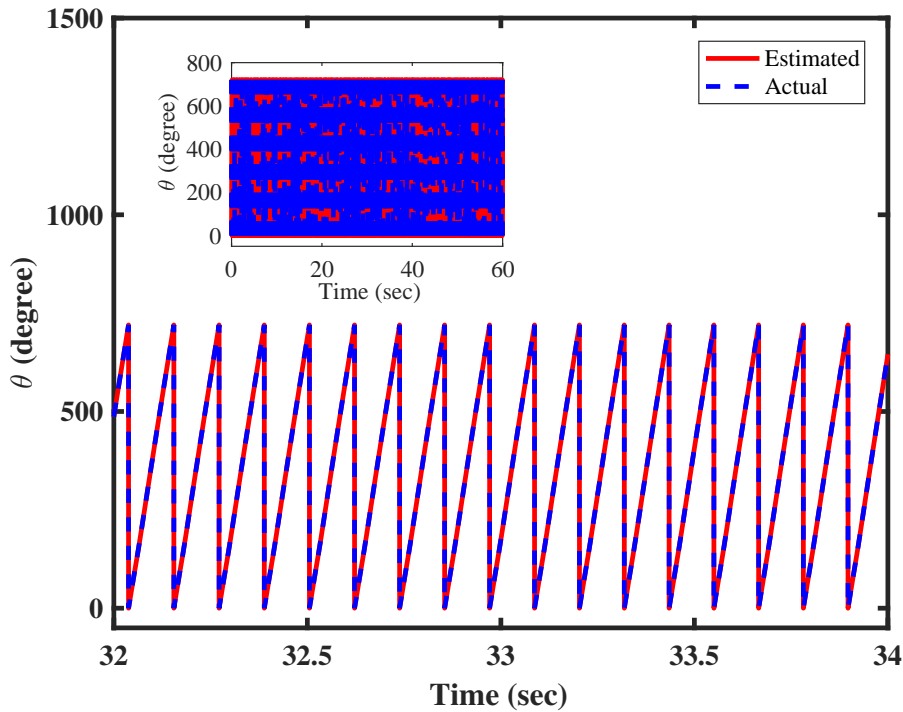


FIGURE 4.13: Estimation of Engine Angular Position (θ_1)

As estimated states $\hat{\theta}_1$, $\hat{\omega}_1$ converged to actual states θ_1 , ω_1 ; error in state estimation of engine speed dynamics converged to the origin. It demonstrated swift and exact convergence of estimated states to actual states. A surge was noted in estimation error at $t = 0$ as initial conditions were different for both models;

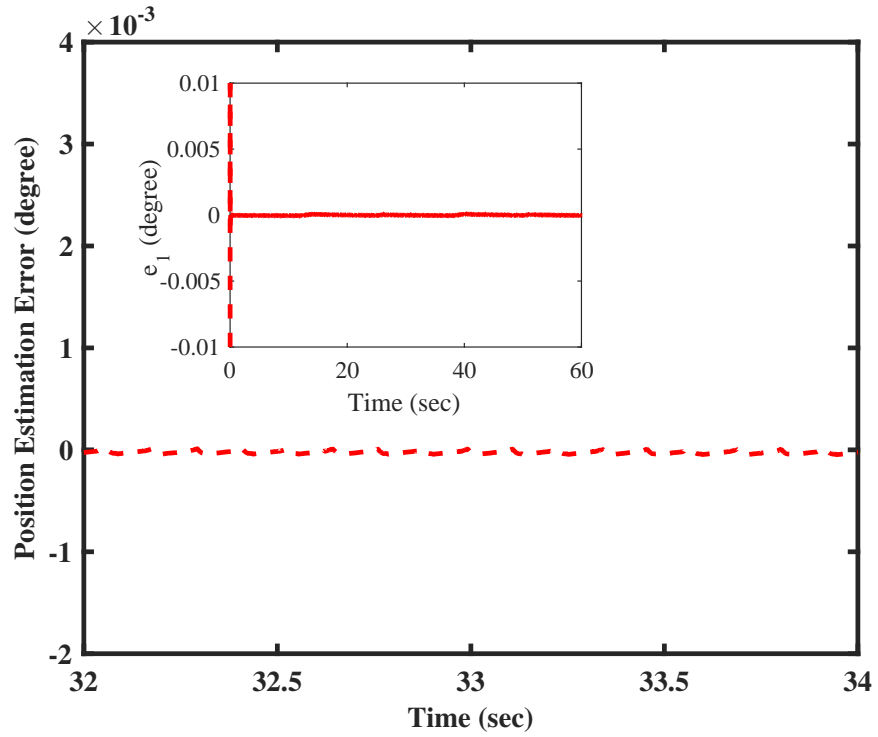


FIGURE 4.14: Error in Estimation of Engine Angular Position

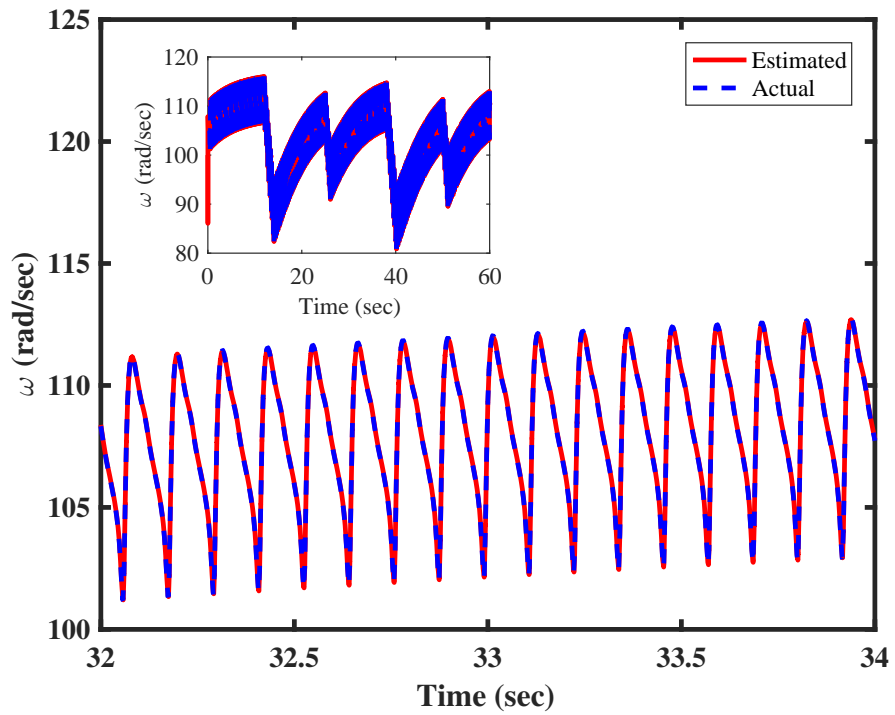


FIGURE 4.15: Estimation of Engine Rotational Speed (ω_1)

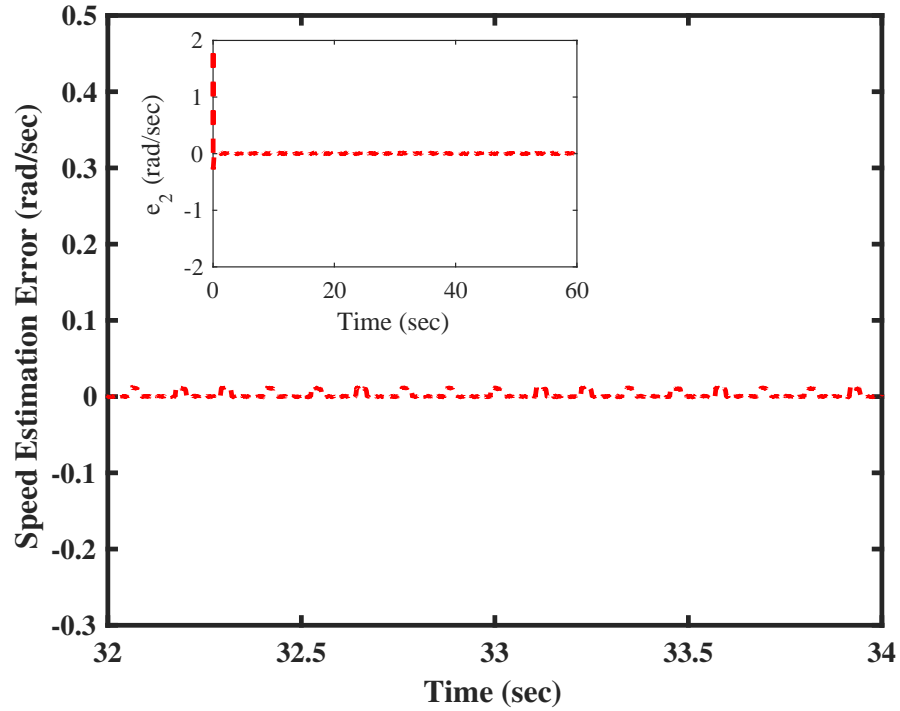


FIGURE 4.16: Error in Estimation of Engine Rotational Speed

however, estimated states converged to actual states in less than 0.03 sec. Also, as estimation errors converged to the origin i.e., $\hat{\theta}_1 \rightarrow \theta_1$ and $\hat{\omega}_1 \rightarrow \omega_1$; injection term (z_2) in the observer represented unknown input i.e., net piston force (f_n). Mean value of net piston force (f_n) was extracted from injection signal by using a LPF.

Both measured and estimated net piston force (f_n) are shown in Figure 4.17. Enlarged view of force estimation is shown in Figure 4.18, as cyclic torque imbalance occur at $t = 25$ sec. As evident in Figure 4.18, cyclic torque imbalance is detected as net piston force (f_n) vary in magnitude due to decrease in injected fuel mass.

Imbalance in the cyclic torque can be detected by comparison of estimated net piston force (\hat{f}_n) with no fault in fuel injection, shown in Figure 4.10, 4.11 with estimated net piston force (\hat{f}_n) with fault in fuel injection, shown in Figure 4.17, 4.18. Nominal values of net piston force (f_n) was acquired as 25 kN, as shown in shown in Figure 4.10 and 4.11. In gasoline engines, combustion variability of 10% has been considered within drivability limit [65, 167]. Thus, a threshold of $\pm 10\%$ variations around nominal values of net piston force was defined to detect imbalance in the cyclic torque, as shown in Figure 4.19.

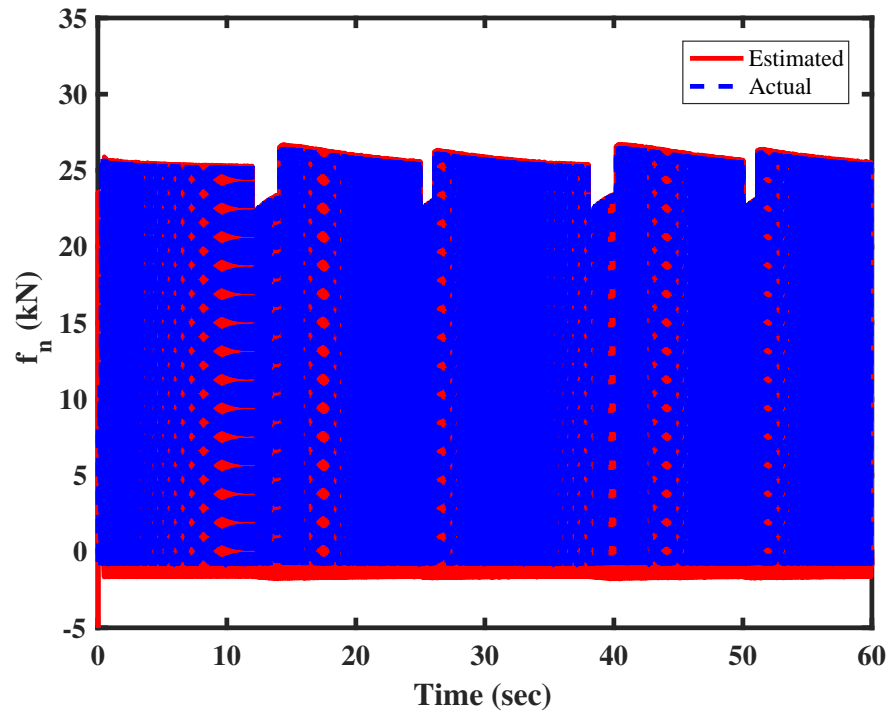


FIGURE 4.17: Estimated Net Piston Force (f_n) for Imbalanced Cyclic Torque Generation, ($\alpha = 7^\circ$, $\tau_L = 34.5 \text{ Nm}$, $P_{man} = 31 \text{ kPa}$ and $\omega = 110 \text{ rad/sec}$)

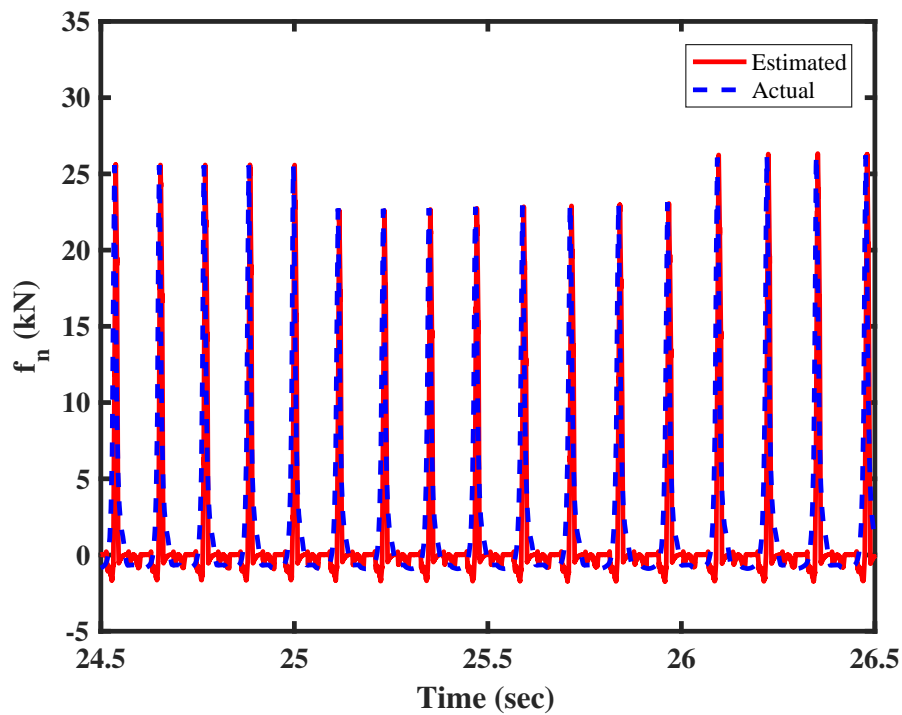


FIGURE 4.18: Magnified View of Estimated Net Piston Force (f_n) for Imbalanced Cyclic Torque Generation, ($\alpha = 7^\circ$, $\tau_L = 34.5 \text{ Nm}$, $P_{man} = 31 \text{ kPa}$ and $\omega = 110 \text{ rad/sec}$)

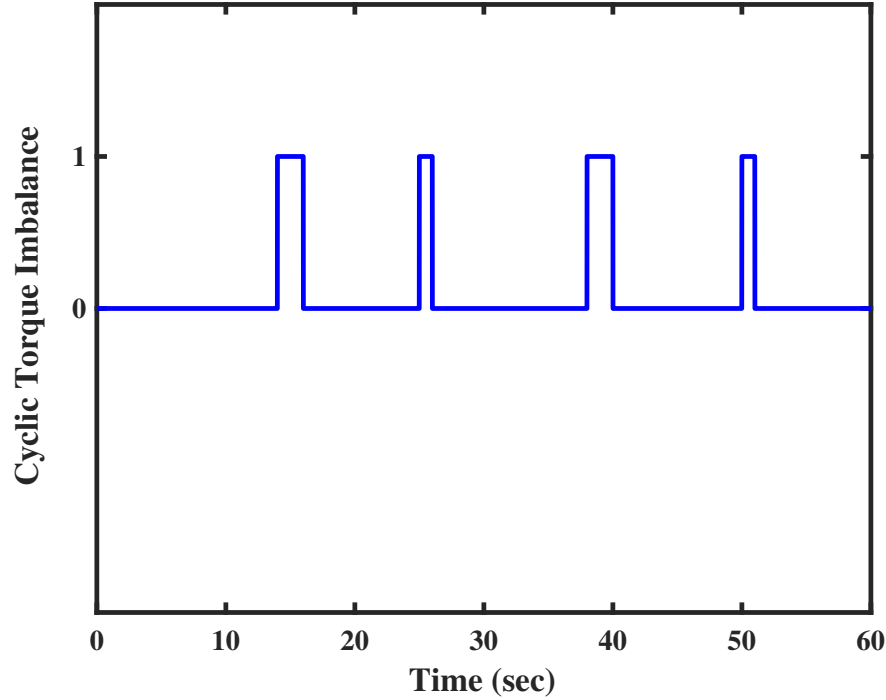


FIGURE 4.19: Detection of Cyclic Torque Imbalance

Estimation of net piston force (f_n) was attained close to actual values with nominal chattering by application of FPEM based USOSM observer. Also, significance of the observer is exhibited by the fact that it does not require any additional equipment. Evaluation of FPEM based USOSM observer for detection of cyclic torque imbalance had demonstrated its instantaneous and accurate performance. Detection of significant variations in cyclic torque of the engine cylinder warrants control of combustion inputs to mitigate torque imbalance and augment performance of the engine.

As discussed in Subsection 2.2.2.1, imbalance in the cyclic torque is generated due to various causes, i.e. variations in the mass of inducted air, injected fuel or spark duration and energy. However, faults in fuel injection subsystem is the most common cause that may increase or decrease the injected fuel mass (m_{fi}) and considered in this research work. Faults, such as clogging or leakage of fuel injector are expressed as % change in desired fuel mass and appear as step signal [66, 168]. whereas, dirty injector nozzle may show ramp or triangular shaped behavior of the faults in fuel injection subsystem. For comparison of fault shapes, triangular

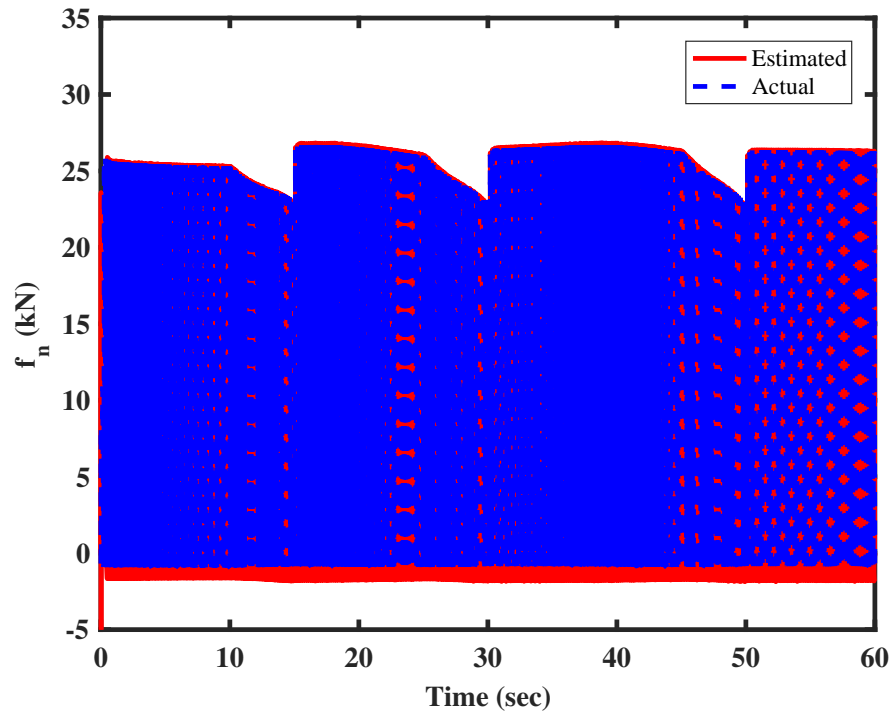


FIGURE 4.20: Estimated Net Piston Force (f_n),
(Triangular Shaped Fault in Fuel Injection)

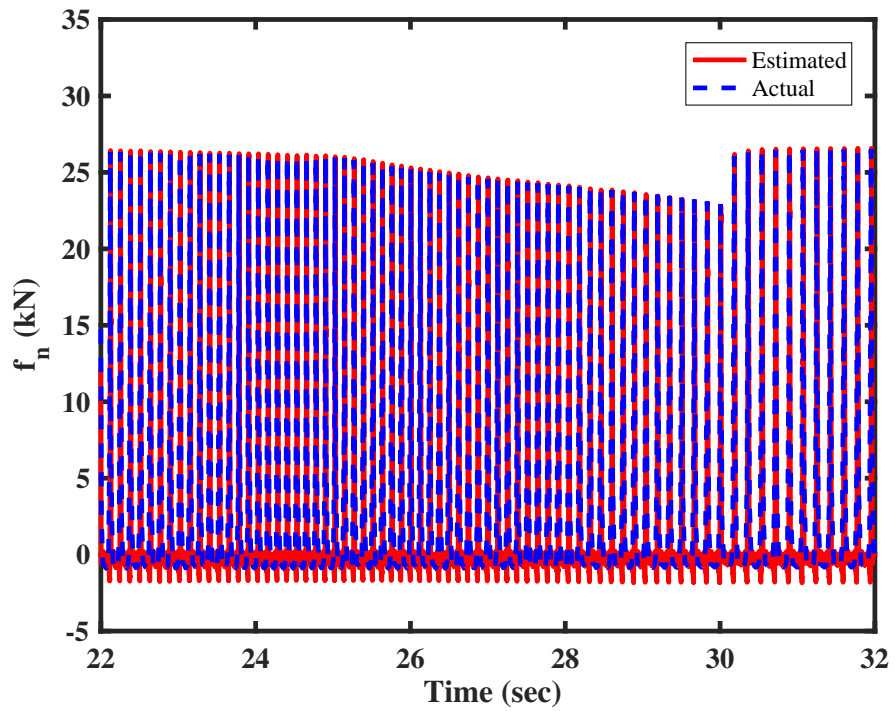


FIGURE 4.21: Magnified View of Estimated Net Piston Force (f_n),
(Triangular Shaped Fault in Fuel Injection)

shape faults have been induced and plots of estimated net piston force (f_n) have been added as Figure 4.20 and 4.21. It has been noted that variations in net piston force was not uniform when triangular shaped fault was induced. However, change in fault shape did not affect performance of the estimation framework as it accurately estimated net piston force (f_n) from engine speed dynamics.

4.6 Chapter Summary

In this chapter, FPEM has been employed to propose a framework for detection of cyclic torque imbalance. FPEM based USOSM observer has been proposed for estimation of net piston force (f_n) to detect imbalance in the cyclic torque from engine speed dynamics. Cyclic torque imbalance has been induced by varying injected fuel mass at multiple instances. Validation of the proposed observer has been carried out by employing GT-Power based engine model. Results of cyclic torque imbalance detection has showed efficacy of the proposed technique. However, this technique has been proposed for implementation under lab conditions. In the next chapter, estimation framework is extended to develop the unified framework for mitigation of cyclic torque imbalance during runtime of the vehicle and achieve degraded performance.

Chapter 5

Mitigation of Cyclic Torque Imbalance

Control systems have become an integral part in the advancement of IC engines with improved fuel efficiency and low exhaust emissions. It is a fundamental technology to enhance safety features in automotive vehicles, such as traction control, anti-lock braking system and active stability control. Moreover, control technology has also contributed toward enhancement of driving experience and comfort, such as air conditioning, active suspensions and cruise control systems.

In the last three decades, considerable research work was carried out to improve control systems of IC engines, which may enable to meet the evolving engine performance criteria. Advancement in the field of digital electronics during third industrial revolution, which is also termed as digital revolution, has influenced working and performance of IC engines. Implementation of complex control methodologies within a compact ECU has become possible due to progression in the field of embedded systems and electronics to achieve the desired performance objectives. Hence, development of automotive control technology parallels with advancement in the field of electronics, which made it possible to propose control techniques on a cycle resolved basis. Mitigation of imbalance in the cyclic torque is essential to

improve the engine performance and acquire uniform torque generation from all combustion cycles.

In previous chapter, detection of cyclic torque imbalance has been carried out under lab conditions. However, unified framework is proposed in this chapter to mitigate cyclic torque imbalance during runtime of the vehicle. It will ensure to achieve graceful performance degradation, in case of fault generation in fuel injection subsystem. Control law of proposed control techniques is designed to detect cyclic torque imbalance from sliding surface and reconfigure the controller accordingly.

In this chapter, two observer based FTC techniques are presented to mitigate imbalance in the cyclic torque. FTC is discussed briefly in Section 5.1. Observer based FTC design, besides assumptions for control design are given in Section 5.2. Transformation in FPEM is also described in this section to derive direct relation between engine speed dynamics and fuel input. Both observer based FTC techniques are presented in Section 5.3 and 5.4, respectively; along with controller structure, stability analysis, control law and numerical simulation results. Summary of the chapter is given in Section 5.5.

5.1 Fault Tolerant Control

In a dynamic system, “*fault*” is described as undesired divergence of at least one system characteristic parameter or property from the nominal range [169]. Sensor loss, actuator blockage or failure of a system component are some of the examples of fault in a system. Coherence between system components or between controller and system is changed by the fault. Thus, closed loop system performance is degraded by the fault, even it can cause complete failure of the system.

Detection, isolation and estimation of a fault are essential requirements to avoid system failure. Fault-tolerance is an important control methodology. It is designed to obtain sustainable performance of closed loop system, despite existence of single

or multiple faults in the system. A system is termed “*fault tolerant*”, if desired performance and stability indices are retained despite presence of faults. Such control technique that ensure fault tolerance in a system, is called “*Fault Tolerant Control*” [169]. Under faulty condition, fault tolerant systems may have performance degradation. However, main purpose of FTC is to keep system operations in acceptable range and provide required repair time to monitoring system.

Diagnosis of a fault and its tolerance are crucial components for safe operation of most applications. Based on intrinsic component properties and fabrication processes, electro-mechanical systems are always prone to faults during their operations. Unsupervised occurrence of a fault could lead to reduced reliability, loss of controllability and even fatal outcomes.

FTC has been an active research area that is motivated by requirement of high level of performance, reliability, availability and maintainability of the system to mitigate effects of a fault during its operations. For example, safety is of paramount importance in case of an airplane and automotive vehicle. Thus, system control must be able to withstand minor faults, otherwise it can lead to system failure. Similarly, for nuclear and chemical plants, results of an inapt control action for a component malfunction can be catastrophic. FTC is developed to keep a part of its control design for a specific fault set. Automatic re-configuration features are incorporated in FTC to attain fault tolerance, after detection and isolation of malfunction in the system.

5.1.1 Fault Tolerant Control for Vehicle Powertrain

The IC engines are complex nonlinear system, which comprises of different subsystems such as air, fuel, output speed, cooling and lubrication. All these subsystems are highly dependent on each other to ensure smooth power generation from the engine. Since early 1980s, the On-Board Diagnostics (OBD) system was introduced in automotive vehicles to monitor performance of major engine subsystems and report faults in these subsystems that can damage the engine. When a fault is

detected, the driver is informed by *malfunction indicator* and fault code is stored in OBD system. However, it is required that satisfactory performance of the engine is maintained in the presence of such faults.

However, concept of FTC is bit different in automotive vehicles from process industry. In case of fault generation, the purpose of FTC is not 100% recovery of the concerned subsystem but to ensure graceful performance degradation to achieve limp home mode. In modern automotive vehicle design, a safety system is incorporated to protect the vehicle engine if any fault is generated in any of the engine subsystem. Such safety system is termed as "*Limp home mode*", which run the engine at reduced speed to ensure drivability of the vehicle to nearest service center or home with that fault.

5.2 Observer Based Fault Tolerant Control Design

In this chapter, observer based FTC techniques are proposed for mitigation of cyclic torque imbalance. FPEM based USOSM observer has already been derived in Section 4.4 for estimation of net piston force (f_n) to detect cyclic torque imbalance. Based on estimated net piston force (\hat{f}_n), control law for FTC techniques is designed to attain the actual net piston force close to desired values.

In this research work, results of numerical simulation are presented for mitigation of imbalance in the cyclic torque. However, for real time implementation, actual net piston force (f_n) can be estimated from speed dynamics of the test engine; whereas, reference values of net piston force (f_n) can be acquired from FPEM to implement the proposed control techniques. Detection of cyclic torque imbalance is carried out by comparison of actual net piston force (f_n) with reference values and controller is reconfigured upon imbalance detection.

Cyclic torque imbalance is generated due to various factors that have been discussed in Subsection 2.2.2.1. However, stochastic faults in fuel injection subsystem

effect run time performance of the engine and FTC techniques are proposed in this chapter to mitigate such faults. All other engine subsystems are assumed fault free. Such faults would decrease the fuel mass injected in the cylinder per combustion cycle (m_{fo}). As mentioned in Subsection 4.1.2, faults in fuel injector could cause under flow or over flow of the fuel injected in the engine cylinder. When faults in fuel injection are generated, control input to engine fuel dynamics i.e., IPW is robustly adjusted to regulate the fuel mass injected per combustion cycle (m_{fo}).

It is pertinent to mention here that load torque has remained a critical issue to implement such techniques. However, calculation and estimation of load torque has always been considered a separate design problem. Thus, it is assumed that either load torque is calculated perfectly under lab conditions or estimate of load torque is available to develop the respective control or estimation problem [13, 112].

5.2.1 Existing Approaches for Mitigation of Cyclic Torque Imbalance

Different techniques were proposed in the existing literature for control of cyclic torque imbalance, which are briefly reviewed in this section.

In [170], a discrete nonlinear model was presented, which predicted combustion phasing in the cylinder on cyclic basis. Combustion phasing was regulated by SMC based control technique, that was coupled with a Kalman filter. Variations in intake manifold pressure as well as temperature and injected fuel equivalence ratio were considered as physical disturbances to the engine.

In [171], spark timing for successive combustion cycles was employed as control input to reduce torque variations in a SI engine. Relation between maximum cylinder pressure and spark timing was used to develop a stochastic model by system identification techniques. Generalized minimum variance controller was proposed, which regulated maximum cylinder pressure by varying spark timing of successive combustion cycles. However, a quartz pressure sensor to measure in-cylinder pressure was required, which is not fitted in commercial vehicle engines.

In [172], estimation of fuel injector mass flow rate for each combustion cycle was presented. Based on feedback signal of cyclic fuel flow, control technique was reconfigured to track injection pulse and realize dwell time for tightly spaced, multiple pulse profiles. In this work, effect of model uncertainties was not considered for estimation as well as control techniques.

5.2.2 Unified Framework for Detection and Mitigation of Cyclic Torque Imbalance

Cyclic torque balancing approach is comprised of detecting imbalance in the torque and mitigating its causes to decrease the difference between work output of successive combustion cycles in an engine cylinder. Detection of imbalance in the cyclic torque is preliminary step to mitigate its causes for uniform torque generation. As discussed in previous subsection and Chapter 2, different approaches were proposed for detection and control of torque imbalance. However, a model based unified framework is rare in existing literature.

FPEM based USOSM observer has been already described for estimation of net piston force (f_n) to detect cyclic torque imbalance. Based on estimated net piston force (\hat{f}_n), observer based FTC techniques are discussed in succeeding sections to mitigate imbalance in the cyclic torque. Thus, model based unified framework for detection and mitigation of cyclic torque imbalance is accomplished by derivation of FPEM based USOSM observer to detect torque imbalance and development of observer based FTC technique for mitigation of imbalance in the cyclic torque.

The proposed unified framework for detection and mitigation of cyclic torque imbalance is presented in Figure 5.1 [173]; that is composed of two modules. One module deals with detection of imbalance in cyclic torque, that is based on estimation of net piston force (f_n). Whereas, other module is comprised of fault tolerance in the applied control technique to mitigate the imbalance. In Figure 5.1, the “*Model based Estimation*” and “*Torque Imabalance Detection*” blocks corresponded with the estimation of net piston force (f_n) and detection of cyclic

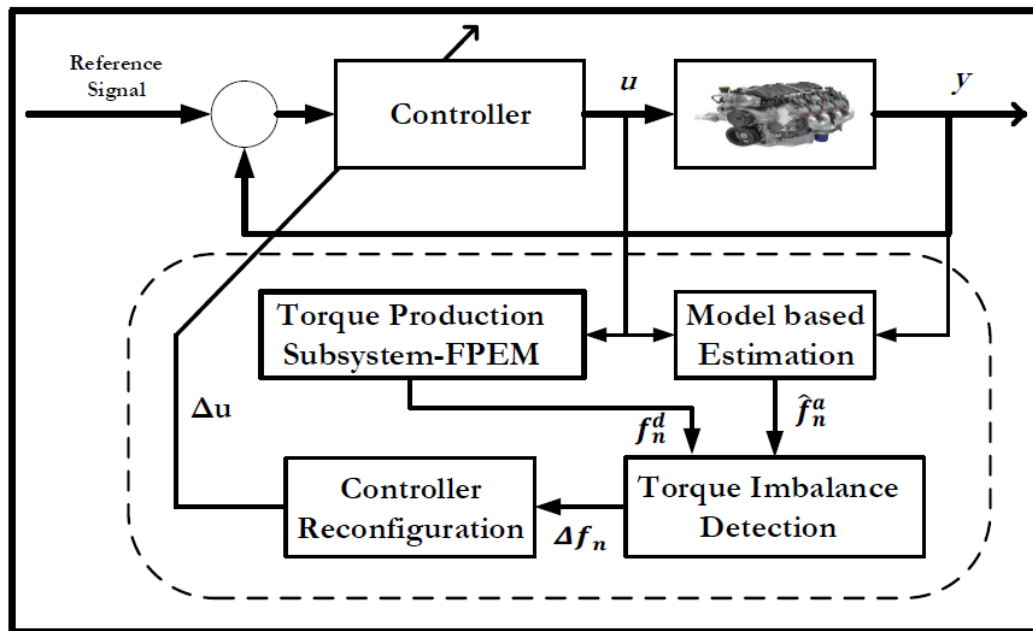


FIGURE 5.1: Proposed Unified Framework for Detection and Mitigation of Cyclic Torque Imbalance

torque imbalance. The “*Controller Reconfiguration*” block represented the fault tolerance in applied control technique to mitigate cyclic torque imbalance, which reconfigured the controller by passing Δu command to the “*Controller*” block.

In the previous chapter, detection of cyclic torque imbalance has been carried out at steady state conditions by keeping throttle valve and load torque constant, which has been implemented under lab conditions. However, proposed unified framework for detection and mitigation of cyclic torque imbalance was applied during runtime of the vehicle to reduce effect of faults in fuel injection subsystem on torque generation and achieve limp home mode.

It was assumed that exact estimate of load torque is available to apply the proposed framework. During runtime of the vehicle, engine speed varies according to drivers torque requirement, which also cause variations in net piston force (f_n^a), generated in the vehicle engine. This net piston force was estimated from speed dynamics of the engine, i.e. \hat{f}_n^a and compared with desired values of net piston force (f_n^d), acquired from FPEM. the sliding surface of the controller is designed in such a way to detect imbalance in the cyclic torque. Based on torque imbalance detection, fuel input was reconfigured to mitigate imbalance in the cyclic torque.

5.2.3 Assumptions for Control Design

Following assumptions were made to design control techniques for mitigation of cyclic torque imbalance:

1. All subsystems of the engine are fault free, except fuel injection subsystem.
2. Faults in fuel injection subsystem are not of extreme nature that may result in complete failure of the system.
3. Faults can be handled by re-configuration of the actuator.

5.2.4 Transformation in First Principle based Engine Model

Relation between net piston force (f_n) and engine speed dynamics was provided in FPEM. However, this relation was required to be transformed for control inputs, i.e., throttle valve angle (α) and IPW to derive their direct relation with engine states. Throttle valve angle (α) controls the flow rate of intake air, as described in Eq. (3.30a), whereas IPW controls the fuel mass injected per combustion cycle. Such relation between fuel input and engine states did not exist in MVEM, which is widely used as control oriented model.

Torque production subsystem of FPEM was transformed to get direct relationship between engine speed dynamics and fuel input i.e. IPW [173]. In Eq.(3.30c), engine speed dynamics was given as follows:

$$\dot{\omega}_1 = \mathbf{g}_1(\theta_1(t), \Gamma) \omega_1^2(t) + \mathbf{g}_2(\theta_1(t), \Gamma) \tau_N + \mathbf{g}_3(\theta_1(t), \Gamma) f_n \quad (5.1)$$

In Eq. (3.17), net piston force (f_n) was given as:

$$f_n = (P_{cyl}(\theta_1) \times A_P) - (P_{crk} \times A_P) \quad (5.2)$$

During intake phase,

$$P_{cyl}(\theta_1) = \eta_v \times P_{man} = P_1 \quad (5.3)$$

In compression phase, cylinder pressure was expressed as:

$$P_{cyl}(\theta_1) = P_1 \left(\frac{V_{ivc}}{V(\theta_1)} \right)^{\gamma_c} = P_2 \quad (5.4)$$

In combustion process, pressure dynamics are directly controlled by injected fuel. Fuel mass injected per combustion cycle (m_{fo}) is function of fuel input, as shown in Eq. (3.27), Eq. (3.28) and Eq. (3.29). Thus, a relationship between net piston force (f_n) and fuel input was established.

During combustion process, cylinder pressure was expressed by following relation:

$$P_{comb}(\theta_1) = P_{cyl}(\theta_1) \left[\frac{T_{comb}}{T_{cyl}(\theta_1)} \right] = P_3 \quad (5.5)$$

$$T_{comb} = T_{cyl}(\theta_1) + \Delta T \quad (5.6)$$

where,

$$\Delta T = \frac{\Delta m_{fb}(\theta_1) \times QHV \times \eta_c \times m_{fo}}{c_v \times m_{total}} \quad (5.7)$$

By putting Eq. (5.6) in Eq. (5.5) and using Eq. (5.7) for ΔT , following relation was obtained:

$$P_{comb}(\theta_1) = B_1(\theta_1) + B_2(\theta_1) m_{fo} \quad (5.8)$$

where,

$$B_1(\theta_1) = P_{cyl}(\theta_1)$$

$$B_2(\theta_1) = \frac{\Delta m_{fb}(\theta_1) \times QHV \times \eta_c \times P_{cyl}(\theta_1)}{c_v \times m_{total} \times T_{cyl}(\theta_1)}$$

In combustion process,

$$P_{cyl}(\theta_1) = P_{comb}(\theta_1) \quad (5.9)$$

By putting Eq. (5.8) in Eq. (5.9), relation between net piston force (f_n) and fuel mass injected per combustion cycle (m_{fo}) was established from Eq. (5.2) and given as following:

$$f_n = A_1(\theta_1) + A_2(\theta_1) m_{fo} \quad (5.10)$$

where,

$$A_1(\theta_1) = \{(P_{cyl}(\theta_1) A_P) - (P_{crk} A_P)\} = B_1(\theta_1) A_P - C_1$$

$$A_2(\theta_1) = \frac{\Delta m_{fb}(\theta_1) \times Q_{HV} \times \eta_c \times P_{cyl}(\theta_1)}{c_v \times m_{total} \times T_{cyl}(\theta_1)} A_P = B_2(\theta_1) A_P$$

or

$$f_n = A_1(\theta_1) + A_2(\theta_1) \Upsilon(t) IPW \quad (5.11)$$

whereas, P_{cyl} , T_{cyl} is cylinder pressure and temperature. ΔT is change in temperature due to combustion, $\Delta m_{fb}(\theta_1)$ is change in mass fraction burnt per combustion cycle, Q_{HV} is fuel heating value, η_c is combustion efficiency, c_v is specific heat at constant volume, $C_1 = (P_{crk} A_P)$ and m_{total} is total charge trapped in the cylinder. $\Upsilon(t)$ represent dynamics of the fuel injection subsystem from IPW to fuel mass injected into cylinder per combustion cycle (m_{fo}).

Using Eq. (5.11), following expression between engine rotational speed (ω_1) and fuel input IPW was obtained from Eq. (5.1):

$$\dot{\omega}_1(t) = f(\theta_1, t) + g(\theta_1, t) IPW \quad (5.12)$$

where,

$$f(\theta_1, t) = \mathbf{g}_1(\theta_1(t)) \omega_1^2(t) + \mathbf{g}_2(\theta_1(t)) \tau_N + \mathbf{g}_3(\theta_1(t)) A_1(\theta_1) \quad (5.13)$$

$$g(\theta_1, t) = \mathbf{g}_3(\theta_1(t)) A_2(\theta_1) \Upsilon(t)$$

Direct relationship between engine rotational speed (ω_1) and fuel input is one of the novel features of FPEM. This relation can be employed to study fuel injection subsystem in further detail, especially if fault is generated in it.

During expansion phase, cylinder pressure was given as:

$$P_{cyl}(\theta) = P_3 \times \left(\frac{V_3}{V(\theta)} \right)^{\gamma_e} \quad (5.14)$$

and in exhaust phase, cylinder pressure was expressed as:

$$P_{cyl}(\theta) = P_{exh} \quad (5.15)$$

where P_{exh} is pressure in exhaust manifold.

By using Eq. (5.3), (5.4), (5.9), (5.14) and Eq. (5.15), net piston force (f_n) was calculated for each combustion cycle in FPEM.

By employing the above transformation in FPEM, following control techniques are proposed for mitigation of imbalance in the cyclic torque:

1. STA based FTC technique.
2. Certainty Equivalence Super Twisting Algorithm (CESTA) based FTC technique.

Both STA and CESTA based FTC techniques are presented in following subsection along with controller structure, existence of sliding mode, control law and respective results along with discussion.

5.3 STA based FTC Technique

SMC based algorithms are mostly employed due to robustness against external disturbances as well as parametric uncertainties. Main drawback of first order SMC is existence of high frequency oscillations in control signal, known as *chattering*. These oscillations could wear out mechanical and electrical actuators, which can degrade their performance.

One of the ways to reduce chattering is the application of HOSM, which employ the concept of first order SMC but utilize derivatives of the sliding surface. HOSM has same performance and robustness as of first order SMC; however, chattering is reduced [158]. Computation of the derivatives of sliding surface is a constraint to apply HOSM. This limitation was relaxed by STA, proposed by Levant et.al., [158] and discussed briefly in Section 4.3.

5.3.1 Controller Structure

Structure of STA is composed of two continuous terms, which are given in Eq. (5.16a). First term is continuous function of the sliding variable, as described in Eq. (5.16b); whereas, second term contains integral of the discontinuous action, given in Eq. (5.16c).

$$\bar{u} = u_a(t) + z(t) \quad (5.16a)$$

$$u_a(t) = \begin{cases} -k_1 |S_0|^\rho \text{sign}(S) & |S| > |S_o| \\ -k_1 |S|^\rho \text{sign}(S) & |S| \leq |S_o| \end{cases} \quad (5.16b)$$

$$\dot{z}(t) = \begin{cases} -\bar{u} & |\bar{u}| > 1 \\ -k_2 \text{sign}(S) & |\bar{u}| \leq 1 \end{cases} \quad (5.16c)$$

Finite time convergence of STA was given by following conditions:

$$\begin{aligned} k_2 &> \frac{\Phi}{\Gamma_m} \\ k_1^2 &\geq \frac{4\Phi \Gamma_M (k_2 + \Phi)}{\Gamma_m^2 \Gamma_m (k_2 - \Phi)} \\ 0 &< \rho \leq 0.5 \end{aligned} \quad (5.17)$$

where $k_1, k_2, \Gamma_M, \Phi, \Gamma_m$ are positive constants [158].

5.3.2 Existence of Sliding Mode

Following system was considered for stability analysis:

$$\begin{aligned} \dot{x}(t) &= f(x) + g(x)(u + F(x, t)) \\ y(t) &= h(x) \end{aligned} \quad (5.18)$$

where, $x(t) \in \mathfrak{R}^n$, $u \in \mathfrak{R}^m$, $y \in \mathfrak{R}^r$ and $F(x, t)$ represents bounded uncertainty in the input. Vector fields $f(x)$, $g(x)$, $h(x)$ represents system dynamics, input

dynamics and output of the system, respectively. These vector fields are assumed smooth and known.

Sliding surface was designed according to the control objective. Internal dynamics of the system in Eq. (5.18) were assumed stable. Also, relative degree of S with respect to u was found to be one. Sliding surface dynamics was represented as:

$$\dot{S} = \frac{\partial S}{\partial x} [f(x, t) + g(x, t)\{u + F(x, t)\}] \quad (5.19)$$

In compact form, it was expressed as follows:

$$\dot{S} = \Psi(S, t) + G(S, t)\{u + F\} \quad (5.20)$$

where, $\Psi(S, t) = \left[\frac{\partial S}{\partial x} f(x, t)\right]^T$ and $G(S, t)\{u + F\} = \frac{\partial S}{\partial x} g(x, t)\{u + F(x, t)\}$

It was assumed that $G(S, t)^{-1}$ exists. Thus, u was taken as:

$$u = G(S, t)^{-1}\{-\Psi(S, t) + \bar{u}\}, \quad (5.21)$$

where known term was handled by $G(S, t)^{-1}\{-\Psi(S, t)\}$ to give desired output for the nominal plant. Actuator fault/uncertain term was handled by \bar{u} . Rest of the system was given by:

$$\dot{S} = F(x, t) + \bar{u}. \quad (5.22)$$

Uncertainty in the input was assumed bounded. Thus,

$$\begin{aligned} |F(x, t)| &\leq \Omega |S(x)|^{\frac{1}{2}}, \\ \Omega &> 0. \end{aligned} \quad (5.23)$$

Lyapunov function, proposed in [174] was considered to analyze stability of the proposed control technique. Following weak Lyapunov function was considered:

$$V = [k_2 |S| + \frac{1}{2}z^2]. \quad (5.24)$$

Taking derivative of Lyapunov function:

$$\dot{V} = [k_2 \text{sign}(S) \dot{S} + z \dot{z}]. \quad (5.25)$$

Putting sliding mode dynamics in Eq. (5.25):

$$\dot{V} \leq [k_2 \text{sign}(S) \{\Omega |S|^{\frac{1}{2}} - k_1 |S|^{\frac{1}{2}} \text{sign}(S) + z - \dot{z}\}]. \quad (5.26)$$

which can be written as:

$$\dot{V} \leq [k_2 \text{sign}(S) \{\Omega |S|^{\frac{1}{2}} - k_1 |S|^{\frac{1}{2}} \text{sign}(S)\}]. \quad (5.27)$$

By selecting $k_1 > \Omega$, \dot{V} becomes negative semi-definite.

Nevertheless, using the invariance principle of Krasovskii-LaSalle for the system in Eq. (5.16a) and Eq. (5.22); all states of the system were bounded and asymptotic stability of the closed loop system was ensured.

5.3.3 Control Law

Control law ensure convergence of system state trajectories toward sliding surface. Structure of SOSM based control techniques are generic in nature. However, control laws and controller gains are always system specific. Depending upon the control problem, sliding surface is designed by using one or more states of the system; whereas, controller gains depended on system dynamics.

Engine states, given in Eq. (3.30a-3.30c) can be presented in following form:

$$\dot{x} = f(x) + g(x, U) \quad (5.28)$$

where, $x = [P_{man}, m_{fo}, \omega_1]^T \in \mathfrak{R}^n$; $u \in \mathfrak{R}^m$; $f : \mathfrak{R}^n \rightarrow \mathfrak{R}^n$; $g : \mathfrak{R}^n \rightarrow \mathfrak{R}^n$. Also, $f(x)$ and $g(x, U)$ are smooth vector fields. Control input vector (U) is comprised of throttle valve angle (α) and IPW , which appear in the expression of manifold pressure and engine speed.

As discussed in [175], SMC design is comprised of two steps. Sliding surface is defined in the first step, followed by control law design in the second step. Sliding surface design was based on control objective. Estimated values of net piston force (\hat{f}_n) was employed to design the control law for proposed observer based FTC technique. Following sliding surface was defined in first step:

$$S(t, x) = \hat{f}_n^a - f_n^d \quad (5.29)$$

where, f_n^d is desired net piston force and \hat{f}_n^a is estimated value of actual net force that is generated on piston head. Sliding variable is represented by $S(t, x)$ that is required to be steered to equilibrium point along with its first total time derivative.

Control law was designed that guaranteed $S = \dot{S} = 0$. It also ensured convergence of estimated values of actual net piston force to desired values of net piston force i.e., $\hat{f}_n^a = f_n^d$ in the presence of external disturbances.

Thus, sliding variable dynamics was expressed as:

$$\dot{S} = A_1(\hat{\theta}_1) + \{A_2(\hat{\theta}_1) \mathcal{Y}(t) + A_2(\hat{\theta}_1) \dot{\mathcal{Y}}(t)\} u \quad (5.30)$$

Faults such as dirty fuel injector, clogged nozzles of the injectors and leakage in fuel injection that can affect the fuel injection subsystem were considered to cause torque imbalance. It included actuation mechanism faults, blockade in actuator and leakages in fuel injection subsystem. Such faults were classified into two types i.e., underflow or overflow through the actuator. It was assumed that upper bound of these faults is known.

By including these faults, following relation was obtained:

$$\dot{S} = A_1(\hat{\theta}_1) + \{A_2(\hat{\theta}_1) \mathcal{Y}(t) + A_2(\hat{\theta}_1) \dot{\mathcal{Y}}(t)\} (u + F(x, t)) \quad (5.31)$$

The control action was proposed as:

$$u = u_{eq} + \bar{u} \quad (5.32)$$

where, u_{eq} is equivalent control and \bar{u} is STA control law that was designed by using Eq. (5.16a). Equivalent control (u_{eq}) was computed from nominal system, given in Eq. (5.30) by solving for u , such that $\dot{S} = 0$. The controller was made model based by computing the equivalent control (u_{eq}), as it incorporated system dynamics in the control law. Controller design parameters, k_1 , k_2 and ρ were calculated according to controller conditions, given in Eq. (5.17). Thus,

$$u_{eq} = -\frac{A_1(\hat{\theta}_1)}{A_2(\hat{\theta}_1)\Upsilon(t) + A_2(\hat{\theta}_1)\dot{\Upsilon}(t)} \quad (5.33)$$

5.3.4 Results and Discussion-STA based FTC Technique

Estimation of net piston force (f_n) was performed to detect imbalance in the cyclic torque. Based on estimated net piston force (\hat{f}_n), control law for STA based FTC technique was designed, which was applied to mitigate imbalance in the cyclic torque. Numerical simulation of the engine model was carried out under steady-state conditions as throttle valve angle and load torque were kept constant. It was assumed that estimate of load torque was available to implement the control technique, as already discussed in existing techniques [13, 112]. In [173], the proposed unified framework was implemented to detect and mitigate imbalance in the cyclic torque.

Fault in fuel injection subsystem was induced to generate imbalance in the cyclic torque. For $t \geq 15$ sec, fuel mass injected per combustion cycle (m_{fo}) was reduced due to such fault by 15% of the desired fuel mass, that was required to be injected. Such faults in fuel injection subsystem have been discussed in detail in Section 4.1.

Intake manifold pressure of the engine model is shown in Figure 5.2. Imbalance in cyclic torque can be observed as manifold pressure is varied as fault is induced in fuel injection subsystem at $t = 15$ sec.

As discussed in Section 5.2, estimated net piston force (\hat{f}_n) was employed to design the control law. Engine angular position and rotational speed were observed to estimate net piston force (f_n), which acted as unknown input to engine speed

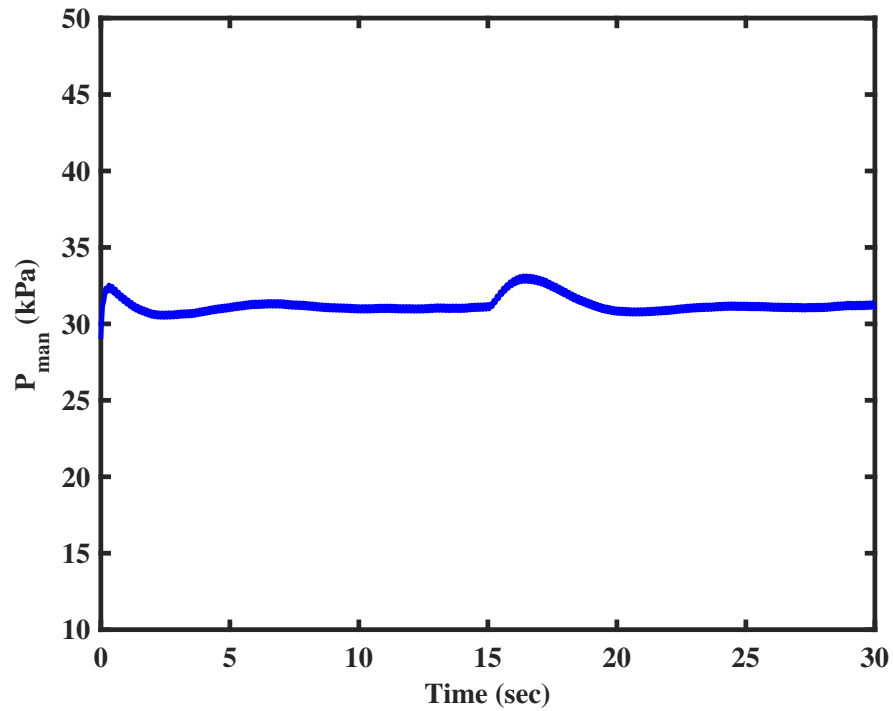


FIGURE 5.2: Intake Manifold Pressure

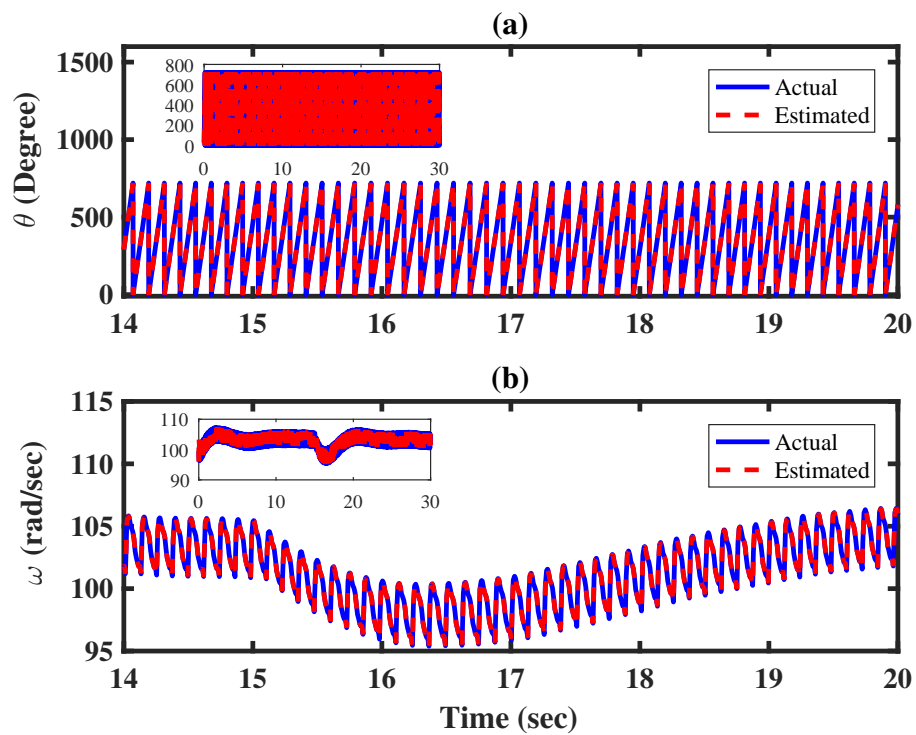


FIGURE 5.3: Estimation of (a) Engine Angular Position (b) Engine Rotational Speed

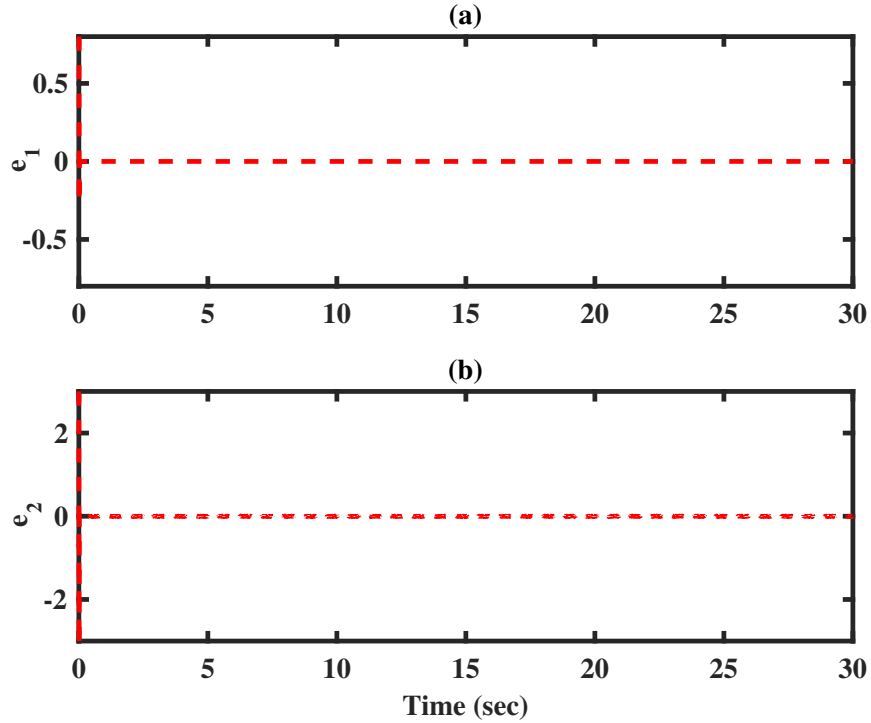


FIGURE 5.4: Estimation Error (a) Engine Angular Position (b) Engine Rotational Speed

dynamics. Plot for estimation of engine angular position is shown in Figure 5.3(a); whereas, for rotational speed it is shown in Figure 5.3(b).

As estimated states of engine speed dynamics converged to actual states, estimation error for both engine angular position and rotational speed converged to the origin, as shown in Figure 5.4. Estimation errors showed exact and swift convergence of observed states to actual states of engine speed dynamics. At $t = 0$, a surge can be observed due to difference in initial conditions; however, it is diminished in 0.03 sec as sliding mode is achieved by FPEM based USOSM observer.

As estimated states converged to actual states i.e., $\hat{\theta}_1 \rightarrow \theta_1$ and $\hat{\omega}_1 \rightarrow \omega_1$; injection term (z_2) in the observer represented unknown input i.e., net piston force (f_n). LPF was applied to extract net piston force (f_n) from the injection signal.

STA based FTC approach was implemented to mitigate cyclic torque imbalance by applying the control law, that was formulated in Subsection 5.3.3. Uncertainties of the system $F(x, t)$ were assumed bounded as $|F(x, t)| \leq \Omega |S(x)|^{\frac{1}{2}}$, where $\Omega > 0$. Accordingly, gains of STA based FTC technique were selected as $k_1 > \Omega$.

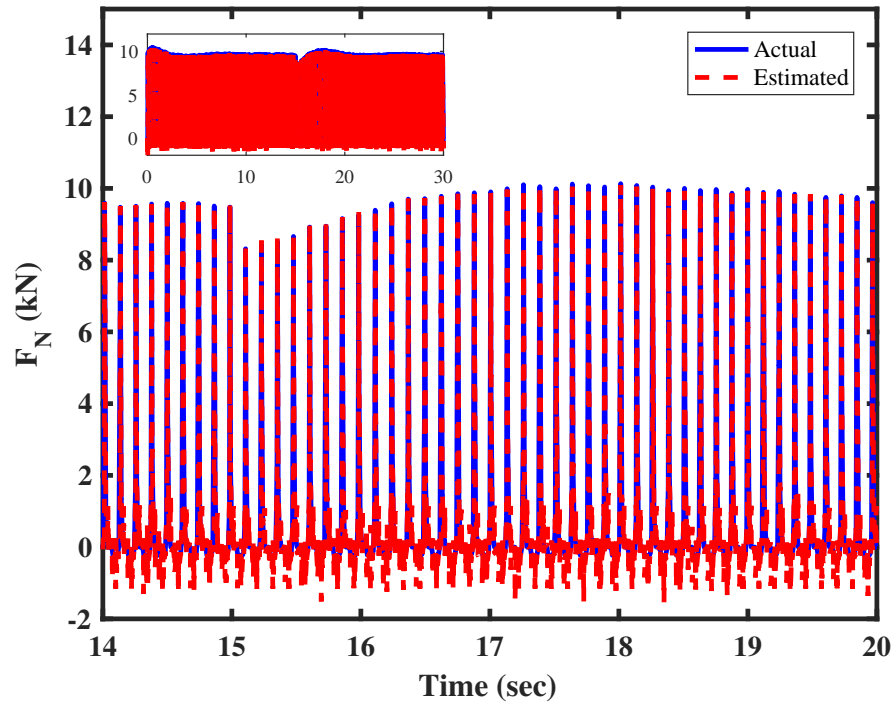


FIGURE 5.5: Estimation of Net Piston force (f_n) by FPEM based USOSM Observer

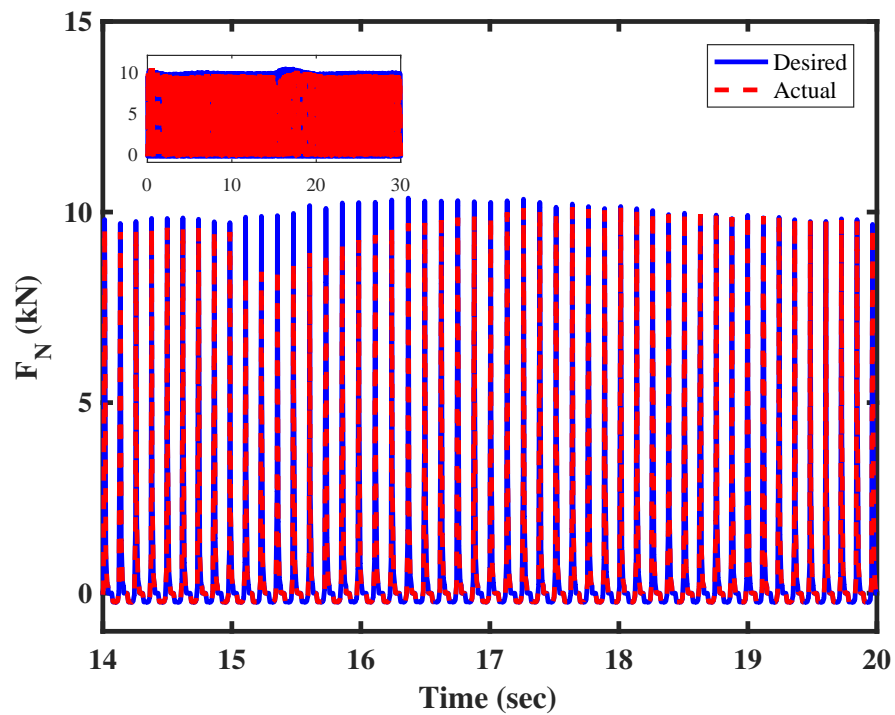


FIGURE 5.6: Mitigation of Cyclic Torque Imbalance by STA based FTC Technique - Desired and Actual Net Piston force (f_n)

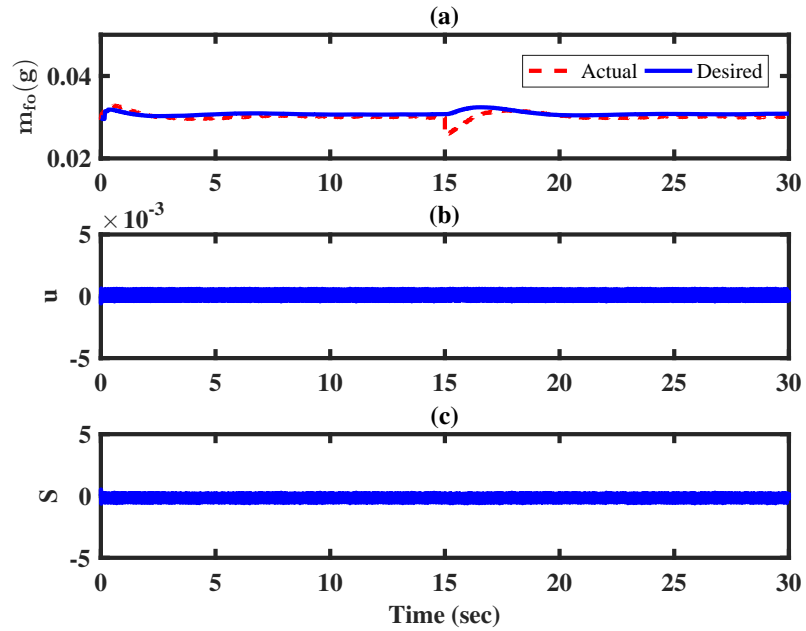


FIGURE 5.7: (a) Fuel Mass Injected per Combustion Cycle (b) Control Input (c) Sliding Surface

Both estimated and actual net piston force (f_n) are shown in Figure 5.5; whereas, in Figure 5.6, actual and desired net piston force (f_n) are shown. In proposed unified framework, both observer and controller were implemented simultaneously. Imbalance in the cyclic torque was detected by FPEM based USOSM observer, which provided estimated net piston force (\hat{f}_n) to design the control law; whereas, STA based FTC technique kept the actual net piston force (f_n) close to desired values. For $t \geq 15$ sec, variations were generated in actual net piston force due to fault in fuel injection subsystem; however, proposed control technique robustly adjusted the input to mitigate the fault and keep actual net piston force (f_n) close to desired values.

Plots of fuel mass injected per combustion cycle (m_{fo}), control input (IPW) and sliding surface are presented in Figure 5.7. It can be noted in Figure 5.7(a) that actual fuel mass injected per combustion cycle (m_{fo}) remained close to desired values, even after occurrence of the fault in fuel injection subsystem. Control input, IPW is shown in Figure 5.7(b), whereas sliding surface is shown in Figure 5.7(c). Evaluation of proposed STA based FTC technique for mitigation of cyclic torque imbalance has demonstrated its instantaneous and accurate performance.

5.4 CESTA based FTC Technique

Performance of STA based control technique is considered satisfactory, if the system with matched uncertainties is stabilized by it in finite time. However, *apriori* knowledge about fault bound is required in STA based control technique, as gains are selected to be higher than fault bound. Controller parameters are affected by upper bound of uncertainties. Large control effort is applied as gains of STA based control techniques are calculated for worst case scenario [176].

This drawback was addressed by *adaptive* STA in [177]. Adaptive control law was proposed in this algorithm that would increase gains of the controller if sliding variable move away from a certain domain around sliding manifold. Prior to controller design, estimation of upper bound of uncertainty was not required. Controller gains can be kept small at start, which would increase as uncertainty bound increases. Stability was achieved even if uncertainty bound was unknown. However, structure of uncertainty was not considered in proposed control technique.

In [178], combination of STA with certainty equivalence adaptation was proposed. This technique was termed as “Certainty Equivalence Super Twisting Algorithm (CESTA)”. Structured and unstructured part of uncertainty are not distinguished by conventional STA based technique. However, these parts of the uncertainty are distinguished by CESTA based control technique to gain maximum information about nature of the uncertainty.

STA based technique is more effective if uncertainty bound remains small; however, chattering increases as magnitude of uncertainty increases. On the other hand, structural information of uncertainty is incorporated in CESTA, which would assist to reduce gains of STA based part of the controller. Adaptive algorithm based on principle of certainty equivalence is added in the algorithm by using Lyapunov approach. Adaptive part of CESTA could estimate structured fault/uncertainty and cancels it out. STA based part of the algorithm could compensate unstructured uncertainty, which reduces the chattering.

5.4.1 Controller structure

Consider the following system:

$$\begin{aligned}\dot{x}(t) &= f(x) + g(x)(u + F(x, t)) \\ y &= h(x)\end{aligned}\quad (5.34)$$

where, $F(x, t)$ represents uncertain term and $x(t) \in \mathfrak{R}^n$, $u \in \mathfrak{R}^m$ and $y \in \mathfrak{R}^r$. Vector fields $f(x)$, $g(x)$ and $h(x)$ were assumed smooth and known.

Uncertain term $F(x, t)$ was expressed as sum of unstructured $f_u(x, t)$ and structured $f_s(x, t)$ parts:

$$F(x, t) = f_u(x, t) + f_s(x, t) \quad (5.35)$$

Structured uncertainty was written as product of a known base function $\Psi(x)$ and unknown constant parameter Δ as:

$$f_s(x) = \Delta \Psi(x) \quad (5.36)$$

Sliding surface $S = S(x)$ was designed according to desired control objective. Internal dynamics of the system were assumed to be stable. Relative degrees of S with respect to u was found to be one.

Sliding surface dynamics can be written as:

$$\begin{aligned}\dot{S} &= \frac{\partial S}{\partial x} [f(x) + g(x)\{u + F(x, t)\}], \\ &= \frac{\partial S}{\partial x} f(x) + \frac{\partial S}{\partial x} g(x)\{u + F(x, t)\}.\end{aligned}\quad (5.37)$$

In compact form, sliding mode dynamics were expressed as:

$$\dot{S} = \Psi(S, t) + G(S, t)(u + F) \quad (5.38)$$

where, $\Psi(S, t) = \left[\frac{\partial S}{\partial x} f(x, t)\right]^T$ and $G(S, T)\{u + F\} = \frac{\partial S}{\partial x} g(x, t)\{u + F(x, t)\}$

It was assumed that $G(S, t)^{-1}$ exists. Thus, u was taken as:

$$u = G(S, t)^{-1}\{-\Psi(S, t) + \bar{u}\} \quad (5.39)$$

where $G^{-1}(x)\{-N(x)\}$ handled known term; whereas, actuator fault/uncertain term was handled by \bar{u} .

Selection of u had decoupled the system and left over system was comprised of only matched uncertainties. Left over system was written as:

$$\begin{aligned} \dot{S} &= F + \bar{u}, \\ \dot{S} &= \Delta\Psi(x) + f_u(x, t) + \bar{u} \end{aligned} \quad (5.40)$$

Unstructured uncertainties were assumed bounded as:

$$\begin{aligned} |f_u(x, t)| &\leq \Omega |S(x)|^{\frac{1}{2}}, \\ \Omega &> 0. \end{aligned} \quad (5.41)$$

CESTA resorts to STA based controller as a nominal controller. Structure of the controller was expressed as [178]:

$$\bar{u} = -k_1 |S|^{\frac{1}{2}} \text{sign}(S) + z - \hat{\Delta}\Psi(x), \quad (5.42)$$

$$\dot{z} = -k_2 \text{sign}(S), \quad (5.43)$$

where controller gains $k_1, k_2 > 0$ allowed to deal with unstructured uncertainties. $\hat{\Delta}$ is the estimate of unknown parameter Δ and z is a controller state.

5.4.1.1 Lyapunov Stability Analysis-I

To apply the controller, stability of the system was analyzed by taking following Lyapunov function [174]:

$$V = \left[k_2 |S| + \frac{1}{2} z^2 + \frac{1}{2\beta} \tilde{\Delta}^2 \right], \quad (5.44)$$

where,

$$\begin{aligned}\beta &> 0 \\ \tilde{\Delta} &= \hat{\Delta} - \Delta\end{aligned}$$

Taking derivative of Lyapunov function that is given in Eq. (5.44),

$$\dot{V} = \left[k_2 \text{sign}(S) \dot{S} + z\dot{z} + \frac{1}{\beta} \tilde{\Delta} \dot{\Delta} \right]. \quad (5.45)$$

By putting Eq. (5.40-5.43) in Eq. (5.45), following relation was obtained:

$$\begin{aligned}\dot{V} &= \left[k_2 \text{sign}(S) \{f_u(x, t) - k_1 |S|^{\frac{1}{2}} \right. \\ &\quad \left. \text{sign}(S) - (\hat{\Delta} - \Delta)\Psi(x)\} + \frac{1}{\beta} \tilde{\Delta} \dot{\Delta} \right] \\ \dot{V} &= \left[k_2 \text{sign}(S) \{\Omega |S|^{\frac{1}{2}} - k_1 |S|^{\frac{1}{2}} \right. \\ &\quad \left. \text{sign}(S)\} + \tilde{\Delta} \left\{ -k_2 \text{sign}(S) \Psi(x) + \frac{1}{\beta} \dot{\Delta} \right\} \right] \quad (5.46)\end{aligned}$$

If $\hat{\Delta}$ is known exactly, then error $\tilde{\Delta} = 0$ and \dot{V} reduced to:

$$\dot{V} \leq [k_2 \text{sign}(S) \{\Omega |S|^{\frac{1}{2}} - k_1 |S|^{\frac{1}{2}} \text{sign}(S)\}] \quad (5.47)$$

Selecting $k_1 > \Omega$, \dot{V} becomes negative semi definite.

Asymptotic stability of proposed control technique was evaluated by using Krasovskii LaSalle's invariance principle; as $\dot{V} = 0$ gives $S = 0$. Only possible solution is $z = 0$, if Eq. (5.40) to Eq. (5.43) are considered. Thus, asymptotic stability of closed loop system was ensured. As $\hat{\Delta}$ is not known, thus adaptation laws was taken as:

$$\dot{\hat{\Delta}} = \beta k_2 \text{sign}(S) \Psi(x) \quad (5.48)$$

Value of adaptation parameter $\hat{\Delta}$ remained close to zero, when no fault or structured uncertainty exist in the system. However, as the fault was induced in fuel

injection subsystem, adaptation parameter value increased according to fault magnitude. Occurrence of fault was indicated by non-zero value of adaptation parameter.

The left over system became:

$$\dot{V} \leq [k_2 \text{sign}(S) \{\Omega |S|^{\frac{1}{2}} - k_1 |S|^{\frac{1}{2}} \text{sign}(S)\}] \quad (5.49)$$

Select $k_1 > \Omega$, \dot{V} comes out to be negative semi definite. However, system converged to $S = 0$, if internal dynamics are assumed stable and z as well as $\hat{\Delta}$ are non-zero. Thus, all states of closed loop system are bounded.

Structure of complete CESTA was expressed as:

$$\begin{aligned} \dot{u} &= -k_1 |S|^{\frac{1}{2}} \text{sign}(S) + z - \hat{\Delta} \Psi(x) \\ \dot{z} &= -k_2 \text{sign}(S) \\ \dot{\hat{\Delta}} &= \beta k_2 \text{sign}(S) \Psi(x) \end{aligned} \quad (5.50)$$

5.4.1.2 Lyapunov Stability Analysis-II

In Subsection 5.4.1.1, Lyapunov function was evaluated along trajectories of the system in Eq. (5.40) to get negative semi-definite derivative of Lyapunov function. However, asymptotic stability of system states cannot be deduced without additional analysis. Following positive definite Lyapunov function, proposed in [179] was adapted for system analysis:

$$V = \left[\frac{2}{3} k_1 |S|^{\frac{3}{2}} - Sz + \frac{2}{3k_1^2} |z|^3 + \frac{1}{2\beta} \tilde{\Delta}^2 \right] \quad (5.51)$$

where $\beta > 0$ and $\tilde{\Delta} = \hat{\Delta} - \Delta$.

Taking derivative of Lyapunov function, that is given in Eq. (5.51):

$$\dot{V} = \left[\dot{S} \left\{ k_1 |S|^{\frac{1}{2}} \text{sign}(S) - z \right\} + \dot{z} \left\{ \frac{2}{k_1^2} |z|^2 \text{sign}(S) - S \right\} + \frac{1}{\beta} \tilde{\Delta} \dot{\hat{\Delta}} \right] \quad (5.52)$$

Considering Eq. (5.40), (5.42) and Eq. (5.43), the relation obtained was given by following expression:

$$\begin{aligned} \dot{V} = & \left[-|S| (k_1^2 - k_2) + 2k_1 |S|^{\frac{1}{2}} \text{sign}(S) z - |z|^2 + \tilde{\Delta} \right. \\ & \left. \left\{ \frac{1}{\beta} \dot{\tilde{\Delta}} - \Psi(x) \left(k_1 |S|^{\frac{1}{2}} \text{sign}(S) - z \right) \right\} - \frac{2k_2}{k_1^2} |z|^2 \text{sign}(S z) \right. \\ & \left. + f_u(x, t) \left(k_1 |S|^{\frac{1}{2}} \text{sign}(S) - z \right) \right] \end{aligned} \quad (5.53)$$

By applying *Certainty Equivalence Principle*, it was assumed that no uncertainties existed in the system i.e., $\tilde{\Delta} = 0$ and $f_u(x, t) = 0$.

Thus, following relation was obtained:

$$\begin{aligned} \dot{V}_0 = & \left[-|S| (k_1^2 - k_2) + 2k_1 |S|^{\frac{1}{2}} \text{sign}(S) z \right. \\ & \left. - |z|^2 - \frac{2k_2}{k_1^2} |z|^2 \text{sign}(S z) \right] \\ = & \left[-|S| (k_1^2 - k_2) + 2k_1 |S|^{\frac{1}{2}} \text{sign}(S) z \right. \\ & \left. - |z|^2 \left(1 + \frac{2k_2}{k_1^2} \text{sign}(S z) \right) \right] \end{aligned} \quad (5.54)$$

Following relations were assumed to achieve stability:

$$\delta_1 = k_1^2 - k_2, \quad (5.55)$$

$$\delta_2 = 2k_1, \quad (5.56)$$

$$\delta_3 = 1 - \frac{2k_2}{k_1}, \quad (5.57)$$

$$\delta_4 = 1 + \frac{2k_2}{k_1}. \quad (5.58)$$

Which provided following expression:

$$\dot{V}_0 \leq \begin{bmatrix} -\delta_1 |S| + \delta_2 |S|^{\frac{1}{2}} z - \delta_3 |z|^2 & S z \geq 0 \\ -\delta_1 |S| - \delta_2 |S|^{\frac{1}{2}} z - \delta_4 |z|^2 & S z < 0 \end{bmatrix}. \quad (5.59)$$

Eq. (5.59) was written as:

$$\dot{V}_0 \leq \begin{bmatrix} -\varsigma^T A_1 \varsigma & S z \geq 0 \\ -\varsigma^T A_2 \varsigma & S z < 0 \end{bmatrix} \quad (5.60)$$

where,

$$A_1 = \begin{bmatrix} \delta_1 & -\frac{\delta_2}{2} \\ -\frac{\delta_2}{2} & \delta_3 \end{bmatrix}$$

$$A_2 = \begin{bmatrix} \delta_1 & -\frac{\delta_2}{2} \\ -\frac{\delta_2}{2} & \delta_4 \end{bmatrix}$$

$$\varsigma^T = \left[|S|^{\frac{1}{2}} \quad \text{sign}(S) \quad z \right]$$

Both matrices A_1 and A_2 became positive definite by taking $k_1^2 > 2k_2$, which implied that \dot{V}_0 is negative definite.

For the case of non-zero uncertainties i.e., $\tilde{\Delta} \neq 0$ and $f_u(x, t) \neq 0$, following relation was obtained:

$$\begin{aligned} \dot{V} = & \dot{V}_0 + \left[\tilde{\Delta} \left\{ \frac{1}{\beta} \dot{\tilde{\Delta}} - \Psi(x) \left(k_1 |S|^{\frac{1}{2}} \text{sign}(S) - z \right) \right\} \right. \\ & \left. + f_u(x, t) \left(k_1 |S|^{\frac{1}{2}} \text{sign}(S) - z \right) \right] \end{aligned} \quad (5.62)$$

Estimate of uncertainty was taken as:

$$\dot{\tilde{\Delta}} = \beta \Psi(x) \left(k_1 |S|^{\frac{1}{2}} \text{sign}(S) - z \right) \quad (5.63)$$

Which provided following relation:

$$\begin{aligned} \dot{V} & \leq \dot{V}_0 + \left[f_u(x, t) \left(k_1 |S|^{\frac{1}{2}} \text{sign}(S) - z \right) \right] \\ & \leq \dot{V}_0 + [\Gamma \|\varsigma\| \|f_u(x, t)\|] \end{aligned} \quad (5.64)$$

where $\Gamma = \sqrt{k_1^2 + 1}$.

For $Sz \geq 0$, Eq. (5.64) was written as:

$$\begin{aligned}\dot{V} &\leq [-\varsigma^T A_1 \varsigma + \Gamma \|\varsigma\| |f_u(x, t)|] \\ &\leq [-\lambda \|\varsigma\|^2 + \Gamma \|\varsigma\| |f_u(x, t)|]\end{aligned}\quad (5.65)$$

where, minimum eigenvalue of A_1 was denoted by $\lambda = \lambda_m\{A_1\}$.

\dot{V} became negative definite, when following condition was satisfied:

$$\|\varsigma\| > \frac{\Gamma}{\lambda} |f_u(x, t)|. \quad (5.66)$$

As $Sz < 0$, conditions for $\dot{V} < 0$ was [179]

$$\frac{\delta_1}{k_1} |S|^{\frac{1}{2}} + \frac{\delta_3}{k_1} |z| > |f_u(x, t)|, \quad (5.67)$$

$$\delta_2 |S|^{\frac{1}{2}} + \delta_4 |z| > |f_u(x, t)|, \quad (5.68)$$

where, constants δ_1 , δ_2 , δ_3 and δ_4 were chosen as in Eq. (5.55-5.58).

Absolute values of state variables S and z were required to be greater than certain values to dominate the uncertainty $f_u(x, t)$ and meet the inequalities, given in Eq. (5.66-5.68). $\dot{V} < 0$ and S as well as z converged to origin, when inequalities given in Eq. (5.66-5.68) were satisfied.

When these conditions were not satisfied, \dot{V} became positive and S as well as z increased, until inequalities in Eq. (5.66-5.68) were satisfied again and \dot{V} was negative. Thus, Lyapunov function V along with states and estimation errors remained bounded for all time.

When unstructured uncertainties were bounded, as given in Eq. (5.41), Eq. (5.66-5.68) was expressed as:

$$\begin{aligned}\frac{\lambda}{\Gamma} &> \Omega, \\ \frac{\delta_1}{k_1} &> \Omega, \\ \delta_2 &> \Omega.\end{aligned}$$

Complete structure of the controller was expressed as:

$$\begin{aligned}\bar{u} &= -k_1 |S|^{\frac{1}{2}} \text{sign}(S) + z - \hat{\Delta}\Psi(x) \\ \dot{z} &= -k_2 \text{sign}(S) \\ \dot{\hat{\Delta}} &= \beta\Psi(x) \left(k_1 |S|^{\frac{1}{2}} \text{sign}(S) - z \right)\end{aligned}\quad (5.69)$$

5.4.2 Control Law

Control law of CESTA based FTC was derived to satisfy sliding condition $S = \dot{S} = 0$, despite presence of modeling errors, actuators faults and parametric uncertainties. Control law ensure convergence of system state trajectories toward sliding surface. Structure of the SOSM based control technique is generic in nature. However, the control law and controller gains are always system specific. Depending upon the control problem, sliding surface is designed by using one or more states of the system; whereas, controller gains depended on system dynamics.

Estimated values of net piston force (\hat{f}_n) was employed to design the control law for CESTA based FTC technique. Keeping in view the defined objective, following sliding surface was defined in first step:

$$S(t, x) = \hat{f}_n^a - f_n^d \quad (5.70)$$

where, f_n^d is desired net piston force and \hat{f}_n^a is estimated value of actual net force generated on piston head. Sliding variable is represented by $S(t, x)$, which is required to be steered to equilibrium point along with its first total time derivative.

Control law was designed that guaranteed $S = \dot{S} = 0$. It also ensured convergence of estimated value of actual net piston force to desired value i.e., $\hat{f}_n^a = f_n^d$ in the presence of external disturbances.

Thus, sliding dynamics was expressed as:

$$\dot{S} = A_1(\hat{\theta}_1) + \{A_2(\hat{\theta}_1) \Upsilon(t) + A_2(\hat{\theta}_1) \dot{\Upsilon}(t)\} (u + \Theta + f_u) \quad (5.71)$$

Where, Θ represent structured fault of over or under flow of injected fuel. Effect of the fault in fuel injection subsystem was classified as underflow or overflow through actuator. Such fault can be caused by actuator chocking due to blockage, leakages in fuel injection subsystem that cause fuel dripping, fault in actuation mechanism that result as offset in actuator position and wearing of actuator components. In terms of flow rates, structured fault was represented as:

$$\Theta = \Delta\Psi(x) = \Delta IPW, \quad (5.72)$$

The term Δ is percentage fault in flow rate of the fuel, which is unbounded and unknown. The term Δ is estimated by adaptation law, that is given in Eq. (5.48). In CESTA, apriori knowledge about fault occurrence or fault bound was not required to design the control law.

Unstructured uncertainty was represented as f_u and assumed bounded, which was given as:

$$\begin{aligned} |f_u(x, t)| &\leq \Omega |S(x)|^{\frac{1}{2}}, \\ \Omega &> 0, \end{aligned} \quad (5.73)$$

Control action was proposed in Eq. (5.39). Perturbation and fault in sliding variable dynamics were ignored to calculate u :

$$\dot{S} = A_1(\dot{\hat{\theta}}_1) + \{A_2(\dot{\hat{\theta}}_1)\Upsilon(t) + A_2(\hat{\theta}_1)\dot{\Upsilon}(t)\}u \quad (5.74)$$

Control action was proposed as:

$$u = u_{eq} + \bar{u} \quad (5.75)$$

where, u_{eq} is equivalent control and \bar{u} is CESTA control law, which was designed by using Eq. (5.69). Equivalent control (u_{eq}) was computed from nominal system, given in Eq. (5.74), by solving for u , such that $\dot{S} = 0$. The controller was made model based by computing the equivalent control (u_{eq}), as it incorporated system

dynamics in the control law.

$$u_{eq} = -\frac{A_1(\hat{\theta}_1)}{A_2(\hat{\theta}_1)\mathcal{Y}(t) + A_2(\hat{\theta}_1)\dot{\mathcal{Y}}(t)} \quad (5.76)$$

5.4.3 Results and Discussion-CESTA based FTC Technique

CESTA based FTC was implemented to mitigate cyclic torque imbalance, under same conditions of STA based technique. Estimation of net piston force (f_n) was performed to detect imbalance in the cyclic torque. Based on estimated net piston force (\hat{f}_n), control law for CESTA based FTC technique was designed, which was applied to mitigate imbalance in the cyclic torque. Numerical simulation of the engine model was carried out under steady-state conditions as throttle valve angle and load torque were kept constant. It was assumed that estimate of load torque was available to implement the control technique, as already discussed in existing techniques [13, 112].

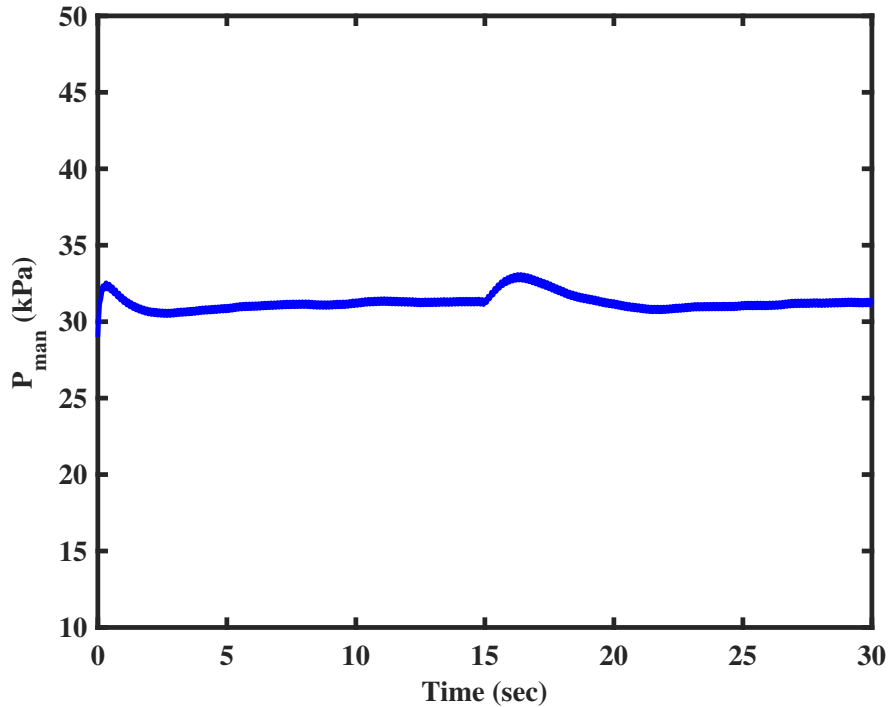


FIGURE 5.8: Intake Manifold Pressure

Fault in fuel injection subsystem was induced to generate imbalance in the cyclic torque. For $t \geq 15$ sec, fuel mass injected per combustion cycle (m_{fo}) was reduced due to such fault by 15% of the desired fuel mass, that was required to be injected. Intake manifold pressure of the engine model is shown in Figure 5.8. Imbalance in cyclic torque can be observed as manifold pressure is varied, when the fault is induced in fuel injection subsystem at $t = 15$ sec.

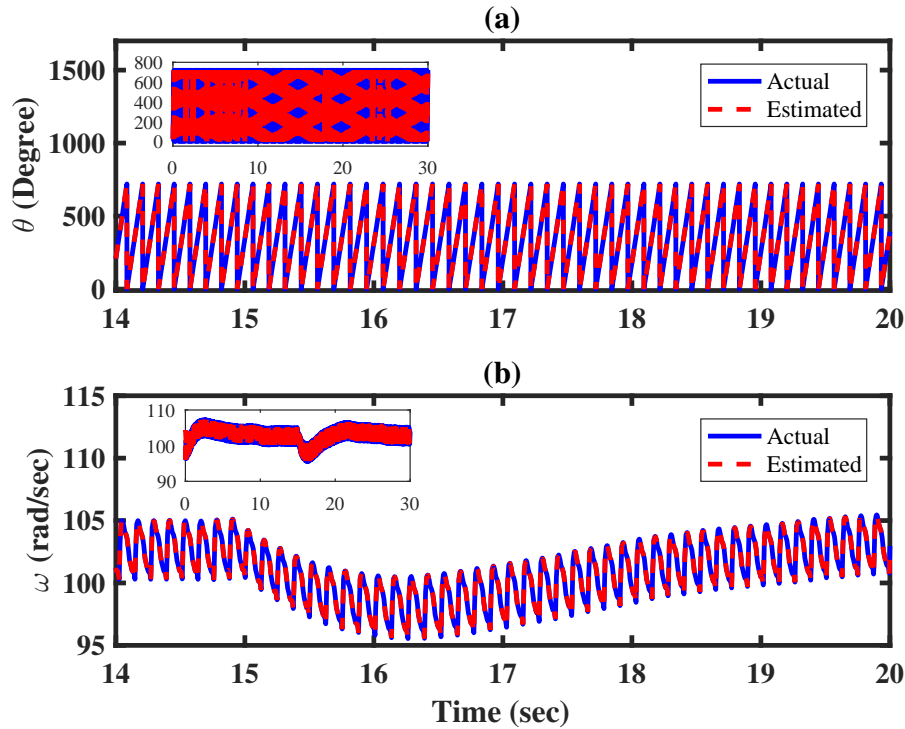


FIGURE 5.9: Estimation of (a) Engine Angular Position (b) Engine Rotational Speed

As discussed in Section 5.2, estimated net piston force (\hat{f}_n) was employed to design the control law. Engine angular position and rotational speed were observed to estimate net piston force (f_n), which acted as unknown input to engine speed dynamics. Plots for estimation of engine angular position and rotational speed are shown in Figure 5.9(a) and Figure 5.9(b), respectively.

As estimated states of engine speed dynamics converged to actual states, estimation error for both engine angular position and rotational speed converged to the origin as shown in Figure 5.10. Estimation errors showed exact and swift convergence of observed states to actual states of engine speed dynamics. At $t = 0$, a

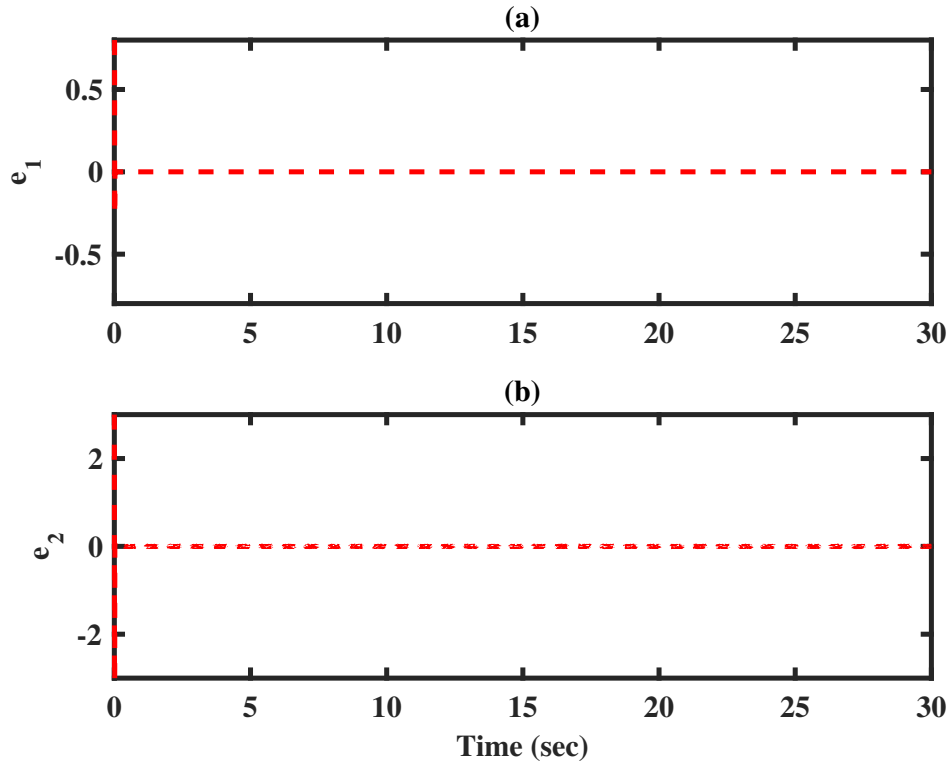


FIGURE 5.10: Estimation Error (a) Engine Angular Position
(b) Engine Rotational Speed

surge can be observed due to difference in initial conditions; however, it is diminished in 0.03 sec as sliding mode is achieved by FPEM based USOSM observer.

As estimated states converged to actual states i.e., $\hat{\theta}_1 \rightarrow \theta_1$ and $\hat{\omega}_1 \rightarrow \omega_1$; injection term (z_2) in the observer represented unknown input i.e., net piston force (f_n). LPF was applied to extract net piston force (f_n) from the injection signal. Both estimated and actual net piston force (f_n) are shown in Figure 5.11; whereas, in Figure 5.12, actual and desired net piston force (f_n) are shown.

In proposed unified framework, both observer and controller were implemented simultaneously. Imbalance in the cyclic torque was detected by FPEM based USOSM observer, which provided estimated net piston force (\hat{f}_n) to design the control law for mitigation of torque imbalance. Variations in actual net piston force (f_n) is noted for $t \geq 15$ sec; however, proposed control technique robustly adjusted the input to mitigate the fault in fuel injection subsystem and keep actual net piston force (f_n) close to desired values.

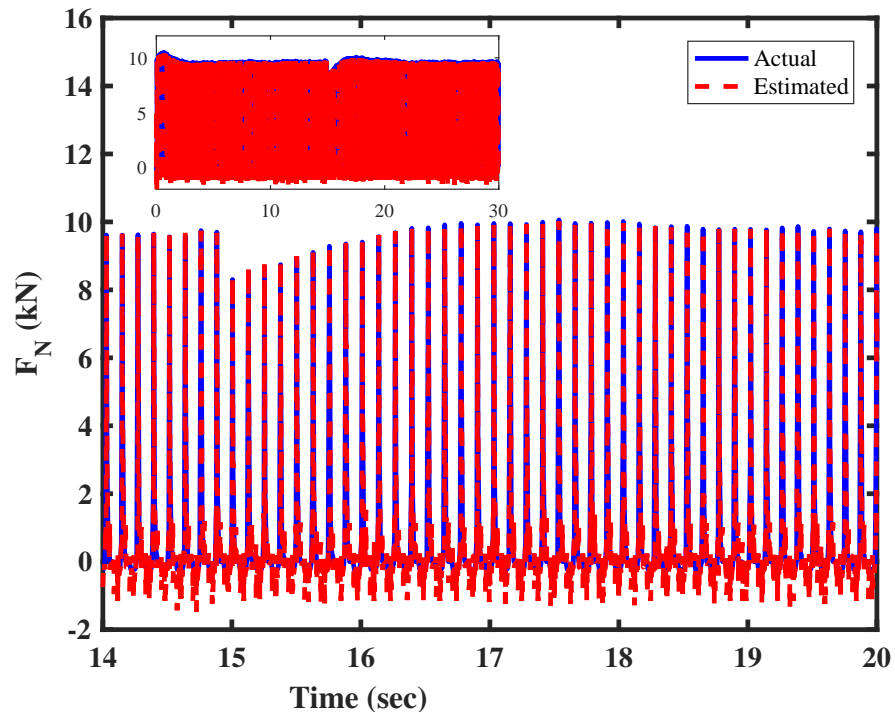


FIGURE 5.11: Estimation of Net Piston force (f_n) by FPEM based USOSM Observer

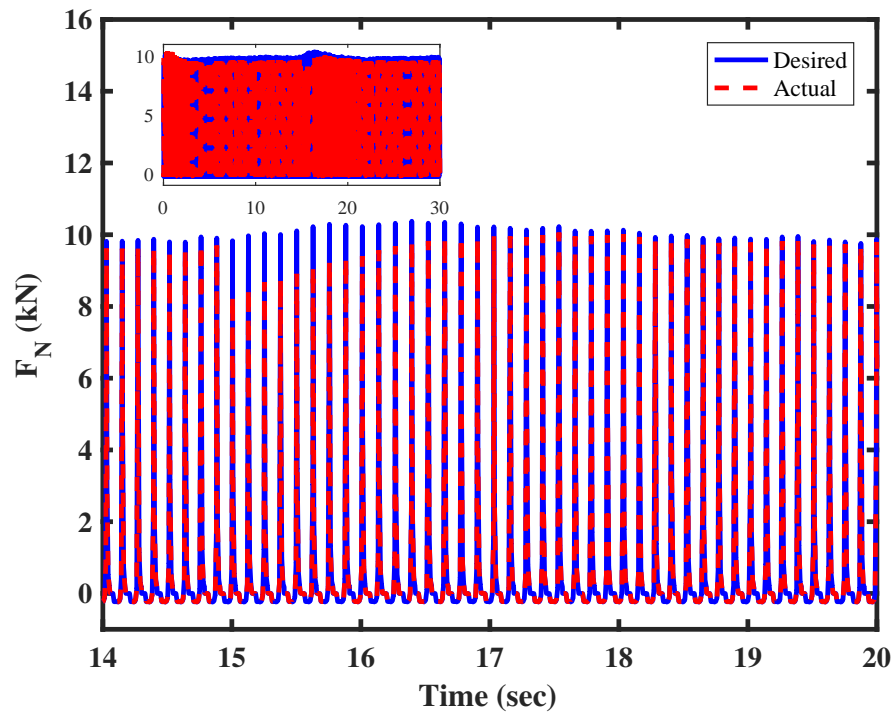


FIGURE 5.12: Mitigation of Cyclic Torque Imbalance by CESTA based FTC Technique - Desired and Actual Net Piston force (f_n)

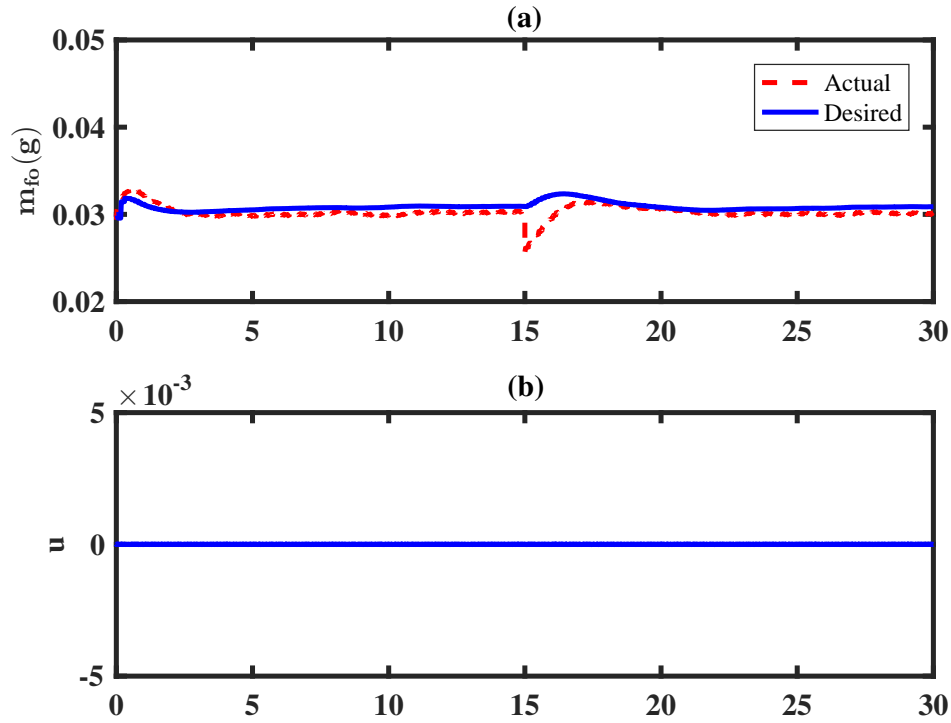


FIGURE 5.13: (a) Fuel Mass Injected per Combustion Cycle (b) Control Input

Plots of fuel mass injected per combustion cycle (m_{fo}) and control input (IPW) are presented in Figure 5.13(a) and Figure 5.13(b), respectively. It is noted in Figure 5.13(a) that actual fuel mass injected per combustion cycle (m_{fo}) remained close to desired fuel mass, even after occurrence of fault in fuel injection subsystem. Evaluation of proposed CESTA based FTC technique for mitigation of cyclic torque imbalance has demonstrated its instantaneous and accurate performance.

In CESTA based technique, fault in the actuator is estimated by using Eq. (5.63). Fault was induced in fuel injection subsystem for $t \geq 15$ sec, which reduced fuel flow into engine cylinder by 15%. Estimated fault $\hat{\Delta}$ is shown in Figure 5.14.

Chattering in sliding surfaces of STA and CESTA based FTC technique is shown in Figure 5.15 and Figure 5.16, respectively. As compared to STA based FTC technique, chattering was reduced significantly by CESTA based FTC technique. As compared to STA based FTC technique, smaller value of controller gains was used for CESTA based FTC technique. STA based part of the algorithm compensated unstructured uncertainty, which reduces the chattering.

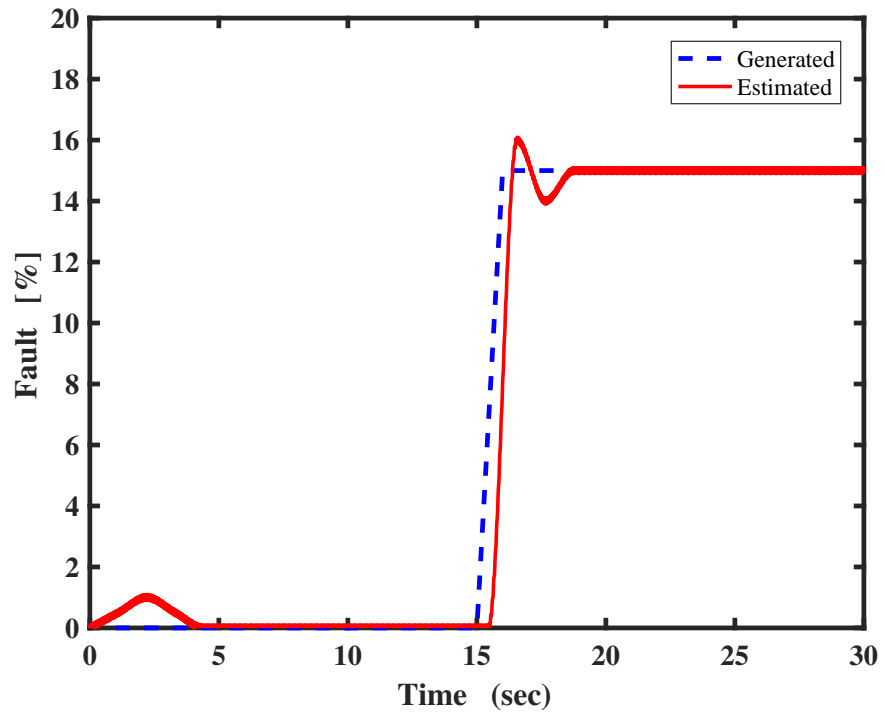
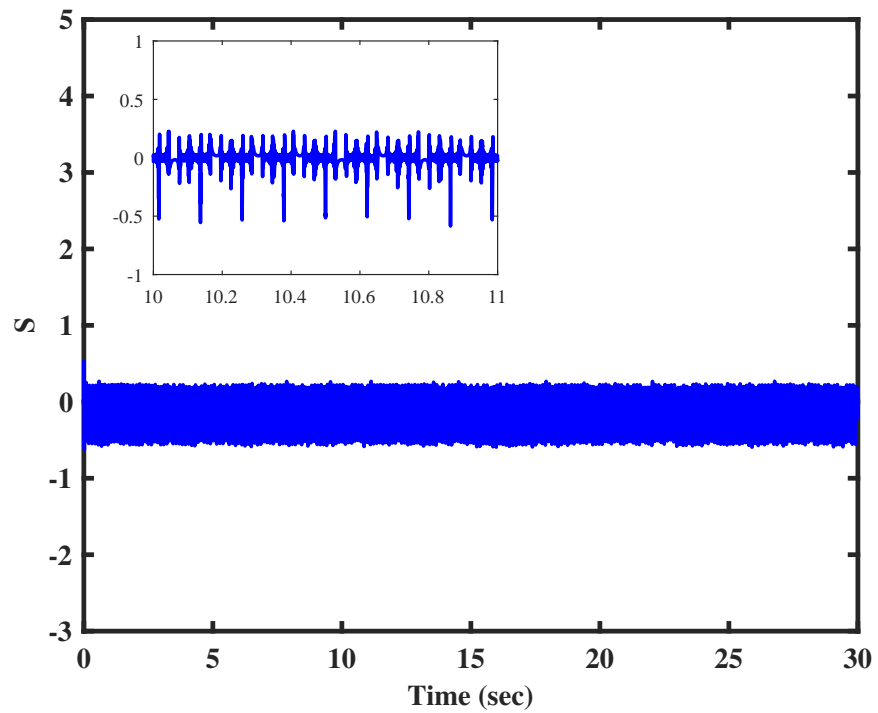
FIGURE 5.14: Fault Induced in Fuel Injection Subsystem at $t \geq 15$ sec

FIGURE 5.15: Sliding Surface of STA based FTC Technique

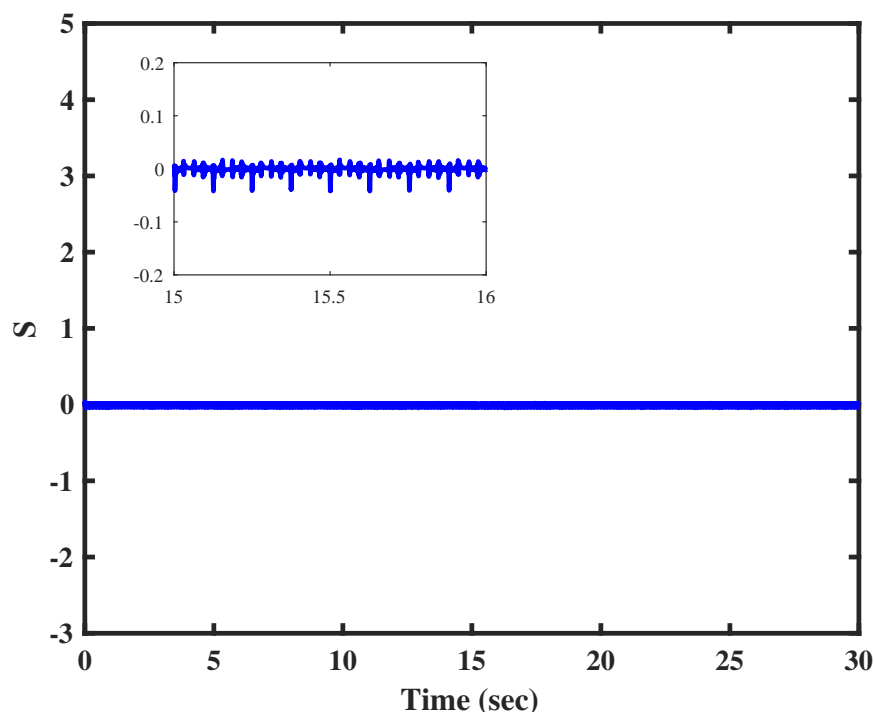


FIGURE 5.16: Sliding Surface of CESTA based FTC Technique

5.5 Chapter Summary

In this chapter, two observer based FTC techniques have been proposed to mitigate cyclic torque imbalance. Model based unified framework, that is comprised of FPEM based USOSM observer and observer based FTC technique has been presented in this chapter. This unified framework has been based on FPEM to detect and mitigate imbalance in the cyclic torque. Transformation in FPEM has been presented to develop the direct relationship between engine speed dynamics and fuel input. Performance of proposed FTC techniques has been demonstrated by numerical simulations.

In the next chapter, a framework is proposed to carryout robust speed tracking control for engine torque management. Variations appear in engine speed due to torque imbalance; whereas, desired speed set points are required to be followed by mitigating the fault that cause such imbalance. SSTA based FTC technique is proposed to mitigate effects of the fault in fuel injection subsystem and track desire speed profile.

Chapter 6

Robust Speed Tracking Control

The increasing complexity of engine control systems and its integration with control of vehicle dynamics has led to torque-based management of IC engines. One of the basic modules of engine control is speed tracking to meet the desired torque requirements. Undesired stresses in driveline, fuel consumption and exhaust emissions could increase if engine does not operate at optimal points, that are coordinated by engine torque and crankshaft speed. Improved performance of speed response under any operating conditions is the main motivation of engine speed tracking control.

The work presented in this chapter was not part of main research problem. However, it demonstrates significance of the transformation in FPEM to develop the techniques for mitigation of faults in fuel injection subsystem. In this chapter, SSTA based robust technique is proposed for engine speed tracking by employing the transformation in FPEM. Torque Imbalance cause variations in the engine speed. Tracking of desired speed set points is important to achieve required torque from the engine. In Section 6.1, speed tracking is described in conjunction with engine torque management. A brief review of different techniques for speed tracking of IC engines is presented in Section 6.2. SSTA based technique is discussed in Section 6.3, along with control law design. In Section 6.4, engine test rig is described, that is used to acquire desired set points of engine speed. Robust speed

tracking control is discussed in Section 6.5, followed by summary of the chapter in Section 6.6.

6.1 Engine Speed Tracking and Torque Management

Gasoline engine control has been focused on various problems, that included control of idle speed [180], AFR [80], spark timing [171], knock [181] and engine torque [114]. Many techniques were proposed to formulate solution for these problems, out of which some were focused on engine torque management [182] and speed tracking control [183]. Speed control has been one of the extensively researched problem related to engine control.

As already discussed, output torque generated by engine cylinders is usually not uniform. Fluctuations in output speed is inevitable due to cylinder to cylinder or cyclic imbalance in torque generation. Engine performance criteria, such as exhaust emissions, fuel efficiency and drivability are degraded due to such variations in speed. Thus, speed control is essential to improve the engine performance.

Engine speed depended on torque demand that is passed by the driver. Engine systems could be split into two subsystems from input throttle valve angle to output speed. One of the subsystems is from input throttle valve to generation of the torque in engine cylinder, whereas other subsystem is from generated torque to output speed. Speed tracking problem encompass the computation of torque demand and control of torque production to track desired set points of engine speed.

Working principle of speed generation in gasoline engines is based on various subsystems, which are shown in Figure 6.1. Throttle valve angle manages the flow of air into intake manifold. ECU calculates the fuel mass that is required to be injected, that is mainly based on air mass flow rate along with input from different sensors. Fuel injection signal controls mass flow rate of the injected fuel; whereas,

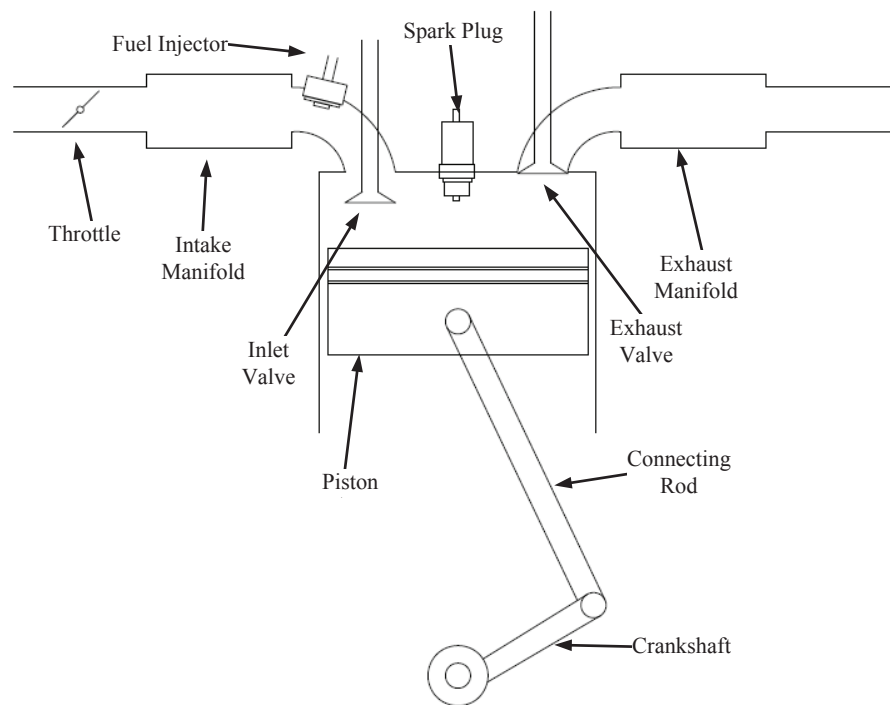


FIGURE 6.1: Speed Generation Subsystems in Gasoline Engine

spark command controls combustion process in the cylinder. During combustion process, air fuel mixture burns to produce mechanical work in the cylinder, which generates engine torque by rotational motion of the crankshaft. Conventionally, control signals to generate desired speed have included throttle valve angle, fuel injection and ignition timing command. For speed generation subsystems, throttle valve angle is primary control input, which controls mass flow rate of the air into intake manifold. Based on mass of air inducted in the cylinder, fuel mass is injected to regulate the AFR; whereas, spark timing influences the combustion process for engine speed generation to meet the torque requirements.

Accurate tracking of speed for engine torque management allows to implement various control functions of engine powertrain. Depending upon the requirement, engine torque management control the actuators that can influence generation of the torque by varying the engine speed. Torque management enhances engine performance by reducing exhaust emissions and improving fuel economy, that can be accomplished by complete combustion of air fuel mixture in engine cylinder. Torque management is used in both speed control and torque control modes. Signal

for actuator control is provided by torque control module to achieve desired engine speed under varying load conditions [184].

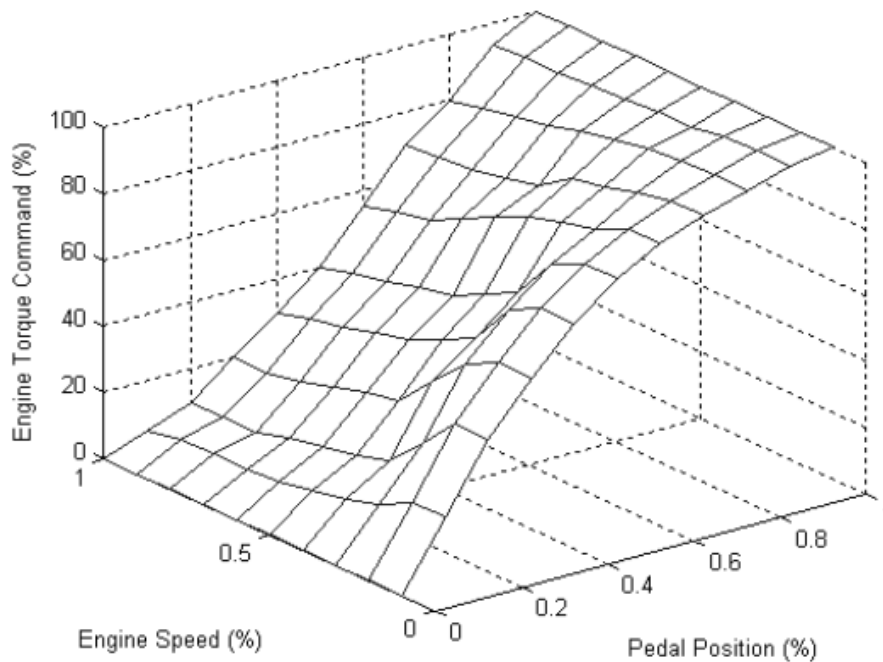


FIGURE 6.2: Map between Torque Demand, Position of Accelerator Pedal and Engine Speed [182]

Control techniques for speed tracking are usually based on mapping between throttle valve angle and engine speed to meet the torque requirements [182]. In general, torque generated by gasoline engine is directly related to mass flow of the air into intake manifold. Desired torque information is passed to the engine by varying the throttle valve angle; whereas, load torque acts as disturbance to engine torque management. Thus, both throttle valve angle and load torque characterize requirement of the torque generation. Also, information of desired torque does not exist in reality as accelerator pedal position acts as driver's input for torque requirement. Signal of pedal position is interpreted as desired torque that must be delivered by vehicle driveline. Driver's torque demand is given by pedal map, which correlate position of accelerator pedal and engine speed. Also, throttle position corresponds with position of accelerator pedal. Thus, only interface between position of accelerator pedal and torque management are set points of the desired speed. Pedal map for torque demand is shown in Figure 6.2, which gives the relation between torque demand, position of accelerator pedal and engine speed.

6.2 Existing Approaches for Engine Speed Tracking Control

Speed control techniques for gasoline engines were mainly focused on idle speed control and considered nonlinearities of the system and disturbances in the form of external torque [185]. However, control techniques were also proposed for speed tracking.

Optimal speed tracking by torque control of the gasoline engine was described in [183]. Cost function was derived to provide the tradeoff between fuel consumption and speed tracking performance. Based on the cost function, optimal torque demand for desired speed profile was provided by applying the dynamic programming. An observer was derived to estimate the engine torque by employing MVEM; whereas, engine speed was estimated by using the crankshaft model. Based on estimated torque, PI controller was implemented to track the torque demand. In [186], engine speed tracking based on Model Predictive Control (MPC) was discussed for heavy-duty vehicles. With a torque-based control architecture, this technique was proposed to track speed by variable weight factor and engine load estimation; whereas, torque was estimated from engine speed and fuel mass. Based on torque requirement, variable weighting factor method was proposed to optimize the control objective and compared with gain-scheduled Proportional Integral Derivative (PID) controller. Relationship between speed response and engine torque was also discussed in [187], which used speed oscillations to calculate the torque. An electrical circuit model, which represented engine dynamics was proposed and engine torque was estimated by crankshaft acceleration measurements in [99].

One of the recent works on speed tracking control was described in [188]. In this work, speed tracking performance of the gasoline engine was analyzed in the presence of time-varying uncertain parameters. Uncertainty was induced due to variations in either spark timing, air path or fuel efficiency. Proposed control technique was based on double closed-loop cascade active disturbance rejection. Both

inner and outer loops were comprised of extended state observer and disturbance rejection controller. The outer loop catered for errors in speed signal; whereas, the inner loop handled errors in manifold pressure. To acquire desired engine speed, set points of the inner loop were driven by time varying uncertainty, load torque and outer loop. Set points for manifold pressure were matched by throttle valve angle; which were driven by pumping fluctuations of air charge, mass flow rate of the air leaving intake manifold and inner loop. Gains of both controllers as well as observers for the inner and outer loop were calculated by Linear Matrix Inequalities (LMI).

In [189], speed control during vehicle deceleration was discussed. Engine speed is required to be kept close to speed of turbine, when bypass clutch is opened, which ensured better vehicle response for succeeding acceleration. It is required that torque disturbances are not present during crossing between turbine and engine speed to maintain vehicle drivability. In this work, engine speed was controlled during deceleration of the vehicle by coordinating air flow rate and spark timing of the gasoline engine. Also, different constraints were managed, which included stability of combustion, engine stall and limit of actuators. MPC based technique was proposed to control spark timing and air flow rate to track reference speed, despite presence of different constraints. In [190], SMC based technique was proposed for engine speed control. Also, effect of parameter variations on engine performance were investigated. Parameters of the controller were applied to nominal as well as perturbed models. In [191], control technique was presented that was based on MVEM of the gasoline engine. Proposed control technique was comprised of dual control loops. One loop improved speed tracking performance by receding horizon optimization, whereas other loop controlled injected fuel mass.

Although different techniques were proposed for engine speed tracking control; however, these techniques employed MVEM to track the desired speed set points. MVEM has throttle valve angle as explicit control input and does not provide direct relation between engine states and other control inputs i.e, ignition timing, valve timing and injected fuel mass. In MVEM, throttle valve angle has been employed as explicit control input to develop the engine control and diagnosis

techniques [80, 81]. However, spark timing, valve timing and fuel injection have been computed from empirical relations; as MVEM does not provide direct relationship between these control variables and engine states. For example, AFR relationship is used to compute mass of the fuel required to be injected from air mass inducted into engine cylinder [80]. Thus, it is not possible to consider faults in these actuators and develop control methodologies for such faults. Whereas in next section, speed tracking framework is presented by applying (*IPW*) as explicit input to control engine speed.

6.3 Robust Speed Tracking Control

Torque imbalance also cause variations in engine speed. Desired engine speed profile is required to be followed by mitigating the fault that cause torque imbalance. One of the research contributions of this dissertation, is *transformation in FPEM to develop the direct relation between engine speed and fuel input (IPW)*. The robust technique presented in this chapter is based on this transformation in FPEM, that has been already discussed in Subsection 5.2.4. A framework has been proposed to carryout speed tracking control for torque management of gasoline engines. In [192, 193], this framework was applied to track set points of engine speed to meet desired torque by employing the transformation in FPEM.

In robust speed tracking control, set points of engine speed are tracked despite occurrence of the fault in engine subsystems. During normal driving conditions, engine torque management use throttle valve to attain desired torque from drive-line of the vehicle. Based on mass of the air inducted into engine cylinder (m_{ao}), fuel mass injected per combustion cycle (m_{fo}) is calculated to keep the AFR at stoichiometric value. As discussed in Section 6.1, throttle valve angle is varied to change mass flow rate of the air into intake manifold (\dot{m}_{ai}) and achieve desired set points of engine speed.

In subsequent sections, SSTA based robust technique is presented to carryout speed tracking for engine torque management. Fuel mass injected per combustion

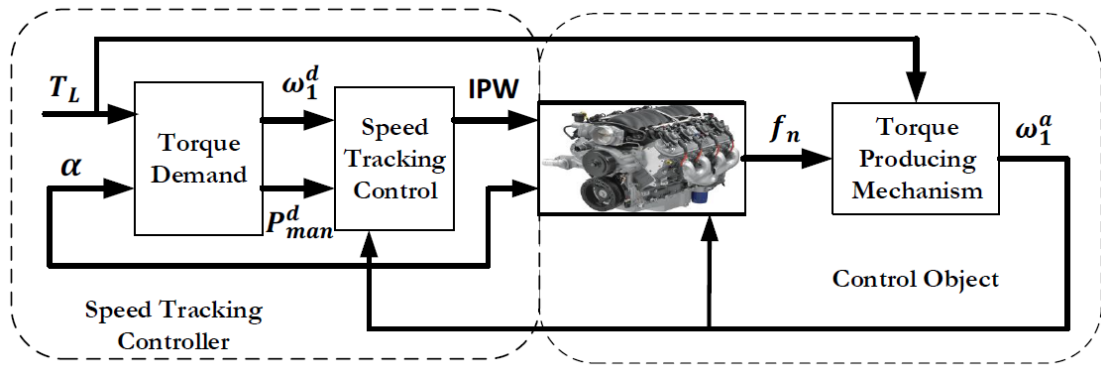


FIGURE 6.3: Proposed Framework for Engine Speed Tracking Control

cycle (m_{fo}) may decrease due to faults in fuel injection subsystem. Hence, desired speed profile of engine could not be tracking as mass of combustion mixture is reduced. The proposed technique ensured tracking of desired speed set points, despite occurrence of the fault in fuel injection subsystem. The control input i.e. (IPW) is robustly adjusted by proposed technique to regulate injected fuel mass and mitigate the effect of fault in it.

The SMC has certain advantages as compared to other nonlinear control techniques, which includes, better convergence rate, robustness to disturbances/perturbations, uncertainties, reduction in system order on sliding surface and invariance with respect to parametric variations. The proposed framework is for engine speed tracking control by using appropriate controller; however, Sliding Mode Control (SMC) based technique was applied for robust speed tracking control to mitigate the effect of faults in fuel injection subsystem. SMC has inherent feature of robustness to uncertainties and disturbances [152, 158]. As sliding mode is achieved, order of the system is reduced and system depended on sliding dynamics due to invariance property of SMC. Uncertainties in the system, such as matched disturbance in the form of faults in fuel injection subsystem is rejected due to inherent feature of invariance of SMC. Thus, robustness is added in speed tracking control framework by application of SMC based techniques.

Proposed control framework for engine speed tracking is shown in Figure 6.3; where ω_1^d represent desired engine speed, ω_1^a represent actual engine speed and P_{man}^a represent the actual manifold pressure of the engine. This framework has

two modules; speed tracking controller and gasoline engine. In speed tracking controller module, “*Torque Demand*” block represent calculation of the torque that is required to be generated by gasoline engine. Based on load torque and position of the throttle valve angle, torque required by the engine is calculated as desired engine speed depend on torque requirement. Torque demand was already computed by ECU of the test rig engine and desired engine speed was acquired from it. Based on desired speed, “*Speed Tracking Control*” block passed the fuel control command to “*Fuel Subsystem*” of the engine module. Throttle valve angle varied the flow rate of the air that entered into “*Air Intake Subsystem*”. The “*Fuel Subsystem*” and “*Air Intake Subsystem*” control the flow rate of the fuel and air, respectively, which are inducted into the cylinder. Net piston force (f_n) was produced in engine cylinder that acted on “*Torque Producing Mechanism*” to generate the actual engine speed.

6.3.1 Smooth Super-Twisting Algorithm

Computation of sliding surface derivatives is a constraint to apply HOSM. This limitation was relaxed by STA, proposed in [158]. In a multi-loop system, STA does not improve performance when a continuous signal is required by inner loop from the outer loop [194]. To overcome such shortcoming, SSTA was proposed in [195]. Structure of SSTA is composed of two continuous terms, as given in Eq. (6.1a). First term is the continuous function of sliding variable, as mentioned in Eq. (6.1b); whereas, second term contain the integral of discontinuous action, given in Eq. (6.1c).

$$\bar{u} = u_a + u_b \quad (6.1a)$$

$$u_a = -k_1 |S|^{\frac{\rho-1}{\rho}} \text{sign}(S) \quad (6.1b)$$

$$\dot{u}_b = -k_2 |S|^{\frac{\rho-2}{\rho}} \text{sign}(S) \quad (6.1c)$$

Sufficient conditions for finite time convergence of SSTA are given in Eq. (6.2). Parameters k_1 , k_2 , ν , ϵ , χ , ρ are positive constants, such that $0 < \nu < 1$, $\gamma > 1$

and $\nu\epsilon > 2$ [194].

$$\begin{aligned} k_1 &= \frac{\chi}{y} \sqrt{\frac{2\epsilon L}{(1-\nu)\psi}} \\ k_2 &= L \left[\frac{\rho(1+\nu) - \nu}{\rho(1-\nu) + \nu} \right] \\ \rho &\geq 2 \end{aligned} \tag{6.2}$$

6.3.2 Control Law

Robust engine speed tracking was accomplished by developing the SSTA based control technique, which is robust to parametric uncertainties, disturbances and unmodeled system dynamics. Sliding surface was designed to meet the desired control objective. As SMC design is comprised of two steps; thus, sliding surface was defined in first step, followed by design of control law in second step. The control law forces trajectories of system states toward sliding manifold.

Engine states, given in Eq. (3.30a-3.30c) can be expressed as:

$$\dot{x} = f(x) + g(x, U) \tag{6.3}$$

where, $x = [P_{man}, m_{fo}, \omega_1]^T \in \mathfrak{R}^n$; $U \in \mathfrak{R}^m$; $f : \mathfrak{R}^n \rightarrow \mathfrak{R}^n$; $g : \mathfrak{R}^m \rightarrow \mathfrak{R}^m$. Also, $f(x)$ and $g(x, U)$ are smooth vector fields. Control input vector (U) is comprised of throttle valve angle (α) and IPW .

Keeping in view the control objective, following sliding surface was defined:

$$S(t, x) = m_{fo}^a - m_{fo}^d \tag{6.4}$$

where, m_{fo}^a is actual fuel mass injected per combustion cycle, m_{fo}^d is desired fuel mass injected per combustion cycle that was calculated from manifold pressure (P_{man}) acquired from engine test rig. $S(t, x)$ is sliding variable, required to be steered to zero along with its first total time derivative.

Desired fuel mass injected per combustion cycle (m_{fo}^d) was calculated from mass of the air inducted into engine cylinder (m_{ao}). Manifold pressure (P_{man}) acquired from engine test rig was employed to calculate mass of air inducted into engine cylinder (m_{ao}) from following relation [1]:

$$m_{ao}^d = \eta_v \times \frac{(V_d + V_c)P_{man}^d}{RT_{man}} \quad (6.5)$$

Using following relation, desired fuel mass injected per combustion cycle (m_{fo}^d) was computed from desired mass of air (m_{ao}^d), given in Eq. (6.5):

$$m_{fo}^d = \frac{m_{ao}^d}{AFR} \quad (6.6)$$

IPW is the time duration for which a fuel injector delivers fuel. It acts as control input to fuel injection subsystem and regulate the mass of fuel injected per combustion cycle (m_{fo}). As discussed in Chapter 3, *IPW* was converted into crank angle rotation to calculate mass flow rate of injected fuel (\dot{m}_{fi}) from mass flow rate of fuel injector (\dot{m}_{fInj}).

Based on *IPW*, actual fuel mass injected per combustion cycle (m_{fo}^a) was computed from mass flow rate of injected fuel (\dot{m}_{fi}) by using following relations of engine fuel dynamics, already given in Eq. (3.30b).

$$\dot{m}_{fo}^a = \dot{m}_{fv} + \dot{m}_{ff} \quad (6.7)$$

where,

$$\begin{aligned} \dot{m}_{fv} &= (1 - X_f)\dot{m}_{fi} \\ \dot{m}_{ff} &= \frac{1}{\tau_f}(-\dot{m}_{ff} + X_f\dot{m}_{fi}) \end{aligned} \quad (6.8)$$

Proposed control law guaranteed that $S = \dot{S} = 0$. It also ensured convergence of actual fuel mass to desired value i.e., $m_{fo}^a = m_{fo}^d$, despite presence of disturbance and faults in fuel injection subsystem.

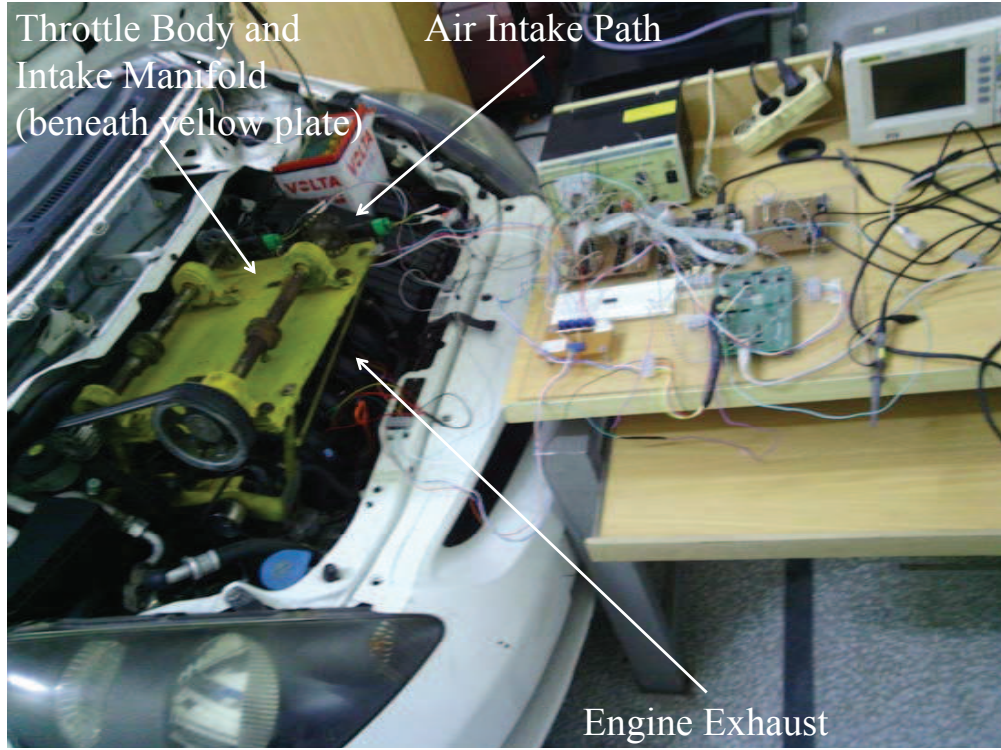


FIGURE 6.4: Engine Experimental Setup

Following dynamics of the sliding variable were derived:

$$\dot{S} = \frac{\partial}{\partial t}S(t, x) + \frac{\partial}{\partial x}S(t, x).(f(x) + g(x, u)) \quad (6.9)$$

Accordingly, the control law was designed, which was based on SSTA, given in Eq. (6.1a). Design parameters of the proposed control technique i.e., k_1 , k_2 , ρ were calculated to satisfy the conditions given in Eq. (6.2).

The complete control action was proposed as:

$$u = u_{eq} + \bar{u} \quad (6.10)$$

where u_{eq} is equivalent control and \bar{u} is designed using SSTA, given in Eq. (6.1a). Equivalent control (u_{eq}) was computed from nominal systems, given in Eq. (6.9) by solving for u such that $\dot{S} = 0$. The equivalent control (u_{eq}) was added to make the control technique model based and enhance its performance by reducing chattering. This control law was applied to achieve the desired objective of engine

speed tracking control despite occurrence of the fault in fuel injection subsystem.

6.4 Engine Test Rig

Reference data was acquired from engine test rig for validation of the proposed technique. A 1300 cc, four cylinder, gasoline engine based test rig formed the basic component of experimental setup, shown in Figure 6.4. Each cylinder was fitted with two spark plugs and two intake valves; whereas separate coil was fitted for each spark plug.

This engine was equipped with Intelligent Duel Sequential Ignition, which ignited the fuel according to engine speed. Test engine had OBD-II compliant data acquisition and logging devices and fitted with ECU. Specifications of the test rig engine are mentioned in Table 6.1.

TABLE 6.1: Specifications of Test Rig Engine

Parameter	Unit	Value
Crank offset	<i>cm</i>	5.1
Mass of the piston	<i>kg</i>	0.5
Engine displacement	<i>cm</i> ³	1294
Mass of crankshaft	<i>kg</i>	11
Mass of connecting rod	<i>kg</i>	0.6
Length of connecting rod	<i>cm</i>	14.5
Compression ratio of the engine	-	10.5

Main components of engine test rig are discussed as follows:

6.4.1 On-board Diagnostic Interface

Engine test rig was fitted with OBD-II compliant ECU. Operational data of the engine was acquired by using standard OBD-II data logging device. Load torque information was provided by OBD-II interface that is based on static modeling approach. Each sample was provided by this interface with a unique time stamp. Data of different parameters along with respective time stamps was obtained and

linear interpolation was applied between these data samples. For each data set, following engine states and parameters were acquired by using OBD-II interface:

1. Throttle valve angle.
2. Intake manifold pressure.
3. Crankshaft rotational speed.
4. Engine load.
5. Spark advance.

Engine sensors passed the measured data to ECU. Sensors, such as Manifold Air Pressure (MAP) and Intake Air Temperature (IAT) were placed in the path of intake air. Oxygen sensor was positioned in exhaust air path. Engine output speed was measured by crankshaft position sensor, that was installed on engine fly wheel. ECU passed the command to fuel injection and spark ignition subsystems, which was based on measurement of these sensors.

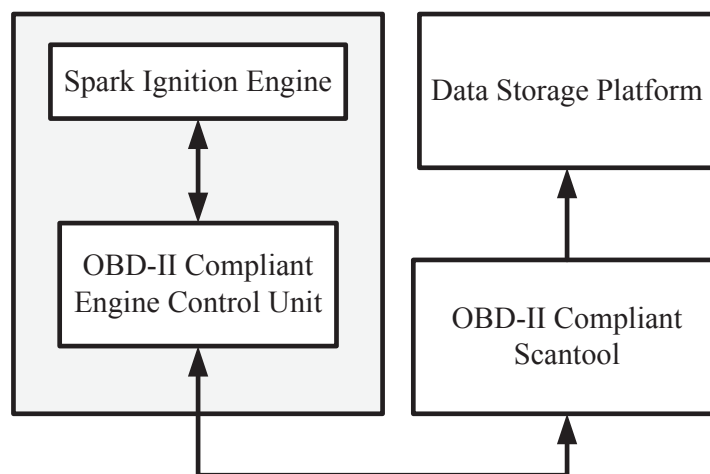


FIGURE 6.5: Data Acquisition System based on OBD-II

6.4.2 Data Acquisition

Engine rotational speed was obtained by using high speed data acquisition interface. A contact less hall effect based rotational encoder was fitted in the engine, with 12 – 1 configuration to indicate reference position. Sensor data was acquired

using NI-DAQ-9001 data acquisition card for engine rotational speed pattern. Architecture of the OBD-II based data acquisition system is shown in Figure 6.5.

6.5 Results and Discussion

SSTA based robust speed tracking control was implemented to track reference engine speed, despite occurrence of the fault in fuel injection subsystem. Reference data was acquired from test rig of 1300 cc, four-cylinder gasoline engine by using OBD-II compliant data logging and scanning software. Reference value of throttle valve angle, load torque, manifold pressure and engine speed was acquired from engine test rig to validate the proposed control technique.

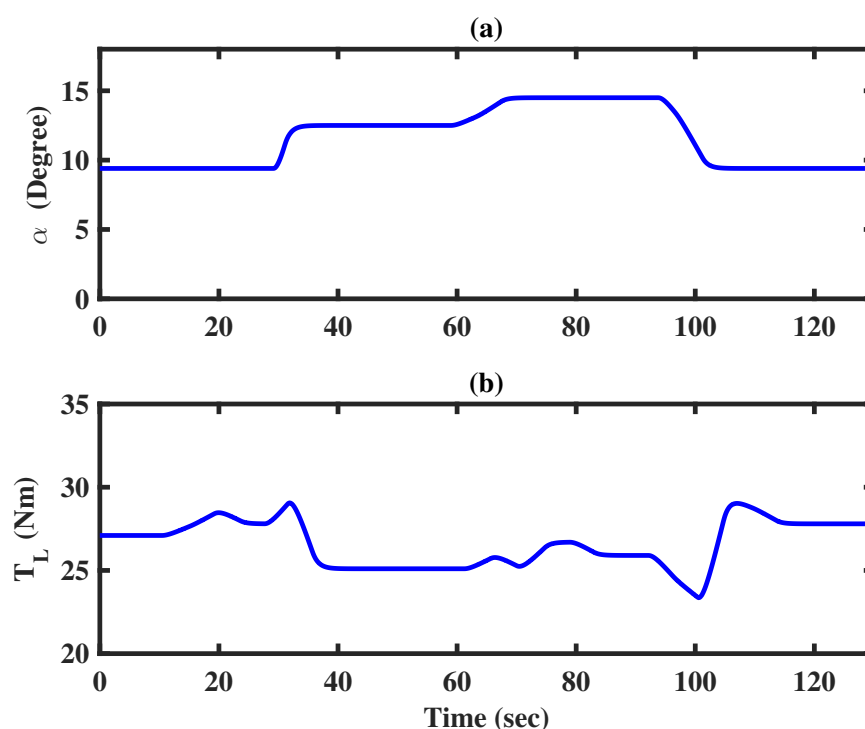


FIGURE 6.6: Plot of (a) Throttle Valve Angle (b) Load Torque

In Figure 6.6(a), throttle valve angle (α) is shown, whereas varying load torque (T_L) is shown in Figure 6.6(b). Both throttle valve angle and load torque were varied to vary the reference engine speed. Throttle valve angle (α) acted as input to manifold pressure dynamics, whereas load torque (T_L) is exerted by vehicle dynamics; which acted as disturbance to engine torque management.

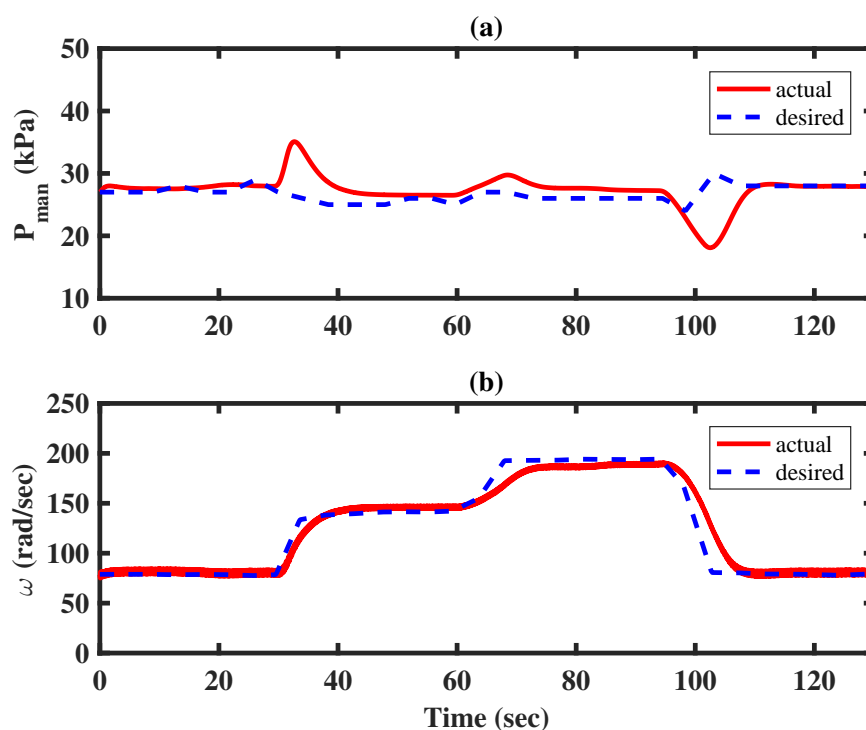


FIGURE 6.7: Plot of Engine States (a) Manifold Pressure (b) Engine Output Speed

Engine states are shown in Figure 6.7. Actual manifold pressure is shown in Figure 6.7(a) along with reference manifold pressure, which was acquired from engine test rig. Actual manifold pressure was calculated by using throttle opening information and its values matched with the reference values.

Desired and actual engine output speed are shown in Figure 6.7(b), which demonstrated performance of the proposed technique by tracking the reference speed profile. Temporary blockage in fuel injection was induced at different time intervals; i.e., from 15 sec to 25 sec, 45 sec to 55 sec and 80 sec to 90 sec. Fuel mass injected per combustion cycle (m_{fo}) was reduced due to such faults by 15% of the desired fuel mass that was required to be injected. However, proposed SSTA based technique robustly adjusted the control input IPW to regulate injected fuel mass and mitigate the induced fault track engine speed set points. It also demonstrated robustness of the proposed technique as speed tracking was attained despite presence of varying load torque, which acted as disturbance to engine torque management. Load torque was assumed know as it was acquired from the engine

using OBD-II data logging and scanning software.

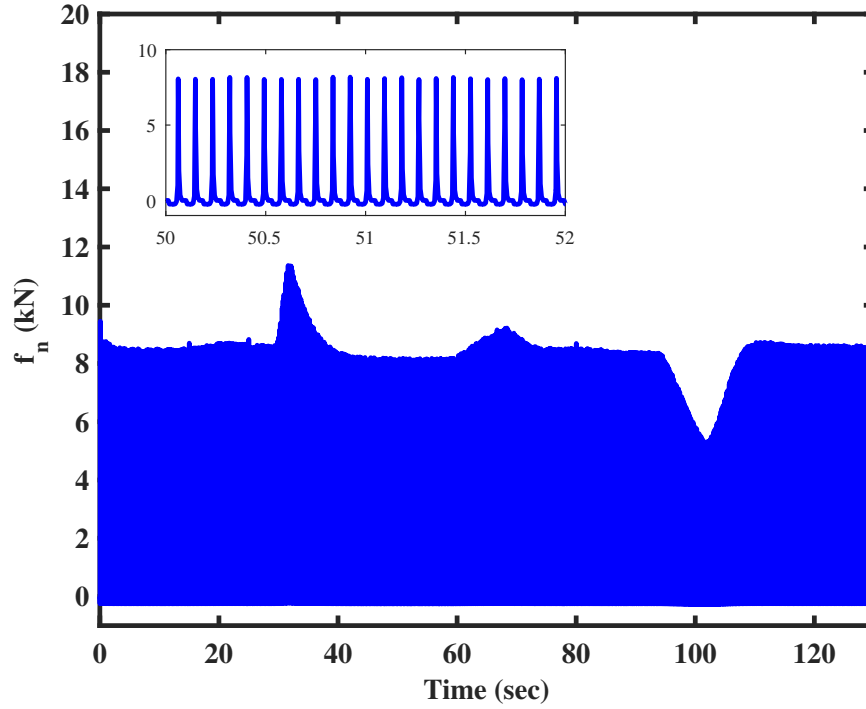


FIGURE 6.8: Net Piston Force (f_n)

Unlike MVEM, net piston force (f_n) is calculated in FPEM as shown in Figure 6.8. Net piston force (f_n) directly corresponded with the torque generated by gasoline engine. Variations in net piston force (f_n) represented variance in engine torque.

Fuel mass injected per combustion cycle (m_{fo}) is shown in Figure 6.9. Mass of injected fuel varied at start and end of the induced fault. Despite occurrence of the fault in fuel injection subsystem, proposed technique guaranteed that actual fuel mass injected per combustion cycle (m_{fo}^a) matched the desired value of fuel mass required to be injected (m_{fo}^d). It ensured that actual engine speed followed the desired speed set points by mitigating the fault in fuel injection subsystem and rejecting disturbance in the form of varying load torque. For comparison, fuel mass injected per combustion cycle (m_{fo}) with no fault in fuel injection subsystem is also shown in Figure 6.10.

Sliding surface and control input IPW are shown in Figure 6.11(a) and Figure 6.11(b), respectively. Sliding surface convergence to equilibrium point exhibited that desired control objective was achieved. Whereas, IPW regulated mass flow

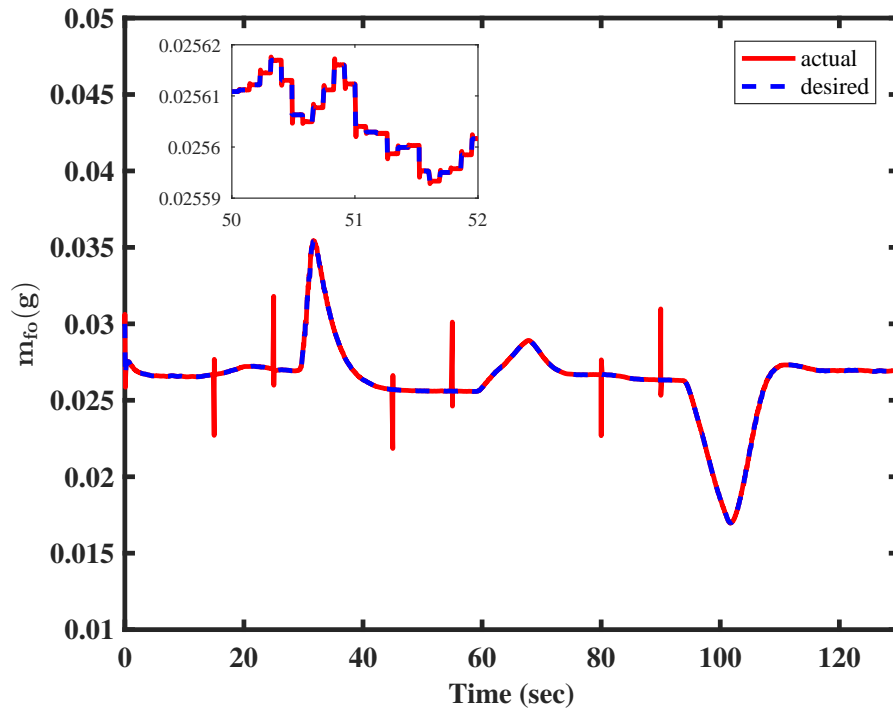


FIGURE 6.9: Fuel Mass Injected per Combustion Cycle (m_{fo}) with Faults in Fuel Injection Subsystem

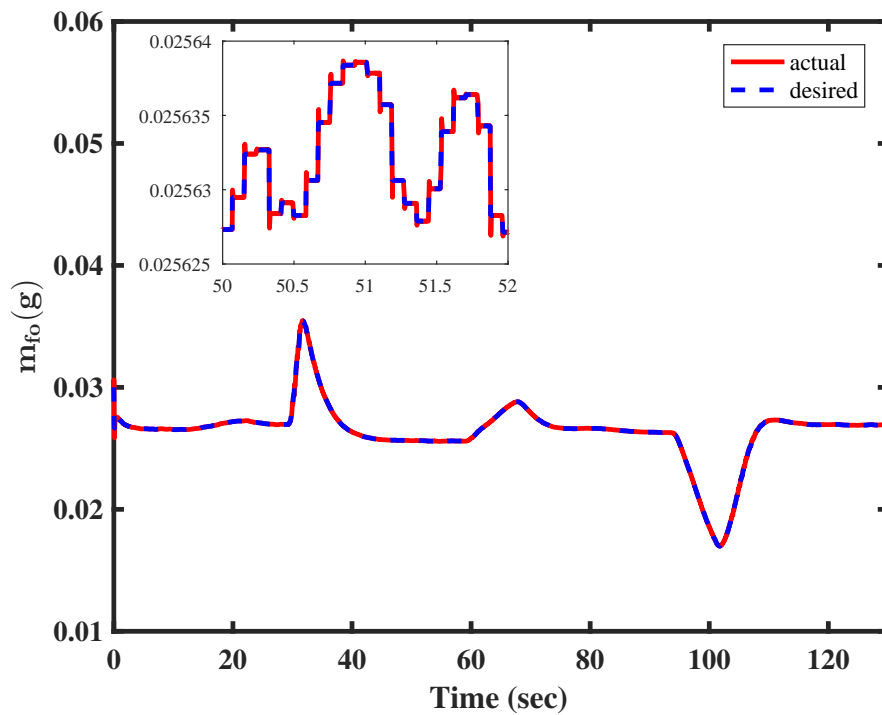


FIGURE 6.10: Fuel Mass Injected per Combustion Cycle (m_{fo}) with no Fault in Fuel Injection Subsystem

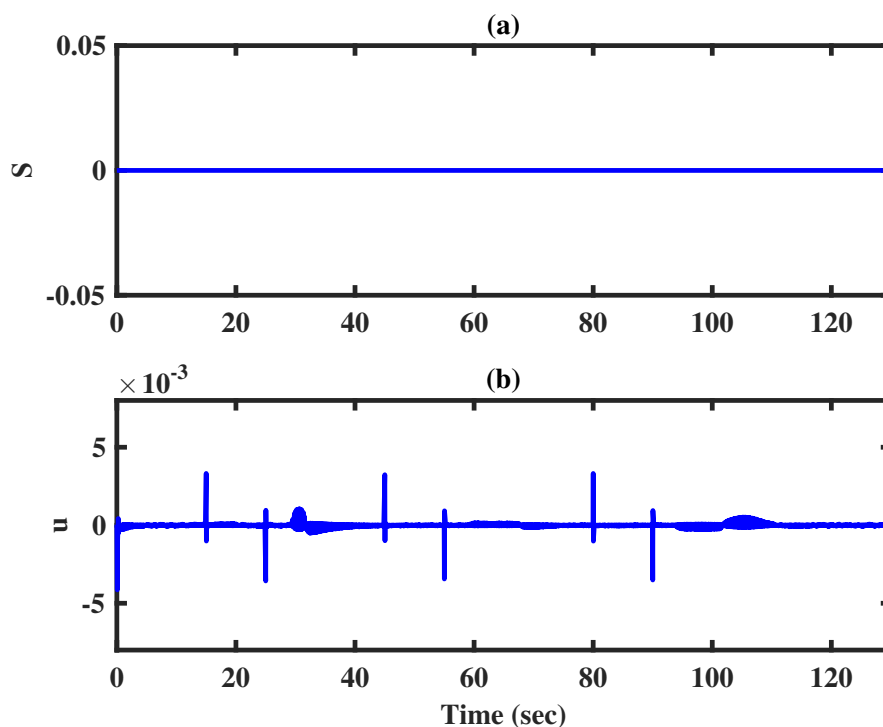


FIGURE 6.11: Plot of (a) Sliding Surface (b) Control Input

rate of the injected fuel (\dot{m}_{fi}) to ensure that actual fuel mass injected per combustion cycle (m_{fo}^a) followed the desired values (m_{fo}^d).

6.6 Chapter Summary

Speed tracking is one of the basic modules of engine control to meet the torque requirements. Accurate tracking of engine speed under different conditions allows to implement various control functions of vehicle powertrain.

In this chapter, SSTA based technique has been proposed for robust speed tracking control to manage the engine torque. Engine speed tracking has been discussed in conjunction with engine torque management. Transformed FPEM has been utilized to develop the proposed control technique; which ensured to follow desired speed set points despite occurrence of faults in fuel injection subsystem. Proposed control technique has also been robust as it rejected disturbances in the form of varying load torque.

Chapter 7

Conclusion and Future Work

In this dissertation, a model based novel unified framework has been proposed for detection and mitigation of cyclic torque imbalance. Engine torque imbalance is generated due to non-uniform contents of the engine cylinder, caused by disparities in the fuel injection, air intake path, stochastic features of combustion process and aging of engine components.

This manuscript starts with discussion on cyclic torque imbalance. An overview of engine balancing with main focus on torque balancing has been presented. Classes of torque balancing are described, besides causes, impact and application of cyclic torque imbalance. Main methodologies for detection and mitigation of torque imbalance along with review of existing approaches have been presented. Cyclic torque imbalance detection and engine rotational speed based approaches have been reviewed; followed by research analysis and problem statement.

In this research work, FPEM has been employed to model the gasoline engine, instead of MVEM. Modeling approaches for gasoline engines have been discussed besides crankshaft models that were proposed in existing literature to model oscillations in engine rotational speed. Review of modeling approaches to incorporate torque production subsystem in engine models has also been presented. FPEM has been described along with derivation of torque production subsystem model.

Validation of torque production subsystem model has been presented by its comparison with speed dynamics of GT-Power based engine model.

In the first part of contributed work, detection of imbalance in the cyclic torque has been presented by derivation of FPEM based USOSM observer for estimation of net piston force (f_n) from engine speed dynamics. Variations in the estimated net piston force (\hat{f}_n) provides a direct measure of imbalance in the cyclic torque. Fault in fuel injection subsystem has been induced to generate cyclic torque imbalance. The proposed FPEM based USOSM observer has been validated by employing speed dynamics of GT-Power based engine model. Detection of cyclic torque imbalance has been conducted under lab conditions. The engine was operated at steady state by keeping throttle valve angle and load torque at constant values.

In the second part, observer based FTC techniques have been proposed for mitigation of cyclic torque imbalance. Estimated net piston force (\hat{f}_n) has been employed to design the control law for FTC techniques. FPEM has been transformed to derive the direct relation between engine speed dynamics and IPW and employed to develop STA and CESTA based FTC techniques.

Model based unified framework for detection and mitigation of cyclic torque imbalance has been accomplished by derivation of FPEM based USOSM observer to detect torque imbalance and development of observer based FTC techniques for mitigation of imbalance in the cyclic torque. The proposed unified framework has been applied to mitigate cyclic torque imbalance during runtime of the vehicle. It will ensure to achieve graceful performance degradation, in case of fault generation in fuel injection subsystem.

Torque imbalance also cause variations in engine speed. Desired engine speed profile is required to be followed by mitigating the faults that cause torque imbalance. Transformation in FPEM has been employed for robust speed tracking to manage the engine torque. Speed tracking is one of the basic modules of engine control to meet the torque requirements. Accurate tracking of engine speed under different conditions allows to implement various control functions of vehicle powertrain. In robust speed tracking control, set points of engine speed has been tracked in the

presence of fault in engine subsystems by application of SSTA based technique. Proposed robust technique has also been robust as it rejected disturbances in the form of varying load torque. Reference data has been acquired from engine test rig to validate the proposed technique.

7.1 Contributions of Research Work

After a brief review of the dissertation, following contributions of the research work can be enumerated:

- Model based unified framework for detection and mitigation of cyclic torque imbalance has been accomplished by derivation of FPEM based USOSM observer to detect torque imbalance and development of observer based FTC techniques for mitigation of imbalance in the cyclic torque.
- Detection of cyclic torque imbalance by estimation of net piston force (f_n), that is generated in engine cylinder. It acted as input to torque production subsystem of the engine; however, it could not be measured directly. Net piston force (f_n) has been assumed as unknown input to engine speed dynamics. FPEM based USOSM observer has been proposed to estimate states of engine speed dynamics and unknown input i.e., net piston force (f_n) has been estimated from observed states. Variations in net piston force (f_n) provided a direct measure of imbalance in the cyclic torque.
- Observer-based FTC techniques have been proposed to mitigate cyclic torque imbalance. Control laws for both STA and CESTA based techniques have been designed by employing the estimated net piston force (\hat{f}_n).
- In FPEM, relationship has been provided between net piston force (f_n) and engine speed dynamics. However, spark timing, valve timing and fuel injection acted as control input to produce net piston force (f_n). Thus, FPEM has been transformed to derive direct relation between engine speed dynamics and fuel input i.e. IPW . Such relation does not exist in MVEM which only has throttle

valve angle as explicit control input. Thus, faults in fuel injection subsystem could not be mitigated by using MVEM.

- Validation of torque production subsystem model in FPEM by using speed dynamics of GT-Power based engine model.
- Robust speed tracking control for engine torque management has been carried out to track set points of engine speed, despite occurrence of the fault in fuel injection subsystem. Significance of transformation in FPEM has been demonstrated by tracking reference speed profile to manage the engine torque.

7.2 Future Directions

Research work presented in the dissertation can be extended in following research directions:

- Detection and mitigation of cyclic torque imbalance has been main focus of the presented research work. Proposed model based unified framework can be extended to study cylinder to cylinder torque imbalance by using FPEM with multi-cylinder dynamics. As discussed in Chapter 1, problem of engine power balancing could be investigated in multi-cylinder engines by employing the proposed unified framework.
- Proposed novel framework for detection and mitigation of cyclic torque imbalance can be applied to analyze cyclic torque imbalance in Diesel cycle and Atkinson cycle engines.
- FPEM based USOSM observer has been proposed for estimation of unknown input, which can be influenced by different factors. It included time constant of LPF, gains and initial conditions of the observer as well as type and sampling time of the numerical solver. Results of the observer are applicable for given values of these factors, that are tuned after many iterations. Sensitivity analysis of the observer results could be carried out to find dependency of observer results on these factors. It can save time to tune and contribute to improve the estimation results.

- Estimation of engine and combustion parameters can be carried out in future work by employing the proposed estimation framework. Different engine parameters like moment of inertia as well as combustion parameters, such as Wiebe shape factor, SoC and EoC can be estimated to improve the engine model.
- A separate simulation was carried out during model validation to estimate computational complexity of the model. A simulation of 133 seconds took 300 seconds on a machine with 1.00 GHz Core2Duo Processor, 1GB RAM, Windows 7 64-bit platform and MATLAB R2016. This became rather a slow model and it was concluded that implementation of the model in embedded system would require special considerations. The mathematical expressions presented in **Appendix A**, other than geometric parameters of the torque producing mechanism are the function of θ_1 and ω_1 . The look-up tables are well known and validated technique that is implemented in automotive systems. Thus, look-up tables for expressions in the **Appendix A** can be developed to make the model feasible for implementation in embedded systems and improve real-time performance of proposed technique.
- Only actuator faults have been considered in the presented research work. It has been assumed that rest of engine subsystems are fault free. Effect of sensor faults on overall system performance needs further investigation. Fault detection techniques can be combined with supervisory control and on-line controller re-configuration to accommodate sensor faults.
- Step shaped faults has been induced in fuel injection subsystem. Other faults shapes, such as ramp shaped, triangular pulse can also be considered in detail in future research work.
- Proposed model based unified framework for cyclic torque imbalance can be applied in research technologies, such as VCD and DSF to mitigate NVH in these techniques.

Bibliography

- [1] W. W. Pulkrabek, *Engineering Fundamentals of the Internal Combustion Engine*. Pearson Prentice Hall Upper Saddle River, NJ, pp. 68-121, 2014.
- [2] N. Ozdor, M. Dulger, and E. Sher, “Cyclic Variability in Spark Ignition Engines, a Literature Survey,” *SAE Transactions*, pp. 1514–1552, 1994.
- [3] M. B. Young, “Cyclic Dispersion—Some Quantitative Cause-and-Effect Relationships,” SAE Technical Paper, Tech. Rep., pp. 382-394, 1980.
- [4] M. Kao and J. J. Moskwa, “Model-based Engine Fault Detection using Cylinder Pressure Estimates from Nonlinear Observers,” in *Proceedings of the 33rd IEEE Conference on Decision and Control, 1994.*, vol. 3. IEEE, 1994, pp. 2742–2747.
- [5] J. Williams, “An Overview of Misfiring Cylinder Engine Diagnostic Techniques based on Crankshaft Angular Velocity Measurements,” SAE Technical Paper, Tech. Rep., pp. 317-329, 1996.
- [6] P. Azzoni, G. Minelli, D. Moro, R. Flora, and G. Serra, “Indicated and Load Torque Estimation using Crankshaft Angular Velocity Measurement,” *SAE transactions*, pp. 752–758, 1999.
- [7] J.-E. Saxén, T. Hyvämäki, J. Björkqvist, F. Ostman, and H. T. Toivonen, “Power Balancing of Internal Combustion Engines—A Time and Frequency Domain Analysis,” *IFAC Proceedings Volumes*, vol. 47, no. 3, pp. 10 802–10 807, 2014.
- [8] D. Taraza, N. Henein, and W. Bryzik, “The Frequency Analysis of the Crankshaft’s Speed Variation: A Reliable Tool for Diesel Engine Diagnosis,” *Journal of Engineering for Gas Turbines and Power*, vol. 123, no. 2, pp. 428–432, 2001.

- [9] A. Walter, C. Lingenfelter, U. Kiencke, S. Jones, and T. Winkler, "Cylinder Balancing based on Reconstructed Engine Torque for Vehicles Fitted with a Dual Mass Flywheel (dmf)," *SAE International Journal of Passenger Cars-Mechanical Systems*, vol. 1, no. 2008-01-1019, pp. 810–819, 2008.
- [10] F. Zhou, J. Fu, J. Shu, J. Liu, S. Wang, and R. Feng, "Numerical Simulation Coupling with Experimental Study on the Non-Uniform of Each Cylinder Gas Exchange and Working Processes of a Multi-Cylinder Gasoline Engine under Transient Conditions," *Energy Conversion and Management*, vol. 123, pp. 104–115, 2016.
- [11] J. Green Jr, C. S. Daw, J. S. Armfield, C. Finney, R. M. Wagner, J. Drallmeier, M. Kennel, and P. Durbetaki, "Time Irreversibility and Comparison of Cyclic-Variability Models," *SAE transactions*, pp. 355–362, 1999.
- [12] O. California's, "Regulation, Section 1968.1, title 13," *California Code of Regulation, Resolution*, pp. 93–40, 1993.
- [13] L. Guzzella and C. Onder, *Introduction to Modeling and Control of Internal Combustion Engine Systems*. Springer Science & Business Media, pp. 21–137, 2009.
- [14] A. Yar, A. Bhatti, and Q. Ahmed, "First Principle-based Control Oriented Model of a Gasoline Engine," *Journal of Dynamic Systems, Measurement and Control*, vol. 139, no. 5, pp. 353–367, 2017.
- [15] A. Yar, A. I. Bhatti, and Q. Ahmed, "First Principle based Control Oriented Model of a Gasoline Engine including Multi-Cylinder Dynamics," *Control Engineering Practice*, vol. 70, pp. 63–76, 2018.
- [16] A. Yar, "Control Oriented Modeling of Gasoline Engines: A New Paradigm," Ph.D. dissertation, Capital University of Science & Technology, Islamabad, pp. 34-65, 2017.
- [17] E. Zervas, "Correlations between Cycle-to-Cycle Variations and Combustion Parameters of a Spark Ignition Engine," *Applied Thermal Engineering*, vol. 24, no. 14-15, pp. 2073–2081, 2004.
- [18] R. L. Norton, *Design of Machinery: An Introduction to the Synthesis and Analysis of Mechanisms and Machines*. McGraw-Hill Boston, pp. 188-213, 1999, vol. 924.

- [19] C. Taylor, *The Internal Combustion Engine in Theory and Practice, Volume 1: Thermodynamics, Fluid Flow, Performance*. MIT, Cambridge, MA., pp. 162-188, 1985.
- [20] F. Vasile, D. Catana, I. Serbanescu, C. P. Mirea, and D. D. Velcea, "Analysis of the Engine Thermal Balance. Determination of Energy Quantity Necessary for Cooling a Naval Engine," *4th International Conference on Computational Mechanics and Virtual Engineering.*, pp. 45–50, 2011.
- [21] K. M. Chun and K. W. Kim, "Measurement and Analysis of Knock in a SI Engine using the Cylinder Pressure and Block Vibration Signals," *SAE transactions*, pp. 56–62, 1994.
- [22] M. Geveci, "Robust Cylinder Health Monitoring for Internal Combustion Engines," Ph.D. dissertation, Purdue University, pp. 6-32, 2005.
- [23] M. Van Nieuwstadt and I. Kolmanovsky, "Detecting and Correcting Cylinder Imbalance in Direct Injection Engines," *Journal of Dynamic Systems, Measurement and Control*, vol. 123, no. 3, pp. 413–424, 2001.
- [24] J. B. Heywood, *Internal Combustion Engine Fundamentals*. Mcgraw-hill New York, pp. 371-470, 1988, vol. 930.
- [25] A. Medina, P. L. Curto-Risso, A. C. Hernández, L. Guzmán-Vargas, F. Angulo-Brown, and K. S. Asok, *Quasi-Dimensional Simulation of Spark Ignition Engines*. Springer, pp. 107-145, 2014.
- [26] J. Ball, R. Raine, and C. Stone, "Combustion Analysis and Cycle-by-Cycle Variations in Spark Ignition Engine Combustion part 2: A New Parameter for Completeness of Combustion and its Use in Modelling Cycle-by-Cycle Variations in Combustion," *Proceedings of the Institution of Mechanical Engineers, Part D: Journal of Automobile Engineering*, vol. 212, no. 6, pp. 507–523, 1998.
- [27] G. Grünefeld, V. Beushausen, P. Andresen, and W. Hentschel, "A Major Origin of Cyclic Energy Conversion Variations in SI Engines: Cycle-by-Cycle Variations of the Equivalence Ratio and Residual Gas of the Initial Charge," *SAE Transactions*, pp. 882–893, 1994.
- [28] S. Joo, K. Srinivasan, K. Lee, and S. Bell, "The Behaviour of Small-and Large-Scale Variations of In-Cylinder Flow During Intake and Compression

- Strokes in a Motored Four-Valve Spark Ignition Engine,” *International Journal of Engine Research*, vol. 5, no. 4, pp. 317–328, 2004.
- [29] P. Aleiferis, Y. Hardalupas, A. Taylor, K. Ishii, and Y. Urata, “Flame Chemiluminescence Studies of Cyclic Combustion Variations and Air-to-Fuel Ratio of the Reacting Mixture in a Lean Burn Stratified Charge Spark Ignition Engine,” *Combustion and Flame*, vol. 136, no. 1-2, pp. 72–90, 2004.
- [30] N. Ozdor, M. Dulger, and E. Sher, “An Experimental Study of the Cyclic Variability in Spark Ignition Engines,” SAE Technical Paper, Tech. Rep., pp. 386-398, 1996.
- [31] D. Scholl and S. Russ, “Air-Fuel Ratio Dependence of Random and Deterministic Cyclic Variability in a Spark-Ignited Engine,” SAE Technical Paper, Tech. Rep., pp. 264-274, 1999.
- [32] H. Li, W. Neill, and W. Chippior, “Cycle-to-Cycle Variation of a HCCI Engine Operated with n-Hptane,” *2007 Spring Technical Meeting, Combustion Institute Canadian Section, Banff, Canada*, pp. 418–424, 2007.
- [33] C. Manzie, H. C. Watson, and P. Baker, “Modeling the Effects of Combustion Variability for Application to Idle Speed Control in SI Engines,” SAE Technical Paper, Tech. Rep., pp. 358-368, 2002.
- [34] C. Schenk and P. Dekraker, “Potential Fuel Economy Improvements from the Implementation of cEGR and CDA on an Atkinson Cycle Engine,” SAE Technical Paper, Tech. Rep., pp. 1833-1845, 2017.
- [35] K. Eisazadeh-Far and M. Younkins, “Fuel Economy Gains through Dynamic-Skip-Fire in Spark Ignition Engines,” SAE Technical Paper, Tech. Rep., pp. 672-684, 2016.
- [36] J. Serrano, G. Routledge, N. Lo, M. Shost, V. Srinivasan, and B. Ghosh, “Methods of Evaluating and Mitigating NVH when Operating an Engine in Dynamic Skip Fire,” *SAE International Journal of Engines*, vol. 7, no. 2014-01-1675, pp. 1489–1501, 2014.
- [37] M. Wilcutts, J. Switkes, M. Shost, and A. Tripathi, “Design and Benefits of Dynamic Skip Fire Strategies for Cylinder Deactivated Engines,” *SAE International Journal of Engines*, vol. 6, no. 2013-01-0359, pp. 278–288, 2013.

- [38] J. Meyer, “Calibration Reduction in Internal Combustion Engine Fueling Control: Modeling, Estimation and Stability Robustness,” Ph.D. dissertation, The Ohio State University, pp. 20-27, 2011.
- [39] H. Husted, D. Kruger, G. Fattic, G. Ripley, and E. Kelly, “Cylinder Pressure-based Control of Pre-Mixed Diesel Combustion,” SAE Technical Paper, Tech. Rep., pp. 266-279, 2007.
- [40] R. Reitz and J. Von der Ehe, “Use of In-Cylinder Pressure Measurement and the Response Surface Method for Combustion Feedback Control in a Diesel Engine,” *Proceedings of the Institution of Mechanical Engineers, Part D: Journal of Automobile Engineering*, vol. 220, no. 11, pp. 1657–1666, 2006.
- [41] B. He, T. Shen, J. Kako, and M. Ouyang, “Input Observer-based Individual Cylinder Air-Fuel Ratio Control: Modelling, Design and Validation,” *IEEE Transactions on Control Systems Technology*, vol. 16, no. 5, pp. 1057–1065, 2008.
- [42] J. Chauvin, N. Petit, P. Rouchon, P. Moulin, and G. Corde, “Six Degrees Crankshaft Individual Air Fuel Ratio Estimation of Diesel Engines for Cylinder Balancing Purpose,” *SAE Technical Paper*, pp. 411-419, 2006.
- [43] J. Yang, T. Shen, and X. Jiao, “Model-based Stochastic Optimal Air-Fuel Ratio Control with Residual Gas Fraction of Spark Ignition Engines,” *IEEE Transactions on Control Systems Technology*, vol. 22, no. 3, pp. 896–910, 2014.
- [44] C. Daw, C. Finney, J. Green Jr, M. Kennel, J. Thomas, and F. Connolly, “A Simple Model for Cyclic Variations in a Spark-Ignition Engine,” *SAE transactions*, pp. 2297–2306, 1996.
- [45] C. E. Finney, B. C. Kaul, C. S. Daw, R. M. Wagner, K. D. Edwards, and J. B. Green Jr, “A Review of Deterministic Effects in Cyclic Variability of Internal Combustion Engines,” *International Journal of Engine Research*, vol. 16, no. 3, pp. 366–378, 2015.
- [46] W. Dai, N. Trigui, and Y. Lu, “Modeling of Cyclic Variations in Spark-Ignition Engines,” *SAE Transactions*, pp. 1851–1861, 2000.
- [47] M. Wenig, M. Grill, and M. Bargende, “A New Approach for Modeling Cycle-to-Cycle Variations within the Framework of a Real Working-Process

- Simulation,” *SAE International Journal of Engines*, vol. 6, no. 2013-01-1315, pp. 1099–1115, 2013.
- [48] Y. Chen, Y. Wang, and R. Raine, “Correlation Between Cycle-by-Cycle Variation, Burning rate, and Knock: A Statistical Study from PFI and DISI Engines,” *Fuel*, vol. 206, pp. 210–218, 2017.
- [49] M. Sjeric, D. Kozarac, and I. Taritas, “Experimentally Supported Modeling of Cycle-to-Cycle Variations of SI Engine using Cycle-Simulation Model,” SAE Technical Paper, Tech. Rep., pp. 468-480, 2014.
- [50] M. Kang, K. Sata, and A. Matsunaga, “Control Oriented Cyclic Modeling Method for Spark Ignition Engines,” *IFAC*, vol. 51, pp. 448–453, 2018.
- [51] A. Suyabodha, A. Pennycott, and C. J. Brace, “A Preliminary Approach to Simulating Cyclic Variability in a Port Fuel Injection Spark Ignition Engine,” *Proceedings of the Institution of Mechanical Engineers, Part D: Journal of Automobile Engineering*, vol. 227, no. 5, pp. 665–674, 2013.
- [52] M. Reyes, F. Tinaut, B. Giménez, and A. Pérez, “Characterization of Cycle-to-Cycle Variations in a Natural Gas Spark Ignition Engine,” *Fuel*, vol. 140, pp. 752–761, 2015.
- [53] M. Pan, G. Shu, H. Wei, T. Zhu, Y. Liang, and C. Liu, “Effects of EGR, Compression Ratio and Boost Pressure on Cyclic Variation of PFI Gasoline Engine at WOT Operation,” *Applied Thermal Engineering*, vol. 64, no. 1-2, pp. 491–498, 2014.
- [54] V. De Bellis, F. Bozza, D. Siano, and G. Valentino, “A Modeling Study of Cyclic Dispersion Impact on Fuel Economy for a Small Size Turbocharged SI Engine,” *SAE International Journal of Engines*, vol. 9, no. 4, pp. 2066–2078, 2016.
- [55] A. Karvountzis-Kontakiotis, L. Ntziachristos, Z. Samaras, A. Dimaratos, and M. Peckham, “Experimental Investigation of Cyclic Variability on Combustion and Emissions of a High-Speed SI Engine,” SAE Technical Paper, Tech. Rep., pp. 1295-1309, 2015.
- [56] J. Franco, M. A. Franchek, and K. Grigoriadis, “Real-Time Brake Torque Estimation for Internal Combustion Engines,” *Mechanical Systems and Signal Processing*, vol. 22, no. 2, pp. 338–361, 2008.

- [57] Y. Wang and F. Chu, "Real-Time Misfire Detection via Sliding Mode Observer," *Mechanical Systems and Signal Processing*, vol. 19, no. 4, pp. 900–912, 2005.
- [58] F. Cruz-Peragon, F. J. Jimenez-Espadafor, J. M. Palomar, and M. P. Dorado, "Combustion Faults Diagnosis in Internal Combustion Engines using Angular Speed Measurements and Artificial Neural Networks," *Energy & Fuels*, vol. 22, no. 5, pp. 2972–2980, 2008.
- [59] M. Desbazeille, R. Randall, F. Guillet, M. El Badaoui, and C. Hoisnard, "Model-based Diagnosis of Large Diesel Engines based on Angular Speed Variations of the Crankshaft," *Mechanical Systems and Signal Processing*, vol. 24, no. 5, pp. 1529–1541, 2010.
- [60] C. Bennett, J. Dunne, S. Trimby, and D. Richardson, "Engine Cylinder Pressure Reconstruction using Crank Kinematics and Recurrently-Trained Neural Networks," *Mechanical Systems and Signal Processing*, vol. 85, pp. 126–145, 2017.
- [61] S. J. Popović and M. V. Tomić, "Possibilities to Identify Engine Combustion Model Parameters by Analysis of the Instantaneous Crankshaft Angular Speed," *Thermal Science*, vol. 18, no. 1, pp. 97–112, 2014.
- [62] C. Kallenberger, H. Hamedović, F. Raichle, J. Breuninger, W. Fischer, K. Benninger, A. Nistor, and A. M. Zoubir, "Estimation of Cylinder-Wise Combustion Features from Engine Speed and Cylinder Pressure," *SAE International Journal of Engines*, vol. 1, no. 2008-01-0290, pp. 198–207, 2008.
- [63] F. Ostman and H. T. Toivonen, "Adaptive Cylinder Balancing of Internal Combustion Engines," *IEEE Transactions on Control Systems Technology*, vol. 19, no. 4, pp. 782–791, 2011.
- [64] S. A. Ali and S. Saraswati, "Cycle-by-Cycle Estimation of Cylinder Pressure and Indicated Torque Waveform using Crankshaft Speed Fluctuations," *Transactions of the Institute of Measurement and Control*, vol. 37, no. 6, pp. 813–825, 2015.
- [65] S. A. Ali and S. Saraswati, "Cycle-by-Cycle Estimation of IMEP and Peak Pressure using Crankshaft Speed Measurements," *Journal of Intelligent & Fuzzy Systems*, vol. 28, no. 6, pp. 2761–2770, 2015.

- [66] H. Li, Y. Huang, G. Li, and Y. Yang, "Research on the Cylinder-by-Cylinder Variations Detection and Control Algorithm of Diesel Engine," SAE Technical Paper, Tech. Rep., pp. 108-118, 2015.
- [67] F. Östman and H. T. Toivonen, "Active Torsional Vibration Control of Reciprocating Engines," *Control Engineering Practice*, vol. 16, no. 1, pp. 78–88, 2008.
- [68] F. Östman and H. Toivonen, "Model-based Torsional Vibration Control of Internal Combustion Engines," *IET Control Theory & Applications*, vol. 2, no. 11, pp. 1024–1032, 2008.
- [69] K. Min, J. Chung, and M. Sunwoo, "Torque Balance Control for Light-Duty Diesel Engines using an Individual Cylinder IMEP Estimation Model with a Single Cylinder Pressure Sensor," *Applied Thermal Engineering*, vol. 109, pp. 440–448, 2016.
- [70] J. Wang, F. Yang, and M. Ouyang, "Cylinder by Cylinder Indicated Torque and Combustion Feature Estimation based on Engine Instantaneous Speed and One Cylinder Pressure through Error Similarity Analysis," SAE Technical Paper, Tech. Rep., pp. 75-88, 2015.
- [71] F. Taglialatela, M. Lavorgna, E. Mancaruso, and B. Vaglieco, "Determination of Combustion Parameters using Engine Crankshaft Speed," *Mechanical Systems and Signal Processing*, vol. 38, no. 2, pp. 628–633, 2013.
- [72] D. Moro, N. Cavina, and F. Ponti, "In-Cylinder Pressure Reconstruction based on Instantaneous Engine Speed Signal," *Journal of Engineering for Gas Turbines and Power*, vol. 124, no. 1, pp. 220–225, 2002.
- [73] A. Al-Durra, "Adaptive Sliding Mode Observer for Engine Cylinder Pressure Imbalance under Different Parameter Uncertainties," *IEEE Access*, vol. 2, pp. 1085–1091, 2014.
- [74] M. Kassa and C. Hall, "Cylinder-to-Cylinder Variations in Power Production in a Dual Fuel Internal Combustion Engine Leveraging Late Intake Valve Closings," *SAE Int. J. Engines*, vol. 9, pp. 1049–1058, 2016.
- [75] M. Kassa, C. Hall, A. Ickes, and T. Wallner, "In-Cylinder Oxygen Mass Fraction Estimation Method for Minimizing Cylinder-to-Cylinder Variations," SAE Technical Paper, Tech. Rep., pp. 1-10, 2015.

- [76] G. Vichi, M. Becciani, I. Stiaccini, G. Ferrara, L. Ferrari, A. Bellissima, and G. Asai, "Analysis of the Turbocharger Speed to Estimate the Cylinder-to-Cylinder Injection Variations-part 1-Time Domain Analysis," SAE Technical Paper, Tech. Rep., pp. 251-263, 2016.
- [77] H. Yun, J.-M. Kang, M.-F. Chang, and P. Najt, "Improvement on Cylinder-to-Cylinder Variation using a Cylinder Balancing Control Strategy in Gasoline HCCI Engines," SAE Technical Paper, Tech. Rep., pp. 252-265, 2010.
- [78] E. Hendricks and S. C. Sorenson, "Mean Value Modelling of Spark Ignition Engines," *SAE transactions*, pp. 1359–1373, 1990.
- [79] H. Adibi Asl, "Acausal Powertrain Modelling with Application to Model-based Powertrain Control," Ph.D. dissertation, University of Waterloo, pp. 12-24, 2014.
- [80] R. Anjum, I. Khan, A. Yar, and A. I. Bhatti, "Air-to-Fuel Ratio Control of Gasoline Engines using Smooth Sliding Mode Algorithm," in *13th International Conference on Emerging Technologies (ICET)*. IEEE, 2017, pp. 1–6.
- [81] Q. Ahmed, "Fault Diagnosis Methodologies for Automotive Engine Air Intake Path," Ph.D. dissertation, Faculty of Engineering and Applied Sciences, Mohammad Ali Jinnah University, Islamabad, Pakistan, pp. 64-99, 2012.
- [82] D. J. Dobner, "A Mathematical Engine Model for Development of Dynamic Engine Control," *SAE Transactions*, pp. 373–381, 1980.
- [83] D. J. Dobner and R. D. Fruechte, "An Engine Model for Dynamic Engine Control Development," in *American Control Conference, 1983*. IEEE, 1983, pp. 73–78.
- [84] C. F. Aquino, "Transient A/F Control Characteristics of the 5 liter Central Fuel Injection Engine," *SAE Transactions*, pp. 1819–1833, 1981.
- [85] B. Powell, "A Dynamic Model for Automotive Engine Control Analysis," in *18th IEEE Conference on Decision and Control including the Symposium on Adaptive Processes, 1979*, vol. 2. IEEE, 1979, pp. 120–126.
- [86] P. Crossley and J. Cook, "A Nonlinear Engine Model for Drivetrain System Development," in *International Conference on Control 1991*. IET, 1991, pp. 921–925.

- [87] W. Yuen and H. Servati, "A Mathematical Engine Model including the Effect of Engine Emissions," SAE Technical Paper, Tech. Rep., pp. 526-537, 1984.
- [88] J. J. Moskwa, "Automotive Engine Modeling for Real Time Control," Ph.D. dissertation, Massachusetts Institute of Technology, pp. 44-73, 1988.
- [89] E. Hendricks and S. C. Sorenson, "SI Engine Controls and Mean Value Engine Modelling," SAE Technical paper, Tech. Rep., pp. 36-44, 1991.
- [90] H. A. Asl, M. Saeedi, R. Fraser, P. Goossens, and J. McPhee, "Mean Value Engine Model including Spark Timing for Powertrain Control Application," SAE Technical Paper, Tech. Rep., pp. 745-755, 2013.
- [91] M. Saeedi, "A Mean Value Internal Combustion Engine Model in Maplesim," Master's thesis, University of Waterloo, pp. 60-94, 2010.
- [92] L. Mianzo and H. Peng, "Modeling and Control of a Variable Valve Timing Engine," in *Proceedings of the American Control Conference, 2000.*, vol. 1. IEEE, 2000, pp. 554-558.
- [93] S. P. S. Sitthiracha and S. Koetnuyom, "An Engine Model for Dynamic Engine Control Development,," *The 20th Conference of Mechanical Engineering Network of Thailand, 18-20 October 2006.*, pp. 483-489, 2006.
- [94] J. Karlsson and J. Fredriksson, "Cylinder-by-Cylinder Engine Models vs Mean Value Engine Models for Use in Powertrain Control Applications," SAE Technical Paper, Tech. Rep., pp. 968-973, 1999.
- [95] L. Xingyu, S. Gequn, D. Lihui, W. Bin, and Y. Kang, "Progress and Recent Trends in the Torsional Vibration of Internal Combustion Engine," in *Advances in Vibration Analysis Research*. InTech, 2011, pp. 245-272.
- [96] E. Nestorides, *A Handbook on Torsional Vibration*. Cambridge University Press, pp. 45-49, 1958.
- [97] Y. W. Kim, G. Rizzoni, and Y.-Y. Wang, "Design of an IC Engine Torque Estimator using Unknown Input Observer," *Journal of Dynamic Systems, Measurement and Control*, vol. 121, no. 3, pp. 487-495, 1999.
- [98] M. Geveci, A. W. Osburn, and M. A. Franchek, "An Investigation of Crankshaft Oscillations for Cylinder Health Diagnostics," *Mechanical Systems and Signal Processing*, vol. 19, no. 5, pp. 1107-1134, 2005.

- [99] G. Rizzoni, "Estimate of Indicated Torque from Crankshaft Speed Fluctuations: A Model for the Dynamics of the IC Engine," *IEEE Transactions on Vehicular Technology*, vol. 38, no. 3, pp. 168–179, 1989.
- [100] J. Chauvin, G. Corde, P. Moulin, M. Castagné, N. Petit, and P. Rouchon, "Real-Time Combustion Torque Estimation on a Diesel Engine Test Bench using Time-Varying Kalman Filtering," in *43rd IEEE Conference on Decision and Control (CDC), 2004.*, vol. 2. IEEE, 2004, pp. 1688–1694.
- [101] J. Yang, L. Pu, Z. Wang, Y. Zhou, and X. Yan, "Fault Detection in a Diesel Engine by Analysing the Instantaneous Angular Speed," *Mechanical Systems and Signal Processing*, vol. 15, no. 3, pp. 549–564, 2001.
- [102] W. Changmin and Z. Dejun, "Calculation of Torsional Stiffness of Engine Crankthrow by Finite Element Method," *Transactions of CSICE*, vol. 9, no. 2, pp. 177–183, 1991.
- [103] D. Eriksson, L. Eriksson, E. Frisk, and M. Krysander, "Flywheel Angular Velocity Model for Misfire and Driveline Disturbance Simulation," *IFAC Proceedings Volumes*, vol. 46, no. 21, pp. 570–575, 2013.
- [104] L. Eriksson and L. Nielsen, *Modeling and Control of Engines and Drivelines*. John Wiley & Sons, pp. 145-210, 2014.
- [105] G. Rizzoni and Y. Zhang, "Identification of a Non-Linear Internal Combustion Engine Model for on-line Indicated Torque Estimation," *Mechanical Systems and Signal Processing*, vol. 8, no. 3, pp. 275–287, 1994.
- [106] S. Schagerberg and T. McKelvey, "Instantaneous Crankshaft Torque Measurements Modeling and Validation," SAE Technical Paper, Tech. Rep., pp. 735-748, 2003.
- [107] R. Potenza, J. Dunne, S. Vulli, and D. Richardson, "A Model for Simulating the Instantaneous Crank Kinematics and Total Mechanical Losses in a Multicylinder in-line Engine," *International Journal of Engine Research*, vol. 8, no. 4, pp. 379–397, 2007.
- [108] P. Falcone, M. C. De Gennaro, G. Fiengo, L. Glielmo, S. Santini, and P. Langthaler, "Torque Generation Model for Diesel Engine," in *Proceedings of 42nd IEEE Conference on Decision and Control (CDC), 2003.*, vol. 2. IEEE, 2003, pp. 1771–1776.

- [109] Y. Shiao, C.-h. Pan, and J. J. Moskwa, “Advanced Dynamic Spark Ignition Engine Modelling for Diagnostics and Control,” *International Journal of Vehicle Design*, vol. 15, no. 6, pp. 578–596, 1994.
- [110] K. Nagaosa, N. Miyagi, T. Yamazaki, and M. Iwase, “Combustion Process Estimation in Cylinders based on an Integrated Engine Model of the Wiebe Function and a Piston-Crank Mechanism,” in *54th Annual Conference of the Society of Instrument and Control Engineers of Japan (SICE)*. IEEE, 2015, pp. 1397–1402.
- [111] B. Lee, G. Rizzoni, Y. Guezennec, A. Soliman, M. Cavalletti, and J. Waters, “Engine Control using Torque Estimation,” *SAE Transactions*, pp. 869–881, 2001.
- [112] J. Na, A. S. Chen, G. Herrmann, R. Burke, and C. Brace, “Vehicle Engine Torque Estimation via Unknown Input Observer and Adaptive Parameter Estimation,” *IEEE Transactions on Vehicular Technology*, vol. 67, no. 1, pp. 409–422, 2018.
- [113] I. Haskara and L. Mianzo, “Real-Time Cylinder Pressure and Indicated Torque Estimation via Second Order Sliding Modes,” in *American Control Conference, 2011.*, vol. 5. IEEE, 2011, pp. 3324–3328.
- [114] M. Kang, M. Alamir, and T. Shen, “Nonlinear Constrained Torque Control for Gasoline Engines,” *IFAC-Papers online*, vol. 49, no. 18, pp. 784–789, 2016.
- [115] M. Pasricha and F. Hashim, “Effect of the Reciprocating Mass of Slider-Crank Mechanism on Torsional Vibrations of Diesel Engine Systems,” *Asean Journal on Science and Technology for Development*, vol. 23, no. 1, pp. 71–81, 2007.
- [116] H. Ferenbach, “Model Based Combustion Pressure Computation through Crankshaft Angular Acceleration Analysis,” in *Proc XXII Int., Symposium on Automotive Technology and Automation, Florence, Italy*, 1990, pp. 375–381.
- [117] A. Yar, A. Bhatti, and Q. Ahmed, “First Principle based Control Oriented Gasoline Engine Model including Lumped Cylinder Dynamics,” *Journal of Dynamic Systems, Measurement and Control*, vol. 140, no. 8, pp. 641–650, 2018.

- [118] R. Anjum, A. Yar, Q. Ahmed, and A. Bhatti, "Cyclic Torque Imbalance Detection in Gasoline Engines using Second Order Sliding Mode," in *2nd IEEE Conference on Control Technology and Applications (CCTA)*. IEEE, 2018, pp. 1046–1051.
- [119] C. Cooney, J. Worm, D. Michalek, J. Naber *et al.*, "Wiebe Function Parameter Determination for Mass Fraction Burn Calculation in an Ethanol-Gasoline Fuelled SI Engine," *Journal of KONES*, vol. 15, pp. 567–574, 2008.
- [120] K. Z. Mendera, A. Spyra, and M. Smereka, "Mass Fraction Burned Analysis," *Journal of KONES*, vol. 3, pp. 193–201, 2002.
- [121] D. B. Brown, "Diesel Exhaust Control During Limp-Home Mode," Aug. 9 2011, pp. 5-9, US Patent 7,992,377.
- [122] G. Technologies, "GT-Power User Manual," *Version 7.4*, pp. 47–79, 2013.
- [123] R. Anjum, A. I. Bhatti, A. Yar, and Q. Ahmed, "Cyclic Torque Imbalance Detection in Gasoline Engines using a Uniform Second-Order Sliding Mode Observer," *Proceedings of the Institution of Mechanical Engineers, Part D: Journal of Automobile Engineering*, vol. 233, pp. 3515–3527, 2019.
- [124] E. Johansson and S. Wagnborg, "Analysis of Engine Cold Start Simulation in GT-Power," Master's thesis, Department of Applied Mechanics, Division of Combustion, Chalmers University of Technology, Sweden, pp. 15-31, 2014.
- [125] M. Nilsson and J. Larsson, "The Potential of Increased Efficiency and Power for a Turbocharged PFI-SI Engine through Variable Valve Actuation and DEP," Master's thesis, Department of Combustion Engines, Faculty of Engineering, Lund University, Sweden, pp. 52-66, 2015.
- [126] Srinivasa, K. S. Banavathy, Shankaregowda, and P. Kagganagadde, "A Novel Approach to a Two-Stroke Dual Stage Expansion Engine Concept," Master's thesis, Department of Applied Mechanics, Chalmers University of Technology, Sweden., pp. 19-37, 2016.
- [127] M. Fam and E. Hendricks, "A Load Torque Estimator," SAE Technical Paper, Tech. Rep., pp. 1-16, 2004.
- [128] D. Pavkovic, I. Kolmanovsky, and J. Deur, "Adaptive Kalman Filter-based Load Torque Compensator for Improved SI Engine Idle Speed Control,"

- IEEE Transactions on Control Systems Technology*, vol. 17, no. 1, pp. 98–110, 2008.
- [129] R. Rajamani, *Vehicle Dynamics and Control*. Springer Science & Business Media, pp. 87-112, 2011.
- [130] R. Van Basshuysen and U. Spicher, *Gasoline Engine with Direct Injection: Processes, Systems, Development, Potential*. Vieweg+ Teubner, pp. 147-173, 2009.
- [131] T. K. Garrett, “Automotive Fuels and Fuel Systems,” *Society of Automotive Engineers*, pp. 156–180, 1991.
- [132] R. Isermann, *Fault-Diagnosis Systems: An Introduction from Fault Detection to Fault Tolerance*. Springer, pp. 13-29, 2006.
- [133] S.-H. Wang, E. Wang, and P. Dorato, “Observing the States of Systems with Unmeasurable Disturbances,” *IEEE Transactions on Automatic Control*, vol. 20, no. 5, pp. 716–717, 1975.
- [134] N. Kobayashi and T. Nakamizo, “An Observer Design for Linear Systems with Unknown Inputs,” *International Journal of Control*, vol. 35, no. 4, pp. 605–619, 1982.
- [135] P. Kudva, N. Viswanadham, and A. Ramakrishna, “Observers for Linear Systems with Unknown Inputs,” *IEEE Transactions on Automatic Control*, vol. 25, no. 1, pp. 113–115, 1980.
- [136] Y. Guan and M. Saif, “A Novel Approach to the Design of Unknown Input Observers,” *IEEE T AUTOMAT CONTR*, vol. 36, no. 5, pp. 632–635, 1991.
- [137] S. S. Delshad, A. Johansson, M. Darouach, and T. Gustafsson, “Robust State Estimation and Unknown Inputs Reconstruction for a Class of Nonlinear Systems: Multiobjective Approach,” *Automatica*, vol. 64, pp. 1–7, 2016.
- [138] K. Veluvolu, M. Defoort, and Y. Soh, “High-Gain Observer with Sliding Mode for Nonlinear State Estimation and Fault Reconstruction,” *Journal of the Franklin Institute*, vol. 351, no. 4, pp. 1995–2014, 2014.
- [139] S. H. Saida, F. M’Sahli, and M. Farza, “Simultaneous State and Unknown Input Reconstruction using Cascaded High-Gain Observers,” *International Journal of Systems Science*, pp. 1–9, 2017.

- [140] A. Pertew, H. Marquez, and Q. Zhao, “Design of Unknown Input Observers for Lipschitz Nonlinear Systems,” in *Proceedings of the American Control Conference, 2005*. IEEE, 2005, pp. 4198–4203.
- [141] K. Lee and W. Lee, “State Estimation for Motorized Seat Belt System using Sliding-Mode Observer,” *International Journal of Automotive Technology*, vol. 16, no. 2, pp. 301–308, 2015.
- [142] Q. Ahmed and A. I. Bhatti, “Estimating SI Engine Efficiencies and Parameters in Second Order Sliding Modes,” *IEEE Transactions on Industrial Electronics*, vol. 58, no. 10, pp. 4837–4846, 2011.
- [143] R. Salehi, G. Vossoughi, and A. Alasty, “A Second-Order Sliding Mode Observer for Fault Detection and Isolation of Turbocharged SI Engines,” *IEEE Transactions on Industrial Electronics*, vol. 62, no. 12, pp. 7795–7803, 2015.
- [144] L. Fridman, Y. Shtessel, C. Edwards, and X.-G. Yan, “Higher-Order Sliding-Mode Observer for State Estimation and Input Reconstruction in Nonlinear Systems,” *International Journal of Robust and Nonlinear Control*, vol. 18, no. 4-5, pp. 399–412, 2008.
- [145] T. Floquet and J.-P. Barbot, “Super Twisting Algorithm-based Step-by-Step Sliding Mode Observers for Nonlinear Systems with Unknown Inputs,” *International Journal of Systems Science*, vol. 38, no. 10, pp. 803–815, 2007.
- [146] M. Saif, W. Chen, and Q. Wu, “High Order Sliding Mode Observers and Differentiators—Application to Fault Diagnosis Problem,” in *Modern Sliding Mode Control Theory*. Springer, 2008, pp. 321–344.
- [147] T. Floquet, C. Edwards, and S. K. Spurgeon, “On Sliding Mode Observers for Systems with Unknown Inputs,” *International Journal of Adaptive Control and Signal Processing*, vol. 21, no. 8-9, pp. 638–656, 2007.
- [148] J. Davila, L. Fridman, and A. Levant, “Second-Order Sliding-Mode Observer for Mechanical Systems,” *IEEE Transactions on Automatic Control*, vol. 50, no. 11, pp. 1785–1789, 2005.
- [149] E. Cruz-Zavala, J. A. Moreno, and L. Fridman, “Uniform Second-Order Sliding Mode Observer for Mechanical Systems,” in *11th International Workshop on Variable Structure Systems (VSS), 2010*. IEEE, 2010, pp. 14–19.

- [150] V. Utkin, "Variable Structure Systems with Sliding Modes," *IEEE Transactions on Automatic Control*, vol. 22, no. 2, pp. 212–222, 1977.
- [151] J.-P. Richard, "Time-Delay Systems: An Overview of Some Recent Advances and Open Problems," *Automatica*, vol. 39, no. 10, pp. 1667–1694, 2003.
- [152] V. Utkin, J. Guldner, and J. Shi, *Sliding Mode Control in Electro-Mechanical Systems*. CRC press, pp. 42-96, 2009.
- [153] V. Utkin, *Sliding Modes in Optimization and Control Problems*. Springer Verlag, New York, pp. 38-61, 1992.
- [154] A. Levant and L. Alelishvili, "Integral High-Order Sliding Modes," *IEEE Transactions on Automatic Control*, vol. 52, no. 7, pp. 1278–1282, 2007.
- [155] H. Sira-Ramírez, "Dynamical Sliding Mode Control Strategies in the Regulation of Nonlinear Chemical Processes," *International Journal of Control*, vol. 56, no. 1, pp. 1–21, 1992.
- [156] R. Isermann, *Fault-Diagnosis Applications: Model-based Condition Monitoring: Actuators, Drives, Machinery, Plants, Sensors, and Fault-Tolerant Systems*. Springer Science & Business Media, pp. 285-314, 2011.
- [157] H. K. Khalil and J. W. Grizzle, *Nonlinear Systems*. Prentice Hall Upper Saddle River, NJ, pp. 137-151, 2002, vol. 3.
- [158] A. Levant, "Sliding Order and Sliding Accuracy in Sliding Mode Control," *International journal of control*, vol. 58, no. 6, pp. 1247–1263, 1993.
- [159] A. F. Filippov, *Differential Equations with Discontinuous Righthand Sides: Control Systems*. Springer, pp. 48-117, 2013, vol. 18.
- [160] G. Bartolini, L. Fridman, and E. Usai, *Modern Sliding Mode Control Theory: New Perspectives and Applications*. Springer, pp. 293-319, 2008, vol. 375.
- [161] J. Davila, L. Fridman, and A. Poznyak, "Observation and Identification of Mechanical Systems via Second Order Sliding Modes," *International Journal of Control*, vol. 79, no. 10, pp. 1251–1262, 2006.
- [162] A. Marouf, M. Djemaï, C. Sentouh, and P. Pudlo, "Driver Torque and Road Reaction Force Estimation of an Electric Power Assisted Steering using Sliding Mode Observer with Unknown Inputs," in *13th International IEEE Conference on Intelligent Transportation Systems*. IEEE, 2010, pp. 354–359.

- [163] J. M. Daly and D. W. Wang, "Time-Delayed Output Feedback Bilateral Teleoperation with Force Estimation for n -DOF Nonlinear Manipulators," *IEEE Transactions on Control Systems Technology*, vol. 22, no. 1, pp. 299–306, 2013.
- [164] C.-T. Chen, *Linear System Theory and Design*. Oxford University Press, Inc., pp. 207-240, 1998.
- [165] H. Sira-Ramirez and S. K. Agrawal, *Differentially Flat Systems*. CRC Press, pp. 117-130, 2004.
- [166] U. Kiencke and L. Nielsen, *Automotive Control Systems: For Engine, Driveline and Vehicle*. IOP Publishing, pp.164-207, 2000.
- [167] S. B. Han, "Investigation of Cyclic Variations of IMEP under Idling Operation in Spark Ignition Engines," *KSME international journal*, vol. 15, no. 1, pp. 81–87, 2001.
- [168] Y.-W. Kim, G. Rizzoni, and V. I. Utkin, "Developing a fault tolerant powertrain control system by integrating design of control and diagnostics," *International Journal of Robust and Nonlinear Control: IFAC-Affiliated Journal*, vol. 11, no. 11, pp. 1095–1114, 2001.
- [169] M. Blanke, M. Kinnaert, J. Lunze, M. Staroswiecki, and J. Schröder, *Diagnosis and Fault-Tolerant Control*. Springer, pp. 215-273, 2006, vol. 2.
- [170] M. Bidarvatan, M. Shahbakhti, S. Jazayeri, and C. Koch, "Cycle-to-Cycle Modeling and Sliding Mode Control of Blended-Fuel HCCI Engine," *Control Engineering Practice*, vol. 24, pp. 79–91, 2014.
- [171] A. Kaleli, M. A. Ceviz, and K. Erenturk, "Controlling Spark Timing for Consecutive Cycles to Reduce the Cyclic Variations of SI Engines," *Applied Thermal Engineering*, vol. 87, pp. 624–632, 2015.
- [172] C. A. Satkoski, N. S. Ruikar, S. D. Biggs, and G. M. Shaver, "Piezoelectric Fuel Injection: Cycle-to-Cycle Control of Tightly Spaced Injections," *Control Engineering Practice*, vol. 20, no. 11, pp. 1175–1182, 2012.
- [173] R. Anjum, A. Yar, S. Shah, Q. Ahmed, and A. Bhatti, "Observer based Robust Control Design for Mitigation of Cyclic Torque Imbalance in Gasoline Engines," in *3rd IEEE Conference on Control Technology and Application (CCTA), 19-21 August 2019*. IEEE, 2019, pp. 1020–1026.

- [174] G. Murtaza, "Sliding Mode Fault Tolerant Control of Air Path Actuators in a Turbocharged Diesel Engine," Ph.D. dissertation, Capital University of Science & Technology Islamabad, pp. 114-146, 2018.
- [175] Y. Shtessel, C. Edwards, L. Fridman, and A. Levant, *Sliding mode control and observation*. Springer, pp.142-182, 2014.
- [176] V. Brégeault, F. Plestan, Y. Shtessel, and A. Poznyak, "Adaptive Sliding Mode Control for an Electropneumatic Actuator," in *2010 11th International Workshop on Variable Structure Systems (VSS)*. IEEE, 2010, pp. 260–265.
- [177] Y. Shtessel, M. Taleb, and F. Plestan, "A Novel Adaptive-Gain Supertwisting Sliding Mode Controller: Methodology and Application," *Automatica*, vol. 48, no. 5, pp. 759–769, 2012.
- [178] A. Barth, M. Reichhartinger, K. Wulff, M. Horn, and J. Reger, "Certainty Equivalence Adaptation Combined with Super-Twisting Sliding-Mode Control," *International Journal of Control*, vol. 89, no. 9, pp. 1767–1776, 2016.
- [179] A. Barth, M. Reichhartinger, J. Reger, M. Horn, and K. Wulff, "Certainty-Equivalence based Super-Twisting Control using Continuous Adaptation Laws," in *2016 14th International Workshop on Variable Structure Systems (VSS)*. IEEE, 2016, pp. 92–97.
- [180] Y. Sakai, M. Kanai, and M. Yamakita, "Torque Demand Control by Non-linear MPC for Speed Control of Vehicles with Variable Valve Lift Engine," *IFAC Proceedings Volumes*, vol. 43, no. 7, pp. 494–499, 2010.
- [181] M. Abu-Qudais, "Exhaust Gas Temperature for Knock Detection and Control in Spark Ignition Engine," *Energy Conversion and Management*, vol. 37, no. 9, pp. 1383–1392, 1996.
- [182] N. Heintz, M. Mews, G. Stier, A. Beaumont, and A. Noble, "An Approach to Torque-based Engine Management Systems," SAE Technical Paper, Tech. Rep., pp. 208-220, 2001.
- [183] M. Hong, T. Shen, M. Ouyang, and J. Kako, "Optimal Speed Tracking Control for Torque-Based Engine Management Systems," in *Proceedings of the 51th Japan Joint Automatic Control Conference*, 2008, pp. 216–216.
- [184] M. Livshiz, M. Kao, and A. Will, "Engine Torque Control Variation Analysis," SAE Technical Paper, Tech. Rep., pp. 71-77, 2008.

- [185] J. Zhang, J. Gao, and T. Shen, “Adaptive Idling Control Scheme and its Experimental Validation for Gsoline Engines,” *Science China, Information Sciences*, vol. 60, no. 2, pp. 1–10, 2017.
- [186] D. Jiang, Y. Huang, G. Li, D. Hao, and Z. Zuo, “Design of a Speed Tracking Controller for Heavy-Duty Vehicles with an All-Speed Governor based on a Model Predictive Control Strategy,” *International Journal of Engine Research*, vol. 18, no. 9, pp. 930–940, 2017.
- [187] S. J. Citron, J. E. O’Higgins, and L. Y. Chen, “Cylinder by Cylinder Engine Pressure and Pressure Torque Waveform Determination utilizing Speed Fluctuations,” *SAE Transactions*, pp. 933–947, 1989.
- [188] M. Feng, X. Jiao, and Z. Wang, “Cascade Active Disturbance Rejection Control-based Double Closed-Loop Speed Tracking Control for Automotive Engine,” *International Journal of Engine Research*, pp. 1410–1424, 2019.
- [189] S. Di Cairano, J. Doering, I. V. Kolmanovsky, and D. Hrovat, “Model Predictive Control of Engine Speed during Vehicle Deceleration,” *IEEE Transactions on Control Systems Technology*, vol. 22, no. 6, pp. 2205–2217, 2014.
- [190] D. Malkhede and B. Setht, “Robust Sliding Mode Controller for Turbocharged Diesel Engine with Parameter Perturbations,” in *2007 Mediterranean Conference on Control and Automation*. IEEE, 2007, pp. 1–6.
- [191] F. Li, T. Shen, and X. Jiao, “Model-based Design Approach for Gasoline Engine Control part i: Modeling and validation,” in *Proceedings of the 32nd Chinese Control Conference*. IEEE, 2013, pp. 7774–7779.
- [192] R. Anjum, A. Yar, I. Yousufzai, Q. Ahmed, and A. Bhatti, “Second Order Sliding Mode based Speed Tracking Control for Torque Management of Gasoline Engines,” in *12th Asian Control Conference (ASCC), 2019*. IEEE, 2019, pp. 555–560.
- [193] R. Anjum, A. Yar, A. Bhatti, I. Yousufzai, and Q. Ahmed, “Dual Loop Speed Tracking Control for Torque Management of Gasoline Engines,” in *2019 18th European Control Conference (ECC)*. IEEE, 2019, pp. 3084–3089.
- [194] I. Khan, A. I. Bhatti, A. Arshad, and Q. Khan, “Robustness and Performance Parameterization of Smooth Second Order Sliding Mode Control,”

International Journal of Control, Automation and Systems, vol. 14, no. 3, pp. 681–690, 2016.

- [195] Y. B. Shtessel, I. A. Shkolnikov, and A. Levant, “Smooth Second-Order Sliding Modes: Missile Guidance Application,” *Automatica*, vol. 43, no. 8, pp. 1470–1476, 2007.

Appendix A

Mathematical Expressions of FPEM

Complete mathematical expressions of the torque producing mechanism have been presented in this appendix. All d_i , n_i and \mathbf{g}_i are functions of θ_1 , ω_1 and Γ :

$$\mathbf{d}_0(\theta_1(t)) = 2l_2^2 - 2l_1^2 \sin^2(\theta_1(t))$$

$$\mathbf{d}_1(\theta_1(t)) = -16 J_1 (l_2^2 - l_1^2 \sin^2(\theta_1(t)))^{\frac{3}{2}}$$

$$\begin{aligned} \mathbf{d}_2(\theta_1(t)) = & -8 l_1 l_2^2 (m_2 - 2m_3) \sin(2\theta_1(t)) \sin(\theta_1(t)) \\ & + 16 l_1^3 (m_2 - 2m_3) \sin^4(\theta_1(t)) \cos(\theta_1(t)) \\ & + 4 l_1^2 \sin^2(\theta_1(t)) \sqrt{l_2^2 - l_1^2 \sin^2(\theta_1(t))} (4m_2 \sin^2(\theta_1(t)) \\ & + 4 m_3 \cos(2\theta_1(t)) + m_1) \\ & - 2 l_2^2 \sqrt{l_2^2 - l_1^2 \sin^2(\theta_1(t))} (-8 m_3 \sin^2(\theta_1(t)) \\ & + m_2 (5 - 3 \cos(2\theta_1(t))) + 2 m_1) \end{aligned}$$

$$\mathbf{d}(\theta_1(t)) = d_0(d_1 + d_2 l_1^2)$$

$$\begin{aligned} \mathbf{n}_1(\theta_1(t)) = & l_2^4 (4m_3 - 3m_2) \sin(2\theta_1(t)) \sqrt{l_2^2 - l_1^2 \sin^2(\theta_1(t))} \\ & + l_1 l_2^4 (m_2 - 2m_3) (\sin(\theta_1(t)) - 3 \sin(3\theta_1(t))) \\ & - 4 l_1^5 (m_2 - 2m_3) \sin^5(\theta_1(t)) \cos(2\theta_1(t)) \end{aligned}$$

$$\begin{aligned}
& + 2l_1^3 l_2^2 (m_2 - 2m_3) \sin^3(\theta_1(t)) (5 \cos(2\theta_1(t)) + 1) \\
& - l_1^2 l_2^2 \sin(2\theta_1(t)) \sqrt{l_2^2 - l_1^2 \sin^2(\theta_1(t))} (m_2(4 \cos(2\theta_1(t)) - 3) \\
& + 4 m_3(1 - 2\cos(2\theta_1(t)))) \\
& - 8 l_1^4 (m_2 - 2m_3) \sin^5(\theta_1(t)) \cos(\theta_1(t)) \sqrt{l_2^2 - l_1^2 \sin^2(\theta_1(t))}
\end{aligned}$$

$$\mathbf{n}_2(\theta_1(t)) = 8 J_1 (l_2^2 - l_1^2 \sin^2(\theta_1(t)))^{\frac{5}{2}}$$

$$\begin{aligned}
\mathbf{n}_3(\theta_1(t)) &= 8 l_1 \sin(\theta_1(t)) (l_2^2 - l_1^2 \sin^2(\theta_1(t)))^2 \\
&\left(\sqrt{l_2^2 - l_1^2 \sin^2(\theta_1(t))} + l_1 \cos(\theta_1(t)) \right)
\end{aligned}$$

$$\begin{aligned}
\mathbf{g}_1(\theta_1(t)) &= \frac{-4 \mathbf{n}_1 l_1^2}{\mathbf{d}} \\
\mathbf{g}_2(\theta_1(t)) &= \frac{-4 \mathbf{n}_2}{\mathbf{d}} \\
\mathbf{g}_3(\theta_1(t)) &= \frac{-4 \mathbf{n}_3}{\mathbf{d}}
\end{aligned}$$

$$\psi(\theta_1(t), \omega_1(t)) = \mathbf{g}_1(\theta_1(t)) \omega_1^2(t) + \mathbf{g}_2(\theta_1(t)) \tau_N$$

Rotational speed of the gasoline engine can be expressed as:

$$\dot{\omega}_1(t) = \psi(\theta_1, \omega_1) + \mathbf{g}_3(\theta_1(t)) f_n$$